SYNTHESIS, STRUCTURE, SPECTRA, DNA BINDING, BSA INTERACTION AND CYTOTOXICITY OF COPPER(II) COMPLEXES



Thesis submitted to Bharathidasan University, Tiruchirappalli in partial fulfilment of the requirements for the award of the degree of

DOCTOR OF PHILOSOPHY IN CHEMISTRY

By J. MANIVEL

(Reg. No. 36247-A/Ph.D.K2/Chemistry/Part Time/Re-Regn.-January 2016)

Under the Guidance and Supervision of **Dr. M. MURALI**



PG AND RESEARCH DEPARTMENT OF CHEMISTRY

NATIONAL COLLEGE (Autonomous)

(Nationally Re-Accredited with 'A" Grade by NAAC)
College with Potential for Excellence by UGC

TIRUCHIRAPPALLI 620 001, INDIA

FEBRUARY 2022



PG AND RESEARCH DEPARTMENT OF CHEMISTRY NATIONAL COLLEGE (Autonomous)

Nationally Re-Accredited at 'A⁺⁺, grade by NAAC College with Potential for Excellence by UGC

Dr. M. Murali Assistant Professor (SG)

Tiruchirappalli 620 001 Tamil Nadu, INDIA

CERTIFICATE

The research work embodied in this thesis entitled 'Synthesis, Structure, Spectra, DNA Binding, BSA Interaction and Cytotoxicity of Copper(II) Complexes' is original and was done by Mr. J. Manivel at Department of Chemistry, National College (Autonomous), Tiruchirappalli 620 001 India. It has not previously formed the basis for the award of any Degree, Diploma, Associateship, Fellowship or other similar title of Bharathidasan University or any other University.

Dr. M. Murali Research Supervisor

e-mail: ma66mu@gmail.com, murali@nct.ac.in

Mobile: +91-9790180077



PG AND RESEARCH DEPARTMENT OF CHEMISTRY NATIONAL COLLEGE (Autonomous) Nationally Re-Accredited at 'A'++, grade by NAAC

College with Potential for Excellence by UGC

Tiruchirappalli 620 001 Tamil Nadu, INDIA

DECLARATION

The research work embodied in this thesis entitled 'Synthesis, Structure, Spectra, DNA Binding, BSA Interaction and Cytotoxicity of Copper(II) Complexes' is original and was done by me at Department of Chemistry, (National college (Autonomous)), Tiruchirappalli 620 001 India. It has not previously formed the basis for the award of any Degree, Diploma, Associateship, Fellowship or other similar title of Bharathidasan University or any other University.

J. Manivel



PG & RESEARCH DEPARTMENT OF CHEMISTRY NATIONAL COLLEGE (Autonomous) TIRUCHIRAPPALLI 620 001 TAMILNADU, INDIA

CERTIFICATE OF PLAGIARISM CHECK

1	Name of the Research Scholar	J. Manivel
2	Course of Study	Ph.D. Chemistry
3	Title of the Thesis / Dissertation	Synthesis, Structure, Spectra, DNA Binding, BSA Interaction and Cytotoxicity of Copper(II) Complexes
4	Name of the Research Supervisor	Dr. M. Murali
5	Department / Institution / Research Centre	PG & Research Department of Chemistry National College (Autonomous) Tiruchirapalli 620 001
6	Acceptable Maximum Limit for Preliminary Chapters	15%
7	Acceptable Maximum Limit for Remaining Chapters	10%
8	Percentage of Similarity of Content Identified for Preliminary Chapters	0%
9	Percentage of Similarity of Content Identified for Remaining Chapters	4%
10	Software Used	Ouriginal
11	Date of Verification	13.01.2022

Report on plagiarism check, item with % of similarity is attached.

Signature of the Research Supervisor

Signature of the Candidate



Document Information

Analyzed document Manivel J Reg.No_36247 A Introduction and Review of Literarture.pdf (D124782383)

Submitted 2022-01-13T11:03:00.0000000

Submitted by Sureshkumar T

Submitter email sureshkumart@nct.ac.in

Similarity 09

Analysis address sureshkumart.bdu@analysis.urkund.com

Sources included in the report



Document Information

Analyzed document Manivel J Reg.No. 36247 A Remaining Thesis pdf (D124782342)

Submitted 2022-01-13T11:03:00.0000000

Submitted by Sureshkumar T

Submitter email sureshkumart@nct.ac.in

Similarity 49

Analysis address sureshkumart.bdu@analysis.urkund.com

Sources included in the report

Jour	ces included in the report	
w	URL https://pubmed.ncbi.nlm.nih.gov/21671566/ Fetched: 2022-01-13T11:14:04.9330000	2 2
w	URL: https://pubs.rsc.org/en/content/getauthorversionpdf/C4DT03879G Fetched: 2021-10-22T02:24:46.2270000	11
J	URL 03f7c0a2-1b6c-4741-9116-dd691b58f588 Fetched: 2019-02-15T22:24;24.6370000	留 16
w	URL: https://www.banglajol.info/index.php/JSR/article/view/42745/32538 Fetched: 2021-06-16T22:45.03.4100000	RR 3

ACKNOWLEDGEMENT

This is by far the most important part of my thesis. I realize that my greatest achievements have been professional and personal relationships. I have developed important relationships that have brought me to this stage in life. So it is with tremendous gratitude that I write this acknowledgement to show my appreciation to some of the people who have helped me throughout the years.

First and foremost, I have an immense pleasure in expressing my deep sense of gratitude to my research adviser and mentor, **Dr. M. Murali**, Assistant Professor, Coordination and Bioinorganic Chemistry Research Laboratory, Department of Chemistry, National College (Autonomous). His guidance, excellent suggestions, keen observations and constructive comments have helped me to establish the overall direction of research and motivate me in my research work. He is not only my guide but is also a father figure to me especially while I am frustrated with my family issues.

I express my sincere thanks to **Dr. R. Sundararaman**, Principal, National College (Autonomous), **Dr. K. Anbarasu**, Former Principal and Director for allowing me to use all the necessary facilities in the college.

I am grateful to **Dr. K. Vivekanandan**, Head, Department of Chemistry, National College (Autonomous) for his kind support during my research work. I also owe my thanks to all the faculty members in the Department of Chemistry for their assistance and encouragement.

I wish to place on record my deep sense of gratitude to my doctoral committee members, **Dr. M. Marappan**, Assistant Professor, Department of Chemistry, Government Arts College, Nandanam, Chennai and **Dr. G. Rajagopal**, Assistant Professor and Head, Department of Chemistry, Chikkanna Government Arts College, Tirupur, for their active support, motivation, timely assistance, encouragement and valuable suggestions rendered throughout my work.

I would like to thank the administrative and technical staff members of the National College (Autonomous) who have been kind enough to help me in their respective roles. I also thank all non-teaching staff for their help.

I wish to express my gratitude to Professor **Dr. M. Palaniandavar, FRSC, FASc, FNA,** INSA Honorary Scientist, School of Chemistry, Bharathidasan University,
Tiruchirappalli, for his interesting suggestions in this study.

I wish to thank **Dr. A. Ramu**, School of Chemistry, Madurai Kamaraj University, Madurai, **Dr. Balachandran Unni Nair**, Emeritus Scientist, Central Leather Research Institute, Chennai for providing Circular Dichroism facility and **Dr. P. K. Sudhadevi** and **Mr. N. Sivaramakrishnan**, Sophisticated Analytical Instrumentation Facility (SAIF), Indian Institute of Science and Technology Madras, Chennai for helping me to solve X-ray crystal structures and record EPR Spectra respectively and **Dr. N. Adhirajan**, Professor, KMCH College of Pharmacy, Coimbatore, who is greatly acknowledged for anticancer activity studies and **Dr. M. S. Mohamed Jabbir**, **Mr. P. Arulprakash**, National College (Autonomous), for supporting the anticancer mechanism.

I would like to extend my sincere thanks to **Ayya. A. Srinivasan**, Honorable Chairman, Dhanalakshmi Srinivasan Educational Institutions for providing the necessary facilities to do the research work. I also thank the Principals of Dhanlakshmi Srinivasan Engineering College for their encouragement during my research work. I wish to express my gratitude to the Head and faculty members, Department of Science and Humanities for their assistance and encouragement.

I wish to express my gratitude to my friend **Dr. V. T. Paventhan**, for his support and tutelage during my Ph.D. Degree and **Dr. S. P. Anand**, National College

(Autonomous), for providing the hostel accommodation during my research work and **Dr. S. Thirumurugan**, National College (Autonomous), for his assistance and support in the hostel.

I would like to thank my seniors and my sisters, **Dr. S. Sangeetha** and **Dr. V. Sathya** for all their support, guideline, advice and help during the entire work and colleagues **Mr. V. Ravisankar**, **Mrs. J. Latha**, for their cooperation, useful discussion and generous help throughout my research period.

I would like to offer my special thanks to **Mr. B. Selvakumaran**, Research Scholar, for being with me day and night, offering help and support for all technical and non-technical works. His timely help was very crucial in the completion of my thesis. I would like to thank my friends, lab mates, colleagues and research team for a cherished time spent together in the lab, and in social settings.

I would also like to give special thanks to my wife Mrs. P. Poornima, for her continuous support and understanding during my research undertaking and thesis writing. Your prayer for me was what sustained me this far. In addition, I would like to thank my parents for their wise counsel and sympathetic ear. You are always there for me. Finally, I could not have completed this dissertation without the support of my friends, who provided stimulating discussions as well as happy distractions to rest my mind outside of my research.

This work is dedicated to my son **M. Pravanth**. You have made me stronger, better and more fulfilled than I could have ever imagined. I love you to the moon and back.

I finish with a final silence of gratitude to the Almighty God for granting me the wisdom, health and strength to undertake this research task and enabling me to its completion.

J. Manivel

CONTENTS

Chapter No.			Title	Page No.
1.	Introduction			1
	1.1	Structure of DNA		4
	1.2	Interac	tion of Small Molecules with DNA	9
	1.3	DNA c	leavage	12
	1.4	Protein	ı	15
		1.4.1	Serum Albumin	15
		1.4.2	Structure of Bovine serum albumin	16
		1.4.3	Intrinsic fluorescence of BSA	17
		1.4.4	Importance of binding analysis study	18
	1.5	Cancer	(A silent killer)	20
		1.5.1	Causes of Cancer	23
		1.5.2	Treatment of Cancer	23
		1.5.3	Cancer treatment with chemotherapy	24
		1.5.4	Apoptosis	24
		1.5.5	Necrosis	26
	1.6	Metal-	based anticancer drugs	27
		1.6.1	Mode of action of cisplatin analogous drugs	29
		1.6.2	Copper complexes as anticancer agents	29
	1.7	Scope	of present investigation	44
	Refere	ences		50
2.	General Experimental Materials, Methods and Techniques			60
	2.1	Materia	als	60
		2.1.1	Chemicals	60
		2.1.2	Solvents	60
		2.1.3	Preparation and purification of supporting electrolytes Tetra-N-butylammonium perchlorates (TBAP)	61
		2.1.4	Purification of solvents	61
		2.1.5	Preparation of metal complexes	61

	2.2	Techniques		62
		2.2.1	Physical Measurements	62
		2.2.2	Electroanalytical techniques	63
		2.2.3	DNA binding studies	63
		2.2.4	Electronic absorption titration	64
		2.2.5	Fluorescence studies	65
		2.2.6	Circular dichroic spectra	65
	2.3	BSA bi	nding studies	66
		2.3.1	Fluorescence quenching measurements	66
		2.3.2	Binding parameters	68
		2.3.3	Thermdynamic parameters and nature of the binding forces	68
		2.3.4	Förster's non-radiative energy transfer	69
		2.3.5	UV-Visible absorption spectra	70
	2.4	DNA c	leavage experiments	70
	2.5	Cell lin	ies	71
	2.6	Cell cu	lture	71
	2.7	Cell via	ability assay	72
	2.8	Cell cycle		
	2.9	ROS generation		
	2.10	Apopto	osis	74
	2.11	DAPI s	staining	74
	Refere	ences		75
3.	Cytoto	oxicity of	SA Interaction, DNA Cleavage and <i>in vitro</i> Copper(II) Complexes: [Cu(bba)(phen)] (ClO ₄) ₂ is demotherapeutic Scaffold	77
	3.1	Introduction		77
	3.2	Experi	mental	79
		3.2.1	Synthesis of copper(II) complexes	79
		3.2.2	X-ray crystallography	81
	3.3	Results	and discussion	83
		3.3.1	Synthesis general aspects	83
		3.3.2	Description of the crystal structure	84

	3.3.3	Electronic and EPR spectral properties	86
	3.3.4	Electrochemical properties	92
	3.3.5	DNA binding studies	92
	3.3.6	Protein binding studies	104
	3.3.7	DNA cleavage studies	115
	3.3.8	In Vitro Cytotoxicity studies	119
3.4	Conclu	sion	121
Refere	ences		122
Synth	esis, St	Copper(II) Complexes with CuN ₅ Chromophore: ructure, DNA binding and Cleavage, BSA d Cytotoxicity	127
4.1	Introdu	ection	127
4.2	Experi	mental	129
	4.2.1	Synthesis of (6-methylpyridin-2-ylmethylene)- (pyridine-2-ylmethyl) amine,L1	129
	4.2.2	Synthesis of (6-methylpyridin-2-ylmethylene)- (pyridine-2-ylethyl) amine,L2	130
	4.2.3	Synthesis of copper(II) complexes	131
	4.2.4	X-ray structure determination	132
4.3	Results	and discussion	133
	4.3.1	Synthesis and general properties	133
	4.3.2	Description of crystal structure	134
	4.3.3	Electronic and EPR spectral properties	138
	4.3.4	Electrochemical properties	141
	4.3.5	DNA binding studies	145
	4.3.6	DNA cleavage	154
	4.3.7	BSA binding	166
	4.3.8	Cytotoxic activity	172
4.4	Conclu	sion	174
Refere	ences		176
	nism of	, In Vitro Cytotoxicity and Anticancer Drugs Copper(II) Complex Containing Pyridyl-Triazine	182
5.1	Introdu	ection	182

5.2	Experimental		
	5.2.1	Synthesis of complex, [Cu(dppt) ₂ (H ₂ O) ₂](ClO ₄) ₂ (1)	184
	5.2.2	X-Ray crystallography	185
5.3	Results and discussion		
	5.3.1	Synthesis and characterization of $[Cu(dppt)_2 (H_2O)_2]$ $(ClO_4)_2$ (1)	186
	5.3.2	Structure description	186
	5.3.3	Electronic and EPR spectra	190
	5.3.4	Redox properties	192
	5.3.5	DNA binding studies	194
	5.3.6	Ethidium Bromide (EtBr) displacement assay	195
	5.3.7	Voltammetric studies	197
	5.3.8	Cytotoxic activity	200
	5.3.9	Anticancer drug mechanism	202
	5.3.9a	Cell cycle arrest studies	202
	5.3.9b	DCFDA assay for ROS	202
	5.3.9c	Cell death pathway	204
5.4	Conclu	sion	206
Refere	nces		207
Summary		211	

Chapter 1

Introduction

The meeting of two personalities is like the contact of two chemical substances: if there is any reaction, both are transformed.

1 Introduction

The discovery of the structure of DNA [1] by James D. Watson and Francis H. C. Crick in 1953 is often regarded as the beginning of modern molecular biology, and it is crucial since it establishes the foundation for the central molecule of life. DNA is the library of the cell. It is a polymer of deoxyribose nucleotides. A double helical structure is formed by phosphate groups and hydrogen bonding between nucleotides of opposing chains (strands). The double helix is coiled around histone proteins in the cell to produce the nucleosome, which is then supercoiled to form chromatin, which is then supercoiled to higher-order structures to form the chromosome. DNA is found in chromosomes and tiny circular strings called plasmids in bacteria. Figure 1.1 depicts the chromosomal organization of DNA schematically.

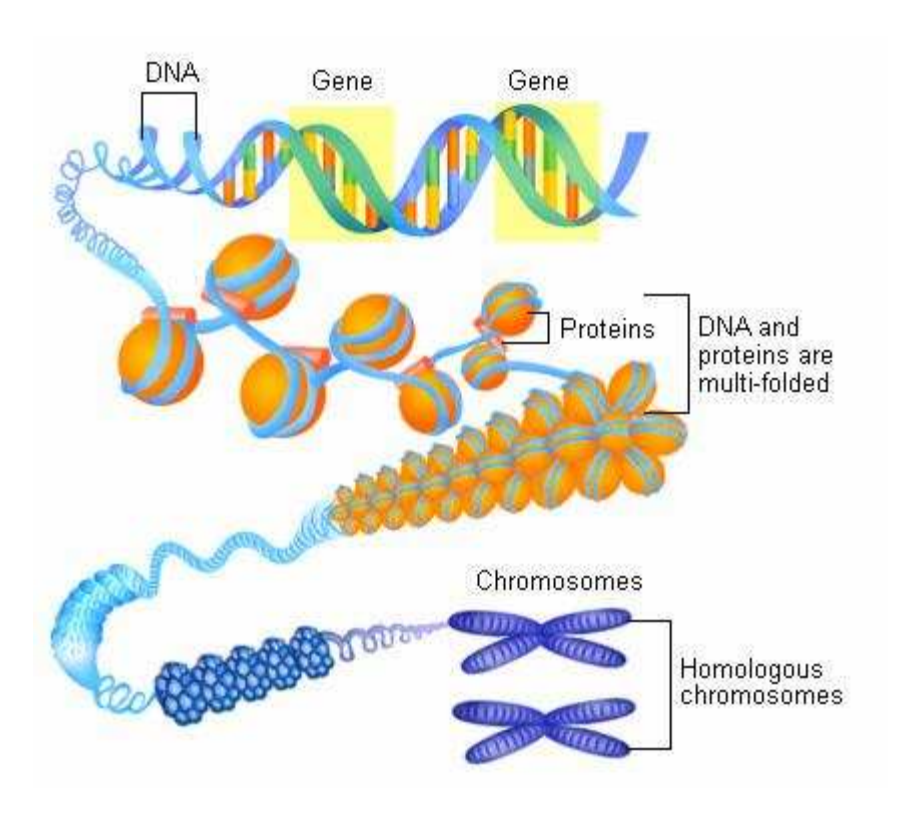


Figure 1.1 Simplified view of the DNA organization in the chromosome.

Despite the incredible diversity of living species on Earth, they are all built on the same fundamental unit, the cell, from minuscule bacteria (µm) to enormous plants and animals. For thousands of years, humans have been fascinated by the genetic enigma, which includes the conservational characteristics and evolutional mutations of each generation. The mystery of heredity was not solved until nucleic acids were firmly identified as the main genetic substance in living cells in 1952. Deoxyribonucleic acid, DNA, is the carrier of genetic information and plays a critical function in all living creatures. Watson and Crick demonstrated the DNA double helix structure a year later, in 1953 [2]. These developments marked a watershed moment in human scientific progress in the twentieth century. The genetic information is encoded in the double helix of DNA, which acts as a template for protein synthesis by transcription of DNA into messenger ribonucleic acid (mRNA). Following that, mRNA is [3,4] translated into amino acid sequences in the ribosome, which, after folding into the correct 3-dimensional structure, creates a functional protein expressing the biological characteristics. The Human Genome Project, International Cooperation, evaluated the sequences of the 46 chromosomes in humans, and the results were published in Nature and Science in 2001 [5,6].

Because DNA is the "terminal controller" of human life, every sickness and dysfunction of the body should logically correlate to a mistake in the appropriate DNA code region. Proteins are still a common target for illness therapy today, although DNA-targeting medicines can also affect protein activity at the transcription level [7]. DNA-targeted therapeutic regulation is a treatment method for genetic diseases including cancer [8]. DNA-binding small molecules play a vital function in

controlling protein expression and cell cycles to prevent uncontrolled cell proliferation and other genetic diseases. The most difficult issue in curing genetic diseases without endangering normal cells is to design a specialized DNA-targeted molecule that can attach to specific DNA sequences. Chemical and physical qualities are two of the most essential considerations for choosing tiny compounds as DNA-binding drugs. Distinguishing between normal and cancerous cells is particularly important since the two types of cells are surprisingly similar, and most anticancer medicines have negative side effects [9]. Transition metal complexes have recently been reported to act as very effective anticancer medicines with specific target selectivity for cancerous cells.

The double helix structure has encouraged chemists to overcome biological challenges for the past 65 years. DNA-binding small molecules have shown great promise as diagnostic probes, reactive agents, and therapeutics. Antineoplastic drugs such as cisplatin have been successfully employed in the past. Transition metal complexes of 1,10-phenanthrolines cleaving DNA under physiological conditions are also of current interest in nucleic acid chemistry for their numerous applications. Metallobleomycins, a non-covalent DNA-binding metal complex first discovered from Streptomyces verticillus in the late 1960s, is a well-studied class of glycopeptide antibiotics that have had some effectiveness in the treatment of cancer [10]. As a result, in our lab, we are particularly interested in the study of non-covalent DNA binding of transition metal complexes. The synthesis of certain copper(II) complexes and their interaction with commercially available calf thymus DNA, as well as their capacity to cleave supercoiled pUC19 DNA, are the subjects of this thesis. The interaction has been researched using a variety of physical methods to better understand the DNA-complex binding behavior. Fluorescence and absorption spectral methods

were used to investigate their interaction with bovine serum albumin. The complexes are being tested for cytotoxicity against a human cervical cancer cell line. Various biochemical approaches have been used to determine the anticancer mode of cell death, such as apoptosis and necrosis.

1.1 Structure of DNA

Nucleic acids are chain-like macromolecules that are composed of pyrimidine and purine bases, sugars, and phosphates (Figure 1.2). The four bases characteristic of deoxyribonucleotide units of DNA are the purine derivatives, adenine (A), and guanine (G) and the pyrimidine derivatives, Cytosine (C), and Thymine (T). Similarly, RNA too has four characteristic bases, adenine, guanine, and cytosine, and uracil instead of thymine. Also, the pentose sugar in RNA is Ribose whereas it is deoxyribose in DNA. The purine and pyrimidine nitrogenous bases are called nucleobases. A base linked to a sugar is called a nucleotide (Figure 1.3). Nucleotides provide the building blocks from which nucleic acids are constructed. The nucleotides are linked into a polynucleotide chain of alternating sugar and phosphate residues, which form the backbone. The 5'-position of one pentose ring is connected to a 3'-position of the next pentose ring via a phosphate group. Thus the sugar-phosphate backbone consists of 5',3'-phosphodiester linkages.

The DNA model proposed by Watson and Crick contains two polynucleotide chains wound into a right-handed helix wherein the phosphodiester bonds of the DNA chains run in the opposite direction, i.e., they are antiparallel. One strand runs in the 5'-3' direction while the other runs in the 3'-5' direction (**Figure 1.4**). There is a specificity of hydrogen bonds, whereas between bases: adenine pairs with thymine

with three hydrogen bonding and guanine pairs with cytosine with two hydrogen bonds. Such specificity in pairing is known as base pairing. The ability of DNA to form a double helix is of prime importance in considering its function in the cell. The double helical structure immediately suggests a mechanism for the accurate replication of genetic information.

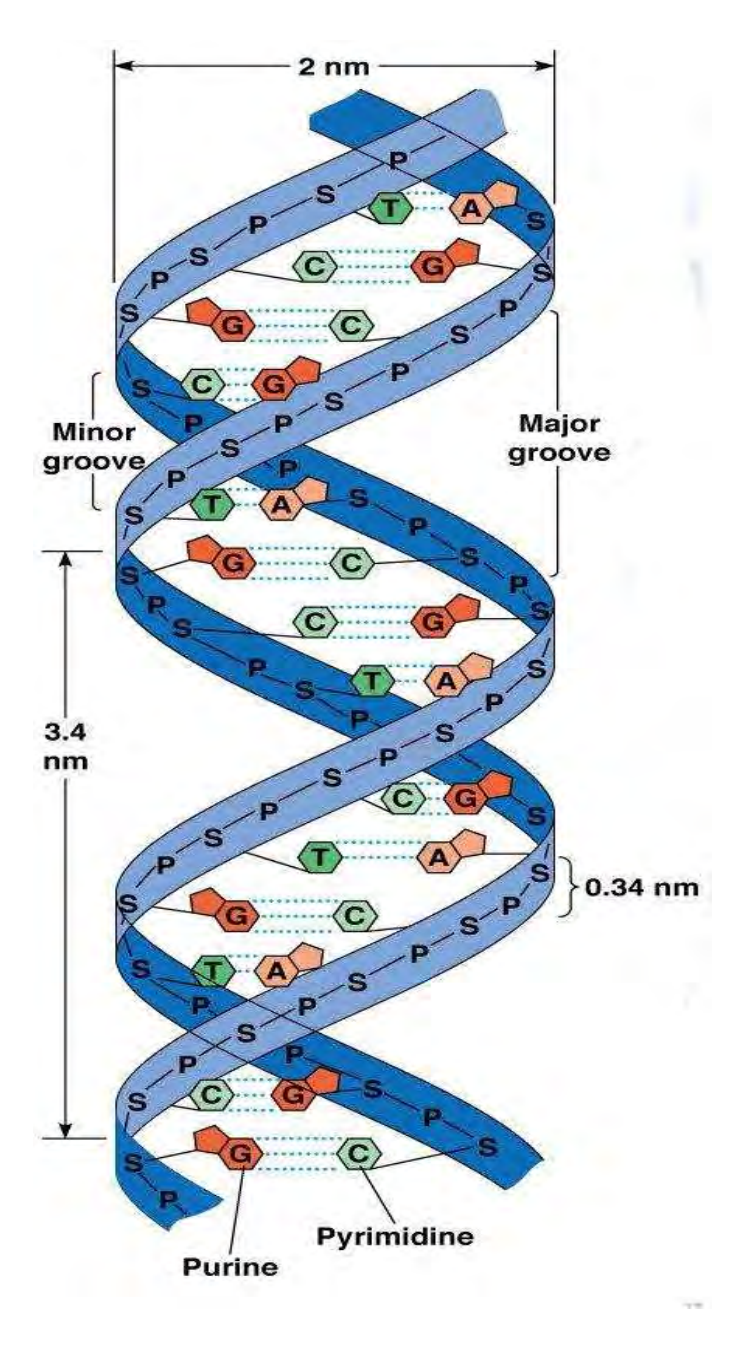


Figure 1.2 Structure of deoxyribonucleic acid (DNA).

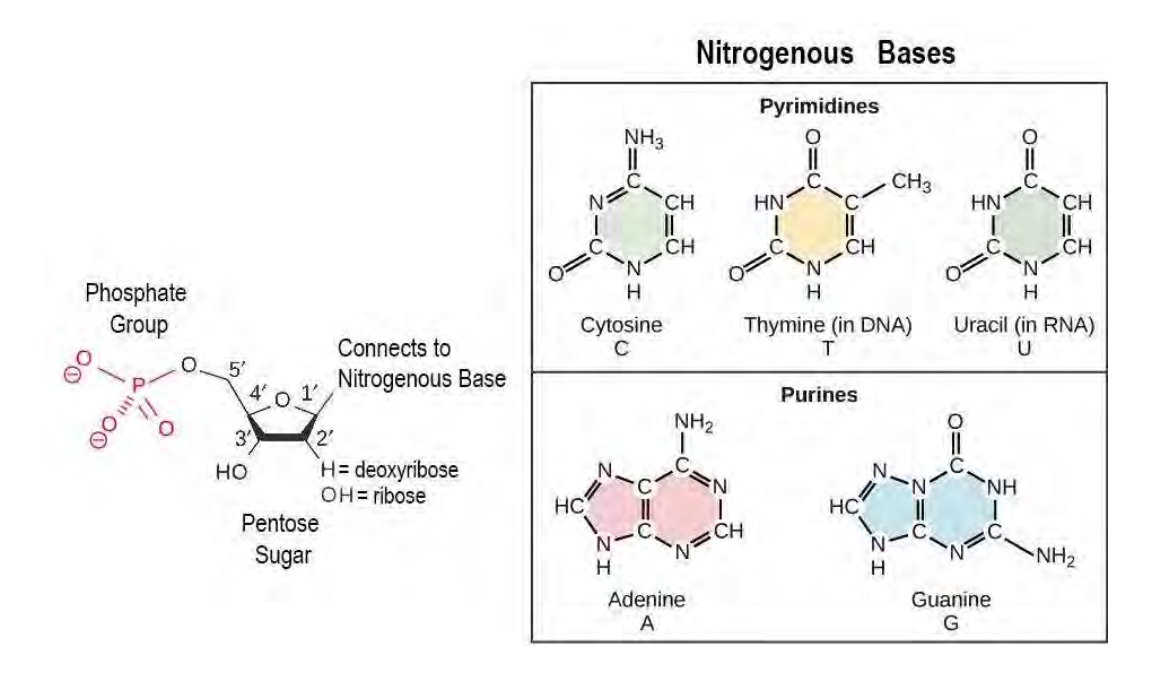


Figure 1.3 Structures of purine and pyrimidine bases and of the corresponding nucleosides and nucleotides.

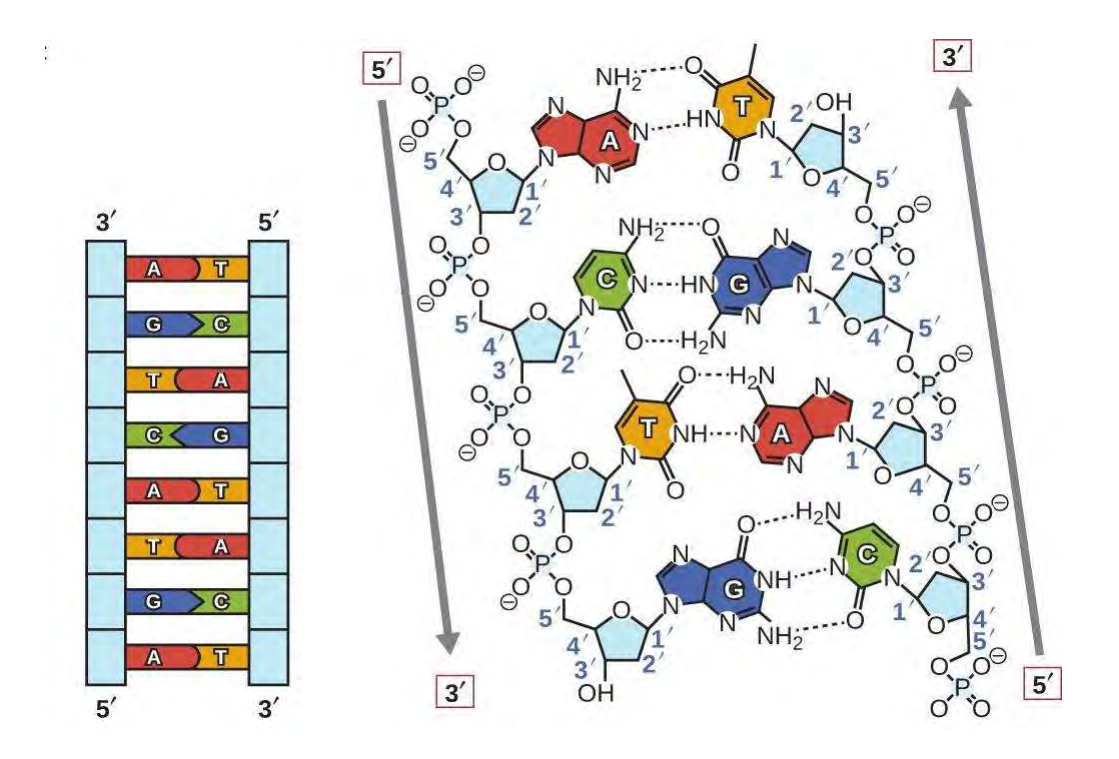


Figure 1.4 Structure of two poly nucleotide chains run in opposite direction (antiparallel); hydrogen bonding involving the Adenine - Thymine and Guanine - Cytosine pairs.

6

The DNA double helix has three structurally characterized conformations. i.e., A, B and, Z forms (Figure 1.5). These three conformation structures are all double helical and rely upon the Watson and Crick hydrogen bonding interaction between the two antiparallel strands of nucleic acid. However, the resulting shapes of the conformations are different. The B form, considered to be the most common is a right-handed helix, with base pairs stacked in the center of the helix and the average base plane aligned normal to the helical axis. A remarkable and biologically important structural feature of B-DNA is the presence of the two grooves in the outer envelope of the double helix. The grooves, called the major and minor grooves, are of different width and depth and are a consequence of the glycosyl bonds between the sugars and bases of a given base pair not being directly opposite to one another, i.e., the asymmetric attachment of the base pair to the backbone results in a groove becoming wider than the other thereby leading to the major and minor grooves. The A conformation is also a right-handed helix, but it is distinctly different from the B conformation concerning the helical grooves. Due to the sugar puckering, the bases are pushed outward towards the minor groove and are tilted substantially to the helix axis. Thus the helix has a deep major groove and virtually no minor groove as it is pulled deeply into the interior of the structure thereby becoming inaccessible to the molecules in solution. The Z DNA is the third form and is characterized structurally by a double helical conformation. This conformation is distinctly different since it spirals into a left-handed rotation. The repeating unit is a dinucleotide, resulting in a zigzag helix, because of

(A)

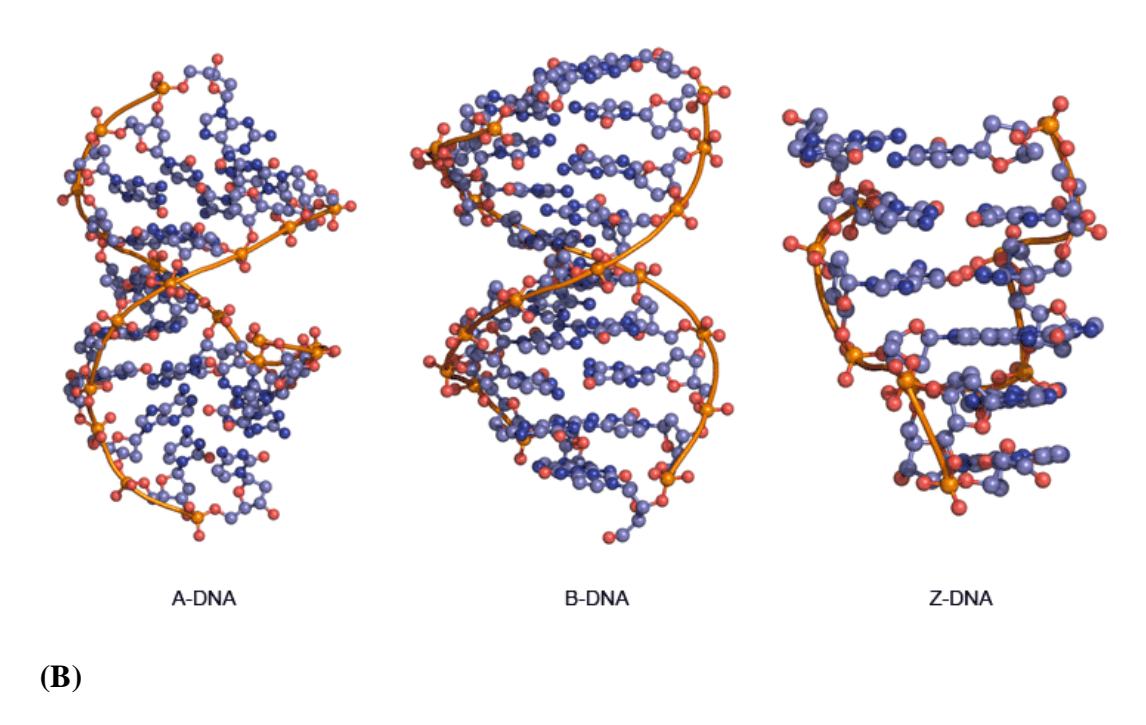


Figure 1.5 (A) Structures of A, B and Z DNA. (B) Diagrams of left- and right-handed helices.

the alteration in sugar pucker and disposition of the bases about the glycosidic bond. The nucleotides alternate in *syn* and *anti* conformations of the bases since the *syn* conformation is more stable for purines than for pyrimidines. In B DNA, all of the nucleotides have the *anti* conformation and a C2′ endo pucker of the deoxyribose ring. Z DNA displays a *syn-anti* alternation in base geometry and an alternating C2′ endo C3′ endo sugar puckering, both of which lead to the overall zigzag geometry of the helix characteristic of the Z DNA. Also, the helix is long and slender than the A or B DNA forms. The conformation of DNA is dependent on humidity, salt content, and base pair composition. The most important biological form of DNA is B, which is present in aqueous solutions and cells, but Z DNA has also been observed in the cell. The major finding is the formation and stabilization of Z DNA by negative supercoiling. It has also been proposed that the energy necessary to form and stabilize Z DNA *in vivo* can be generated during the transcription process.

1.2 Interaction of small molecules with DNA

The interaction of metal complexes with DNA is a thriving area of research since the discovery of cisplatin (*cis* diamminedichloroplatinum(II)), *cis*-[PtCl₂(NH₃)₂], 60 years ago. Cisplatin when bound to DNA generates intrastrand crosslink's that kink the DNA structure, inhibits transcription leading to the death of cancerous cells. The mechanism of DNA-binding and behavior of the metal complexes as novel cancer therapeutic agents are strongly attributed to the size, shape, and planarity of the intercalative ligands. It is also known that metal complexes may interact with DNA either covalently or non-covalently. (**Figure 1.6**)

1. Covalent DNA interactions

It is widely believed that the primary mechanism for cisplatin-induced cancer cell death arises from its ability to form covalent adducts with DNA (Figure 1.7), primarily at purine bases. It has been shown that the formation of cisplatin-DNA adduct leads to a disruption of biological functions such as protein/DNA binding, DNA replication, and transcription which causes cell death.

2. Non-covalent DNA interactions

a. Intercalation

Intercalation results when a small molecule or the drug interacts into the non-polar interior of the DNA helix. The aromatic group is stacked between the base pairs in this type of binding (**Figure 1.8**). This happens when ligands of an appropriate size and chemical nature fit themselves in between base pairs of DNA. The ligands suitable for interaction are mostly polycyclic, aromatic, and planar and therefore often make good nucleic acid stains [11].

b. Groove binding (Major and Minor Groove)

Groove binding involves direct interaction of the bound molecules with edges of base pairs in either of the major (G-C) or minor (A-T) grooves of the nucleic acids (**Figure 1.9**). The antibiotic netropisn is a model groove binder in which methyl groups prevent intercalation. Binding within the major groove of the double helix is rare for small molecules [12].

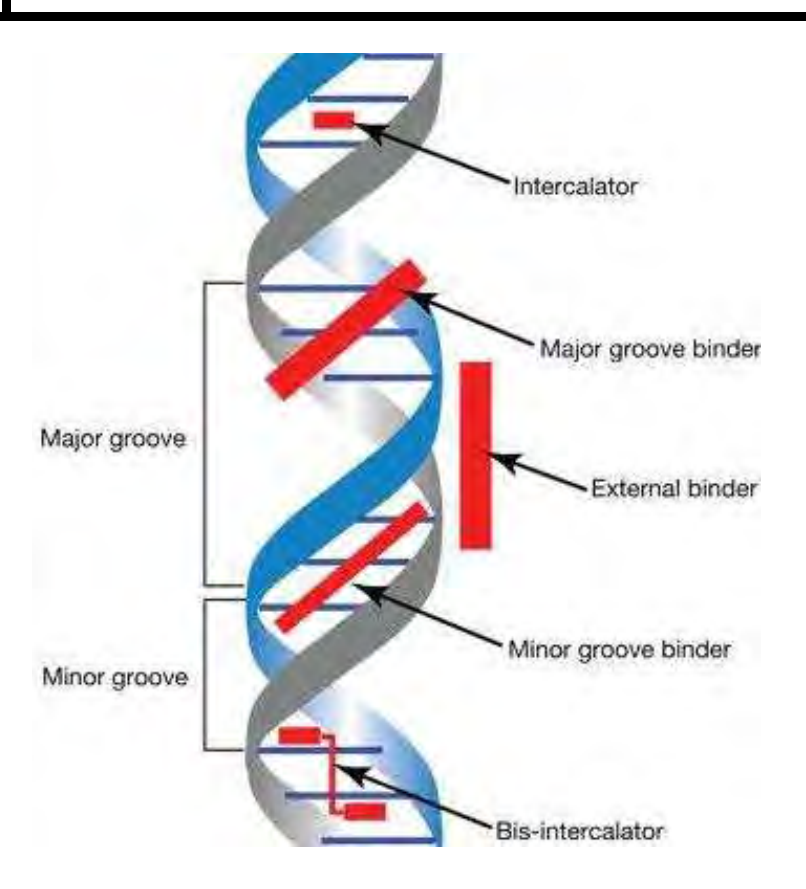


Figure 1.6 Schematic diagrams of different modes of binding in DNA.

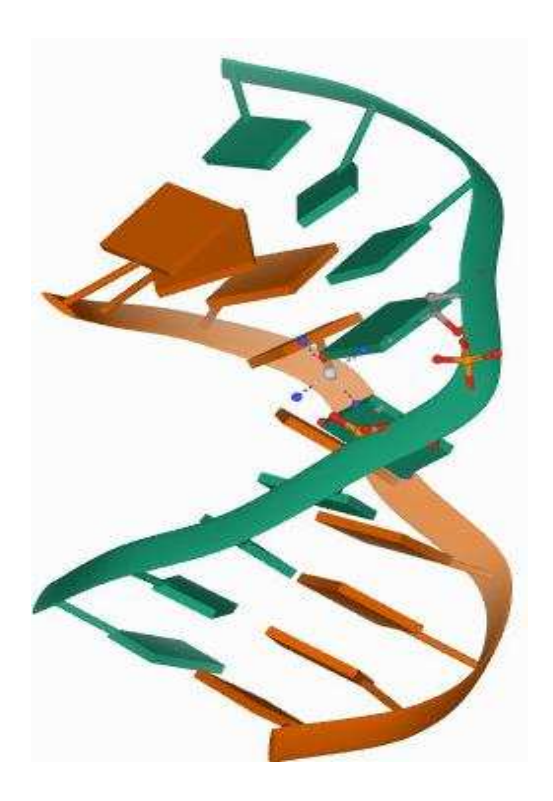


Figure 1.7 View of cisplatin when bound to DNA.

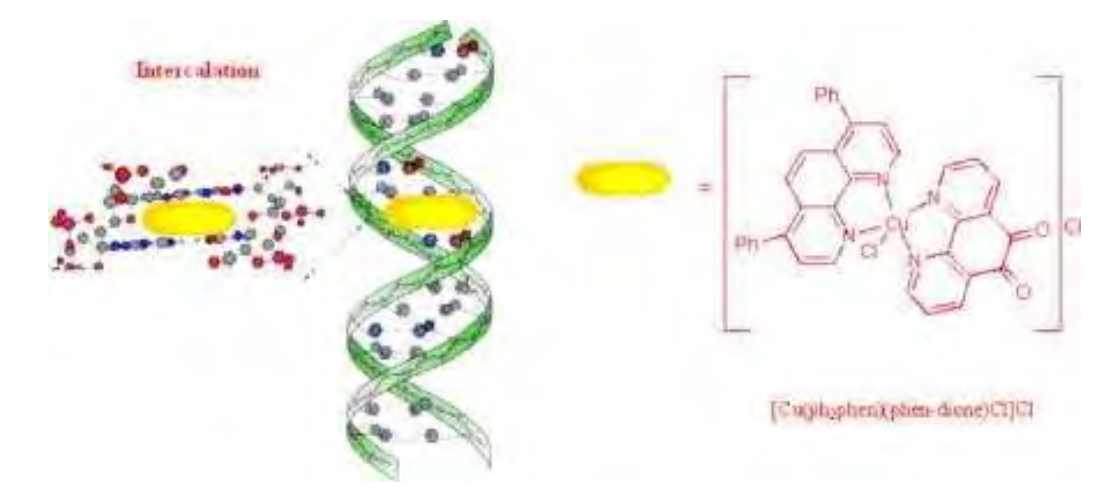


Figure 1.8 Intercalative binding models.

c. Electrostatic/External binding

This type of interaction happens in the case of positively charged molecules (**Figure 1.10**) interacting with a negatively charged phosphate backbone of the DNA chain. Electrostatic interaction is generally weak under physiological conditions cations such as Mg^{2+} usually interact in this way [13].

1.3 DNA cleavage

Cleavage of DNA is a vital process in all living systems. For example, topoisomerase enzymes resolve topological problems of DNA in replication, transcription, and other cellular transactions by cleaving one or both strands of the DNA [14]. Another example is restriction enzymes (or restriction endonucleases), which protect the cell against virus infection by cleavage of the foreign DNA, [15] or by degrading cellular DNA during apoptosis of the affected cell [16]. Finally, the activity of many anticancer drugs relies on their ability to introduce extended damage to the DNA in the (affected) cells (*e.g.* bleomycin), [17] which can trigger apoptosis, [10] leading to cell death [18]. In general, three different types of DNA cleavage can

be distinguished, namely i) DNA hydrolysis, ii) photochemical cleavage, and iii) oxidative cleavage, although the last two categories are quite closely related.

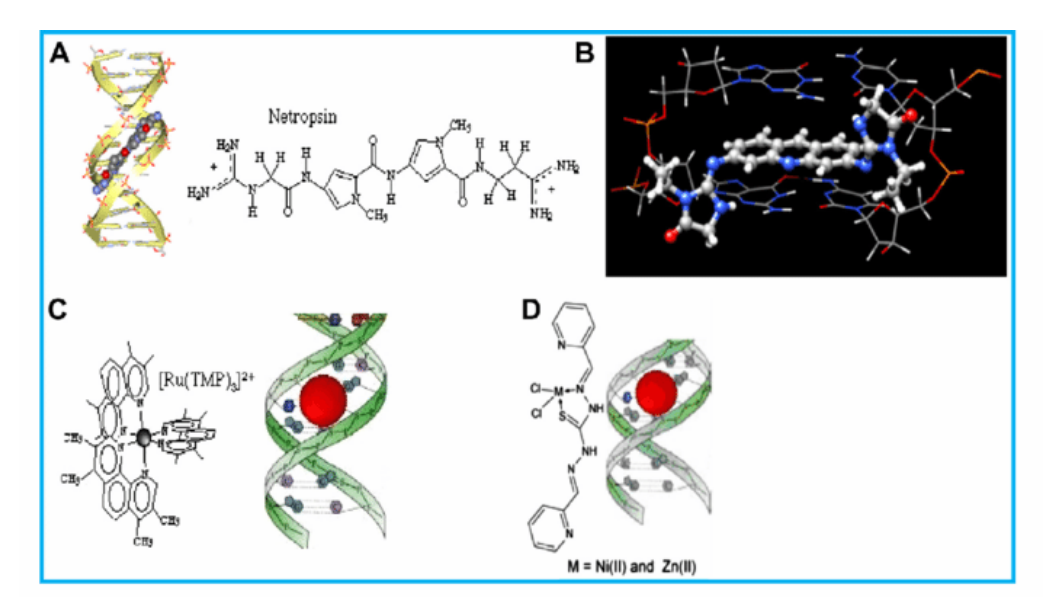


Figure 1.9 Groove binding models.

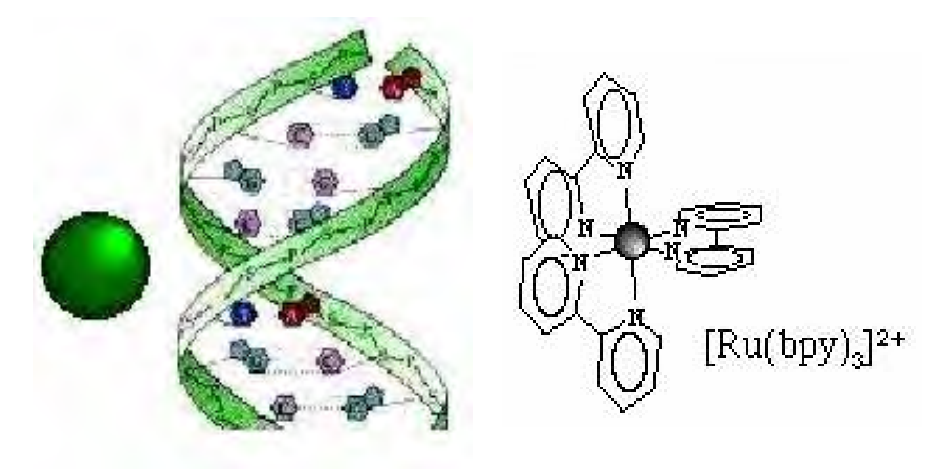


Figure 1.10 External/Electrostatic binding models.

Transition metal complexes capable of cleaving DNA are of importance for their potential use as new structural probes in nucleic acids chemistry and as therapeutic agents. Transition metal complexes of Fe, Cu, Ni, Pt, Ru, Rh, V, Cr, Co, Mn, Os, and Pd have been reported to mediate DNA oxidation in the presence of oxidants or reductants or without any other assistant agents [19]. Transition metal complexes

cleave DNA after activation by reducing agents in presence of molecular oxygen or hydrogen peroxide and thus act as synthetic nucleases. All these nucleolytic agents can be distinguished from other DNA-modifying compounds by their sugar-directed reactivity. These complexes attack the sugar or base moieties of DNA [19]. The first metal complex capable of cleaving DNA is $[Cu(phen)_2]^+$ (phen = 1,10-phenanthroline), discovered by Sigman and his coworkers. [20] In this reaction, there are two essential co-reactants, the $[Cu(phen)_2]^+$ complex and hydrogen peroxide. Possibly the unique reactivity of the 1,10-phenanthroline nucleus in the DNA cleavage reaction can be attributed to the transfer of charge from the phenanthroline to the metal ion. Several well-known and best-characterized nucleolytic agents are: $[Fe(EDTA)]^{2-}$ (H₂EDTA = ethylenediaminetetraacetic acid), [21] Fe-BLM (BLM = bleomycin), [22] metalloporphyrins, [23] Ni-peptides, [24] and metalsalen [H₂salen = N,N'-ethylenebis(salicylideneimine)] [25].

The fidelity of DNA replication carried out by DNA polymerases and their attendant proofreading functions is essential for the accurate transmission of genetic information during cell division. Yet errors in polymerization occasionally occur and, if not corrected, may alter by agents that are naturally present in the cell or the cell's external environment. In many cases, damaged DNA can be repaired. Severe lesions, however, may be irreversible, leading to the loss of genetic information and, often, cell death. Even when damaged DNA can be mended, the restoration may be imperfect, producing a **mutation**, a heritable alteration of genetic information. In multicellular organisms, genetic changes are usually notably only when they occur in germ-line cells so that the change is passed on to all the cells of the organism's offspring. Damage to the DNA of a somatic cell, in contrast, rarely has an effect beyond that cell unless the mutation contributes to a malignant transformation (**cancer**).

1.4 Protein

Proteins are the eminent molecules among those essential for life and are the most abundant biological macromolecule in cells. Their importance stems from the remarkable diversity of their functional roles within living organisms, like catalyzing biochemical reactions, replication of DNA, transporting molecules to appropriate sites, maintaining the structures of cells and organs, etc. The basic structural unit of a protein is the polypeptide chain with definite protein specific sequences of 20 commonly occurring amino acid residues linked by peptide bonds. These amino acid, which contains a carbonyl group and an amino group bonded to the α -carbon atom, are α -amino acids. Each of these amino acid residues varies in structure, size, and electric charges in physiological conditions. The specific sequence and the composition of amino acids in proteins differ the protein from one another.

1.4.1 Serum Albumin

Albumin, the most abundant extracellular protein accounts for a total of 60 % of the total serum content in the mammals. The investigation of compounds to their binding to albumins becomes important because of the pharmacokinetics and pharmacodynamics role of binding [26]. Serum albumins are the most abundant proteins in the circulatory system of a wide variety of organisms. They have an important role in bioregulatory functions like maintenance of the colloidal osmotic blood pressure and blood pH. In addition, serum albumins serve as depot proteins and as transport proteins for a variety of endogenous and exogenous substances such as fatty acids, hormones, and drugs [27]. In general, bovine serum albumin (BSA) has been extensively used because of its structural homology with human serum albumin

(HSA) [28]. BSA is the most abundant protein of plasma and has been widely used as a model system to study protein aggregation, biotechnological folding, and other applications. BSA is a well-known protein that displays a tendency to self-assemble in large macromolecular aggregates under a variety of conditions. Therefore, it is always chosen as a relevant protein and has become the best-studied model of general drugprotein interactions [29]. Due to its medical importance, low cost, ready availability, and unusual ligand-binding properties [30].

1.4.2 Structure of Bovine serum albumin

The primary structure of BSA (Figure 1.11) was proposed after the HSA structure elucidation and is composed of 585 amino acid residues. The sequence has 17 disulphide bonds resulting in nine loops formed by the bridges. BSA contains one cysteine and 8 pairs of disulphide bonds similar to HSA [31]. BSA also contains a high content of Asp, Glu, Ala, Leu, and Lys as well as the four amino acid residues in the sequence determined later as Gly–Phe–Gln–Asn [32]. According to the amino acid sequence proposed by Brown, the structural features of BSA show that it is composed of three homologous domains [33]. In the secondary structure of BSA, it has been suggested that the α -helices are uniformly placed in the subdomains and the connections between the domains. Most of the residues in the long loops (except at the end) and the sections linking the domains possibly form α -helices, whereas the intra-domain hinge regions are mainly the non-helical structures. The three long helices in the subdomain are considered principal elements of the structure. These run parallel with each other and a trough is formed owing to the middle helix (Y) being slightly lower in position. The helices are mainly linked together by disulphide

bridges [34]. There occurs almost 76% homology and a repeating pattern of disulphides which is conserved. The major difference between the two occurs for the number and positioning of tryptophan residues in them. HSA has only one tryptophan, located at position 214, which is equivalent to Trp-212 for BSA buried in a hydrophobic pocket at sub domain IIA. BSA has one more additional tryptophan Trp-134, which is more exposed to solvent and found at sub domain IB [35].

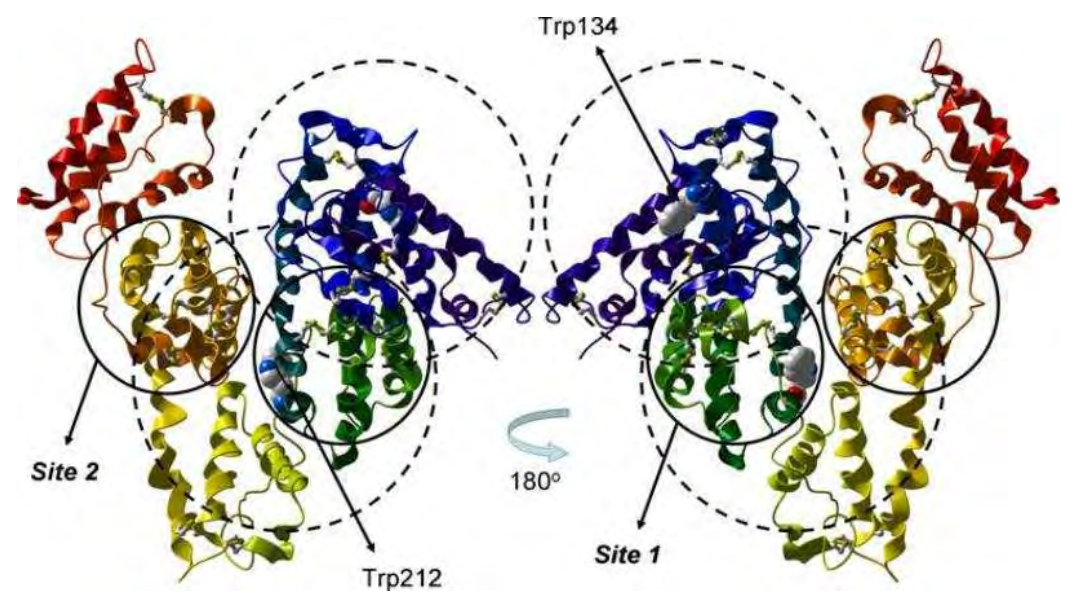


Figure 1.11 Two side-on 3D graphic representation of a BSA model structure based on HSA X-ray crystal structure obtained from the Protein Data Bank (PDB ID:1UOR).

1.4.3 Intrinsic fluorescence of BSA

Protein contains three amino acid residues, namely, tryptophan, phenylalanine, tyrosine which contribute to the intrinsic fluorescence. The fluorescence of a folded protein is a mixture of the fluorescence from individual aromatic residues. Protein fluorescence is observed generally by exciting at 280 nm or higher wavelengths usually at 295 nm. The emissions are due to the excitations of tryptophan residue predominantly when excited at 295 nm and a combination with contributions from the

tryptophan, tyrosine, and phenylalanine residues when excited at 280 nm. These three residues have distinct absorption and emission wavelengths. They differ greatly in their quantum yields and lifetimes.

Tryptophan has a much stronger fluorescence and higher quantum yield than the other two aromatic amino acids. The intensity, quantum yield, and wavelength of maximum fluorescence emission of tryptophan are very much solvent dependent. The fluorescence spectrum shifts to a shorter wavelength and the intensity of the fluorescence increases as the polarity of the solvent surrounding the tryptophan residue decreases. Tryptophan residues that are buried in the hydrophobic core of proteins can have spectra, which are blue or red shifted depending on the polarity experienced by them due to the solvent.

Tyrosine, like tryptophan, has strong absorption bands at 280 nm, and when excited by light at this wavelength, has characteristic emission. Tyrosine is a weaker emitter than the tryptophan, but it may still contribute significantly to protein fluorescence because it is present in larger numbers. The fluorescence from tyrosine can be easily quenched by nearby tryptophan residues because of energy transfer effects.

Phenylalanine with only a benzene ring and a methylene group is weakly fluorescent. The quantum yield and molar absorptivity are low for this residue. Phenylalanine fluorescence is observed only in the absence of both tyrosine and tryptophan.

1.4.4 Importance of binding analysis study

Albumins have been identified as major transport proteins in blood plasma for many compounds such as fatty acids, hormones, bilirubin, and many drugs which are

otherwise insoluble in plasma [36]. Serum Albumins are thus effective in increasing the solubility of hydrophobic drugs in plasma and modulate their delivery to cells in vivo and in vitro. They also play a leading role in drug disposition and efficacy. Furthermore, albumins are the principal biomacromolecules that are involved in the maintenance of colloid-blood pressure and are implicated in the facilitated transfer of many ligands across organ-circulatory interfaces such as in the liver, intestine, kidney, and brain [37]. From a biopharmaceutical point of view, one of the most important biological functions of albumins is their ability to carry drugs as well as endogenous and exogenous substances, and numerous experiments to characterize the binding capacity and sites of albumins have been carried out [38]. The drugs move through the blood by binding with the serum albumins only, so it is necessary to account for their interaction to obtain the needed best results. Understanding the full implications of the human genome project and the emerging field of proteomics has introduced new needs to further probe millions of protein interactions. An analysis is based on monitoring the change of a physicochemical property of the protein-probe system upon binding either directly (direct technique) or after separation of the bound and free probe (indirect technique). Among the direct techniques, fluorescence analysis is extensively used and considered to be superior to the indirect techniques (equilibrium and dynamic dialysis, ultrafiltration, and gel filtration) because it does not disturb the binding equilibrium upon separation [39]. The spectral changes observed on the binding of fluorophores with proteins are an important tool for the investigations of the topology of binding sites, conformational changes, and characterization of the substrate to ligand binding [40]. Besides, the determination of protein quantity in biological liquids is of great importance in biology and medicine and fluorescent

probes are successfully applied to this approach. The capability of serum albumins to bind aromatic and heterocyclic compounds is largely dependent on the existence of two major binding regions, namely Sudlow's site I and site II, [36] which are located within specialized cavities in subdomains IIA and IIIA, respectively. These hydrophobic binding pockets enable the serum albumins to increase the apparent solubility of the hydrophobic drugs in plasma and modulate their delivery to the cells in vivo and in vitro. Many drugs, including anticoagulants, tranquilizers, and general anesthetics, are transported in blood while bound to albumin-often more than 90% of the drug is bound [41]. This has stimulated much research on the nature of drug binding sites as well as investigations on whether fatty acids, natural metabolites, and drugs compete with each other for binding to the protein [42]. Various techniques, including fluorimetry, [43] equilibrium dialysis, [44] circular dichroism spectroscopy, [45] UV spectrophotometry, [46] electrochemistry, [47] FTIR, [48] and NMR [49] are usually used for studying molecular interaction of drugs with serum albumin. Among these methods, fluorescence spectroscopy has been particularly useful with the application of site marker fluorescence probes for investigating the nature of the binding sites as well as their specificity and affinity towards particular drugs. Geometrical effects can be successfully quantified using Förster's resonance energy transfer (FRET) theory where the changes in distance between donor and acceptor centers can be monitored [50].

1.5 Cancer (A silent killer)

All cancers originate from normal cells, which are the body's basic units of life. Cancer is a group of diseases that cause cells in the body to change and grow out of control (**Figure 1.12**). Although there are many kinds of cancer, all of them start because of the out-of-control growth of abnormal cells. The body is made up of

hundreds of millions of living cells. Normal body cells grow, divide, and die in an orderly function. In the beginning stage of a person's life, normal cells divide more rapidly to allow the person to grow. After the person becomes an adult, most cells divide only to replace worn-out, damaged, or dying cells and to repair injuries. However, sometimes this orderly process goes wrong. Cancer cell growth is different from normal cell growth because cancer cells continue to grow and divide. Instead of dying, cancer cells keep on growing and form new cancer cells. Being able to grow out of control and invade other tissues is what makes cells cancerous. Cancer harms the body when damaged cells divide uncontrollably to form lumps and these extra cells form masses of tissue called tumors.

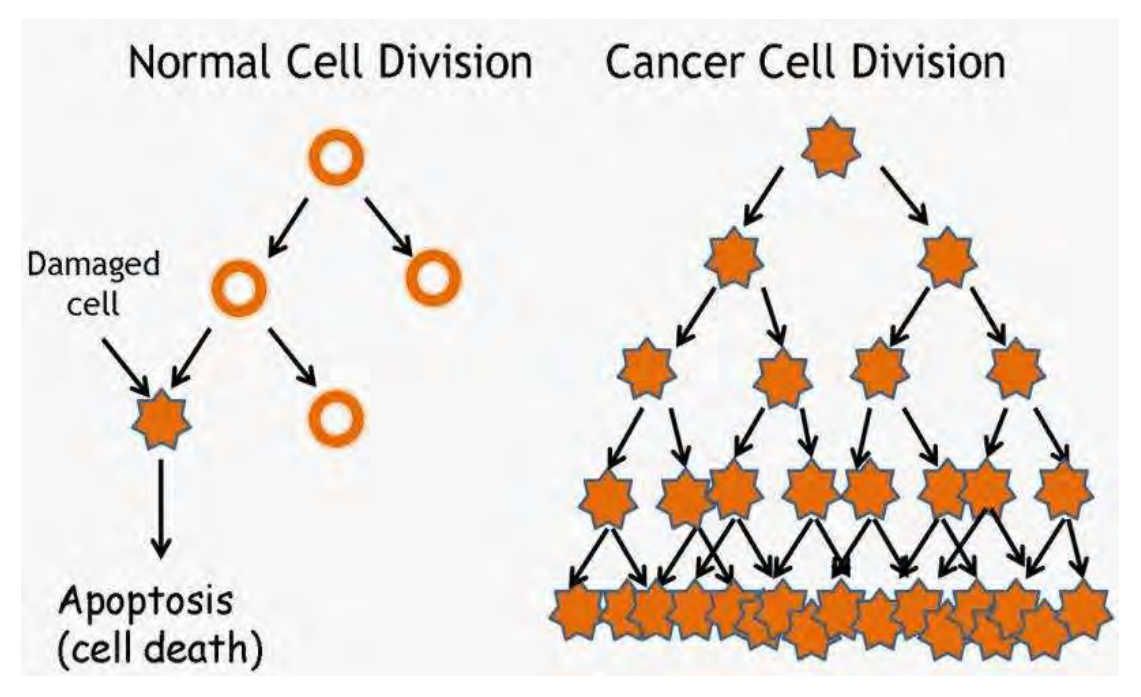


Figure 1.12 Normal and cancer cell division.

Three biological properties that unify or characterize all cancers, *viz.* (namely), (i) they have uncontrolled growth; (ii) the capacity of cancer cells to invade and destroy normal tissue, and (iii) the capacity of the primary tumor to break off seeds

that spread to distant organs throughout the body [51]. Not all tumors are cancerous. There are two types of tumors, which can be benign or malignant. Benign tumors are not cancerous. They usually grow slowly and can be removed; in most cases, they do not come back. The cells in benign tumors are localized and do not spread to other parts of the body or invade and destroy nearby tissue. In contrast, malignant tumors are cancerous. This form of tumor can invade and damage tissues and organs near the tumor. Therefore, the cells in these tumors can spread from one part of the body to another and this process itself is called metastasis. In most cases, the cancer cells form a tumor. But some cancers, such as leukemia, do not form tumors. Instead, these cancer cells are in the blood and bone marrow (American Cancer Society). When cancer cells get into the bloodstream or lymph vessels, they can travel to other parts of the body. When a tumor starts to spread to other parts of the body and begins to grow, invading and destroying other healthy tissues and forming new tumors, it is said to have metastasized [52]. Consequently, this results in a severe conditions that is very difficult to treat.

There are over 200 different types of cancer, and each is classified by the type of cell that is initially affected [53]. Metastatic cells have the same cell type as the original or primary tumor from which they spread. No matter where a cancer may spread, it is always named after the place where it started. According to the American Cancer Society, breast cancer, for example, that has spread to the liver is still called breast cancer, not liver cancer. Different types of cancer can behave very differently. For example, lung cancer and breast cancer are very different diseases. They grow at different rates and respond to different treatments. That is why people with cancer need treatment that is aimed at their kind of cancer (American Cancer Society).

Toumi [53] has reported that cancer causes more deaths than AIDS, tuberculosis, and malaria combined. One in eight deaths worldwide is due to cancer. Based on the GLOBOCAN 2008 estimates, cancer has grabbed the lives of about 7.6 million people in the world which constitutes 2.8 million in economically developed countries and 4.8 million in economically developing countries [54]. Hence, there are about 20,000 cancer deaths a day. Center [54] *et al.* also reported that by 2030, the global burden is expected to grow to 21.4 million new cancer cases and 13.2 million cancer deaths due to the growth and aging of the population, and reductions in childhood mortality and deaths from infectious diseases in developing countries.

1.5.1 Causes of cancer

The unusual cell growth that brings about cancer is the result of DNA damage the substance inside all cells that directs cell behavior. Damaged DNA can be caused
by genetics, by behavior (such as smoking or diet), or by things in the environment
(such as air pollutants, radiation, or occupational exposure to certain chemicals). Usually,
the body can repair damaged DNA, but cancer cells evade this natural process.

1.5.2 Treatment of cancer

The choice on which type of treatment is the most appropriate depends on the type and location of cancer, genetic patterns, and epidemiological factors. The major types of treatment are surgery, radiation, chemotherapy, immunotherapy, hormone therapy, and bone-marrow transplantation. As of now, emerging field combinatorial or target-based chemotherapy is considered the best.

1.5.3 Cancer treatment with chemotherapy

The term 'chemotherapy' refers to the use of drugs to kill or inhibit the growth of cancer cells. Most chemotherapy drugs cause damage to deoxyribonucleic acid (DNA) or prevent chromosomal replication, which leads to programmed cell death (apoptosis). The field has been stimulated by the success of cisplatin, the world's best selling anticancer drug, and platinum complexes with reduced toxicity, oral activity, and activity against resistant tumors are currently in the clinical trial. It is now increasingly accepted that part of the efficacy of anti-cancer drugs is due to their ability to activate apoptosis. Moreover, the resistance of tumor cells to drug-induced apoptosis is promising as the major category of cancer the resistance of treatment failure. Therefore, amongst cancer biologists, there is increasing attention in understanding the regulatory mechanisms of apoptosis. The recent efforts in this field are focused on uncovering the cellular factors that determine the fate of the cell through their ability to control the balance between life and death. Understanding the biological role of these factors will enable the design of more efficient and selective drugs to overcome resistance to apoptosis.

1.5.4 Apoptosis

Apoptosis is a form of programmed cell death (**Figure 1.13**) and it involves a series of biochemical events which leads to a variety of morphological changes, including blebbing, changes to the cell membrane such as loss of membrane asymmetry and attachment, cell shrinking, nuclear fragmentation, chromatin condensation, and chromosomal DNA fragmentation. Kerr, Wyllie, and Currie first created the term apoptosis. The apoptotic process is executed in such a way as to safely dispose of

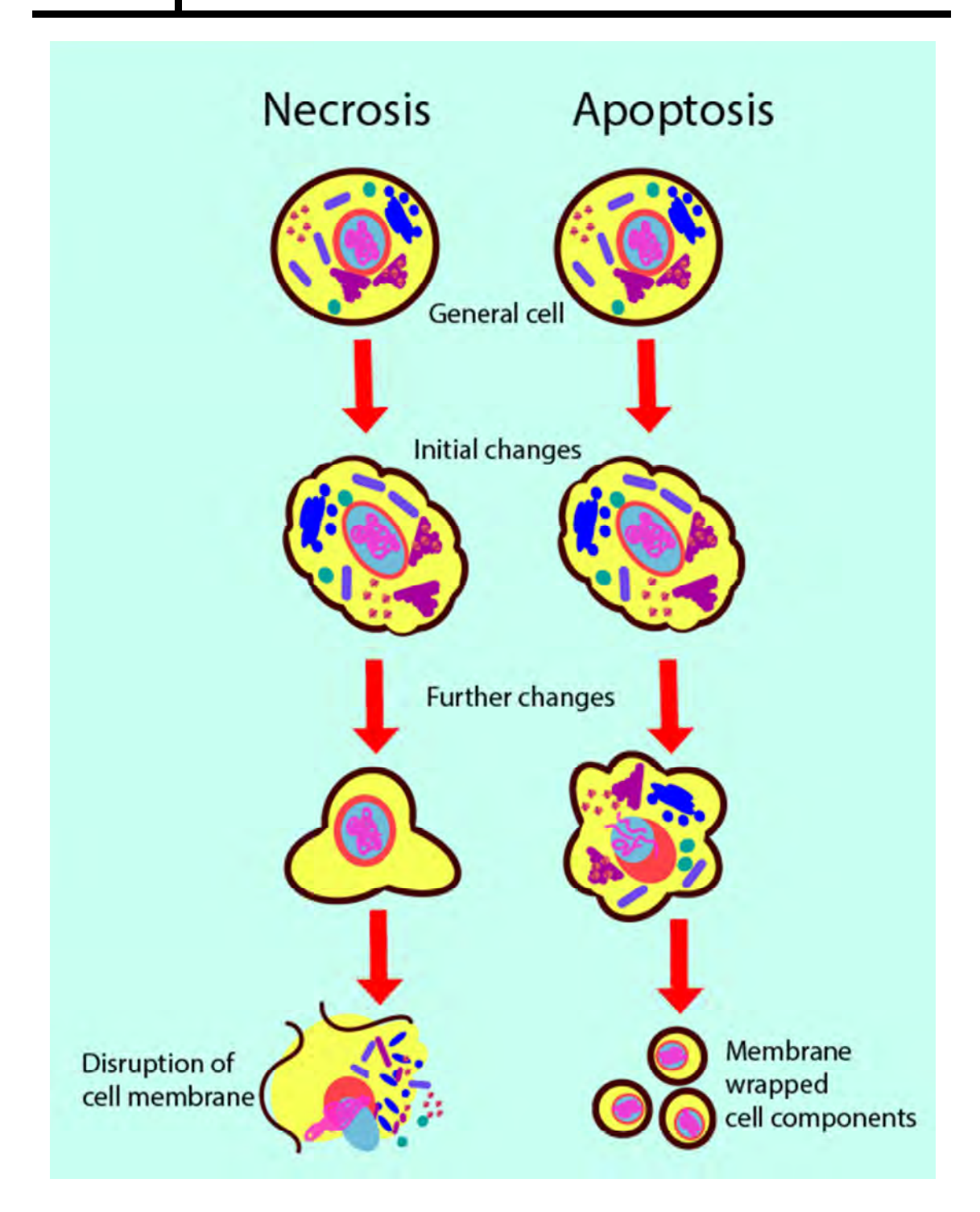


Figure 1.13 Mechanisms of Apoptosis and Necrosis.

cellular debris. In contrast to necrosis, which is a form of traumatic cell death that results from an acute injury, apoptosis is carried out in an orderly process that generally confers advantages during an organism's life cycle.

Apoptosis is triggered through two signaling pathways such as intrinsic pathways and extrinsic pathways. The intrinsic, or mitochondrial, the pathway is initiated from within the cell. This pathway is often activated in response to signals resulting from DNA damage, loss of cell-survival factors, or other types of severe cell stress. Normally, pro-apoptotic proteins are released from the mitochondria to activate caspase proteases and trigger apoptosis. Currently, the intrinsic pathway is more widely implicated as a blockade in tumor genesis. The extrinsic pathway begins outside the cell through the activation of pro-apoptotic receptors on the cell surface. These are activated by molecules known as pro-apoptotic ligands.

1.5.5 Necrosis

Necrosis is the name given to the accidental death of cells (Figure 1.13) and living tissue. Necrosis is less orderly than apoptosis, which is part of programmed cell death. In contrast to apoptosis, cleanup of cell debris by phagocytes of the immune system is generally more difficult, as the disorderly death generally does not send cell signals which tell nearby phagocytes to engulf the dying cell. This lack of signaling makes it harder for the immune system to locate and recycle dead cells, which have died through necrosis than if the cell had undergone apoptosis. The release of intracellular content after the cellular membrane damage is the cause of inflammation in necrosis.

1.6 Metal-based anticancer drugs

The serendipitous discovery of the anticancer activity of cisplatin in the 1960s has opened new horizons for the development of metal-based drugs and the last four decades have seen immense interest in metallopharmaceuticals. The increasing knowledge of molecular structural biology, in particular, information of genomic, proteomic, and other cellular functions has not only helped in the understanding the mechanism of action of existing metal-based drugs but also set the basis for the rational design of new metal-therapeutics.

Cisplatin (**Figure 1.14**) was first synthesized [55] by Michele Peyrone in 1844 and about a hundred years later, its tumor-inhibiting properties were discovered accidentally [56] by Barnett Rosenberg who was investigating the influence of an electric field on the growth of *Escherichia coli* bacteria.



Figure 1.14 Structure of cisplatin.

Today cisplatin is one of the most widely used anticancer drugs with a very impressive cure rate, particularly in testicular and ovarian cancer, and is also used in combination therapy of many other solid tumors, such as bladder, head and neck, and small cell lung cancers [57]. The success of cisplatin in cancer therapy stimulated

scientists to search for novel metal-based antitumor drugs, with improved effectiveness, the broader spectrum of activity, and fewer side effects. Thus thousands of other platinum complexes have been synthesized and biologically evaluated for their antitumor properties, from which about forty entered clinical phase I trials but only two carboplatin and oxaliplatin (Figure 1.15) have received worldwide approval so far. Carboplatin exhibits a tumor-inhibiting profile identical to that of cisplatin, however, with fewer side effects, whereas oxaliplatin is used in combination therapy against metastatic colorectal cancer [58]. In addition, three platinum-based drugs have gained regional approval. These include nedaplatin (Japan), lobaplatin (China), and heptaplatin (South Korea).

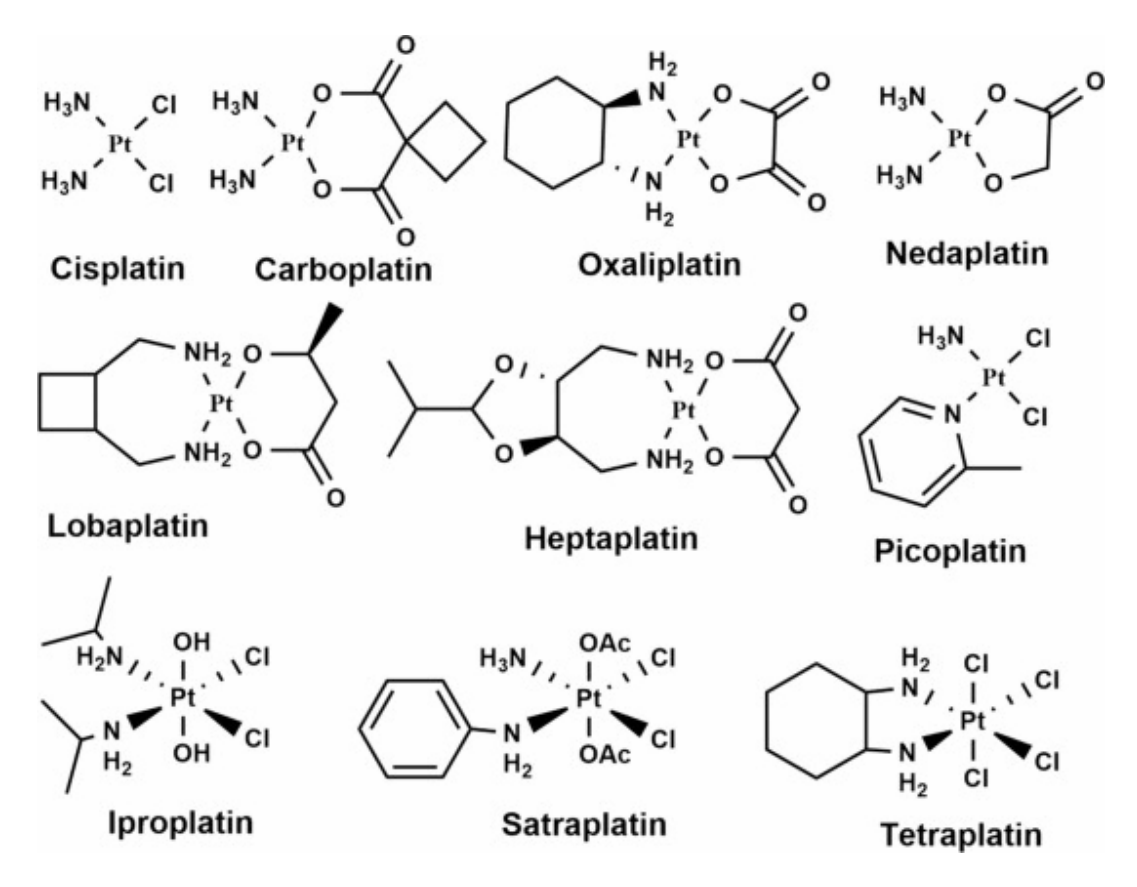


Figure 1.15 Some approved and trial platinum anticancer drugs.

1.6.1 Mode of action of cisplatin and analogous drugs

In the last 40 years, much research has been focused on the understanding of the mechanism by which cisplatin and its analogues induce apoptosis; however, the exact mode of action is still elusive. Cisplatin is administered by intravenous injection or infusion into the bloodstream, [59] where it remains intact due to the presence of relatively high chloride concentration (100 mM), resulting in the suppression of hydrolysis of the drug. It enters the cell by passive diffusion or by active transport mechanisms [60] such as the copper transporter Ctrl [61]. Inside the cell, hydrolysis is promoted due to low chloride concentration (4 mM). Cisplatin undergoes aquation (Figure 1.16) to form mainly monoaqa species *cis*-[Pt(NH₃)₂Cl(H₂O)][†] by exchange of one chloride ligand with a water molecule [62]. This reactive species then binds preferably to nitrogen atoms of the DNA bases, particularly to the N7 of guanine, forming initially monofunctional DNA adducts and later on bifunctional intrastrand cross-links of the type 1,2-d(GpG) and 1,2-d(ApG) [63]. These adducts induce a kink (conformational changes) in the DNA, resulting in the inhibition of DNA replication and transcription which leads towards the programmed cell death in cancerous tissue.

1.6.2 Copper complexes as anticancer agents

Copper(II) complexes are regarded as the most promising alternatives to cisplatin as anticancer substances. Copper(II) is known to play a significant role in biological systems and also as pharmacological agent. Synthetic copper(II) complexes have been reported to act as potential anticancer and cancer-inhibiting agents, [64] and several copper complexes [65] are active both *in vitro* and *in vivo*.

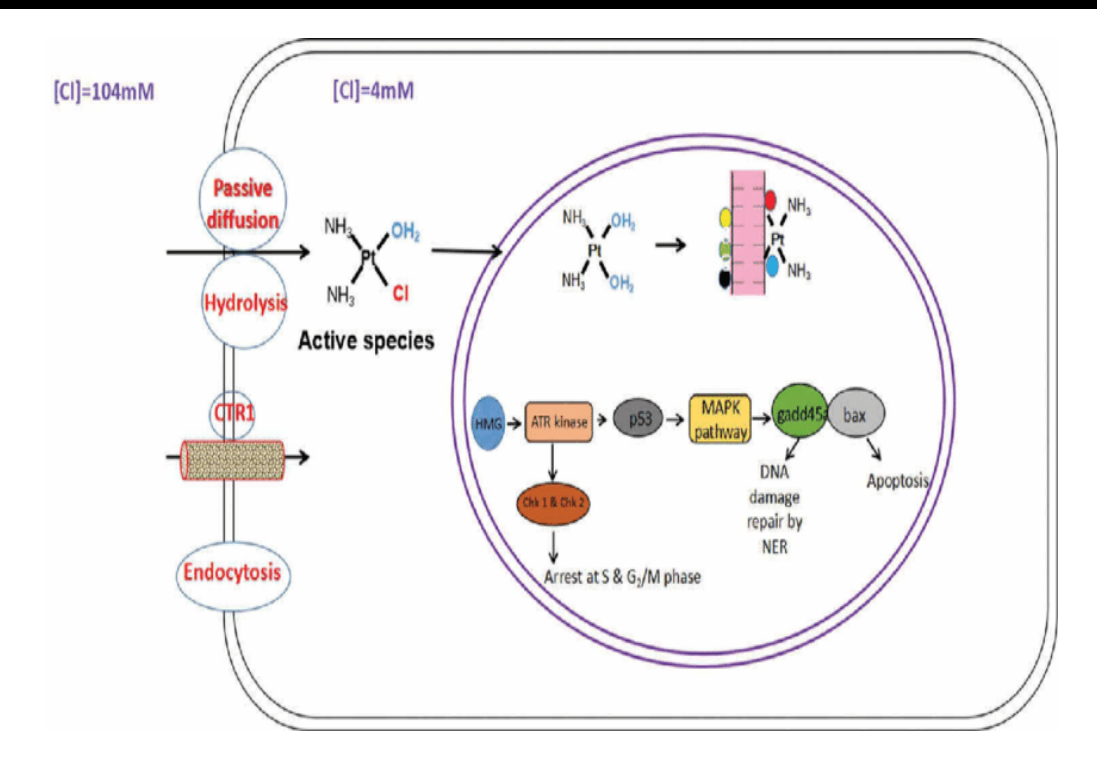


Figure 1.16 Mechanism of cisplatin.

Sigman et al reported the copper(II) complexes of 1,10-phenanthroline ligands, which cleave DNA duplexes, [66] show antiviral activity upon interaction with nucleic acid templates and inhibit proviral DNA synthesis [67]. Sadler and co-workers have isolated mixed ligand bis(salicylato)copper(II) complexes with diimine [68] as coligands to exhibit cytotoxic and antiviral activities. Guo and co-workers have synthesized the ternary Cu(II) complex of 1,10-phenanthroline and L-threonine, [69] which hydrolytically cleave DNA and exhibit cytotoxicity. Recently, there has been substantial interest in the design and study of DNA binding [70] and cleavage properties of mixed-ligand Cu(II) complexes [71] and the development of the complexes as metallo-drugs. The *in vitro* antitumor effect of [Cu(phendione)₃]²⁺ on human epithelial cell lines has been studied [72]. Reedijk and co-workers have reported that the complexes [Cu^{II}(pyrimol)CI] [73] and [Cu(pbt)Br₂], [74] where H(pyrimol) is

4-methyl-2-[(pyrid-2-ylmethyl)amino]phenol and pbt is 2-(2-pyridyl)benzthiazole, show efficient self-activated DNA cleavage and cytotoxic effects on L1210 murine leukemia and A2780 human ovarian carcinoma cell lines. Ng and co-workers have prepared ternary copper(II) complexes of ethylenediaminediacetic acid (H₂edda) and 1,10-phenanthroline, [75] which strongly bind to DNA and also regulate apoptosis.

Neves and co-workers have synthesized cis-aqua/hydroxyl copper(II) complexes containing tridentate ligands [76] that are capable of promoting phosphate diester hydrolysis and DNA damage. The complex [Cu(phen)(N-propylnorfloxacin) Cl] [77] exhibits antileukemic activity, indicating that the synergy between the metal and ligand results in enhancement of their antiproliferative properties. Yan and co-workers prepared copper(II) complexes with planar heterocyclic bases, [Cu(acac)(dpq)Cl] and [Cu(acac)(dppz)Cl] [78] (acac is acetylactonate, dpq is dipyrido[3,2-d:2',3'-f]quinoxaline, dppz is dipyrido[3,2-a:2',3'-c]phenazine). They show more efficient photo-induced DNA cleavage activity and induce apoptosis process against the HeLa cell line.

Cini and co-workers prepared the copper(II) complex, [Cu(HPIR)₂(H₂O)₂], [79] where H₂PIR is Pyroxicam (4-hydroxy-2-methyl-N-pyridin-2-yl-2H-1,2 benzothiazine-3-carboxamide-1,1-dioxide) and performed the release studies from smart hydrogels as carriers for pyroxicam and copper(II)-oxicam complex as an anticancer drug. The amount of Cu(HPIR)₂ released compares well with the IC₅₀ values reported for metal-based drugs like carboplatin against certain human tumor cell lines [80]. Zhang and co-workers synthesized copper(II) complex containing N,N'-dibenzylethane-1,2-diamine [81]. Interaction between the complex and DNA/HSA has been studied that copper(II) complex could bind to DNA and remarkably quench the emission intensity

of the DNA-EB system. The copper(II) complex was a strong quencher of HSA. The interaction was mainly hydrophobic interaction, which coincided with the thermodynamic analysis.

Alzuet and co-workers isolated the complex $[Cu(N9-ABS)(phen)_2]$, [82] where $H_2N9-ABS = N-(9H-purin-6-yl)$ benzenesulfonamide and phen = 1,10-phenanthroline. The interaction of the complex by DNA was classic intercalation and a very efficient cleavage agent of plasmid DNA in the presence of ascorbate. The cytotoxic compound demonstrated a significant ability to induce cell death by apoptosis. Barba-Behrens and co-workers synthesized compounds of copper(II) with 2-methyl-benzimidazole (2mbz), 2-phenylbenzimidazole (2phbz), 2-chlorobenz-imidazole (2cbz), 2-benzimidazolecarbomate (2cmbz) and 2-guanidinobenzimidazole (2gbz) [83]. The copper(II) compounds $[Cu(2cmbz)Br_2]$ and $[Cu(2gbz)Br_2]$ had significant cytotoxic activity against PC3, MCF-7, HCT-15, HeLa, SKLU-1 and U373 human cancer cell lines.

Ferreira and co-workers prepared and verified the cytotoxicity of some oxindole-Schiff base copper(II) complexes toward tumor cells [84]. These complexes can transport copper through the cell membrane, trigger oxidative stress inside the cell and induce apoptosis, targeting mainly the organelles mitochondria and nuclei, in a process modulated by the imine ligand [85]. Oxidative damage to the protein [86] after incubation with these copper(II) complexes in the presence of hydrogen peroxide, was monitored by carbonyl groups formation and was observed to be more severe when conformational features of the protein were modified. They also described apoptosis induction and DNA cleavage studies with some novel imine-copper(II) complexes [87] showing potential antitumor activity, to verify specifically damage to DNA.

Palaniandavar and co-workers [88] synthesized mixed ligand copper(II) complexes exhibit higher cytotoxicity and induce cell death through both apoptosis and necrosis due to more effective ROS generation in cancer cells. They also reported a series of water-soluble copper(II) complexes of the types [Cu(L)Cl] (LH, 2-(2-(1Hbenzimidazol-2-yl)ethyliminomethyl)phenol) or 2-(2-(1H-benzimidazol-2-yl)ethyliminomethyl)-4-methylphenol), and [Cu(L)Cl₂] (L, (2-pyridin-2-yl-ethyl)pyridin-2-ylmethyleneamine or 2-(1H-benzimidazol-2-yl) ethylpyridin -2-yl-methyl eneamine or 2-(1H-benzimidazol-2-yl)ethyl(1Himidazol-2-ylmethylene) amine or and 2-(1Hbenz-imidazol-2-yl)ethyl-(4,4a-dihydroquinolin-2-ylmethylene) amine) bind through covalent mode of DNA interaction. They display remarkable cytotoxicity against the HBL-100 human breast cancer cell line with potency more than that of the widely used drug cisplatin [89]. Palaniandavar and co-workers [90] prepared mixed ligand copper(II) complexes of the types [Cu(L)(phen)](ClO₄) (HL, 2-(2-(1*H*-benzimidazol-2-yl)ethyliminomethyl)phenol or 2-(2-(1*H*-benzimidazol-2-yl)ethylimino)methyl)-4-methylphenol) and [Cu(L)(phen)]-(ClO₄)₂ (L, (2-pyridin-2-ylethyl)pyridin-2ylmethyleneamine or 2-(1H-benzimidazol-2-yl)ethyl)-pyridin-2-ylmethyleneamine or 2-(1*H*-benzimidazol-2-yl)ethyl)(1*H*-imidazol-2-yl-methylene) amine 2-(1*H*benzimidazol-2-yl)ethyl)(4,4a-dihydroquinolin-2-yl-meth-ylene) amine) covalently to CT DNA, exhibit double strand cleavage of supercoiled (SC) plasmid DNA in the absence of an activator and exhibit cytotoxicity against human breast cancer cell lines (HBL-100). They have prepared mononuclear mixed ligand copper(II) complexes of the type [Cu(L)(2,9-dmp)](ClO₄)₂ (L, diethylenetriamine or

N-methyl-*N*'-(pyrid-2-ylmethyl)ethylenediamine or di(2-picolyl)amine or bis(pyrid-2-ylmethyl)-*N*-methylamine), which cleave pUC19 supercoiled DNA in the absence of an activating agent [91]. They show stronger binding with bovine serum albumin (BSA) in the hydrophobic region. The IC₅₀ values for the MCF-7 breast cancer cell line are lower than that of cisplatin. Flow cytometry analysis reveals the higher potency of the complexes to induce apoptosis.

Nair and co-workers [92] reported mononuclear complexes [Cu(Itpy) X(H₂O)]X (Itpy, imidazole terpyridine, X, NO₃, or ClO₄) show the dual mode of binding to DNA and display potent cytotoxicity towards lung carcinoma cell line with an induction of apoptosis. Chao et al [93] synthesized three novel copper(II) complexes $Cu(L^1/L^2/L^3)Cl2$ (L^1 , 4'-(3-methoxyphenyl)-2,2':6'-2"-terpyridine, L_2 , 4'-(4-methoxyphenyl)-2,2':6'-2"-ter-pyridine and L³, 4'-(3,5-dimethoxyphenyl)-2,2':6'-2"-terpyridine). These complexes bind to DNA through an intercalative mode, efficiently cleave pBR322 DNA, and exhibit good anticancer activity against HeLa, Hep-G2, and BEL-7402 cell lines. Ebahimipour et al [94] made a tridentate ONO ligand (E)-N'-((2hydroxynaphthalen-1-yl)-methylene) acetohydrazide and its cationic Cu(II) complex [Cu(L)(H₂O)]NO₃. It was found that [Cu(L)(H₂O)]NO₃ complex showed higher anticancer activity against the MCF-7 cell line. Mahani and co-workers [95] reported two water-soluble copper(II) complexes of the type [Cu(phen-dion)(diimine)Cl]Cl, (phen-dione, 1,10-phenanthroline-5,6-dione). The complexes interact with FS-DNA by electrostatic and partial insertion of pyridyl rings. The quenching mechanism, thermodynamic parameters, the number of binding sites and the effect of the Cu(II) complexes on the secondary structure of BSA have been explored. (MCF-7, A-549, and HT-29) and one normal cell line (DPSC) was evaluated by MTT assay. They

have greater cytotoxicity activity against MCF-7, A-549, and HT-29 cell lines. Hussian et al [96] reported six novel copper(II) complexes of the formula [Cu(R-tpy)(N-O)]NO₃ (R-tpy, 4'-phenyl-2,2':6',2''-terpyridine or 4'-ferrocenyl-2,2':6',2''-terpyridine, N-O is the anion of 8-hydroxyquinoline or 5-chloro-7-iodo-8-hydroxyquinoline or 5-nitro-8-hydroxyquinoline). The DCFDA, annexin-V-FITC, and propidium iodide nuclear staining assays reveal an apoptotic mechanism of cell death which is attributable to the metal-assisted generation of reactive oxygen species. Deng et al [97] prepared three Cu(II) complexes of acetylpyridine benzoyl hydrazone (HL), [Cu(L)(NO₃) (H₂O)]·H₂O, [Cu(L)₂] and [Cu(L)(HL)]·(NO₃)(Sas) (Sas, salicylic acid). All Cu(II) complexes showed significant anticancer activity and promotes A549 cell apoptosis possibly through the intrinsic reactive oxygen species (ROS) mediated mitochondrial pathway, accompanied by the regulation of Bcl-2 family proteins.

Annaraj and co-workers [98] reported new mixed ligand copper(II) complexes of the type [Cu(L)(diimine)](ClO₄) (L is 2-((1H-imidazol-2-yl)methylene)-N-phenylhydrazine carbothio-amide). They efficiently induce a single strand breakage of pUC18 plasmid DNA and underwent a static mode of quenching process with BSA protein. They are promising antitumor agents *in vitro* against AGS cancer cells. Chiniforoshan et al [99] reported three novel copper(II), complexes of juglone (Jug) containing 1,10-phenanthroline ligand, [M(Jug)₂(phen)]. The complex interacted with CT-DNA via the intercalation mode and act as a better catalyst in the DNA cleavage process. They display promising antitumor activity with quite low IC₅₀ values in the range of 0.09-1.2μM against HeLa, HepG-2, and HT-29 cells, which are 75 times lower than those of cisplatin. Jadeja et al [100] reported four Cu(II) mixed ligand complexes [Cu(L)(bpy/phen)NO₃] and[Cu(L)(bpy/phen)NO₃] [L, 3-methyl-5-oxo-1-phenyl-4,5-

di-hydro-1H-pyrazole-4-carbaldehyde; or 4-(1-naphthoyl)-3-methyl-1-(p-tolyl)-1H-pyrazol-5 (4H)-one]. The inhibitory effects of the complexes on the cell population growth of the A549 and L132 cell lines were determined by MTT assay, DAPI staining, and DCFDA staining, which assessed mitochondrial dysfunction, nuclear condensation, and intracellular oxidative stress, respectively. The expression levels of Bax (pro-apoptotic) and BCl2 (anti-apoptotic) genes were also studied in A549 cells wherein, both genes showed moderate down regulation after treatment with all the test complexes. Schindler and co-workers [101] prepared a series of copper(II) complexes with tripodal polypyridylamine ligands derived from the parent ligand tris(2-pyridylmethyl)amine. Some compounds showed similar activity against cervical, colon, ovarian cancers and melanoma cell lines compared to that of cisplatin.

Wang et al [102] synthesized three Cu(II) piperidylthiosemicarbazone complexes and examined their structures. These Cu(II) complexes have significant apoptosis-promoting activity at nanomolar concentrations. Apoptosis mechanism results showed that excessive ROS leads to mitochondrial membrane potential dissipation and promotes the release of apoptotic factors from mitochondria. Le and co-workers [103] made a copper complex, [Cu(HPBM)(L-Phe)-(H₂O)](ClO₄) (HPBM, 5-methyl-2-(2'-pyridyl)benz-imidazole, L-Phe, L-phenylalanine anion) and interacts with CT DNA through minor groove binding. The results of in vitro cytotoxicity, double staining analysis, and comet assay demonstrate that the complex induces apoptosis in Eca-109 cells through DNA-binding and ROS-mediated mitochondrial dysfunctional pathways. Liang et al [104] have developed potential next-generation metal anticancer agents. They have designed and synthesized five Cu(II) 2-pyridine-thiosemicarbazone complexes.

the production of reactive oxygen species to regulate expression of the B-cell lymphoma-2 family of proteins, causing a change in the mitochondrial membrane potential and release of cytochrome c to form a dimer with apoptosis protease activating factor-1, resulting in activation of caspase-9/3 to induce apoptosis. Trávníček et al [105] reported the Cu(II) complexes, [Cu(bpdmpz)Cl]ClO₄, [Cu(bdmpzp)Cl]ClO₄, [Cu(bdmpzp)Cl]PF₆ and [Cu(tdmpza)Cl]ClO₄ (bpdmpzp, [bis[((2-pyridylmethyl)-di(3,5-dimethyl-1H-pyrazolyl)-methyl)]amine, bdmpzp, [bis ((di(3,5-dimethyl-1H-pyrazolyl)-methyl)]- amine and tdmpza, tris[di(3,5-dimethyl-1H-pyrazolyl)-methyl)]amine). One of the complexes was the most cytotoxic one, with IC₅₀ values 1.4 μ M (A2780), 8.3 μ M (A2780R), 4.7 μ M (HOS), and 10.8 μ M (CaCO₂).

Zhang and co-workers [106] synthesized Cu(II) complexes with Schiff bases derived from diethylenetriamine, [Cu(C₂₂H₂₃N₅)(H₂O)(ClO₄)₂] and [Cu(C₁₄H₁₈N₄) (ClO₄)]-(ClO₄). Both the complexes bind to DNA via groove binding mode and are capable of cleave pBR322 DNA efficiently in the presence of ascorbic acid as a reducing reagent. In vitro cytotoxicities were screened against HepG2, MGC-803, EC9706, and MCF-7 cell lines) and the different anticancer activities of the complexes may be correlated with their DNA binding abilities. Pande et al [107] reported that the CT DNA binding interaction of Bis(N-p-naphthylbenzo-hydroxamato) copper(II), was a groove binding. The in vitro cytotoxicity study was carried out against the MCF-7 breast cancer cell line. Kumar and co-workers [108] synthesized a novel copper(II) complex, [{Cu(hpdbal-sbdt)}₂] tethered with a biocompatible ONS²⁻ donor backbone (H₂hpdbal-sbdt is a tridentate ligand derived from S-benzyldithiocarbazate (Hsbdt) and 2-hydroxy-5-(phenyldiazenyl)benzaldehyde (Hhpdbal)). It exhibits significant

growth inhibition of HeLa cells with an IC₅₀ value of 4.46 µM. The interactive behavior of the bioactive copper complex with a drug transporter protein (BSA) was deciphered through multi-spectroscopic investigations. Arjmand et al [109] reported the chiral enantiomeric amino acid Schiff base copper(II) complexes were synthesized and characterized. They interact strongly via the intercalative mode with preferential binding toward the t-RNA biomolecule compared to CT DNA. The cleavage activities toward the pBR322 plasmid DNA mediated by reactive oxygen species radical scavengers involving singlet oxygen (${}^{1}O_{2}$) and superoxide anions ($O_{2}^{\bullet-}$). One of the complexes showed the highest cytotoxicity, being selectively targeted toward the MCF-7 cancer cell line with a GI₅₀ value of <1 µM. Kumar and co-workers [110] reported the synthesis, characterization, spectroscopic properties, redox behavior, and biological activities of the Cu(II) complex [Cu(pabt)(phen)](ClO₄), (Hpabt, N-(2mercaptophenyl)-2'-pyridylmethylenimine). It shows strong intercalative DNA binding and exhibits strong cytotoxicity against A549 (5.26 µM) and A431 (5.41 µM) carcinoma cell lines. The compound is found to be less toxic for the L132 normal cell line. Xie et al [111] prepared three novel copper(II) complexes, $Cu(L)_2$, $Cu(L)_2 \cdot 2DMF$, and Cu(L)₂·2DMF using three arylhydrazone ligands, (E)-2-hydroxy-N'-(1-(pyrazin-2-yl)ethylidene)benzohydrazide or (E)-3-hydroxy-N'-(1-(pyrazin-2-yl)ethylidene) benzohydrazide or (E)-4-hydroxy-N'-(1-(pyrazin-2-yl)ethylidene)benzohydrazide. Complexes bind readily to CT DNA through intercalative and minor groove binding modes. Complexes exhibited oxidative cleavage of supercoiled plasmid DNA (pUC19) in the presence of ascorbic acid as an activator. Cytotoxicity studies showed that complexes possessed high cytotoxicities toward the HeLa cancer cell line, but weak toxicities toward the L929 normal cell line.

Valko and co-workers [112] made up novel mixed copper(II) complexes with NSAIDs: tolfenamic (tolf), mefenamic (mef) and flufenamic (fluf) acids and phenanthroline (phen): [Cu(tolf-O,O')₂(phen)], [Cu(mef-O,O')₂(phen)] and [Cu(fluf- $O,O')_2(phen)$]. The ability of the complexes to cleave DNA in the absence of an external agent and the reactive oxygen species (ROS) scavengers confirmed that singlet oxygen, hydroxyl radicals (Fenton reaction), and superoxide radicals were formed. The fluorescence spectroscopy revealed that albumin may act as a targeted drug delivery vehicle for Cu(II) complexes $(K\sim10^6)$. The anticancer activities of complexes were investigated against HT-29, HeLa, and T-47D cancer cells, and MSC normal cells. Manna et al [113] reported two Schiff bases, having potential tridentate O,N,N' donor sets, have been used for the synthesis of two copper(II) complexes, namely $[Cu(HL)(pdc)]_2$ and $[Cu(L')_2]_2$, (HL, 2-([2-(piperazin-yl)ethylimino]methyl)phenol, pdc, py-2,5-dicarboxylate; HL', 2-(((2-(di-isopropylamino)ethyl)imino)methyl) phenol). The interaction of complexes with CT DNA and BSA shows a higher binding affinity. The anticancer activity of the complexes against the MCF-7 cancer cell line reveals that the complex has moderate growth suppression with an IC₅₀ value of 24 \pm $6.24 \mu M.$

Richardson et al [114] synthesized and characterized a series of eight bis(thiosemicarbazone) ligands and 16 of their respective copper(II) complexes containing a combination of hydrogen, methyl, pyridyl, phenyl, and/or ethyl substituents at the diimine position of the ligand backbone. However, five of the eight bis(thiosemicarbazone) Cu(II) complexes maintained or increased their antiproliferative activity, relative to the ligand alone, and a mechanism of Cu-induced oxidative stress

is suggested. These results provide structure-activity relationships useful for the rational design of bis(thiosemicarbazone) anticancer agents. Montagner and coworkers [115] reported four estrogen-functionalized copper complexes as electrochemical active DNA binding and cleavage agents. Cytotoxic activity was studied over a panel of estrogen-receptor-positive (ER+) and negative (ER-) human cancer cell lines employing both 2D and 3D cell viability studies. The complexes showed high in vitro intercalative interaction with nuclear DNA and demonstrated to be strong DNA cleaving agents. This series of Cu compounds are potent anticancer agents with low and sub-micromolar IC₅₀ values. The estrogen complexes are involved in the cellular redox stress by stimulating the production of ROS. Le et al [116] studied the anticancer and antimetastatic activity of a copper(II) with tropolone (trp), complex [Cu(trp)₂] toward human breast cancer cells in monolayer (2D). Cytotoxicity assays against MCF7 (IC₅₀(complex) = $5.2 \pm 1.8 \mu M$, IC₅₀(CDDP) = $19.3 \pm 2.1 \mu M$) and MDA-MB-231(IC₅₀(complex) = $4.0 \pm 0.2 \mu M$, IC₅₀(CDDP) = $27.0 \pm 1.9 \mu M$) demonstrate that [Cu(trp)₂] exert greater antitumor potency than cisplatin (CDDP) on 2D and 3D human breast cancer cell models. Besides, [Cu(trp)₂] inhibits cell migration by reducing the metalloproteinases activities and the compound undergoes the breast cancer cells to apoptosis at lower concentrations (2.5-10 µM).

Rigamonti and co-workers [117] reported copper(II) complexes of general formula [Cu(^GL)(Cl)] (G is OMe, H and NO₂), bearing tridentate Schiff base ligands (^GL⁻) and chloride as a fourth labile one. In vitro tests on cell viability were conducted on malignant cell lines typical for their poor prognosis and curability, revealing time-dependent and differential cytotoxicity given by the substituent G. All

compounds were capable of formation of intracellular reactive oxygen species and DNA intercalation, acting as nuclease and producing double-strand DNA breaks Alzuet et al [118] have synthesized and characterized seven novel copper(II) complexes, namely [Cu(Am4DHotaz)(H₂O)₂](ClO₄), [Cu(Am4DHotaz)(NO₃) (MeOH)]·H₂O, [Cu(Am4-Motaz)₂(H₂O)](ClO₄)₂·0.83H₂O, [Cu(Am4Motaz)₂ (NO₃)]NO₃·MeOH, [Cu(Am4Eotaz)₂- (NO₃)]₃(NO₃)₃·2H₂O, [Cu(Am4Eotaz)₂(ClO₄)](ClO₄) and [Cu(Am4Eotaz) (ClO₄)-(H₂O)](ClO₄) (HAm4DHotaz, N'-(4-oxothiazolidin-2-ylidene)-pyridine-2-carbohydrazonamide; Am4Motaz, N'-(3-methyl-4-oxothiazolidin-2-ylidene)-pyridine-2-carbohydrazonamide; Am4Eotaz, N'-(3-ethyl-4-oxothiazolidin-2-ylidene)-pyridine-2-carbohydrazonamide)). The ability of complexes to cleave supercoiled pUC18 DNA was assayed with the aid of gel electrophoresis. The complex, [Cu(Am4Motaz)₂(H₂O)](ClO₄)₂·0.83H₂O has been shown to behave as a nuclease, its interaction with DNA was studied using thermal denaturation and viscosimetry measurements.

Masram et al [119] synthesized and characterized two new copper(II) complexes with their excellent binding and cleavage affinity towards DNA and proteins with the general formula [Cu(ENox)bpyCl] and [Cu(phen)₂Cl] (HENox, Enoxacin; bpy, 2,2'-bipyridine; phen, 1,10-phenanthroline). Biological studies revealed that both complexes interact with CT DNA *via* intercalative mode. The interaction of the complexes with proteins (BSA/HSA) indicated that complexes have quenched the intrinsic fluorescence of proteins in a *static quenching* mode. The ability of complexes to cleave the supercoiled plasmid DNA (pBR322) and proteins in the presence of activator-like H₂O₂ as revealed from gel electrophoresis and SDS-PAGE experiments. The *in vitro* cytotoxicity of the complexes was evaluated against MCF-7 cells and the results suggested that both complexes exhibit superior anticancer

activity. Potkin et al [120] reported four new water-soluble copper(II) complexes $[Cu(dmbipy)L_2]$, $[Cu(phen)(H_2O)L_2]$, $[Cu(dmphen)L_2]$ and $[Cu_2(bipy)_2L_4]$ (HL, 4,5dichloro-isothiazole-3-carboxylic acid). They exhibit a significant dose-dependent cytotoxic effect against Hep-2 and MCF-7 cell lines and [Cu(dmphen)L₂] is found to be the most cytotoxic (IC₅₀ = $0.97 \pm 0.03 \mu M$). All complexes exhibit moderate binding affinity toward CT DNA. The effect of [Cu(dmbipy)L₂] and [Cu(dmphen)L₂] on the activity of drug-metabolizing enzymes cytochromes P450 has also been investigated. The addition of complexes to the hepatic microsomes of 3-MC or PBtreated rat, leads to a dose-dependent decrease of CYP's activities. The data obtained indicate that [Cu(dmphen)L₂] and [Cu(phen)(H₂O)L₂] can be potential anticancer agents. Ari et al [121] reported mixed ligand complexes of Cu(II) using quercetin and diimine ligands. Anti-cancer effects of these compounds were tested against A549, PC-3, HeLa, and MCF-7 cancer cells. Apoptosis was identified by fluorescence imaging, caspase cleaved cytokeratin-18, and flow cytometry analysis. Kargar et al [122] prepared a novel series of Cu(II) complexes including: $[Cu(L^1)_2]$, $[Cu(L^2)_2]$, $[Cu(L^3)_2]$, $[Cu(L^4)_2]$ with four halogenated bis-N,O-bidentate Schiff base ligands (HL¹, 2-ethoxy-6-[(4-fluoro-phenyl)iminomethyl]phenol; HL², 2-ethoxy-6-[(4-chlorophenylimino) methyllphenol; HL³, 2-ethoxy-6-[(4-bromophenyl)iminomethyll phenol; HL⁴, 2-ethoxy-6-[(4-iodophenyl-imino)methyl]phenol). The binding ability of the Schiff base ligands and their metal complexes with FS-DNA was studied by spectroscopic methods. The results showed that the ligands bound in minor grooves of DNA. Adolfo and co-workers [123] synthesized three water soluble copper(II) coordination compounds containing the ligands 3,3'-(ethane-1,2-diylbis(azanediyl))dipropanamide (BCEN), 3,3'-(piperazine-1,4-diyl)dipropanamide (BPAP) or 3,3'-(1,4-diazepane-1,4-

diyl)dipropanamide (BPAH). They were screened cytotoxicity against THP-1, U937, Molt-4, Colo-205, and NCIH460 tumor cell lines. The complex containing the homopiperazine unit presented the best antiproliferative effect and selectivity against lung cancer cell line NCI-H460, showing inhibitory concentration (IC₅₀) of 58 μmol dm⁻³ and Selectivity Index (SI) >3.4. The mechanism of cell death promoted by the complex was investigated by Sub-G1 cell population analysis and annexin V and propidium iodide (PI) labeling techniques, suggesting that the complex promotes death by apoptosis.

Murali et al [124] reported a water soluble mononuclear copper(II) complex [Cu(dipica)-(CH₃COO)]ClO₄ (dipica is di-(2-picolyl)amine). Absorption, circular dichroic and emission spectral measurements, and electrochemical measurements demonstrate groove binding of the complex to CT DNA. It exhibits more effective pUC 19 DNA cleavage at acidic pH. It shows significant cytotoxicity (IC₅₀, 55 μM) against the HeLa cell line at 48 h incubation time and is non-toxic to healthy cells. A copper(II) complex [Cu^{II}(quamol)Cl]·H₂O, where H(quamol) is N-2-(quinolylmethylidene) aminophenol, has been isolated by the same group [125]. The complex interacts strongly with DNA through partial intercalation. The electrochemical studies indicate that Cu(II) binds to DNA more strongly than Cu(I). It cleaves \$\phi X174\text{supercoiled}\$ phage DNA in the presence of ascorbic acid as a reducing agent. Meanwhile, the interaction of the complex with BSA indicates that the complex can markedly quench the intrinsic fluorescence of BSA via a static quenching process. The observed IC₅₀ values for the cell lines EVSA-T and M19 MEL are in the range of those observed with cisplatin while the M19 MEL cancer cell line, the complex is more active than 5-fluorouracil. The complex is non-toxic to healthy cells. They have also reported [126]

the mixed ligand copper(II) complexes [Cu(terpy)(mq)]ClO₄ and [Cu(phen)(mq)] ClO₄, (terpy, 2,2':6',2''-terpyridine; phen, 1,10-phenanthroline; H(mq), 2-methyl-8-hydroxyquinoline). The complexes interacted with calf thymus (CT) DNA was found to be groove binding. Interestingly, phen complex cleaves supercoiled \$\phi\x174\ DNA without reductant while terpy complex cleaves with the reductant. The DNA and protein binding affinity and DNA cleavage activity are higher. The cytotoxicity studies on MCF7 and SiHa cell lines show that the IC₅₀ values are lower than cisplatin and illustrate lower cytotoxicity against Jurkat T4 normal cell line. AO/EB and Hoechst 33258 staining assays reveal the higher induction of apoptosis. The alkaline single-cell electrophoresis (comet assay) indicates that the complexes induce DNA fragmentation, which is additional proof of apoptosis.

1.7 Scope of the present investigation

There is a great interest in understanding the factors that control the binding of metal ions to nucleic acids. This has been fuelled to a great extent by the success of several platinum complexes that exert anticancer activity by forming covalent adducts with the purine bases of DNA. In addition, metal complexes that can bind to DNA via non-covalent interaction, groove binding, and electrostatic binding have also attracted interest as antitumor agents.

We can start understanding the chemical principles underlying site-specific DNA recognition in biological systems if we determine how all the ligand and metal ion factors contribute to DNA binding affinity. Such studies on metal ion interactions with nucleic acids indeed have provided the basis for the successful application of cisplatin and related compounds as anticancer drugs. However, Pt-based anticancer drugs

possess inherent limitations such as high toxicity and low administration dosage [127]. Many copper(II) complexes [128,129] have received considerable attention during the past few decades in an attempt to replace cisplatin. Since DNA is considered as a main molecular target in the functioning of anticancer agents, and the design of efficient DNA binding and cleaving metal complexes is of immense interest in the field of metal-based drugs.

Serum albumin functions as a carrier of a large number of endogenous and exogenous compounds including fatty acids, amino acids, drugs, and pharmaceuticals. 111 The drug-serum albumin interaction plays a dominant role in drug disposition and efficacy. The study of the interaction between drugs and serum albumin is not only important in providing salient information about the nature of drugs and pharmacokinetics but also helpful in explaining the relationship between the structures and functions of drugs. So our interest in the present investigation is to synthesize copper(II) complexes with well-defined structures, to study how do they bind and cleave DNA using a variety of approaches, and to examine the interaction of these complexes with the protein bovine serum albumin. Attempts will be made to address metal complexes as sensitive chemical probes for DNA and explore them as cytotoxic agents. Other than DNA intercalation, additional interactions like hydrogen bonding, groove binding, electrostatic and hydrophobic interactions play an important role in determining biological activity. The coordination complexes isolated permit the variation in geometry, size, hydrophobicity, and hydrogen bonding ability by a systematic variation of ligands.

A great deal of the work contained in the present thesis involves the synthesis of copper(II) complexes of bi- and tridentate ligands as primary ligands like (**Scheme 1.1**)

5,6-diphenyl-3-(2-pyridyl)-1,2,4-triazine (dppt), N,N-bis(benzimidazol-2-ylmethyl) amine (bba), (6-methylpyridin-2-ylmethylene)-(pyridin-2-ylmethyl) amine (L1) and (6-methyl-pyridin-2-ylmethylene)-(pyridin-2-ylethyl) amine (L2).

Scheme 1.1 Structure of primary ligands.

An 'affinity' diimine ligands such as 2,2'-bipyridine (bpy), 1,10-phenanthroline phen) and 2,2'-dipyridylamine (dpa) have been selected as co-ligands (**Scheme 1.2**). All the complexes have been interacted with calf thymus (CT) DNA and BSA. The DNA cleavage studies were made by using plasmid pUC19 DNA (agarose gel electrophoresis). The cytotoxicity studies have also been carried out for human cervical carcinoma cell line using different biochemical methods.

Scheme 1.2 Structure of co-ligands.

To address the above issues and to illustrate DNA and protein binding affinities, DNA cleavage ability and prominent cytotoxic activity in killing the cancer cells, we plan to isolate the copper(II) complexes of the type [Cu(bba) (bpy/phen/dpa))](ClO₄)₂ (1-3), where bba is N,N-bis(benzimidazol-2-ylmethyl)-amine, bpy is 2,2'-bipyridine, phen is 1,10-phenanthroline and dpa is 2,2'-dipyridylamine. These complexes are expected to bind polyanionic DNA *via* non-covalent outer sphere interaction. The selection of bpy or phen or dpa as a second ligand is to enhance the affinity of the complex towards DNA through partial intercalative interaction. In addition, the non-planar nature of benzimidazole moiety would be expected to affect the kinetics and cytotoxic properties due to its flexibility and bulkiness. The nature of key DNA binding interaction, the efficiency of transport and distribution by BSA and DNA cleavage activity of the complexes in the presence of H₂O₂ has been investigated and attempts made to understand the chemical principle underlying DNA and BSA recognition and then see whether these can be studied as promising drug for cancer. The results of our study are presented and discussed in Chapter 3.

We have also isolated two redox active copper(II) complexes of the type, $[Cu(L1/L2)(phen)](ClO_4)_2 \ (\textbf{1} \ and \ \textbf{2}) \ where \ L1 \ is \ (6-methylpyridin-2-ylmethylene)- (pyridin-2-ylmethyl))$ (pyridin-2-ylmethyl)

-amine and phen is 1,10-phenanthroline and have investigated DNA and BSA binding affinity, DNA cleavage and cytotoxic activity against human cervical carcinoma cell line. The rationale behind the design of the complex is to understand the structure-activity relationship on DNA and BSA binding and DNA cleavage ability and attempts made to understand the chemical principles underlying the cytotoxic activity. The results of our study are presented and discussed in **Chapter 4**

In this study, a copper(II) complex, which has the potential to bind to DNA non-covalently has been also synthesized with the aim of enhancing the DNA binding affinity and cytotoxicity as well. The complex isolated is the mononuclear copper(II) complex, $[Cu(dppt)_2(H_2O)_2](ClO_4)_2$, where dppt is 5,6-diphenyl-3-(2-pyridyl)-1,2,4-triazine. The dppt N_{py} and N_{tz} donor ligand are chosen to provide donor elements such as pyridine and triazine groups and thus tune the DNA binding property of the complex. Then see whether it can be used as cancer chemotherapeutic potential against human cervical carcinoma cell line. The interesting aspects of the anticancer drug mechanisms underlying the cytotoxic response have been probed and the results are presented and analyzed in **Chapter 5**

At the outset of **Chapters 3** to **5**, a brief introduction and a review of the relevant previous work are provided. The general experimental materials, methods, and techniques are described in **Chapter 2**. The experimental procedures for the synthesis of ligands and the isolation of complexes are included in the respective chapters.

To determine the DNA and protein binding affinity, DNA cleavage ability and cytotoxicities of the present copper(II) complexes, it is proposed to employ several

spectral methods like electronic absorption, emission, and circular dichroic spectroscopy. The extent of DNA interactions will be followed by electrochemical measurements. Agarose gel electrophoresis experiment will be also performed to study the DNA cleavage activity of the complexes. Tryphtophan fluorescence quenching experiment shall be used to determine the protein binding constant. The cytotoxicities of the complexes shall be monitored by using MTT assay. Cell cycle arrest, ROS generation, apoptosis, DAPI staining shall be used to detect the cell pathology upon treating the copper(II) complex.

Parts of the thesis have been published [130,131] before or have been submitted for publication.

References

- [1] J.D. Watson, F.H. Crick, Nature 171 (1953) 737-738.
- [2] A.D. Hershey, M. Chase, J. Gen. Physiol. 36 (1952) 39-56.
- [3] J.D. Watson, F.H. Crick, Cold Spring Harb. Symp. Quant. Biol. 18 (1953) 123-131.
- [4] U. Lagerkvist, Lakartidningen, 65 (1968) 4373-4381.
- [5] E.S. Lander, Nature 409 (2001) 860-921.
- [6] J.C. Venter, Science 291 (2001) 1304-1351.
- [7] D.Gibson, Pharmacogenomics J.2 (2002) 275-276.
- [8] Y.S. Cho-Chung, Curr. Pharm. Des. 11 (2005) 2811-2823.
- [9] A. Fernandez, S. Sessel, Trends Pharmacol. Sci. 30 (2009) 403-410.
- [10] J. Chen, J. Stubbe, Nat. Rev. Cancer 5 (2005) 102-112.
- [11] C. Moucheron, A. Kirsch-De Mesmaeker, S. Choua, Inorg. Chem.36 (1997) 584-592.
- [12] B.A. Armitage, Curr. Chem., 253 (2005) 55-76.
- [13] J. Kelly, A. Tossi, D. McConell, Nucleic Acids Res.13 (1985) 6017-6034.
- [14] K. Fukui, K. Tanaka, Nucleic Acids Res. 24 (1996) 3962-3967.
- [15] J.C. Wang, Nat. Rev. Mol. Cell. Biol. 3 (2002) 430-440.
- [16] T.A. Bickle, D.H. Krüger, Microbiol. Rev. 57 (1993) 434-450.
- [17] K. Samejima, W.C. Earnshaw, Nat. Rev. Mol. Cell. Biol. 6 (2005) 677-688.
- [18] M.O. Hengartner, Nature 40 (2000) 770-776.
- [19] L.M. Mirica, X. Ottenwaelder, T.D.P. Stack, Chem. Rev. 104 (2004)1013-1045.
- [20] D.S. Sigman, T.W. Bruice, A. Mazumder, C.L. Sutton, Acc. Chem. Res. 26 (1992)98-104.

[21] W.J. Pogozelski, T.J. McNeese, T.D. Tullius, J. Am. Chem. Soc.117 (1995) 6428-6433.

- [22] C.A. Claussen, E.C. Long, Chem. Rev. 99 (1999) 2797-2816.
- [23] B. Mestre, A. Jakobs, G. Pratviel, B. Meunier, Biochemistry 35 (1996) 9140-9149.
- [24] Y.Y. Fang, C.A. Claussen, K.B. Lipkowitz, E.C. Long, J. Am. Chem. Soc. 128 (2006) 3198-3207.
- [25] J.L. Czlapinski, T.L. Sheppard, Chem. Commun. 21 (2004) 2468-2469.
- [26] N.M. Urquiza, L.G. Naso, S.G. Manca, L. Lezama, T. Rojo, P.A.M. Williams, E.G. Ferrer, Polyhedron 31 (2012) 530-538.
- [27] G. Vignesh, S. Arunachalam, S. Vignesh, R.A. James, Spectrochim. Acta. A. Mol. Biomol. Spectrosc. 96 (2012) 108-116.
- [28] K.S. Ghosh, S. Sen, B.K. Sahoo, S. Dasgupta, Biopolymers 91 (2009)737-744.
- [29] P. Sathyadevi, P. Krishnamoorthy, E. Jayanthi, R.R. Butorac, A.H. Cowley,N. Dharmaraj, Inorganica Chimica. Acta. 384 (2012) 83-96.
- [30] C.M. Dobson, Semin Cell Dev. Biol. 15 (2004) 3-16.
- [31] X.M. He, D.C. Carter, Nature 358 (1992) 209-215.
- [32] J.R. Brown, Albumin: Structure, Function and Uses Pergamon Press, Oxford, 1977.
- [33] R.N.M. Weijers, Clin. Chem. 23 (1977) 1361-1362.
- [34] D.C. Carter, J.X. Ho, Protein Chem. 45 (1994) 153-203.
- [35] T.J. Peters, Metabolism: albumin in the body In: All about albumin, Biochemistry Genetics and Medical applications, San Diego: Academic Press, 1996, 188.

[36] M. Dockal, D.C. Carter, F. Rüker, J. Biol. Chem. 275 (2000) 3042-3050.

- [37] W.M. Pavdridge, Am. J. Physiol. 252 (1987) 157-164.
- [38] A. Valstar, M. Almgren, W. Brown, M. Vasilescu, Langmuir 16 (2000) 922-927.
- [39] M.E. Georgiou, C.A. Georgiou, M.A. Kouppairs, Anal. Chem. 71 (1999) 2541-2550.
- [40] A.P. Demchenko, Topics in Fluorescence Spectroscopy: Biochemical Applications, Plenum Press, New York, 1992.
- [41] A. Varshiney, P. Sen, E. Ahmad, M. Rehan, N. Subbarao, R.H. Khan, Chirality 22 (2010) 77-87.
- [42] V. Fodera, M. Groenning, V. Vetri, F. Librizzi, S. Spagnolo, C. Cornett, L. Olsen,M. Van de Weert, M. Leone, J. Phys. Chem. B 112 (2008) 15174-15181.
- [43] P.B. Kandagal, S. Ashoka, J. Seetharamappa, S.M.T. Shaikh, Y. Jadegoud,O.B Ijare, J. Pharm. Biomed. Anal. 41 (2006) 393-399.
- [44] I. Girard, S. Ferry, J. Pharmaceut. Biomed. 14 (1996) 583-591.
- [45] P.B. Kandagal, S.M.T. Shaikh, D.H. Manjunatha, J. Seetharamappa, B.S. Nagaralli, J. Photochem. Photobiol. A 189 (2007) 121-127.
- [46] E. Karnaukhova, Biochem. Pharmacol. 73 (2007) 901-910.
- [47] M. Hepel, Electroanalysis 17 (2005) 1401-1412.
- [48] Y. Li, W.Y. He, H.X. Liu, X.J. Yao, Z.D. Hu, J. Mol.Struct. 831 (2007) 144-150.
- [49] A. Sułkowska, B. Bojko, J. Rownicka, P. Rezner, W.W. Sułkowski, J. Mol. Struct. 744 (2005) 781-787.
- [50] T. Jianniao, L. Jiaqin, Z. Hu, C. Xingguo, Bioorg. Med. Chem. 13 (2005) 4124-4129.

[51] H. Toumi, (2010). Cancer kills more people than AIDS, tuberculosis and Malaria combined. URL:http://www.habibtoumi.com/2010/04/22/ Accessed on 18th June 2010. American Cancer Society. (2010). Leukemia-chronic lymphocytic. URL:http://documents.cancer.org/acs/groups/cid/documents/webcontent/003 111-pdf. pdf. Accessed on 1st October 2010.

- [52] I. E. McCutcheon,(2006). The problem of the aggressive pituitary tumor. URL: http://www.touchbriefings.com/pdf/2403/mccutcheon.pdf Accessed on 1st December 2010.
- [53] N. E. Dangoor, (2011). How many different types of cancer are there? URL:http://cancerhelp.cancerresearchuk.org/about-cancer/cancer questions/ how- Many-different-types-of-cancer-are-there Accessed on 1st December 2011.
- [54] M. Center, A. Jemal, R.L. Siegel, (2011). Global cancer facts & figures 2nd edition. (pp 1-60). Atlanta: American Cancer Society.
- [55] M. Peyrone, Ann. Chemie Pharm. 51 (1844) 1-29.
- [56] B. Rosenberg, L. Van Camp, T. Krigas, Nature 205 (1965) 698-699.
- [57] M. Galanski, M.A. Jakupec, B.K. Keppler, Curr. Med. Chem. 12 (2005) 2075-2094.
- [58] J. Graham, M. Muhsin, P. Kirkpatrick, Nat. Rev. Drug Discov. 3 (2004) 11-12.
- [59] L. Kelland, Nat. Rev. Cancer 7 (2007) 573-584.
- [60] D.P. Gately, S.B. Howell, Br. J. of Cancer 67 (1993) 1171-1176.
- [61] X. Lin, T. Okuda, A. Holzer, S. B. Howell, Mol. Pharmacol. 62 (2002) 1154-1159.
- [62] T.G. Appleton, J.R. Hall, S.F. Ralph, C.S.M. Thompson, Inorg. Chem. 28(1989) 1989-1993.

[63] A.J. Fichtinger-Schepman, J.L. Van der Veer, J.H.J. Den Hartog, P.H.M. Lohman, J. Reedijk, J. Biochemistry 24 (1985) 707-713.

- [64] T. Miura, A. Hori-i, H. Mototani, H. Takeuchi, Biochemistry 38 (1999) 11560-11569.
- [65] C. Fernandes, G.L. Parrilha, J.A. Lessa, L.G. Santiago, M.M. Kanashiro, F.S. Boniolo, A.J. Bortoluzzi, N.V. Vugman, M.H. Herbst, A. Jr. Horn, Inorg. Chim. Acta, 359 (2006) 3167-3176.
- [66] B.P. Hudson, J.K. Barton, J. Am. Chem. Soc. 120 (1998) 6877-6888.
- [67] D.S. Sigman, D.R. Graham, V.D. Aurora, A.M. Stern, J. Biol. Chem. 254 (1979) 12269-12272.
- [68] J.D. Ranford, P.J. Sadler, D.A. Tocher, Dalton Trans. 177 (1993) 3393-3399.
- [69] S. Zhang, Y. Zhu, C. Tu, H. Wei, Z. Yang, L. Lin, J. Ding, J. Zhang, Z. Guo, J. Inorg. Biochem. 98 (2004) 2099-2106.
- [70] M. Chikira, Y. Tomizava, D. Fukita, T. Sugizaki, N. Sugawara, T. Yamazaki,
 A. Sasano, S. Shindo, M. Palaniandavar, W.E. Anthroline, J. Inorg. Biochem.
 89 (2002) 163-173.
- [71] M. Barceló-Oliver, A. Garcia-Raso, A. Terrón, E. Molins, M.J. Prieto, V. Moreno, J. Martinez, V. Lladó, I. López, A. Gutiérrez, P.V. Escribá, J. Inorg. Biochem.101 (2007) 649-659.
- [72] C. Deegan, B. Coyle, M. McCann, M. Devereux, D.A. Egan, Chem. Biol. Interact. 115 (2006) 115-125.
- [73] P.U. Maheswari, S. Roy, H.D. Dulk, S. Barends, G.V. Wezel, B. Kozlevcar, P. Gamez, J. Reedijk, J. Am. Chem. Soc. 128 (2006) 710-711.

[74] P.U. Maheswari, M.V.D. Ster, S. Smulders, S. Barendes, G.V. Wezel,C. Massera, S. Roy, H.D. Dulk, P. Gamez, J. R eedijk, J. Inorg. Chem., 47 (2008) 3719-3727.

- [75] C.H. Ng, K.C. Kong, S.T. Von, P. Balraj, P. Jensen, E. Thirthagiri,H. Hamada, M. Chikira, Dalton Trans. 4 (2008) 447-454.
- [76] M. Scarpellini, A. Neves, R. Horner, A.J. Bortoluzzi, B. Szpoganicz,
 C. Zucco, R.A.N. Silva, V. Drago, A.S. Mangrich, W.A. Ortiz, A.C.W.
 Passos, M.C.B. Oliveira, H. Terenzi, Inorg. Chem., 42 (2003) 8353-8365.
- [77] M. Katsarou, E. Efthimiadou, G. Psomas, A. Karliota, D.J. Vourloumis,J. Med. Chem., 51 (2008) 470-478.
- [78] G. Chen, X. Qiao, P. Qiao, G. Xu, J. Xu, J. Tian, W. Gu, X. Liu, S. Yan,J. Inorg. Biochem., 105 (2011) 119-126.
- [79] R. Cini, G. Tamasi, S. Defazio, M.B.J. Hursthouse, J. Inorg. Biochem. 101 (2007) 1140-1152.
- [80] G. Tamasi, F. Serinelli, M. Consumi, A. Magnani, M. Casolaro, R. Cini, J. Inorg. Biochem., 102 (2008) 1862-1873.
- [81] S. Wu, W. Yuan, H. Wang, Q. Zhang, M. Liu, K. Yu, J. Inorg. Biochem. 102 (2008) 2026-2034.
- [82] J.L. García-Giménez, M. González-Álvarez, M. Liu-González, B. Macías, J. Borrás, G. Alzuet, J. Inorg. Biochem. 103 (2009) 923-934.
- [83] O. Sánchez-Guadarrama, H. López-Sandoval, F. Sánchez-Bartéz, I. Gracia-Mora, H. Höpfl, N. Barba-Behrens, J. Inorg. Biochem. 103 (2009) 1204-1213.
- [84] G. Cerchiaro, K. Aquilano, G. Filomeni, G. Rotilio, M.R. Ciriolo, A.M.D.C. Ferreira, J. Inorg. Biochem. 99 (2005) 1433-1440.

[85] G. Filomeni, G. Cerchiaro, A.M.D.C. Ferreira, J.Z. Pedersen, A. De Martino,G. Rotilio, M.R. Ciriolo, J. Biol. Chem. 282 (2007) 12010-12021.

- [86] V.C.D. Silveira, G.F. Caramori, M.P. Abbott, M.B. Goncalves, H.M. Petrilli, A.M.D.C. Ferreira, J. Inorg. Biochem. 103 (2009) 1331-1341.
- [87] V.C.D. Silveira, J.S. Luz, C.C. Oliveira, I. Graziani, M.R. Ciriolo, A.M.D.C. Ferreira, J. Inorg. Biochem. 102 (2008) 1090-1103.
- [88] M. Ganeshpandian, R. Loganathan, S. Ramakrishnan, A. Riyasdeen, M.A. Akbarsha, M. Palaniandavar, Polyhedron 52 (2013) 924–938.
- [89] C. Rajarajeswari, R. Loganathan, M. Palaniandavar, E. Suresh, A. Riyasdeen,M.A. Akbarsha, Dalton Trans. 42 (2013) 8347-8363.
- [90] C. Rajarajeswari, M. Ganeshpandian, M. Palaniandavar, A. Riyasdeen, M.A. Akbarsha, J. Inorg. Bio. Chem, 110 (2014) 255-268.
- [91] M. Ganeshpandian, S. Ramakrishnan, M. Palaniandavar, E. Suresh,A. Riyasdeen, M.A. Akbarsha, J. Inorg. Bio. Chem, 140 (2014) 202-212.
- [92] V.M. Manikandamathavan, B. Unni Nair, Eur. J. Med. Chem. 68 (2013) 244-252.
- [93] J.-W. Liang, Y. Wang, K.-J. Du, G.-Y. Li, R.-L. Guan, L.-N. Ji, H. Chao.,J. Inorg. Bio. Chem 141 (2014) 17–27.
- [94] S.Y. Ebrahimipour, I. Sheikhshoaie, J. Castro, W. Haase, M. Mohamadi,S. Foro, M. Sheikhshoaie, S.E. Mahani, Inorg. Chim. Acta. 430 (2015) 245-252.
- [95] M. Anjomshoa, M.T. –Mahani, Spectrochim. Acta. A Mol. Biomol. Spectrosc. 150 (2015) 390-402.
- [96] B. Deka, T. Sarkar, S. Banerjee, A. Kumar, S. Mukherjee, S. Deka, K.K. Saikia, A. Hussain, Dalton Trans. 46, (2017) 396-409.

[97] J.G. Deng, Y. Gou, W. Chen, X. Fu, H. Deng, Bioorg. Med. Chem. 24 (2016) 2190-2198.

- [98] S. Kathiresan, S. Mugesh, J. Annaraj, New. J. Chem. 6 (2016) 1810-1825.
- [99] L. Tabrizi, M. Fooladivand, H. Chiniforoshan, Biometals 29 (2016) 981-993.
- [100] R.N. Jadeja, K.M. Vyas, K.K. Upadhyay, R.V. Devkar, RSC Adv. 7 (2017) 17107-17116.
- [101] M. Jopp, J. Becker, S. Becker, A. Miska, V. Gandin, C. Marzano, S. Schindler, Eur. J. Med. Chem. 132 (2017) 274-281.
- [102] J. Qi, Q. Yao, L. Tian, Y. Wang, Eur. J. Med. Chem. 158 (2018) 853-862.
- [103] Y.-X. Liu, H.W. Mo, Z.Y. Lv. F. Shen. C.L. Zhang, Y.Y. Qi, Z.W. Mao.X.Y. Le Trans. Met. Chem., 43 (2018) 259-271.
- [104] J. Deng, P. Yu, Z. Zhang, J. Wang, J. Cai, N. Wu, H. Sun, H. Liang, F. Yang, Eur. J. Med. Chem., 158 (2018) 442-452.
- [105] S.S. Massoud, F.R. Louka, G.T. Ducharme, R.C. Fischer, F.A. Mautner, J. Vančo, R. Herchel, Z. Dvořák, Z. Trávníček, J. Inorg. Biochem. 180 (2018) 39-46.
- [106] Z. Fang, J. Yan, W. Yu, N. Zhang, S. Zhang, Trans. Met. Chem., 44 (2019) 463-474.
- [107] Y. Thakur, R. Agrawal, M. Tripathi, M.K. Siddiqi, E. Mohapatra, R.H. Khan,R. Pande, J. Mol. Struct., 1197 (2019) 691-706.
- [108] M. Kongot, D. Reddy, V. Singh, R. Patel, N.K. Singhal, A. Kumar, Spectrochim.
 Acta. A, Mol. Biomol. Spectrosc. 212 (2019) 330-342.
- [109] S. Zehra, T. Roisnel, F. Arjmand, ACS Omega. 4 (2019) 7691–7705.

[110] M. Kumar, S.U. Parsekar, N. Duraipandy, M.S. Kiran, A.P. Koley, Inorg. Chim. Acta, 484 (2019) 219-226.

- [111] P. Yang, D.-D. Zhang, Z.-Z. Wang, H.-Z. Liu, Q.-S. Shi, X.-B. Xie, Dalton Trans., 48 (2019) 17925-17935.
- [112] M. Simunkova, P. Lauro, K. Jomova, L. Hudecova, M. Danko, S. Alwasel, I.M. Alhazza, S. Rajcaniova, Z. Kozovska, L. Kucerova, J. Moncol, L. Svorc, M. Valko, J. Inorg. Biochem. 194 (2019) 97-113.
- [113] S.C. Manna, S. Mistri, A. Patra, M.K. Mahish, D. Saren, R.K. Manne,M.K. Santra, E. Zangrando, H. Puschmann, Polyhedron 171 (2019) 77-85.
- [114] R. Anjum, D. Palanimuthu, D.S. Kalinowski, W. Lewis, K.C. Park, Z. Kovacevic,I.U. Khan, D.R. Richardson, Inorg. Chem. 58 (2019) 13709-13723.
- [115] S. Barrett, M. de Franco, A. Kellett, E. Dempsey, C. Marzano, A. Erxleben,V. Gandin, D. Montagner, J. Biol. Inorg. Chem. 125 (2020) 49-60.
- [116] L.M. Balsa, M.C. Ruiz, L.S.M. de la Parra, E.J. Baran, I.E. Leon., J. Inorg. Biochem. 204 (2020) 110975.
- [117] L. Rigamonti, F. Reginato, E. Ferrari, L. Pigani, L. Gigli, N. Demitri, P. Kopel, B. Tesarova, Z. Heger, Dalton Trans. 49 (2020) 14626-14639.
- [118] G. Alzuet, A. Castiñeiras, I. Cores, I.G.-Santos, M.G.- Álvarez, M. Saa, J. Inorg. Bio. Chem, 203 (2020) 110902.
- [119] M. Kumar, G. Kumar, D.T. Masram, New J. Chem. 44 (2020) 8595-8613.
- [120] J.A. Eremina, E.V. Lider, T.S. Sukhikh, L.S. Klyushova, M.L. Perepechaeva, D.G. Sheven, A.S. Berezin, A.Y. Grishanova, V.I. Potkin, Inorg. Chim. Acta 510 (2020) 119778.

Chapter I Introduction

[121] H.M. Gençkal, M. Erkisa, P. Alper, S. Sahin, E. Ulukaya, F. Ari, J. Biol. Inorg. Chem. 25 (2020) 161-177.

- [122] H. Kargar, R.B.- Ardakani, V. Torabi, M Kashani, Z.C.- Natanzi, Z. Kazemi, V. Mirkhani, A. Sahraei, M.N. Tahir, M. Ashfaq, K.S. Munawar, Polyhedron 195 (2021) 114988.
- [123] W.da S. Terra, E.S. Bull, S.R. Morcelli, R.R. Moreira, L.L.F. Maciel, J.C. de A. Almeida, M.M. Kanashiro, C. Fernandes, A.H. Jr, Biometals 34 (2021) 661-674.
- [124] S. Sangeetha, M. Murali, Inorg. Chem. Comm. 59 (2015) 46-49.
- [125] S. Sangeetha, M. Murali, Int. J. Biol. Macromol. 107 (2018) 2501–2511.
- [126] S. Sangeetha, T. Ajaykamal, M. Murali, New. J. Chem. 45, 2021, 7578-7593.
- [127] E. Wong, C. M. Giandomenico, Chem. Rev. 99 (1999) 2451-2466.
- [128] M. Ganeshpandian, R. Loganathan, S. Ramakrishnan, E. Suresh, A. Riyasdeen,M.A. Akbarsha, M. Palaniandavar, Polyhedron 52 (2013) 924-938.
- [129] C. Rajarajeswari, R. loganathan, M. Planiandavar, E. Suresh, A. Riyasdeen,M.A. Akbarsha, Dalton Trans. 42 (2013) 8347-8363.
- [130] J. Manivel, S. Sangeetha, M. Murali, J. Sci. Res. 12 (2020) 111-133.
- [131] J. Manivel, S. Sangeetha, M. Murali, J. Adv. Sci. Res. 12 (2021) 166-175.

Chapter 2

General Experimental Materials, Methods and Techniques

The observer listens to nature: the experimenter questions and forces him to reveal himself.

2.1 Materials

2.1.1 Chemicals

The following chemicals were used as received. Copper(II) acetate monohydrate (Cu(CH₃COO)₂·H₂O), Copper(II) perchlorate hexahydrate (Cu(ClO₄)₂·6H₂O), 5,6-diphenyl-3-(2-pyridyl)-1,2,4-triazine, 2,2'-bipyridine, 1,10-phenanthroline (Merck), 2,2'-dipyridylamine, 2-aminomethylpyridine, 2-aminoethylpyridine, 2-picoline-6-carbox-aldehyde, *N*,*N*-iminodiacetic acid, o-phenylenediamine, ethidium bromide (EthBr), sodium azide (NaN₃), Potassium Iodide (KI), Sodium hydrogen phosphate monohydrate, di-Sodium hydrogen phosphate dihydrate (**Sigma-Aldrich**), Ascorbic acid (**Fisher scientific**) hydrogen peroxide solution (30% w/v), *tetra-N*-butylammonium bromide, perchloric acid, sodium perchlorate (**Sigma Aldrich**), pUC19 supercoiled DNA and agarose (**Genei**). Calf thymus (CT) DNA (highly polymerized stored at 4°C), superoxide dismutase (SOD) (stored at 4°C), bovine serum albumin (BSA) (stored at 4°C) (**Sigma Aldrich**) were used as received.

2.1.2 Solvents

Methanol, ethanol, diethylether, acetone, and HPLC grade dimethylformamide and acetonitrile were purchased from **Merck**. The HPLC grade methanol was used for the synthesis of copper(II) complexes. Molecular biology grade DMSO (**Sigma**) was used for cell culture. Ultrapure Milli Q water (18.2 $\mu\Omega$) was used for all experiments. All the experiments described in this thesis were carried out in 2% DMF/5 mM Tris HCl/50 mM NaCl buffer at pH 7.1 as mentioned in the respective chapters.

2.1.3 Preparation and purification of supporting electrolytes

Tetra-N-butylammonium perchlorate (TBAP)

This electrolyte was prepared by reacting *tetra-N*-butylammonium bromide (**G**. **F**. **Smith**, **USA**) with perchloric acid in water. The solid thus obtained was recrystallized twice before drying at 100 °C under vacuum. It was also prepared by the addition of sodium perchlorate to a hot ethanol solution of *tetra-N*-butylammonium bromide (**G**. **F**. **Smith**, **USA**). The product was recrystallized from aqueous ethanol and was tested for the absence of bromide.

2.1.4 Purification of solvents

The commercial solvents were distilled and then used for the preparation of complexes. For spectroscopic and electrochemical studies methanol was purified by refluxing it with Mg turnings and iodine and then distilled. Dimethylformamide was distilled (40-50 $^{\circ}$ C) under reduced pressure, after drying it over P₄O₁₀ and neutralizing the resulting phosphoric acid generated by the addition of crystalline NaOH pellets.

2.1.5 Preparation of metal complexes

The procedures employed for the synthesis of ligands and the isolation of metal complexes are described in the respective chapters. The identities of already known ligands and complexes were established based on elemental analysis, ESI-MS, and UV-Visible spectroscopy. For certain new complexes, SCXRD analysis was used to optimize the structure.

Caution: A few complexes described in this thesis contain perchlorate anion. Perchlorate salts of metal complexes with organic ligands are potentially explosive! Only small quantities of materials were prepared and they were handled with great caution.

2.2 Techniques

2.2.1 Physical measurements

The elemental analyses (C, H, N) were carried out using a Perkin-Elmer 2400 series II analyzer. The electrical conductivity was obtained with a Systronic 305 conductivity bridge, using a 1×10^{-3} M solution of the complex in N,N-dimethyl-formamide (DMF). FTIR spectra were recorded using a Perkin Elmer Spectrum RX1 FTIR spectrophotometer in the range 400-4000 cm⁻¹ with a sample prepared at KBr disc. The electronic spectra were recorded using Perkin Elmer Lambda 365 UV-VIS spectrophotometer using cuvettes of 1 cm length. X-band electron paramagnetic resonance (EPR) measurements were performed at room temperature in the solid-state and 77 K in the DMF solution on the JEOL JES-FA200 ESR spectrometer. Emission intensity measurements were carried out using a Shimadzu RF-5301PC spectrofluorophotometer equipped with a thermostatic bath. Finnigan MAT TSQ-700 equipped with a custommade electrospray interface (ESI) was used to perform mass spectrometry experiments. Spectra were collected by constant fusion of the analyte dissolved in DMF. High resolution mass spectrometry (HRMS) was performed on the HRMS Exactive Plus EMR spectrometer. Magnetic susceptibility value at 298 K was obtained using Model 300 Lewis-coil-force magnetometer of George Associate Inc. (Berkley, USA) make. The pH was potentiometrically measured using an Elico LI 120 pH meter equipped with a combined glass electrode. ¹H NMR spectra were recorded on a Bruker 300 MHz with AVANCE II NMR spectrometer in DMSO-d₆.

2.2.2 Electroanalytical technique

Cyclic voltammetry (CV) and differential pulse voltammetry (DPV) on glassy carbon electrode were performed in DMF 25 \pm 0.2 °C. The voltammograms were generated using CH instruments 620C electrochemical analyzer. A three-electrode system has been used to study the electrochemical behavior of complexes (0.001 M) consisting of a glassy carbon working electrode (A = 0.0707 cm²), a platinum wire auxiliary electrode, and saturated calomel reference electrode and TBAP (0.1 M) is used as a supporting electrolyte. Solutions were deoxygenated by purging with nitrogen gas for 15 min before the measurements. Redox titrations with DNA were carried out in 2% DMF/5 mM Tris HCl/50 mM NaCl buffer (pH 7.1). The redox potential ($E_{1/2}$) was calculated from the anodic (E_{pa}) and cathodic (E_{pc}) peak potentials of CV traces as ($E_{pa} + E_{pc}$)/2. The redox potentials were predictable from the DPV peak potential, E_p using the relation [1], $E_{1/2} = E_p + \Delta E/2$ where $E_{1/2}$ is equal to the average of E_{pa} and E_{pc} in CV experiments and ΔE is the pulse amplitude.

2.2.3 DNA binding studies

DNA is believed to be the primary cellular target of many metallodrugs, therefore, the interaction between complex and DNA was investigated by using the following spectroscopic methods.

Solutions of DNA in the 5 mM Tris HCl/50 mM NaCl buffer gave a ratio of UV absorbance at 260 and 280 nm, A_{260}/A_{280} , about 1.9 [2], indicating that the DNA was sufficiently free of protein. Concentrated stock solutions of DNA (13.5 mol dm³) were prepared in buffer and sonicated for 25 cycles, where each cycle consisted of 30 s with 1 min intervals. The concentration of DNA in nucleotide phosphate (NP) was

determined by UV absorbance at 260 nm after 1:100 dilutions. The extinction coefficient, ε_{260} , was taken as 6600 M⁻¹ cm⁻¹ [3]. Stock solutions were stored at 4 °C and used after no more than 4 days. Concentrated stock solutions of metal complexes were prepared by dissolving calculated amounts of metal complexes in respective buffers and diluted suitably with the corresponding buffers to required concentrations for all the experiments. For absorption, emission, circular dichroic spectral, and voltammetric experiments the DNA solutions were pretreated with solutions of metal complexes (the concentrations of which are the same as that used for titration) to ensure no change in concentration of the metal complexes. The titration of DNA was performed by adding small volumes of DNA solutions to the sample cuvette containing a fixed concentration of the complexes. The solutions were thoroughly mixed using a micropipette and allowed to equilibrate for 10 min before measurements wherever required. DNA was also titrated into the reference cuvette to correct for any absorbance or light scattering due to the DNA itself.

2.2.4 Electronic absorption titration

Absorption titration experiments were performed with fixed concentrations of the complexes, while gradually increasing the concentration of CT DNA. To obtain the absorption spectra, the required amount of CT DNA was added to both the compound and reference solutions, to eliminate the absorbance of CT DNA itself. From the absorption titration data, the binding constant (K_b) was determined using the equation [4]:

$$[DNA]/(\epsilon_a\text{-}\epsilon_f) = [DNA]/(\ \epsilon_b\text{-}\epsilon_f) + 1/K_b(\epsilon_b\text{-}\epsilon_f)$$

where [DNA] is the concentration of CT DNA in base pairs, ϵ_a corresponds to the observed extinction coefficient (A_{observed}/[M]), ϵ_f corresponds to the extinction

coefficient of the free compound, ε_b is the extinction coefficient when fully bound to CT DNA, and K_b is the intrinsic binding constant. The ratio of slope to intercept in the plot of [DNA]/(ε_a - ε_f) versus [DNA] gave the value of K_b .

2.2.5 Fluorescence studies

The enhanced fluorescence of EthBr in the presence of DNA can be quenched by the addition of a second molecule [5,6]. The extent of fluorescence quenching of EthBr bound to CT DNA can be used to determine the extent of binding between the second molecule and CT DNA. Competitive binding experiments were carried out in the buffer by keeping [DNA]/[EthBr]=1 and varying the concentrations of compounds. The fluorescence spectra of EthBr were measured using an excitation wavelength of 520 nm and the emission range was set between 550 to 700 nm. The Spectra were analyzed according to the classical Stern-Volmer equation [7]:

$$I_0/I = 1 + K_{sv}[Q]$$

where I_0 and I are the fluorescence intensities at 600 nm in the absence and presence of the quencher, respectively, K_{sv} is the linear Stern-Volmer quenching constant, and [Q] is the concentration of the quencher. In these experiments $[CT\ DNA] = 125 \times 10^{-6}$ M, $[EthBr] = 1.25 \times 10^{-6}$ M. From the plot of the observed intensities against complex concentration the values of apparent DNA binding constant (K_{app}) were calculated using the equation [8]:

$$K_{app} \times [complex] = K_{EthBr} \times [EthBr]$$

2.2.6 Circular dichroic spectra

Circular Dichroic (CD) spectra of DNA were obtained by using JASCO J-716 spectropolarimeter equipped with a peltier temperature control device. All experiments

were done using 0.2 cm path quartz cell. Each CD spectrum was collected after averaging over at least 4 accumulations using a scan speed of 100 nm min⁻¹ and a 1s response time. Machine plus cuvette baselines were subtracted and the resultant spectrum zeroed 50 nm outside the absorption bands.

2.3 BSA binding studies

The stock solution of protein $(1.0 \times 10^{-4} \text{ mol L}^{-1})$ was prepared by dissolving the solid BSA in 0.05 M phosphate buffer at pH 7.4 and stored at 0-4 °C in the dark for about a week and then diluted to 1.0×10^{-6} mol L⁻¹ using phosphate buffer (pH 7.4, 0.05 M) when used. The concentration of BSA was determined from optical density measurements, using the value of molar absorptivity of $\varepsilon_{280} = 44720 \text{ M}^{-1} \text{ cm}^{-1}$ [9]. All fluorescence measurements were performed using a Shimadzu RF-5301PC spectrofluorophotometer equipped with a thermostatic bath and a 10 mm quartz cuvette. Fluorescence emission spectra were recorded at two different temperatures (300 and 310 K).

2.3.1 Fluorescence quenching measurements

Quantitative analyses of the interaction between complex and BSA were performed by fluorimetric titration (0.05 M phosphate buffer, pH 7.4). A 3.0 mL portion of an aqueous solution of BSA was titrated by successive additions of the complex. Titrations were done manually by using an Eppendorf micro pipette. For every addition, the mixture solution was shaken and allowed to stand for 20 min at the corresponding temperature (300 and 310 K), and then the fluorescence intensities were measured with an excitation wavelength of 280 nm and emission wavelengths in the interval 290-500 nm. No correction for the inner filter effect was applied since

complex represented very low absorbance (less than 0.1) at excitation and emission wavelengths. The excitation and emission slit width (each 5.0 nm), scan rate (fast) were constantly maintained for all the experiments. In the meantime, the synchronous fluorescence intensity of the mixed solution was measured at $\Delta\lambda=15$ nm and $\Delta\lambda=60$ nm, respectively. In synchronous fluorescence spectroscopy, according to Miller [10], the distinction of the difference between excitation wavelength and emission wavelength ($\Delta\lambda=\lambda_{em}-\lambda_{ex}$) reflects the spectra of a different nature of chromophores, with large $\Delta\lambda$ value such as 60 nm, the synchronous fluorescence of BSA is characteristic of tryptophan residue and with a small $\Delta\lambda$ values such as 15 nm is characteristic of tyrosine [11].

To determine the quenching property, the fluorescence decay data were analyzed *via* the Stern-Volmer equation [12]:

$$F_0/F = 1 + K_{SV}[Q] = 1 + k_0 \tau_0[Q]$$

where F_0 and F are the steady-state fluorescence intensities in the absence and the presence of quencher, respectively. K_{sv} is the Stern-Volmer quenching constant and [Q] is the concentration of quencher. The plot of F_0/F versus [Q] shows the value of K_{SV} . According to the above equation

$$K_{SV} = k_0/\tau_0$$

where K_q is the quenching rate constant and τ_0 is the fluorescence lifetime of protein in the absence of quencher, the value of τ_0 is considered to be 10^{-8} s [13].

To ascertain the static quenching mechanism, the quenching data were analyzed according to modified Stern-Volmer equation [14]:

$$F_0/\Delta F = F_0/F_0-F = 1/f_aK_a \times 1/[Q] + 1/f_a$$

 ΔF is the fluorescence intensity difference in the absence and presence of the quencher at a concentration [Q], K_a is the effective quenching constant for the accessible fluorophores and f_a is the fraction of accessible fluorescence.

2.3.2 Binding parameters

When small molecules bind independently to a set of equivalent sites on a macromolecule, the binding constant (K_b) and the numbers of binding sites (n) can be determined using the following equation [15]:

$$\log[F_0-F/F] = \log K_b + n\log[Q]$$

where K_b is the binding constant, reflecting the degree of interaction of the BSA and complex, and n is the number of binding sites. Thus the plots of $log[(F_0-F)/F]$ *versus* log[Q] give a straight line. The values of n and K_b can be calculated from the slope and intercept of the linear plot respectively.

2.3.3 Thermodynamic parameters and nature of the binding forces

Generally, the binding mode of a drug with biomolecules often contains hydrogen bonds, van der Waals forces, electrostatic force, and hydrophobic interactions [16,17]. The enthalpy change can be regarded as a constant when the temperature does not vary significantly [18]. The sign and magnitude of thermodynamic parameters such as ΔH° (enthalpy change), ΔS° (entropy change), and ΔG° (free energy change) of small molecules with proteins can account for the main forces of interaction. To elucidate the binding forces between complex and BSA, the thermodynamic parameters were calculated from the Van't Hoff equations [18,19]:

$$ln(K_2/K_1) = (1/T_1 - 1/T_2) \Delta H^{\circ}/R$$

$$\Delta G^{\circ} = \Delta H^{\circ} - T\Delta S^{\circ} = -RTlnK$$

where K is the equilibrium binding constant, which is analogous to the effective quenching constants K_a at the corresponding temperature, K_1 and K_2 are the binding constants at temperature T_1 and T_2 , respectively, and R is the gas constant.

2.3.4 Förster's non-radiative energy transfer

Fluorescence resonance energy transfer (FRET) is a non-destructive spectroscopic method that can monitor the proximity and relative angular orientation of fluorophores, the donor and acceptor fluorophores can be entirely separated or attached to the same macromolecule. A transfer of energy could take place through direct electro-dynamic interaction between the primarily excited molecule and its neighbors [20]. The distance between the donor (BSA) and the interacted complex as acceptor was estimated. Förster's non-radiative energy transfer theory is the overlapping of the fluorescence spectrum of BSA with the absorption spectrum of the complex. Thus the energy transfer efficiency, E, is calculated using the following equation [21]:

$$E = 1 - F/F_0 = R_0^6/R_0^6 + r^6$$

Here r is the distance between the donor and acceptor and R_0 is the critical distance when the transfer efficiency equals 50% and the value of R_0 is calculated by the following equation [22]:

$$R_0 = 979 (\kappa^2 n^{-4} \phi J)^{1/6} nm$$

the term κ^2 is the relative orientation of space of the transition dipole of the donor and acceptor (for a random orientation as in fluid, $\kappa^2=2/3$), n is the refractive index of the medium in the wavelength range where the spectral overlap is significant, ϕ is the

fluorescence quantum yield of the donor and overlap integral J expresses the extent of overlap between the donor emission and the acceptor absorption, which could be calculated by the following equation:

$$J = \int F(\lambda) \epsilon(\lambda) \lambda^4 d\lambda / \int F(\lambda) d\lambda$$

where $F(\lambda)$ is the normalized donor emission spectrum in the range from λ to $\lambda + \Delta\lambda$, and $\varepsilon(\lambda)$ is the molar absorption coefficient of the acceptor at wavelength λ .

2.3.5 UV-Visible absorption spectra

The UV-Visible absorption spectra of 1.0 μM free BSA, as well as BSA/complex (equal molar ratio) in 0.5 M phosphate buffer of pH 7.4, were recorded from 200-500 nm.

2.4 DNA cleavage experiments

The cleavage of DNA in the absence and presence of activating agents such as ascorbic acid (20 μ M) or H_2O_2 (50 or 200 μ M) was monitored using agarose gel electrophoresis. A typical reaction mixture, containing pUC19 supercoiled phage DNA (form I, 20 μ M) and copper(II) complex in 2% DMF/5 mM Tris-HCl/50mM NaCl buffer (pH 7.1) was incubated at 37 °C for 1 h. After the incubation period, the reaction was quenched by keeping the samples at -20 °C, followed by the addition of loading buffer (0.025 mg bromophenol blue, 1 mL glycerol, and 1 mL MilliQ water). This was then loaded on a 1% agarose gel containing ethidium bromide (2.54 μ M in the gel as well as in the buffer). The gels were run at a constant voltage of 40 V for 3 h in the 1×TBE buffer (TBE = Tris-Borate-EDTA Buffer) containing ethidium bromide. After washing with distilled water, the gels were visualized under a UV transilluminator

and the bands were documented and quantified using a BioRad Gel Doc 1000 apparatus interfaced with a computer.

The cleavage efficiency was measured by determining the ability of the complex to convert the supercoiled DNA (SC) to nicked circular form (NC) and linear form (LC). To identify the reactive oxygen species (ROS) involved in the cleavage reaction the radical scavengers such as hydroxyl radical (DMSO, 20 μ M), singlet oxygen (NaN₃, 100 μ M), superoxide (SOD, 0.5 units), and Catalase (0.5 or 6 units) were introduced. Also, methyl green (100 μ M) is used to determine the groove binding nature of the copper(II) complexes.

2.5 Cell line

The human cervical cancer cell line (HeLa) was acquired from National Centre for Cell Science (NCCS), Pune. It was grown in Eagles Minimum Essential Medium containing 10% fetal bovine serum (FBS). The cells were preserved at 37 °C, 5% CO₂, 95% air, and 100% relative humidity [23]. Maintenance cultures were channelized weekly and the culture medium was altered twice a week.

2.6 Cell culture

To make single cell suspensions, the monolayer cells were detached with trypsin-ethylenediaminetetraacetic acid (EDTA) and viable cells were counted using a hemocytometer. They were diluted with a medium containing 5% FBS to give a final density of 1×10^5 cells/ml. The cell suspension of one hundred microlitres per well was seeded into 96-well plates at a plating density of 10,000 cells/well. They were incubated to allow for cell attachment at 37 °C, 5% CO₂, 95% air and 100% relative

humidity. The cells were treated with serial concentrations of the test samples after 24 h. They were dissolved in dimethylsulfoxide (DMSO) and an aliquot of the sample solution was diluted twice to the desired final maximum test concentration with a serum-free medium. Also, four serial dilutions were made to give a total of five sample concentrations. Aliquots of $100~\mu l$ of different sample dilutions were added to the suitable wells already containing $100~\mu l$ of the medium, resulting in the required final sample concentrations. The plates were incubated followed by sample addition at $37~^{\circ}C$, $5\%~CO_2$, 95% air and 100% relative humidity for an additional 48~h. The medium alone was served as control and triplicate was maintained for all concentrations.

2.7 Cell viability assay

The cell viability was carried out by using the MTT assay [24]. Complex in the concentration range 0.25-100 μ M dissolved in 2% DMF/5 mM Tris-HCl/50 mM NaCl buffer at pH 7.1 were added to the wells 24 h after seeding of 1×10^5 cells per well in 100 μ L of fresh culture medium. After 48 h, 15 μ L of 3-[4,5-dimethylthiazol-2-yl]2,5-diphenyltetrazolium bromide (MTT, 5 mg/mL) in phosphate buffered saline (PBS) was added to each well and incubated at 37 °C for 4 h. The formed formazan crystals were solubilized in 100 μ L of DMSO after the medium with MTT was flicked off. The microplate reader was used to measure the absorbance at 570 nm. Data were collected for three replicates each and the percentage cell viability and percentage cell inhibition was calculated using the following formulas:

% Cell viability = $[A_s]$ / $[A_c]$ × 100 (where A_s is absorbance of sample and A_c is absorbance of control).

% Cell inhibition = $[100 - ([A_s] / [A_c])] \times 100$

Nonlinear regression graph was plotted between % Cell inhibition and Log concentration and IC_{50} was calculated using GraphPad Prism software.

2.8 Cell cycle

The HeLa cells were seeded in 6 well plates with high-glucose DMEM media after the period of the time cells attained the growth and the cells were treated with copper(II) complex in its IC₅₀ concentration in the medium for 48 h. After 48 h of incubation, cells were trypsinized and resuspended with complete media. Cells were collected and centrifuged at 1000 rpm for 5 min. Then cell pellet was washed with PBS (Phosphate Buffer Saline) twice and subsequently fixed with 1 ml of 70% of ice cold ethanol overnight at 4 °C. Following the ice cold ethanol, the cell pellet was washed twice with cold PBS and added 10 μl of RNase A at 10 g/ml concentration, which was then incubated for 30 min and washed with PBS at the end. Cells were then incubated in 1 ml of PBS with 50 μl of propidium iodide (1 mg/ml stock) for 30 min in darkness [25]. Then cells were analyzed to check the cell cycle phase using the FACSverse flow cytometer (Becton-Dickinson).

2.9 ROS generation

The HeLa cells were seeded in 6 well plates with high glucose DMEM media for the treatment until cell confluency after the cell growth treated with copper(II) complex in 3 h, 2 h, and 1 h time intervals. After the treatment, cells were trypsinized and 10 µM 2',7'-dichlorodihydrofluorescein diacetate (DCHF-DA, Sigma-Aldrich) dye was added to the pellet. This was kept in incubation under darkness for 10 min. The cells were then analyzed to determine ROS level using the FACSverse flow cytometer (Becton-Dickinson) [26].

2.10 Apoptosis

The HeLa cells were treated with copper(II) complex in high-glucose DMEM media for 48 h. After treatment, the cells were trypsinized, resuspended in PBS, washed twice, and centrifuged to remove PBS. The cells were suspended in 100 µl of binding buffer containing 5 µl of Annexin V and propidium iodide (PI) and incubated for 15 mins under darkness. Stained cells were diluted using 450 µl of binding buffer. The cells were analyzed by using the FACSverse flow cytometer (Becton-Dickinson) and the data were analyzed by FACSverse software [27].

2.11 DAPI staining

Cell nuclear morphology was evaluated by fluorescence microscopy following DAPI (4',6-diamidino-2-phenylindole) staining [28]. The HeLa cells were treated with copper(II) complex for 48 h. The cells were washed with PBS (pH 7.4), fixed with ice cold paraformaldehyde, and then cells were then washed with PBS followed by DAPI was added and incubated for 15 min at 37 °C wrapped in aluminum foil. The cells were then washed with PBS and examined under a Zeiss Axio Observer fluorescence microscope.

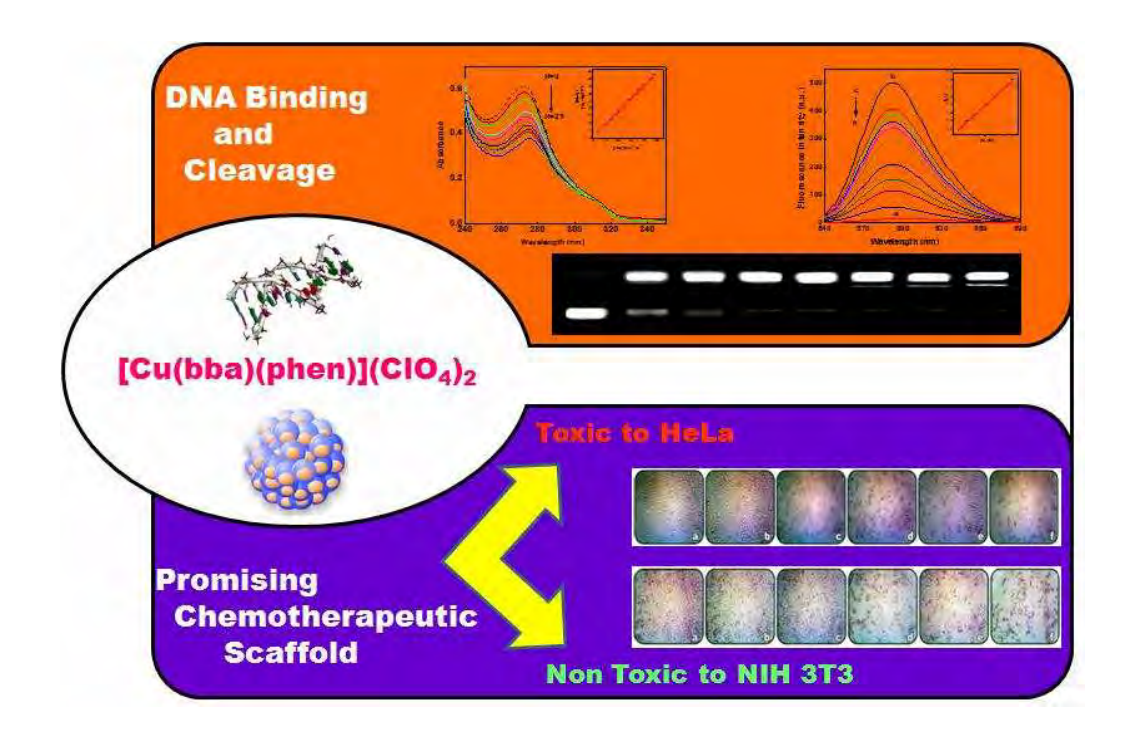
References

- [1] A.J. Bard, L.R. Faulkner, In Electrochemical Methods; Fundamental Applications; Wiley, New York, 1980 p.194.
- [2] J. Marmur, J. Mol. Biol. 3 (1961) 208-218.
- [3] M.E. Reichmann, S.A. Rice, C.A. Thomas, P.J. Poty, J. Am. Chem. Soc. 76 (1954) 3047-3053.
- [4] A.M. Pyle, J.P. Rehmann, R. Meshoyrer, C.V. Kumar, N.J. Turro, J.K. Barton,J. Am. Chem. Soc. 111 (1989) 3051-3058.
- [5] A. Wolfe, G.H. Shimer, T. Meehan, Biochemistry 26 (1987) 6392-6396.
- [6] B.C. Baguley, M.L. Bret, Biochemistry 23 (1984) 937-943.
- [7] O. Stern, M.Z. Volmer, Z. Phys. 20 (1919) 183-188.
- [8] L. Moses, L.R. Andrea, D.W. Michael, F. Stephen, A.H. John, Biochemistry 32 (1993) 4237-4245.
- [9] T.J. Peters, Adv. Protein Chem. 37 (1985) 161-245.
- [10] C.W. Fuller, J.N. Miller, Proc. Anal. Div. Chem. Soc. 16 (1979) 199-208.
- [11] J. Tang, F. Luan, X. Chen, Bioorg. Med. Chem. 2006, 14, 3210-3217.
- [12] J.R. Lakowicz, Principles of Fluorescence Spectroscopy, 3rd ed. Plenum Press, New York, 2006.
- [13] J.R. Lakowicz, G. Webber, Biochemistry 12 (1973) 4161-4179.
- [14] S.S. Lehrer, Biochemistry 10 (1971) 3254-3263.
- [15] A. Divsalar, M.J. Bagheri, A.A. Saboury, H. Mansoori-torshizi, M. Amani,J. Phys. Chem. B 113 (2009) 14035-14042.
- [16] N. Zhou, Y.Z. Liang, P. Wang, J. Mol. Struct. 872 (2008) 190-196.
- [17] I.M. Klotz, Acad. Sci. 226 (1973) 18-35.

- [18] T. Wang, Z. Zhao, B. Wei, L. Zhang, L. Ji, J. Mol. Struct. 970 (2010) 128-133.
- [19] S. Bi, Y. Sun, C. Qiao, H. Zhang, C. Liu, J. Lumin. 129 (2009) 541-547.
- [20] T. Förster, Ann. Phys. 437 (1948) 55-75.
- [21] J. Kang, Y. Liu, M. Xie, S. Li, M. Jiang, Y. Wang, Biochim. Biophys. Acta 1674 (2004) 205-214.
- [22] M. Hof, R. Hutterer, V. Fidler, Fluorescence Spectroscopy in Biology; Springer Science + Business Media: Berlin, 2005.
- [23] V.T. De Vita, Jr S. Hellman, S.A. Rosenberg (Eds.), Cancer: Principles and Practice of Oncology Update, Lippincott, Philadelphia, 1989 Vol. 3 pp. 1-12.
- [24] M.V. Blagosklonny, W.S. El-Diery, Int. J. Cancer. 67 (1996) 386-392.
- [25] C.-C. Zeng, G.-B. Jiang, S.-H. Lai, C. Zhang, H. Yin, B. Tang, D. Wan, Y.-J.Liu, J. Photochem. Photobiol. B 161 (2016) 295-303.
- [26] R. M. Roy, P. Pratheeshkumar, Y-O. Son, L. Wang, J. A. Hitron, S. P.Divya,Z. Zhang, X. Shi, Toxicol Appl Pharmacol., 307 (2016) 81-90.
- [27] M. He, F. Du, W.-Y. Zhang, Q.-Y. Yi, Y.-J. Wang, H. Yin, L. Bai, Y.-Y.Gu,Y.-J. Liu, Polyhedron 165 (2019) 97-110.
- [28] R.N. Jadeja, K.M. Vyas, K.K. Upadhyay, R.V. Devkar, RSC Adv. 7 (2017) 17107-17116.

Chapter 3

DNA and BSA Interaction, DNA Cleavage and *in vitro* Cytotoxicity of Copper(II) Complexes: [Cu(bba)(phen)](ClO₄)₂ is Promising Chemotherapeutic Scaffold



The copper(II) complex, [Cu(bba)(phen)](ClO₄)₂ binds to CT DNA through partial intercalation, binds to BSA and transport in the body, cleaves pUC19 DNA efficiently at 12 μ M and kills the HeLa cancer cells at 2 μ M, more potent than cisplatin and non-toxic to NIH 3T3 normal cells.

3 DNA and BSA Interaction, DNA Cleavage and *in vitro* Cytotoxicity of Copper(II) Complexes: [Cu(bba)(phen)](ClO₄)₂ is Promising Chemotherapeutic Scaffold

3.1. Introduction

The serendipitous discovery of cisplatin [1] has revolutionized cancer treatment; however, side effects associated with the drug restrict its wider use [2]. Copper(II) complexes are regarded as promising and have attracted considerable attention owing to their capability of interacting directly with DNA and BSA [3,4]. Many studies reveal that DNA is the primary intracellular target of anticancer drugs, since the interaction between small molecules and DNA is able to cause DNA damage, block DNA synthesis in cancer cells [5-8]. Therefore, under physiological conditions, metal complexes that possess efficient DNA binding and cleavage are regarded as potential candidates for use as therapeutic agents in medicinal applications and genomic research [9-12]. On the other hand, a vast majority of cytotoxic metal-containing compounds are administered intravenously, special consideration should be given to interactions of the metal drug with macromolecular blood components, which can then be taken up by and accumulate in tumor tissue. In this context, binding toward serum proteins, like albumin or transferrin may perform a transport function for a metal. Such interactions determine the overall drug distribution and excretion and differences in efficacy, activity, and toxicity [13,14].

Benzimidazole moiety is structurally related to purine bases and is found in a variety of naturally occurring compounds such as vitamin B_{12} . Benzimidazole derivatives display a wide variety of pharmacological properties including antitumor activity [15]

and inhibition of nucleic acid synthesis [16]. Transition metal complexes consist of benzimidazole ligands that act as cytotoxic [17,18], antiviral [18] and antiamoebic [19] agents. Moreover, ruthenium(I) [20] and zinc(II) [21] complexes of 2,6-bis(benzimidazol-2-yl)pyridine have DNA cleaving properties. Copper(II) complexes with benzimidazole-derived bidentate chelating ligands show the most active cytotoxic activity [22] with different human tumor cell lines. There are also many examples in the literature of copper complexes of ligands containing α-diimino (-N=C-C=N-) moiety such as phenanthroline that can induce apoptosis [23] and 2-(4'-thiazolyl)benzimidazole that display antimicrobial activity [24]. In particular, the non-planar nature of benzimidazole ligands, their flexibility, and bulkiness affect the kinetics and cytotoxic properties of the corresponding metal complexes. In addition, benzimidazole-based ligands can possess N-H moiety which can facilitate DNA cleavage in cancer cells [25].

Thus, we have synthesized a series of mixed-ligand copper(II) complexes of the type [Cu(bba)(diimine)](ClO₄)₂ [where bba is *N,N*-bis(benzimidazol-2-ylmethyl) amine and diimine is 2,2'-bipyridine (**1**, bpy) or 1,10-phenanthroline (**2**, phen) or 2,2'-dipyridylamine (**3**, dpa)] (**Scheme 3.1**) and investigated their interaction with calf thymus (CT) DNA and bovine serum albumin (BSA), DNA cleavage activity and *in vitro* cytotoxic properties against human cervical carcinoma cell line (HeLa) and normal mouse embryonic fibroblasts cell line (NIH 3T3).

Scheme 3.1 Schematic representation of the copper(II) complex (1-3) and structure of ligands bpy, phen, Hdpa, bba.

3.2 Experimental

3.2.1 Synthesis of copper(II) complexes

[Cu(bba)(bpy)](ClO₄)₂ (1): The complex 1 was prepared by adding a solution of copper(II) perchlorate hexahydrate (0.370 g, 1 mmol) in methanol (10 mL) to a 15 mL methanolic solution of 2,2'-bipyridine (bpy; 0.156 g, 1 mmol) and N,N-bis (benzimidazol -2-ylmethyl)amine (bba; 0.277 g, 1 mmol) and then stirring the solution for 2 h. The blue precipitate obtained was collected by suction filtration, washed with small amounts of cold methanol and diethyl ether and then dried in vacuum over P_4O_{10} . Yield: 0.45 g (65%). Λ_M (Ω^{-1} cm² mol⁻¹) in DMF at 25 °C: 160. μ_{eff} (solid, 298 K): 1.81 μ_B . ESI-MS (CH₃CN) displays a peak at m/z 248.35 [Cu(bba)(bpy)]²⁺. Anal. Calc. for $C_{26}H_{23}N_7O_8Cl_2Cu$. C, 44.87; H, 3.33; N, 14.09. Found: C, 44.82; H, 3.37; N, 14.14%. FT-IR (KBr, cm⁻¹) selected bands: 1528 ν_{bzim} (C=N), 1638 ν_{bzim} (-C=N-C=C-), 1040, 1094 ν_{bzim} (C-N), 3245 ν_{amine} (N-H), 1556 ν_{py} (C=N), 1091, 625 ν (ClO₄). Electronic spectrum in 2% DMF - 5 mM Tris-HCl/50 mM NaCl buffer solution, λ_{max} /nm

 $(\epsilon_{\text{max}}/\text{M}^{-1} \text{ cm}^{-1})$: 271 (22680), 278 (24600), 311 sh, 635 (90). Molecular orbital coefficients such as α^2 (0.83), β^2 (0.70) and γ^2 (0.58) and orbital reduction factors viz. K_{\parallel} (0.76) and K_{\perp} (0.69).

The blue-colored crystals of 1 suitable for X-ray diffraction studies were obtained by dissolving the complex in DMF:MeCN mixture (1:5 v/v) and allowing it to crystallize at 5 °C for 12 days.

[Cu(bba)(phen)](ClO₄)₂ (**2**): The complex **2** was prepared by adopting the procedure used for obtaining **1** by using 1,10-phenanthroline (phen; 0.180 g, 1 mmol) instead of bpy. Yield: 0.43 g (60%). $\Lambda_{\rm M}$ (Ω^{-1} cm² mol⁻¹) in DMF at 25 °C: 161. $\mu_{\rm eff}$ (solid, 298 K): 1.79 $\mu_{\rm B}$. ESI-MS (CH₃CN) displays a peak at m/z 260.43 [Cu(bba) (phen)]²⁺. Anal. Calc. for C₂₈H₂₃N₇O₈Cl₂Cu. C, 46.71; H, 3.22; N, 13.62. Found: C, 46.79; H, 3.24; N, 13.69%. FT-IR (KBr, cm⁻¹) selected bands: 1546 $\nu_{\rm bzim}$ (C=N), 1623 $\nu_{\rm bzim}$ (-C=N-C=C-), 1044, 1081 $\nu_{\rm bzim}$ (C-N), 3241 $\nu_{\rm amine}$ (N-H), 1543 $\nu_{\rm py}$ (C=N), 1084, 623 ν (ClO₄-). Electronic spectrum in 2% DMF - 5 mM Tris-HCl/50 mM NaCl buffer solution, $\lambda_{\rm max}$ /nm ($\varepsilon_{\rm max}$ /M⁻¹ cm⁻¹): 271 (33440), 278 (35900), 311 sh, 638 (130). Mmolecular orbital coefficients such as α^2 (0.82), β^2 (0.72) and γ^2 (0.60) and orbital reduction factors viz. K_{\parallel} (0.77) and K_{\perp} (0.70).

[Cu(bba)(dpa)](ClO₄)₂ (**3**): The complex **3** was prepared by adopting the procedure used for obtaining **1** by using 2,2'-dipyridylamine (dpa; 0.171 g, 1 mmol) instead of bpy. Yield: 0.47 g (66%). $\Lambda_{\rm M}$ (Ω^{-1} cm² mol⁻¹) in DMF at 25 °C: 165. $\mu_{\rm eff}$ (solid, 298 K): 1.83 $\mu_{\rm B}$. ESI-MS (CH₃CN) displays a peak at m/z 255.92 [Cu(bba) (dpa)]²⁺. Anal. Calc. for C₂₆H₂₄N₈O₈Cl₂Cu. C, 43.92; H, 3.40; N, 15.76. Found: C, 43.98; H, 3.49; N, 15.88%. FT-IR (KBr, cm⁻¹) selected bands: 1534 $\nu_{\rm bzim}$ (C=N), 1632 $\nu_{\rm bzim}$

(-C=N-C=C-), 1042, 1090 $v_{\rm bzim}$ (C-N), 3218 $v_{\rm amine}$ (N-H), 1549 $v_{\rm py}$ (C=N), 1105, 621 $v({\rm ClO_4}^-)$. Electronic spectrum in 2% DMF - 5 mM Tris-HCl/50 mM NaCl buffer solution, $\lambda_{\rm max}$ /nm ($\varepsilon_{\rm max}$ /M⁻¹ cm⁻¹): 254 (26930), 271 (25480), 312 (15050), 658 (125). Molecular orbital coefficients such as α^2 (0.81), β^2 (0.67) and γ^2 (0.52) and orbital reduction factors viz. K_{\parallel} (0.73) and K_{\perp} (0.65).

3.2.2 X-ray crystallography

The crystal of **1** with dimensions $0.42\times0.28\times0.12$ mm³ was selected under the polarizing microscope and then mounted on the tip of glass fiber and cemented using epoxy resin. Intensity data for **1** was collected using Mo-K_a (λ = 0.71073 Å) radiation on a Bruker SMART Apex diffractometer equipped with a CCD area detector at 296 K. The SMART program [26] was used for collecting frames of data, indexing the reflections, and determining the lattice parameters. The data integration and reduction were processed with SAINT [27] software. Empirical absorption correction was applied to the collected reflections with SADABS [28]. The structure was solved by direct methods using SHELXS-97 [31-33] and was refined on F² by the full-matrix least-squares technique using the SHELXL-97 [29-31] program package. All the non-hydrogen atoms in **1** were refined anisotropically until convergence is reached. Hydrogen atoms attached to the ligand moieties were stereochemically fixed. The crystallographic data and details of data collection for **1** are given in **Table 3.1**. Crystallographic data for the structural analysis of [Cu(bba)(bpy)](ClO₄)₂ have been deposited with Cambridge Crystallographic Data Center, CCDC No. 1865376.

Table 3.1Crystal data and structure refinement details for [Cu(bba)(bpy)](ClO₄)₂ (1)

Empirical formula	$C_{26}H_{23}Cl_2CuN_7O_8$
Formula weight	695.95
Crystal system	Triclinic
Space group	P-1
a, Å	9.120(3)
b, Å	10.506(4)
c, Å	16.767(6)
α, deg	83.346(6)
β, deg	74.488(6)
γ, deg	64.483(5)
V, Å	1396.9(9)
Z	2
λ, Å (Mo Kα)	0.71073
D _{calc} , g cm ⁻³	1.655
Goodness-of-fit on F ²	1.054
θ for data collection (deg)	1.26-25.00
final R indices $[I > 2\sigma(I)]$	$R_1 = 0.0696$, $wR_2 = 0.1656$
R_1^{a}	0.0871
wR ₂ ^a	0.1776

 $^{^{}a}R_{1}=\Sigma\;||F_{o}|-|F_{c}||/\Sigma|F_{o}|,\;wR_{2}=\{\Sigma w[({F_{o}}^{2}-{F_{c}}^{2})^{2}/\Sigma w[({F_{o}}^{2})^{2}]\}^{1/2}.$

3.3 Results and discussion

3.3.1 Synthesis and general aspects

The mixed ligand copper(II) complexes have been isolated in good yield (60-66%) by the reaction of bba and bpy or phen or dpa and copper(II) perchlorate hexahydrate in methanol at room temperature. All the complexes have been obtained as blue crystalline solids. Based on the elemental analysis the complexes were formulated as [(Cu(bba)(diimine)](ClO₄)₂ and the stoichiometry of 1 was confirmed by single crystal X-ray structure determination. They show strong infrared spectral bands in the range 1528-1546 cm⁻¹ and 1623-1638 cm⁻¹ are assigned to $v_{bzim}(C=N)$ and v_{bzim} (-C=N-C=C-) stretching vibrations respectively of the benzimidazole ring. The very strong band (1040-1048 cm⁻¹) and a medium band (1081-1094 cm⁻¹) are assigned to $\nu_{\text{bzim}}(\text{C-N})$ stretching vibrations. The band in the range 3218-3245 $\text{cm}^{\text{-1}}$ is due to $v_{amine}(N-H)$ stretching mode of the bba ligand while the sharp and strong band $(1543-1556 \text{ cm}^{-1})$ is assigned to $v_{py}(C=N)$ stretching vibration of diimine ligands. The shift in the vibrational bands to lower energy implies the coordination of amine, benzimidazole, and pyridine nitrogens. A broad intense band (1084-1105 cm⁻¹) and a strong sharp band (623-625 cm⁻¹) are observed, which are characteristics of non-coordinated perchlorate ions. The μ_{eff} values (1.79-1.83 μB) are typical of paramagnetic, mononuclear copper(II) species with d⁹ configuration [32]. The ESI-MS data in MeCN $(m/z [Cu(bba)(diimine)]^{2+}$: 1, 248.35; 2, 260.43; 3, 255.92) reveal that the complexes maintain their identity in solution and this is substantiated by values of molar conductivity in DMF ($\Lambda_{\rm M}/\Omega^{-1}$ cm² mol⁻¹: 160-165), characteristics of 1:2 electrolytes [33].

3.3.2 Description of the crystal structure

The ORTEP view (Figure 3.1a) of 1 shows a discrete monomeric copper(II) complex dication and two perchlorate anions. The selected bond distances and bond angles relevant to the copper coordination sphere are given in Table 3.2.

Table 3.2Selected interatomic distances [Å] and bond angles [°] for [Cu(bba)(bpy)](ClO₄)₂ (1)

Cu(1)-N(1)	1.997(4)	Cu(1)-N(2)	1.994(4)
Cu(1)-N(3)	1.987(4)	Cu(1)-N(4)	1.985(4)
Cu(1)-N(7)	2.412(5)	N(4)-Cu(1)-N(3)	87.03(17)
N(4)-Cu(1)-N(2)	170.66(16)	N(3)-Cu(1)-N(2)	96.22(17)
N(4)- $Cu(1)$ - $N(1)$	95.15(17)	N(3)-Cu(1)-N(1)	176.82(16)
N(2)- $Cu(1)$ - $N(1)$	81.28(17)	N(4)-Cu(1)-N(7)	77.50(17)
N(3)-Cu(1)-N(7)	78.90(18)	N(2)-Cu(1)-N(7)	111.69(17)
N(1)-Cu(1)-N(7)	103.82(17)		

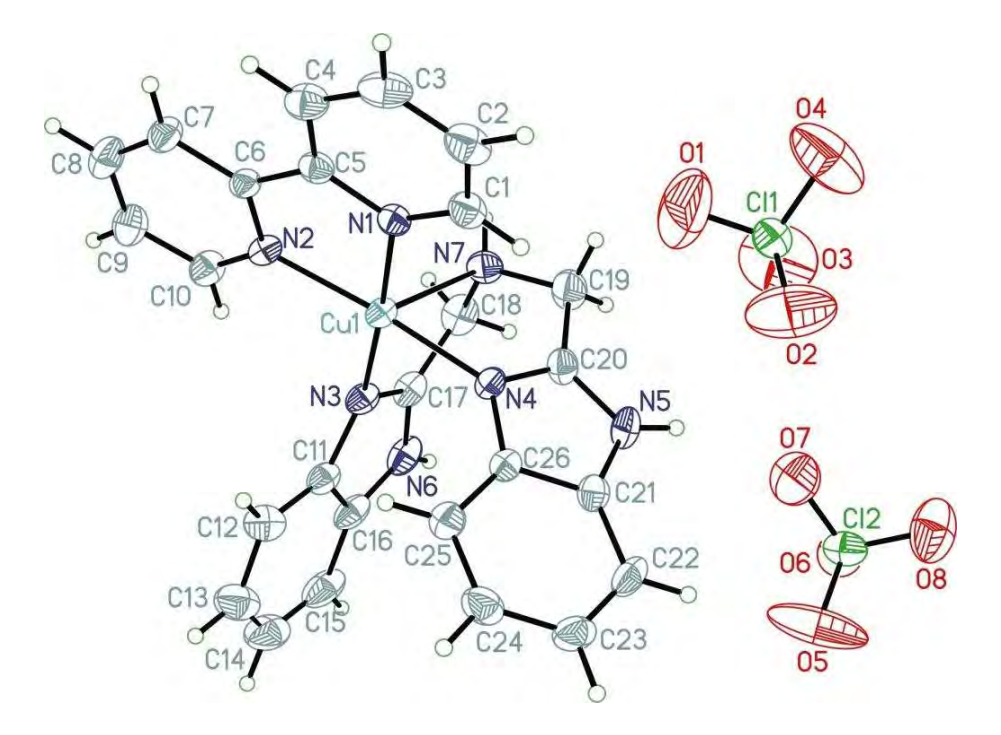


Figure 3.1a An ORTEP view of [Cu(bba)(bpy)](ClO₄)₂ (1) with atom numbering of complex and thermal ellipsoids at 40% probability.

The value of the structural index [34] τ of 0.10 reveals that the coordination geometry around copper(II) is best described as square pyramidal [35,36] with no significant distortion toward trigonal bipyramidal. The tridentate ligand bba is bound facially to Cu(II) with the two bzim nitrogens (Cu-N_{bzim}, 1.987(4), 1.985(4) Å) located in the basal plane and the two imine nitrogens of bpy (Cu-N_{imine}, 1.997(4), 1.994(4) Å) occupying the remaining corners of the basal plane. The strongly bound bpy nitrogens occupy the equatorial sites around Cu(II) with the sterically hindered N7 amine nitrogen atom of bba defaulting to the more weakly bound z-axial position (Cu(1)-N(7), 2.412(5) Å) [37]. The displacement of the copper atom above the N1N2N3N4 plane is 0.094 Å illustrating the importance of the steric effect of the bulky bzim moieties. The Cu-N_{bzim} bond distances are similar to those observed for [Cu(bba)Cl₂] [38,39] and [Cu(bba)₂]²⁺ [37]. The axial Cu-N_{amine} bond is longer than the equatorial Cu-N_{bpy} bonds, which is expected of the presence of two electrons in the d₂₂ orbital of Cu(II).

Interestingly, the molecular packing of **1** shows two different self-assembled molecular associations between different adjacent molecules, viz. interactions between the molecules I and II and II and III (**Figure 3.1b**). The noticeable features are the presence of (i) inter-pair π - π interactions between bpy ligands (I and II) and (ii) C-H··· π non-covalent interactions (II and III). The π - π stacking between C(3) of py and C(5) of py (C(3)···C(5), 3.393 Å) rings of adjacent coordinated bpy ligands giving an average spacing of C_g(p)···C_g(p) (C_g(p), the centroid of the pyridine ring; 3.546 Å). Such an interaction is expected to stabilize the complex in the solid-state [40]. Also, benzene rings of benzimidazole moiety of neighboring molecules display an

attractive C-H··· π non-covalent interaction. It gives C(15)-H(15)···C(21) distance of 3.654 Å and the C(15)-H(15)···C_g(benzene) distance of 3.856 Å and \angle C(15)-H(15)···C_g(benzene) angle of 160.02° (C_g(benzene) is the centroid of the benzene in benzimidazole moiety) showing the closure approach and orientation of the neighbouring molecules [41]. Thus, the separation of Cu···Cu between the adjacent molecules is 8.15 (I and II) and 10.69 Å (II and III).

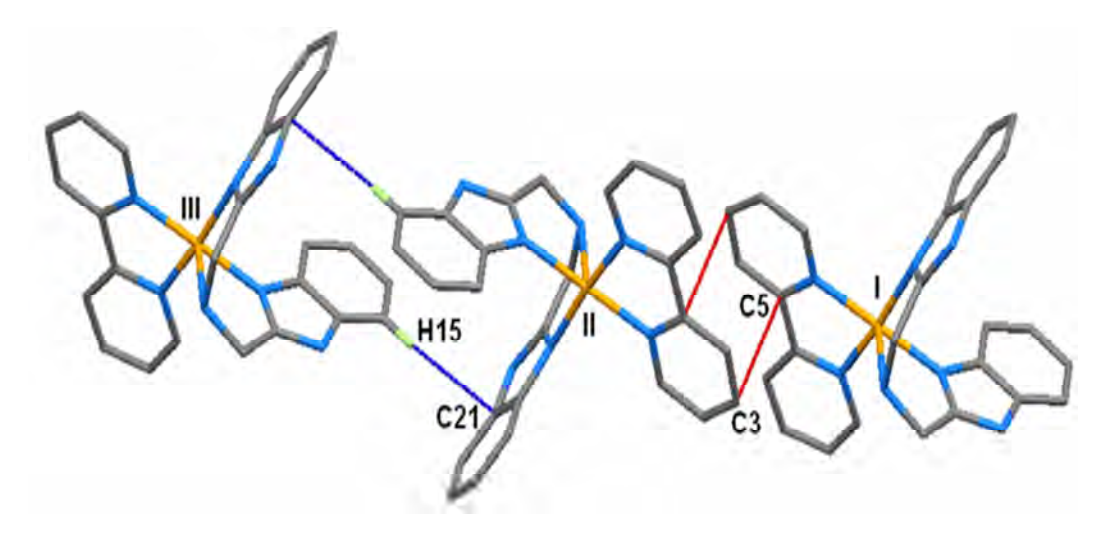


Figure 3.1b Molecular Packing viewed down the a-axis showing intermolecular interactions of $[Cu(bba)(bpy)]^{2+}$ (1) (Blue, C-H··· π ; Red, π ··· π stacking).

3.3.3 Electronic and EPR spectral properties

The complexes (1-3) exhibit only one broad band (λ_{max} , 639-667 nm) in the visible region (**Figure 3.2**) with very low ε_{max} value (70-120 M⁻¹ cm⁻¹), which is typical of a distorted square-based coordination geometry around copper(II) (**Table 3.3**). The strong absorption band is observed in the UV region (λ_{max} , 269-315 nm), which is attributing to the intraligand $\pi \rightarrow \pi^*$ transitions [42] from the coordinated diimines. The EPR spectra of 1-3 display one broad singlet (g_{iso} , 2.053-2.066) in the polycrystalline state at 298 K (**Figure 3.3**) arising from dipolar broadening and

enhanced spin-lattice relaxation The frozen DMF solution EPR spectra (Figure 3.4) of the complexes (**Table 3.3**) are axial $[g_{\parallel} > g_{\perp} > 2.0$; $G = [(g_{\parallel} - 2)/(g_{\perp} - 2)] = 4.9-5.1]$ suggesting the presence of d_{x²-y²} ground state in copper(II) located in square-based geometries [43]. A square-based CuN₄ chromophore is expected [44-46] to show a g_{\parallel} value of 2.200 and A_{\parallel} value in the range $180\text{-}200 \times 10^{\text{-}4} \text{ cm}^{\text{-}1}$ and a tetrahedral distortion from square planar coordination geometry or axial interaction would increase both the ligand field band position (cf. above) and g_{\parallel} value and decrease the A_{\parallel} value [44-46]. So, the observed values of g_{\parallel} (~2.25) and A_{\parallel} (181-186 \times 10⁻⁴ cm⁻¹) for **1-3** are consistent with the presence of a square-based CuN₄ chromophore with no significant distortion from planarity, as evident from the crystal structure of 1 (cf. above). This is supported by the values of $g_{\parallel}/A_{\parallel}$ quotient (122-124 cm) falls in the range of 105–135 cm [47]. Molecular orbital coefficients [48], α^2 (covalent in-plane σ -bonding: 1, 0.83; 2, 0.82; 3, 0.81) and β^2 (covalent in-plane π -bonding; 1, 0.70; 2, 0.72; 3, 0.67) values show that there is a considerable interaction in the in-plane σ -bonding while the in-plane π -bonding is nearly covalent. For complexes 1-3, it is observed that $K_{\parallel} > K_{\perp}$ [49] (K_{\parallel} (1, 0.76; 2, 0.77; 3, 0.73) and K_{\perp} (1, 0.69; 2, 0.70; 3, 0.65) are orbital reduction factors), illustrating the significant out-of-plane π -bonding.

Chapter 3

 Table 3.3

 Electronic absorption and EPR spectral and electrochemical properties of Cu(II) complexes

Complex	λ_{max} in nm (ϵ , M ⁻¹ cm ⁻¹)				EPR spectr	a	Redox properties	
Complex	Ligand field	Ligand based		Solid	Frozen	DMF	DMF	solution
[Cu(bba)(bpy)] ²⁺ 1	643 (70)	279 (33510)	g _{iso}	2.061	g_{\parallel}	2.249	E _{1/2} (V, CV)	-0.074
		273 (32080)			A_{\parallel}	186	$E_{1/2}$ (V, DPV)	-0.081
		315 sh			${f g}_{\perp}$	2.053	$\Delta E_{p} (mV)$	198
					$g_{\parallel}\!/A_{\parallel}$	122	$i_{\rm pa}/i_{ m pc}$	0.9
					G	4.9	$D (10^6 \text{ cm}^2 \text{ s}^{-1})$	7.4
$[Cu(bba)(phen)]^{2+}$ 2	639 (125)	279 (57250)	g_{iso}	2.053	g_{\parallel}	2.254	$E_{1/2}$ (V, CV)	-0.074
		273 (54390)			$\mathbf{A}_{ }$	182	$E_{1/2}$ (V, DPV)	-0.077
		314 sh			g_{\perp}	2.054	$\Delta E_p (mV)$	128
					$g_{\parallel}\!/A_{\parallel}$	124	i_{pa}/i_{pc}	1.0
					G	4.9	$D (10^6 \text{ cm}^2 \text{ s}^{-1})$	7.6
$[Cu(bba)(dpa)]^{2+} 3$	667 (120)	315 (14800)	g_{iso}	2.066	g_{\parallel}	2.242	$E_{1/2}\left(V,CV\right)$	-0.072
		269 (40540)			$\mathbf{A}_{ }$	181	$E_{1/2}$ (V, DPV)	-0.083
					g_{\perp}	2.049	$\Delta E_p (mV)$	206
					$g_{\parallel}\!/A_{\parallel}$	124	i_{pa}/i_{pc}	0.9
					G	5.1	$D (10^6 \text{ cm}^2 \text{ s}^{-1})$	7.8

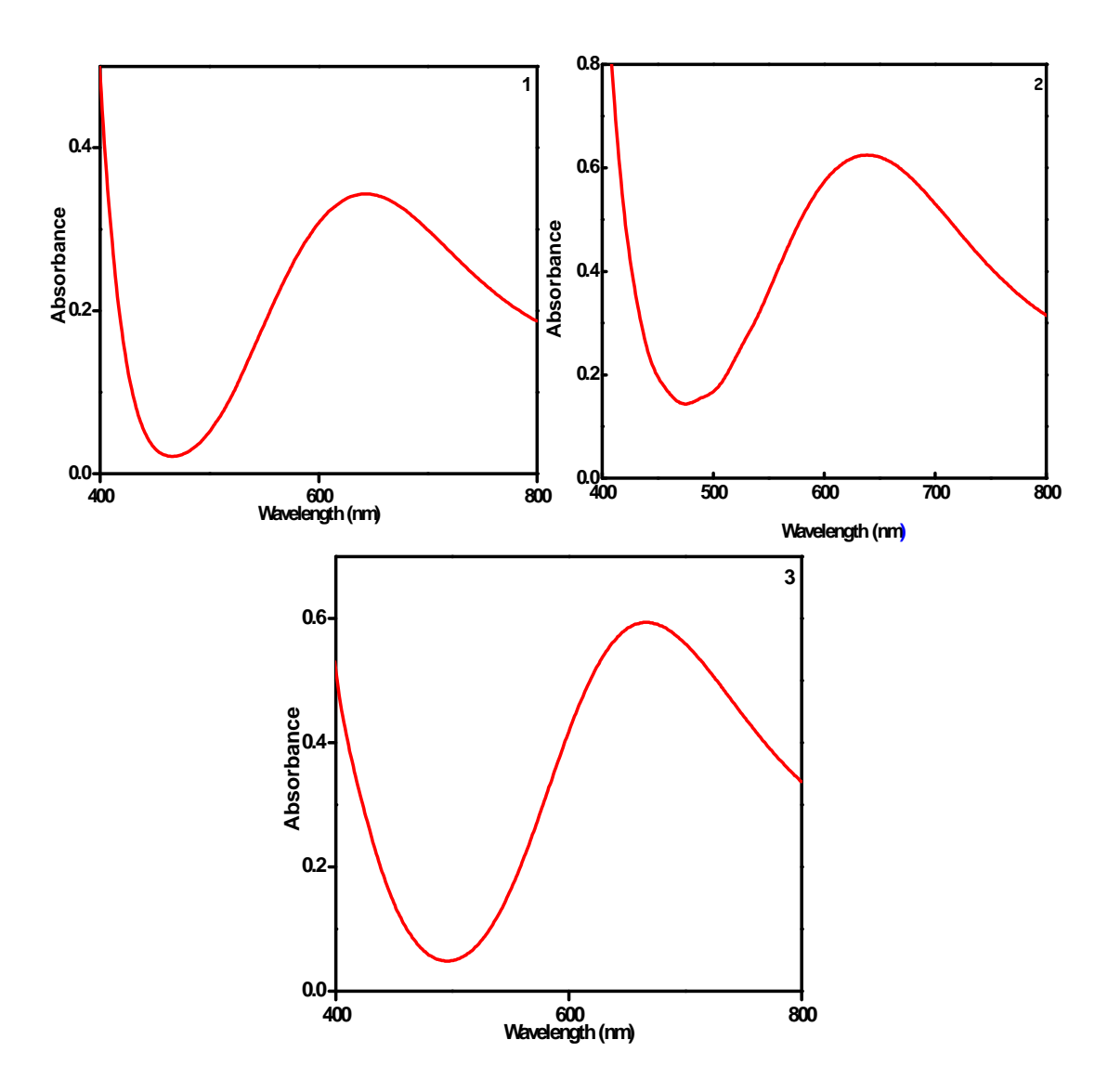


Figure 3.2 Electronic spectra of [Cu(bba)(bpy 1 / phen 2 / dpa 3)](ClO₄)₂ in DMF.

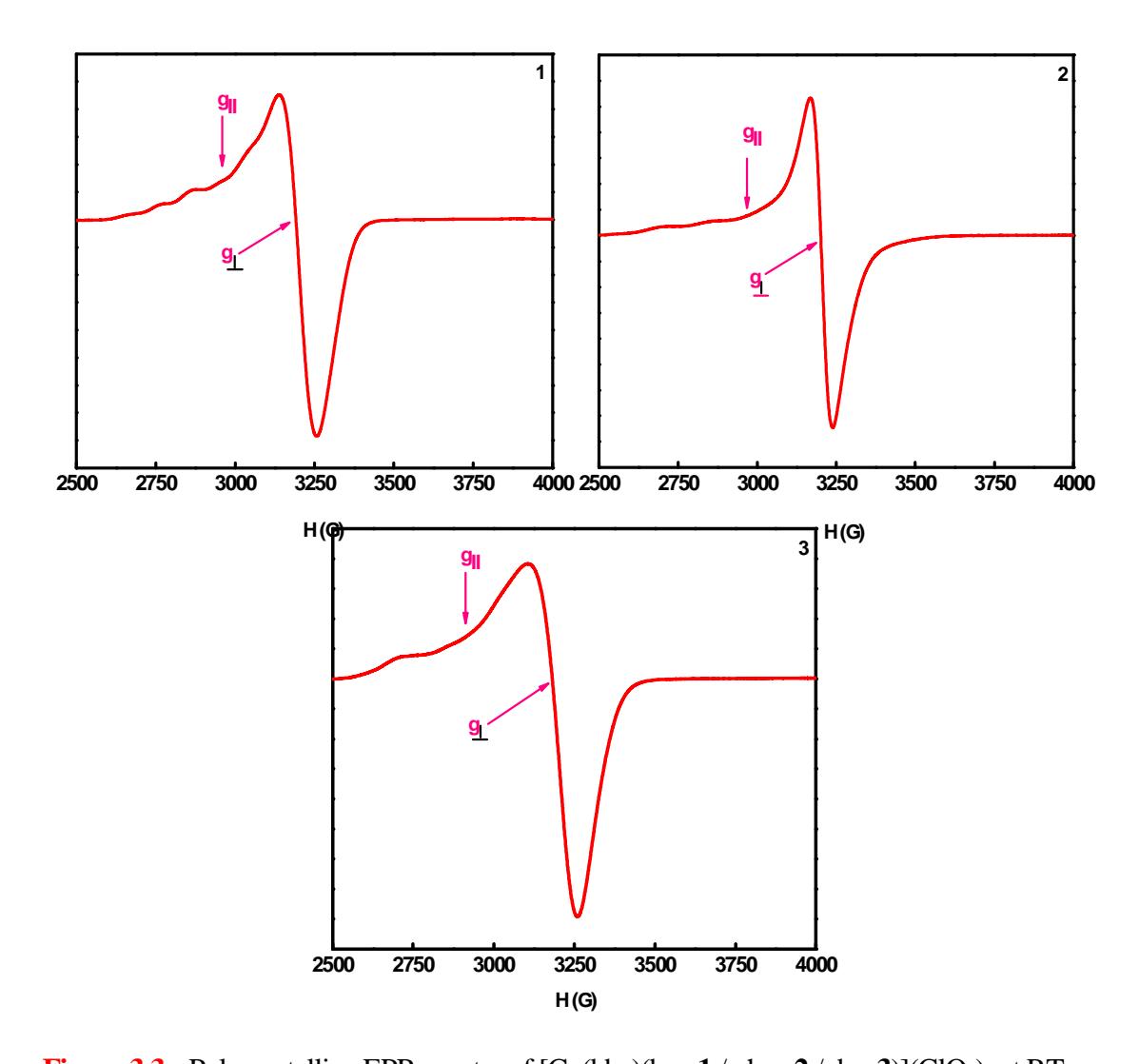


Figure 3.3 Polycrystalline EPR spectra of [Cu(bba)(bpy 1 / phen 2 / dpa 3)](ClO₄)₂ at RT.

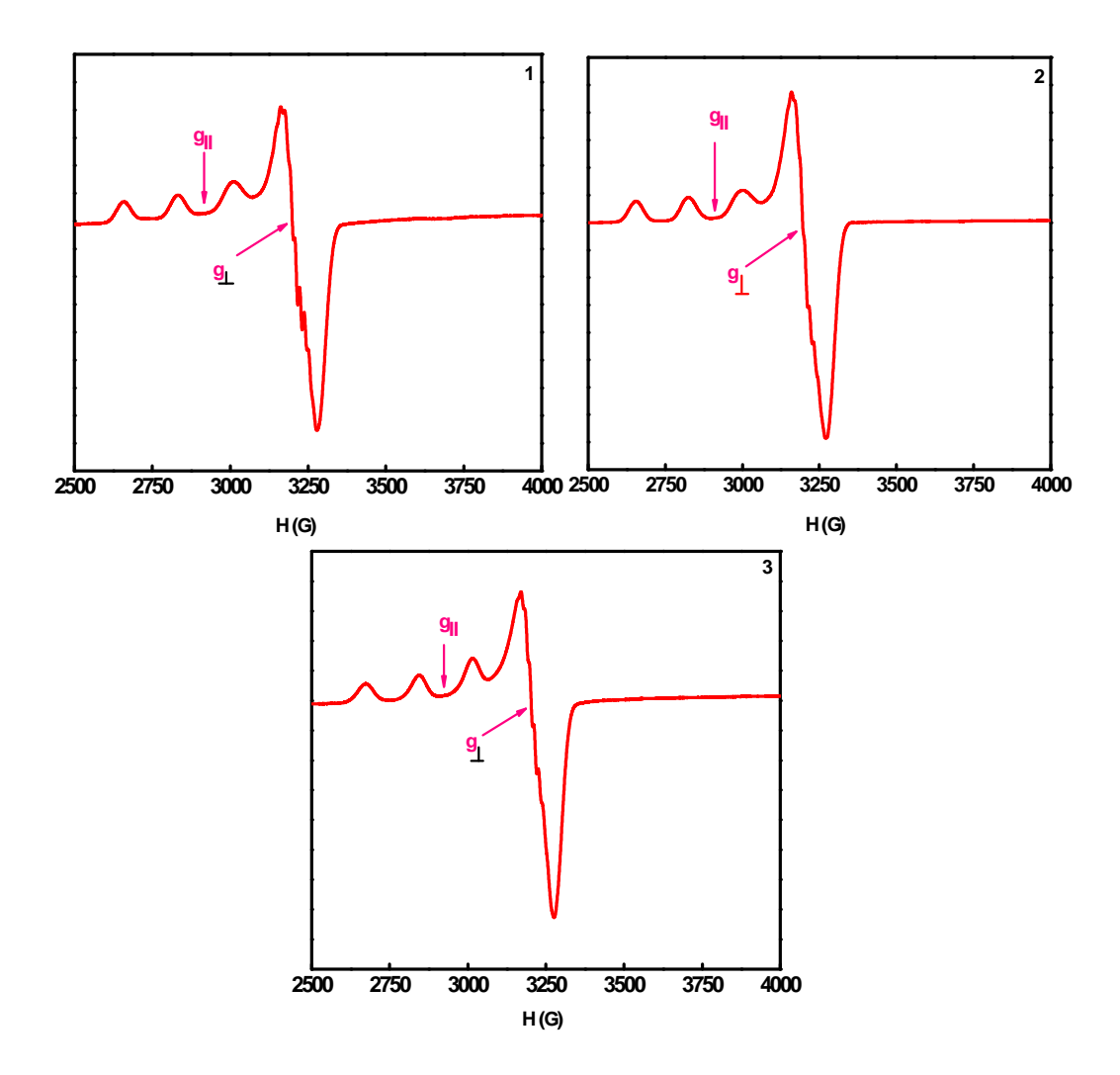


Figure 3.4 EPR spectra of [Cu(bba)(bpy 1 / phen 2 / dpa 3)](ClO₄)₂ in DMF at 77 K.

3.3.4 Electrochemical properties

The complexes are redox-active and show a one-electron quasi-reversible $(\Delta E_{\rm p}: 1, 198; 2, 128; 3, 206 \,\mathrm{mV})$ cyclic voltammetric responses in DMF (**Figure 3.5**) for the Cu(II)/Cu(I) couple $(E_{1/2}: 1, -0.074; 2, -0.074; 3, -0.072 \,\mathrm{V}$ vs SCE) with an $i_{\rm pa}/i_{\rm pc}$ ratio (1, 0.9; 2, 1.0; 3, 0.9) of unity. Though the $E_{1/2}$ values are similar, the $E_{\rm pa}$ $(1, -0.173; 2, -0.138; 3, -0.175 \,\mathrm{V})$ and $E_{\rm pc}$ $(1, 0.025; 2, -0.010; 3, 0.031 \,\mathrm{V})$ values suggest the stability order for the copper(I) species as 2 (phen) > 1 (bpy) > 3 (dpa). A greater stabilization of the Cu(I) species for the phen complex is related to the planar phenyl moiety enhancing the π -acidity of the ligand. Notably, 2 shows very low $\Delta E_{\rm p}$ value compared to 1 and 3 (**Table 3.3**), demonstrating the minimal structural reorganization between copper(II) and copper(I) species. It leads to a facile heterogeneous electron transfer [50] possibly due to the equatorial coordination of planar phen and bulky benzimidazoles of bba. The redox potential of the Cu^{II}/Cu^I couple from the DPV is -0.081 V (1), -0.077 (2) and -0.083 V (3) vs SCE (**Figures 3.6**).

3.3.5 DNA binding studies

DNA is an important cellular target of many metallodrugs for the treatment of multiple pathologies including cancer. Thus, the binding ability of the complexes **1-3** with calf thymus (CT) DNA is characterized by measuring the effects on absorption, emission, and circular dichroism spectral and electrochemical techniques. The absorption spectra of **1-3** in the absence and presence of CT DNA at different concentrations R=25 (R=[DNA] / [Cu complex]; **Figure 3.7**) show interesting changes in the intensity of the intraligand absorption band (**Table 3.4**). This suggests the hypochromism for **1-3**, typical of the metal complex's association with the DNA helix.

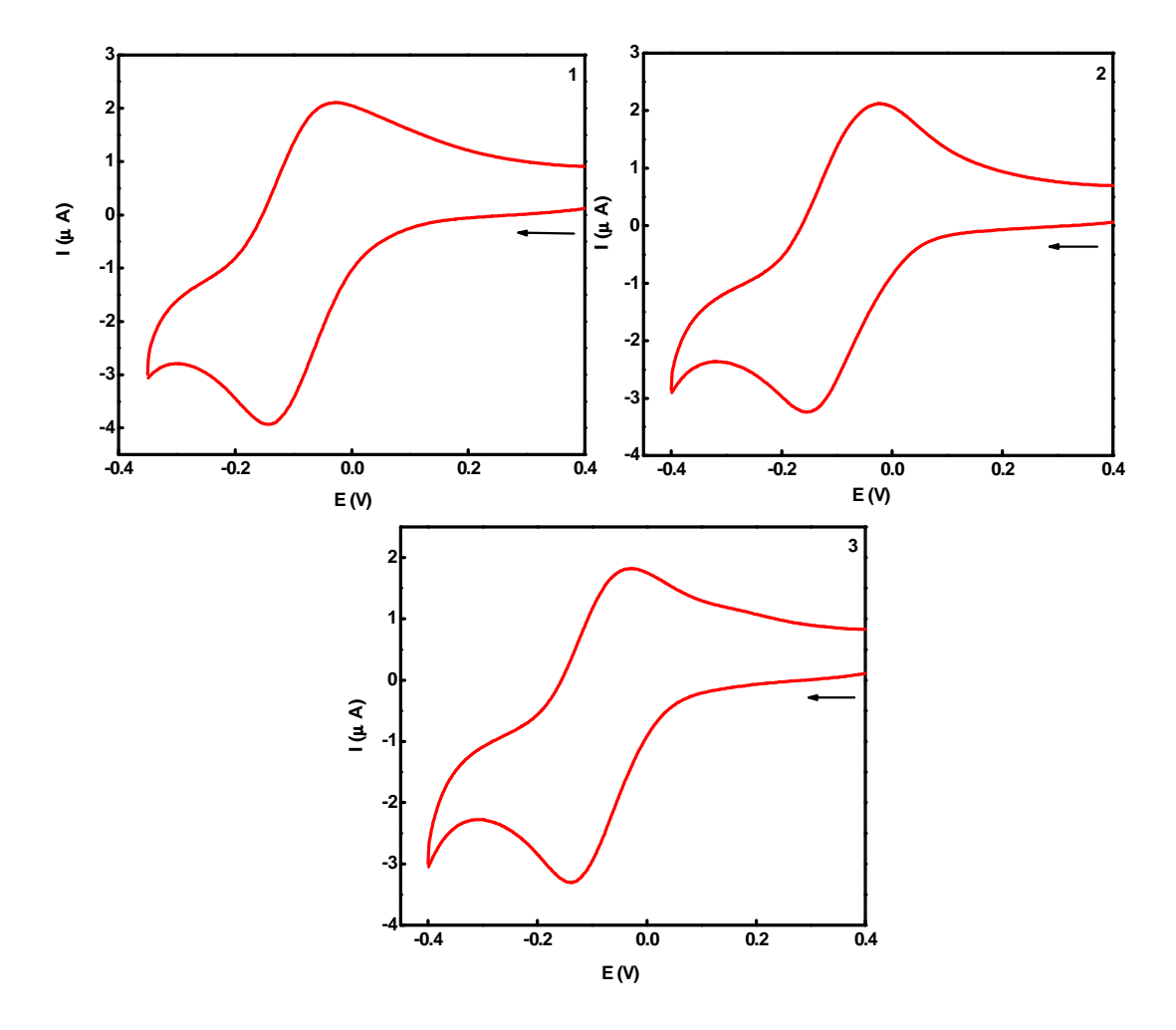


Figure 3.5 Cyclic voltammograms of [Cu(bba)(bpy 1 / phen 2 / dpa 3)](ClO₄) $_2$ at 50 mV s⁻¹ scan rate in DMF.

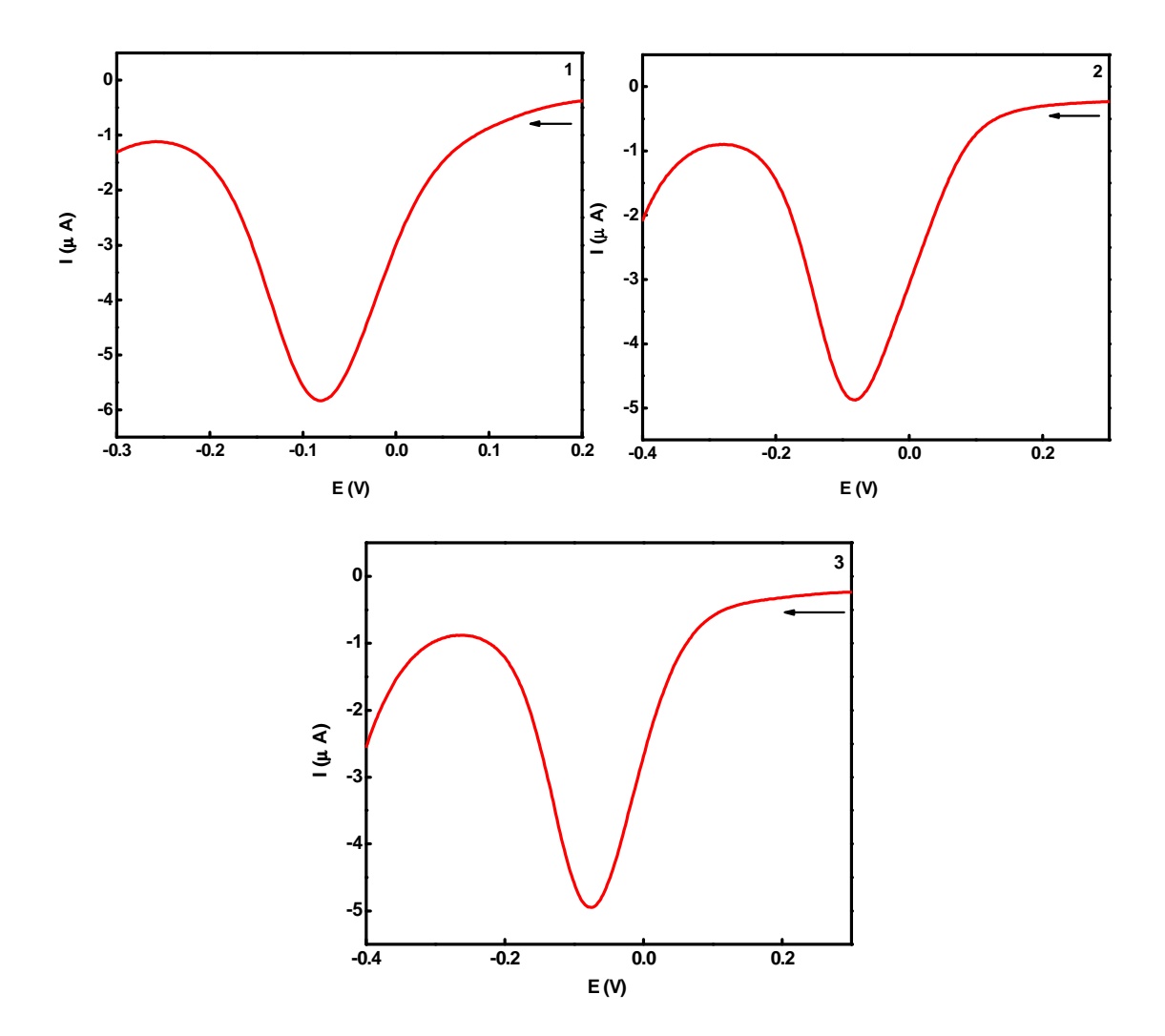


Figure 3.6 Differential pulse voltammogram of [Cu(bba)(bpy 1 / phen 2 / dpa 3)](ClO₄)₂ at 2 mV s⁻¹ scan rate in DMF

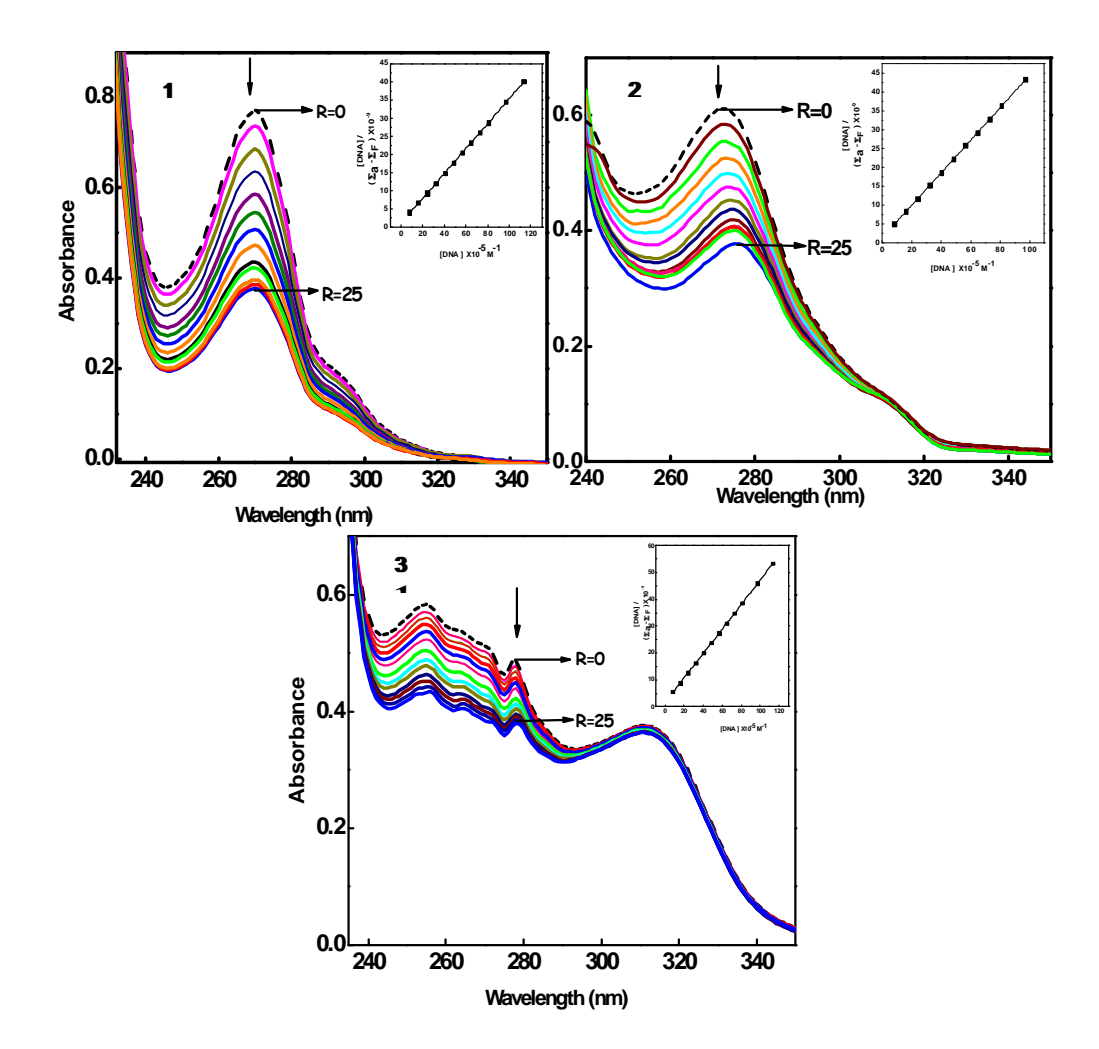


Figure 3.7 Absorption spectra of [Cu(bba)(bpy/phen/dpa)](ClO₄)₂ **1-3** (2.7 × 10⁻⁵ M) in 2% DMF/5mM Tris-HCl/50 mM NaCl buffer at pH 7.1 in the absence (R = 0) and presence (R = 25) of increasing amounts of CT DNA. Inset: Plot of [DNA] vs [DNA]/(ϵ_a - ϵ_f) at R = 25 of **1-3**.

The strong hypochromic effect (61%) along with the 3 nm red shift for 2 reveals the partial intercalative [51] interaction through the active participation of planar phen moiety with DNA. However, the lack of red shift suggests that the binding mode of 1 and 3 (hypochromic effect: 1, 56; 3, 48%) was not intercalative. Because the bulky structure of the complexes as well as the co-ligand is non-planar bpy (1) or dpa (3), the bzim rings cannot completely intercalate. When one of the two bzim rings inserts into the helix, the other ring extends away from the plane due to the stereochemistry effect hence decreasing the effective area of overlap. Therefore, the observed spectral changes were rationalized in terms of feeble intercalation via bzim moiety in 1 and 3. To further illustrate the DNA binding strength, the intrinsic binding constant K_b was determined for 1-3 (Table 3.4) which were found to be $3.26 \times 10^4 \,\mathrm{M}^{-1}$ (1), $3.49 \times 10^4 \,\mathrm{M}^{-1}$ (2), $3.11 \times 10^4 \,\mathrm{M}^{-1}$ (3). The binding constants were lower compared to classical intercalators (EthBr-DNA, $1.4 \times 10^6 \text{ M}^{-1}$) [52], the diminution could be explained by the steric constraints imposed by the ligand framework thus encouraging a partial intercalative binding mode for these complexes and it was found for many other compounds with the same order of K_b values [53].

The observed circular dichroic (CD) spectrum of CT DNA consists of a positive band at 273 nm owing to base stacking and a negative band at 243 nm owing to helicity which is typical of DNA in right-handed B-form. Upon incubation of CT DNA with 1-3, shows conformational changes: (i) the intensity of both the bands of CT DNA increases (1 and 3) with the red shift of 2-3 nm in the positive band and (ii) the intensity of positive band increases while the intensity of the negative band decreases (2) with the red shift of 3 nm in the positive band (Figure 3.8). These observations are consistent with the partial intercalative interaction through planar phen moiety (2) or bzim moiety (1 and 3) supporting the results from UV-vis spectroscopy.

Table 3.4Ligand-based absorption spectral properties^a and fluorescence spectral properties^b of copper(II) complexes bound to CT DNA

Complex	$\begin{matrix} \lambda_{max} \\ (nm) \end{matrix}$	R	Change in Absorbance	Δε (%)	$K_b \times 10^4 \mathrm{M}^{-1})$	K_{app} (× 10^5 M^{-1})
[Cu(bba)(bpy)](ClO ₄) ₂ 1	270	25	Hypochromism	48	3.2 ± 0.1	1.5
[Cu(bba)(phen)](ClO ₄) ₂ 2	272	25	Hypochromism	61	3.4 ± 0.1	2.0
$[Cu(bba)(dpa)](ClO_4)_2$ 3	277	25	Hypochromism	56	3.1 ± 0.1	1.0

^aMeasurements were made at R=25, where R=[DNA]/[complex], concentration of solutions of copper(II) complexes = $2.5-2.7\times10^{-5}$ M (1-3).

^bApparent DNA binding constant from ethidium bromide displacement assay using increasing concentration (0-10 μM) of **1-3**.

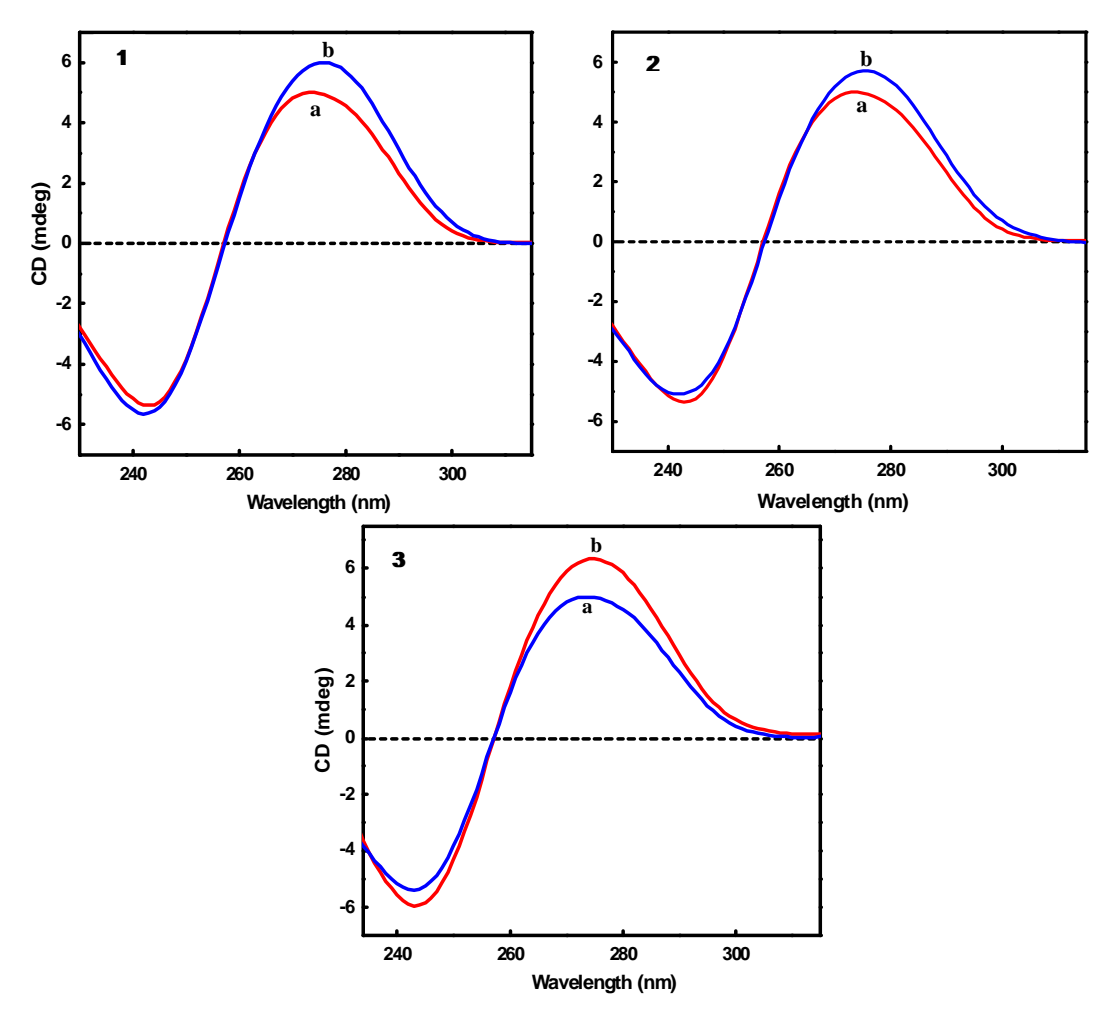


Figure 3.8 Circular dichroism spectra of CT DNA in 2% DMF/5mM Tris-HCl/50 mM NaCl buffer at pH 7.1 and 25 °C in absence (a) and presence (b) of 1-3 at 1/R value of 3.

In a competitive DNA binding experiment, with increasing amounts of 1-3, the fluorescence intensity of the CT DNA-EthBr system (594 nm) was quenched (1, 89; 2, 96; 3, 76%) with the red shift of 5 nm (2) or 1 nm (1) or no shift (3), which was due to the partial intercalation of copper(II) complexes to DNA base pairs displacing some EthBr from CT DNA-EthBr system (Figure 3.9) [54]. The quenching data (K_{sv}) were analyzed according to the Stern-Volmer equation and the binding constant (K_{app}) value obtained using the equation, $K_{EthBr}[EthBr] = K_{app}[Cu(II) Complex]$. The $K_{\text{sv}}(\mathbf{1}, 1.55 \times 10^4; \mathbf{2}, 5.40 \times 10^4; \mathbf{3}, 1.01 \times 10^4 \,\text{M}^{-1}) \text{ and } K_{\text{app}}(\mathbf{1}, 1.54 \times 10^5; \mathbf{2}, 2.06 \times 10^5;$ 3, 1.03×10^5 M⁻¹) values (**Table 3.4**) indicate that the complex 2 binds more strongly (via planar phen moiety) than the complexes 1 and 3 (via bzim moiety) through partial intercalative mode. The cyclic voltammograms of the complexes (Table 3.5) in the absence of DNA reveal a non-Nernstian but a fairly quasi-reversible (ΔE_p : 1, 110; 2, 128; 3, 111 mV) one-electron redox process (i_{pa}/i_{pc} : 1, 1.0; 2, 1.2; 3, 1.0) involving the Cu(II)/Cu(I) couple ($E_{1/2}$: 1, -0.089; 2, -0.091; 3, -0.085 V vs SCE). Upon the addition of excess DNA (r = 5), the complexes show a significant reduction in both cathodic and anodic peak currents (**Figure 3.10**) and reveal quasi-reversible (ΔE_p : 1, 156; 2, 129; 3, 116 mV) one electron (i_{pa}/i_{pc} : 1, 1.0; 2, 1.1; 3, 1.2) electrochemical behavior for Cu(II)/Cu(I) couple ($E_{1/2}$: 1, -0.193; 2, -0.191; 3, -0.198 V vs SCE). Interestingly, the reduction in both the peak currents indicates that the complexes bind through the partial intercalative mode and cause slow diffusion of an equilibrium mixture of the free and DNA-bound complexes to the electrode surface.

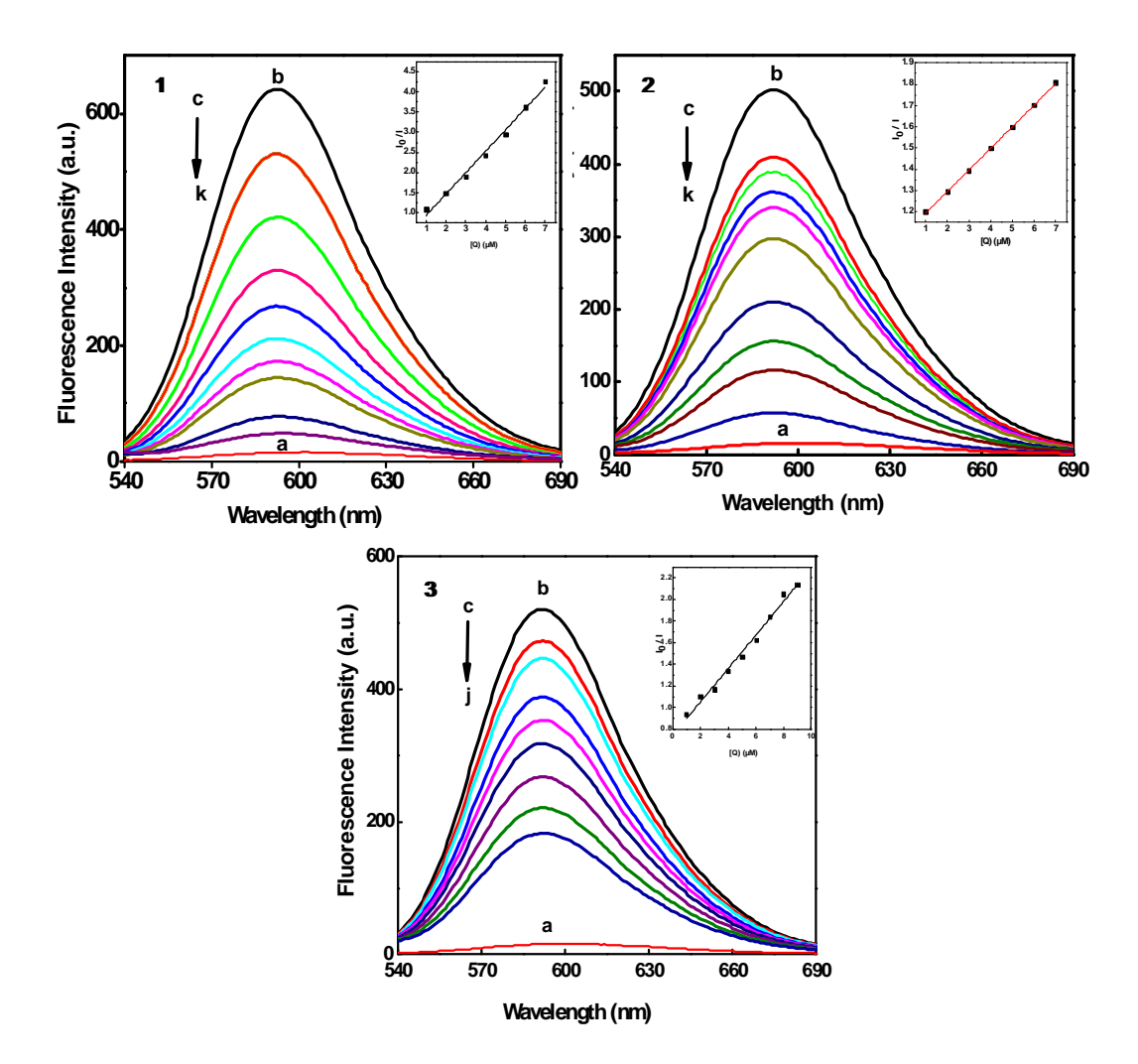


Figure 3.9 Fluorescence quenching curves of ethidium bromide bound to DNA in 2% DMF/5mM Tris-HCl/50 mM NaCl buffer at pH 7.1: (a) EthBr (1.25 μ M); (b) EthBr+DNA (125 μ M); (c-k) EthBr+DNA+ **1-3** (0-10 μ M). Inset: Plot of I_O/I vs [complex] of **1-3**.

Table 3.5 Electrochemical behaviour^{a,b} of the copper(II) complexes on interaction with CT DNA (r = [base-pair]/[Cu(II) complex]

	$_{ m r}$ $_{ m pc}^{ m E_{pc}}$		E_{pa}	E 1/2 (V) CV DPV		; /;	ΔE_p	$\Delta E_{1/2}$	V/V
	1	(V)	(V)	CV	DPV	1 _{pc} /1 _{pc}	(mV)	(V)	K ₊ / K ₂₊
1	0	-0.144	-0.034	-0.089	-0.083	1.0	110	-106	0.02
	5	-0.271	-0.115	-0.193	-0.189	1.0	156		
2	0	-0.155	-0.027	-0.091	-0.084	1.2	128	-104	0.02
	5	-0.255	-0.126	-0.191	-0.188	1.1	129		
3	0	-0.140	-0.029	-0.085	-0.076	1.0	111	-127	0.01
	5	-0.261	-0.145	-0.198	-0.203	1.2	116		

 $[^]aMeasured$ vs. SCE; scan rate: 50 mV s $^{\text{-1}}$; supporting electrolyte: 2% DMF - 5 mM Tris-HCl/50 mM NaCl; complex concentration: $0.5\times10^{\text{-3}}$ M.

Further, the observed shifts (104-127 mV) in $E_{1/2}$ values (DPV) to more negative potentials (**Figure 3.11**) suggest that both Cu(II) and Cu(I) forms of the present complexes bind to DNA but with Cu(II) displaying higher DNA binding affinity than Cu(I) form, which is substantiated by the ratio of the equilibrium constants (K_+/K_{2+}) [55]. The K_+/K_{2+} values (1, 0.02; 2, 0.02; 3, 0.01) are far less than unity (**Table 3.5**) suggesting preferential stabilization of Cu(II) form over Cu(I) form on binding to DNA.

^bDifferential pulse voltammetry (DPV), scan rate 2 mV s⁻¹, pulse height 50 mV.

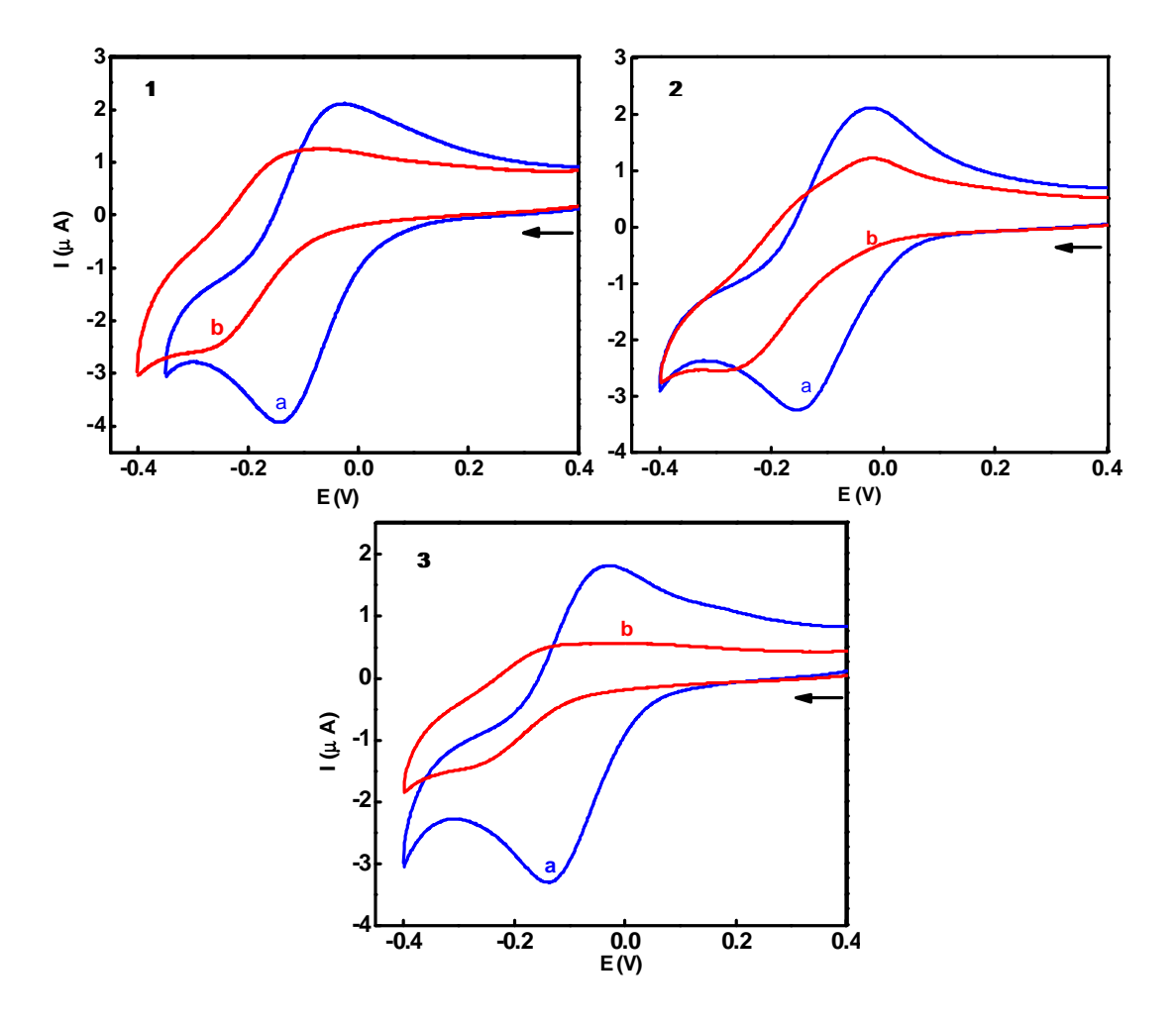


Figure 3.10 Cyclic voltammograms of 1-3 (0.5 mM) in the absence (a) and presence (b) of CT DNA (R = 5) at 25.0 ± 0.2 °C at 50 mV s⁻¹ scan rate in 2% DMF/5mM Tris-HCl/50 mM NaCl buffer at pH 7.1.

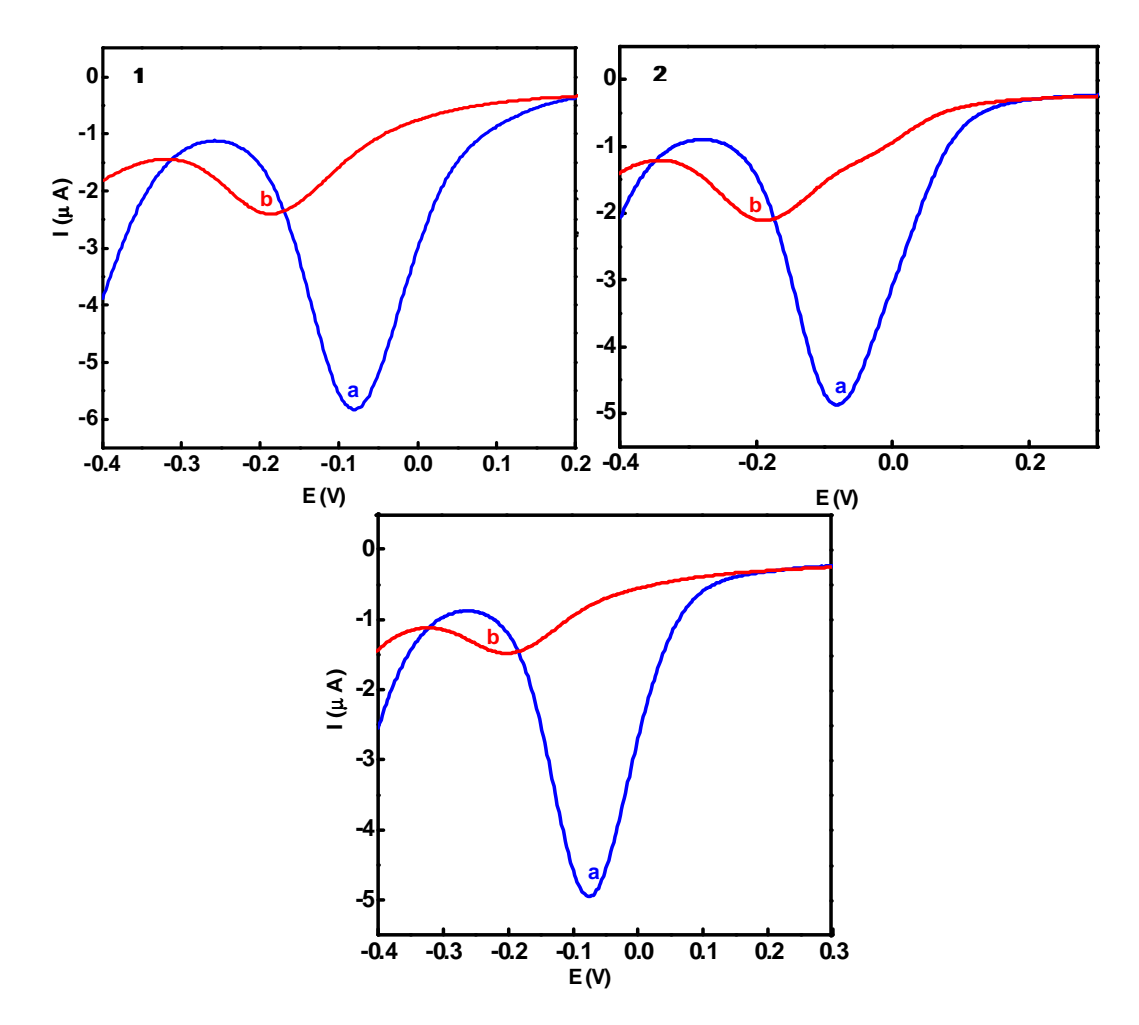


Figure 3.11 Differential pulse voltammograms of 1-3 (0.5 mM) in the absence (a) and presence (b) of CT DNA (R = 5) at 25.0 ± 0.2 °C at 2 mV s⁻¹ scan rate in 2% DMF/5mM Tris-HCl/50 mM NaCl buffer at pH 7.1.

3.3.6 Protein binding studies

Three intrinsic flours present in the protein, such as tryptophan, tyrosine, and phenylalanine residues are responsible for the fluorescence of protein. The intrinsic fluorescence of many proteins is caused mainly by tryptophan alone. Fluorescence quenching corresponds to any process, which is a reduction of the fluorescence intensity from a fluorophore due to a variety of molecular interactions such as molecular rearrangements, reactions at excited-state, energy transfer ground-state complex formation, and collisional quenching. Thus, the emission spectra of BSA (λ_{em} , 340 nm; λ_{ex} , 280 nm) in the presence of increasing concentrations of 1-3 were recorded at 300 K and 310 K. The fluorescence intensity of BSA decreased regularly (Figure 3.12), up to 61.6-74.4% (300 K) and 67.2-71.0% (310 K), accompanied by a hypsochromic shift of 3-14 nm (1 and 2) and bathochromic shift of 4-9 nm (3). The Stern-Volmer plots (Figure 3.13) are linear [K_{SV}: 300 K, 3.16 (1); 2.45 (2); 2.01×10^5 M⁻¹ (3) and 310 K, 3.58 (1); 2.79 (2); $2.15 \times 10^5 \,\mathrm{M}^{-1}$ (3)] and suggest that a single quenching mechanism, either static or dynamic is occurred at these concentrations [56]. The quenching rate constant (k_a) is on the order of 10^{13} M⁻¹s⁻¹, which is 1000-fold higher than the maximum limit $(2.0 \times 10^{10} \,\mathrm{M}^{-1} \mathrm{s}^{-1})$ [57], which indicates that the quenching is not initiated by the dynamic collision but from the formation of the complex. Also, when the temperature is raised $(300 \text{ K}, \mathbf{1}, 2.07; \mathbf{2}, 1.74; \mathbf{3}, 1.05 \times 10^5 \text{ M}^{-1} \text{ and } 310 \text{ K}, \mathbf{1}, 2.31; \mathbf{2}, 2.14; \mathbf{3}, 2.21 \times 10^5 \text{ M}^{-1}),$ the effective quenching constant, Ka (Table 3.6) derived using the modified Stern-Volmer equation (Figure 3.14) [66], increases. On the other hand, upon addition of 1-3 to BSA, a significant decrease in 210 nm absorbance peak of BSA is observed (Figure 3.15), which is attributed, to the induced perturbation of α -helix of BSA.

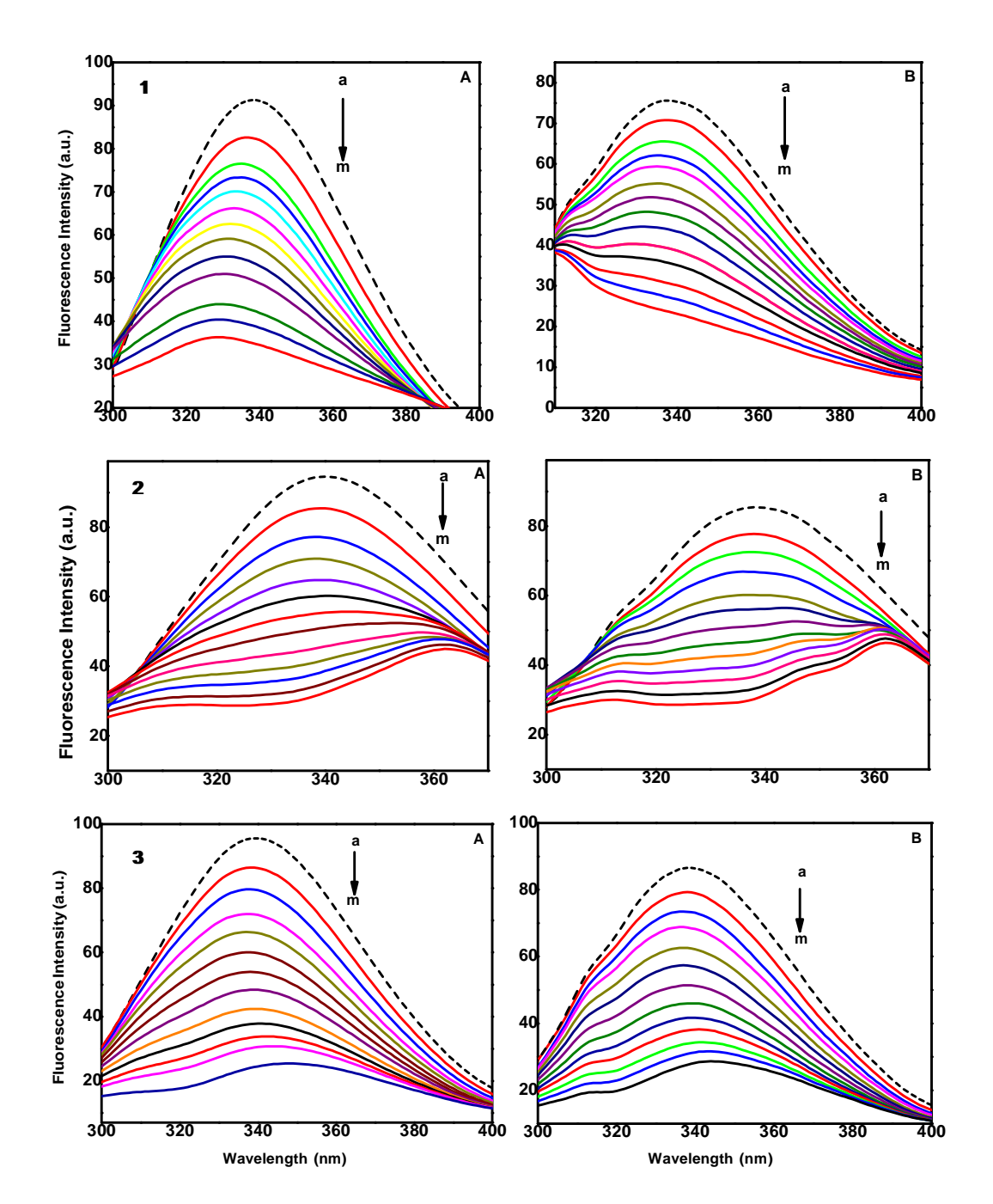


Figure 3.12 Changes in the fluorescence spectra of BSA through the titration with 1-3 at 300 K (left), and 310 K (right). The concentration of BSA is 1×10^{-6} mol L^{-1} , and the concentration of 1-3 was varied from (a) 0.0 to (k) 4.0×10^{-6} mol L^{-1} ; pH 7.4 and λ_{ex} 280 nm.

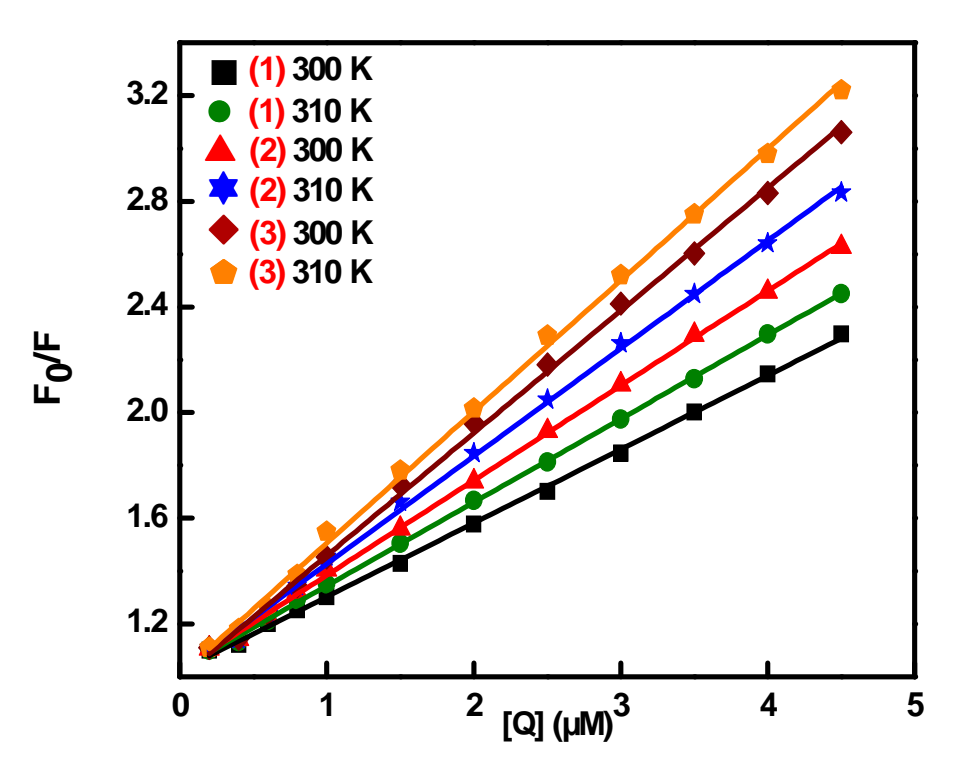


Figure 3.13 The Stern-Volmer plots of BSA on different temperature for 1, 2 and 3. $\lambda_{ex} = 280$ nm; pH = 7.4.

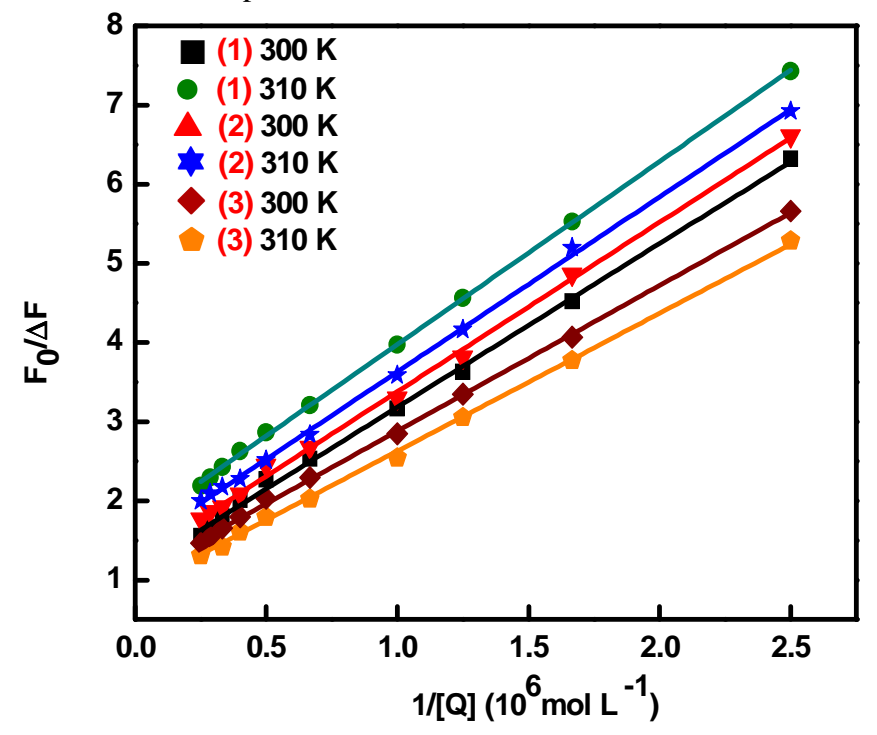


Figure 3.14 The modified Stern-Volmer plots of BSA on different temperature for 1, 2 and 3. $\lambda_{ex} = 280$ nm; pH = 7.4.

Table 3.6Quenching, association, binding and thermodynamic parameters of the interaction of **1-3** with BSA at different temperatures^a

Parameters	300 K	R	310 K	R
[Cu(bba)(bpy)](ClO ₄) ₂ 1				
$K_{SV} (10^5 \mathrm{M}^{-1}) \pm \mathrm{SD}$	3.164 ± 0.002	0.9995	3.582 ± 0.003	0.9989
$k_q (10^{13} M^{-1} s^{-1})$	3.164		3.582	
$K_a (10^5 M^{-1}) \pm SD$	2.065 ± 0.031	0.9980	2.311 ± 0.014	0.9996
$K_b (10^5 M^{-1}) \pm SD$	0.830 ± 0.112	0.9954	0.420 ± 0.048	0.9990
$n \pm SD$	0.877 ± 0.018		0.860 ± 0.008	
$\Delta H^{\circ} (kJ \text{ mol}^{-1})$	79.210			
$\Delta S^{\circ} (J \text{ mol}^{-1} \text{ K}^{-1})$	103.373		100.910	
$\Delta G^{\circ} (kJ \text{ mol}^{-1})$	-30.932		-30.203	
[Cu(bba)(phen)](ClO ₄) ₂ 2				
$K_{SV} (10^5 \mathrm{M}^{-1}) \pm \mathrm{SD}$	2.451 ± 0.005	0.9986	2.786 ± 0.003	0.9993
$k_q (10^{13} M^{-1} s^{-1})$	2.451		2.786	
$K_a (10^5 M^{-1}) \pm SD$	1.739 ± 0.026	0.9980	2.138 ± 0.032	0.9980
$K_b (10^5 M^{-1}) \pm SD$	0.730 ± 0.121	0.9943	0.606 ± 0.061	0.9986
$n \pm SD$	0.859 ± 0.020		0.875 ± 0.010	
$\Delta H^{\circ} (kJ \text{ mol}^{-1})$	77.833			
$\Delta S^{\circ} (J \text{ mol}^{-1} \text{ K}^{-1})$	101.741		101.070	
$\Delta G^{\circ} (kJ \text{ mol}^{-1})$	-30.444		-31.254	
[Cu(bba)(dpa)](ClO ₄) ₂ 3				
$K_{SV} (10^5 \mathrm{M}^{-1}) \pm \mathrm{SD}$	2.008 ± 0.006	0.9984	2.154 ± 0.006	0.9982
$k_q (10^{13} M^{-1} s^{-1})$	2.008		2.154	
$K_a (10^5 M^{-1}) \pm SD$	1.046 ± 0.017	0.9992	2.209 ± 0.022	0.9991
$K_b (10^5 \mathrm{M}^{-1}) \pm \mathrm{SD}$	1.426 ± 0.064	0.9986	0.789 ± 0.062	0.9986
$n \pm SD$	0.897 ± 0.010		0.878 ± 0.010	
$\Delta H^{\circ} (kJ \text{ mol}^{-1})$	78.066			
$\Delta S^{\circ} (J \text{ mol}^{-1} \text{ K}^{-1})$	102.188		101.212	
ΔG° (kJ mol ⁻¹)	-30.578		-31.298	

^aR is the linear correlated coefficient.

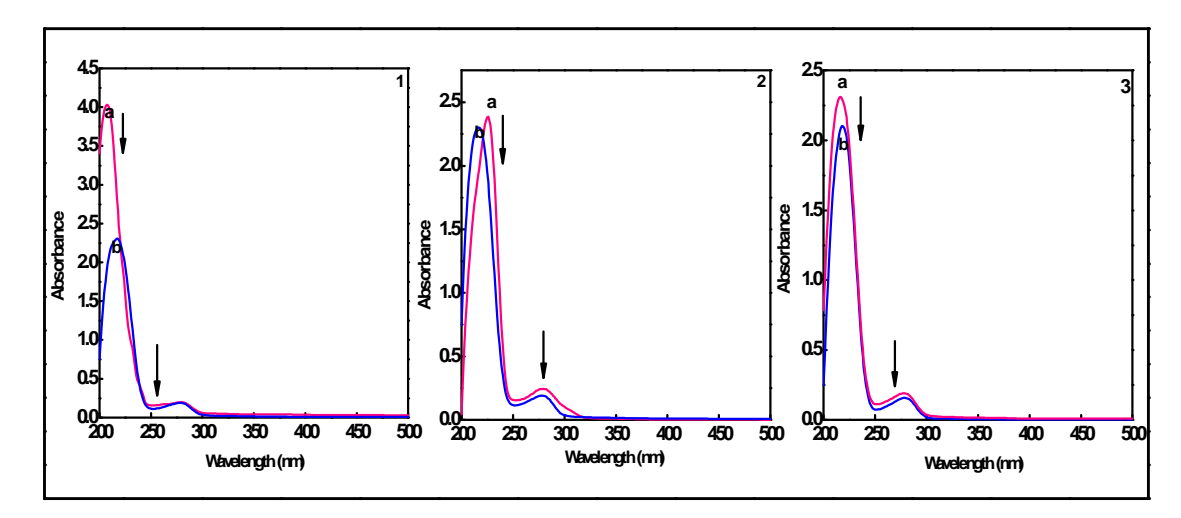


Figure 3.15 UV-Vis absorption spectra of BSA in the absence and presence of 1-3. (a) Absorption spectrum of BSA. (b) Absorption spectrum of BSA in the presence of 1, 2 and 3 at the same concentration, [BSA] = [Cu complex] = 3.5×10^{-6} mol L⁻¹. The absorbance of 1, 2 and 3 is negligible in the spectral region shown.

Meanwhile, the absorption intensity of the 280 nm band is increased due to the alteration in the microenvironment of three amino acid residues followed by the disturbance of the tertiary structure of BSA. Therefore the interaction between 1-3 and BSA leads to an adduct species which undergoes mainly a static quenching process [58]. The binding constant K_b (Figure 3.16) is decreased with increasing temperature [300 K, 0.83 (1); 0.73 (2); 1.42 × 10⁵ M⁻¹ (3) and 310 K, 0.42 (1); 0.60 (2); 0.78 × 10⁵ M⁻¹ (3)], which indicates the formation of stable BSA-(1/2/3) adduct and the number of binding site n is equal to 0.9 (Table 3.6) corresponds to the existence of a single binding site. So, the results suggest that the complex binds to the hydrophobic pocket located in subdomain IIA [59]. To elucidate the interaction forces of 1-3 with BSA, the thermodynamic parameters were calculated (Table 3.6). The spontaneity of the interaction is revealed by the negative ΔG value.

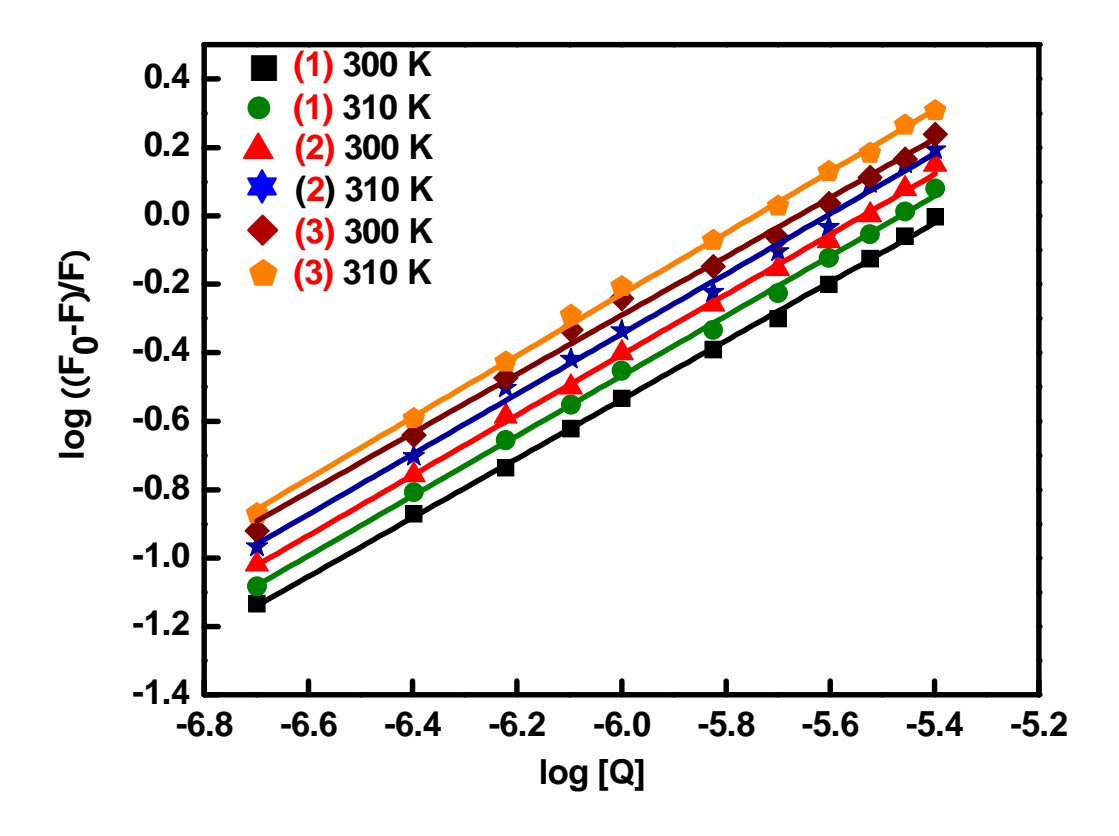


Figure 3.16 Double-log plot of quenching effect of 1, 2 and 3 on BSA fluorescence at pH = 7.4.

The positive values obtained for both ΔH and ΔS indicate that a hydrophobic association is the major binding force and that the interaction is entropy- driven process [60]. Therefore, hydrophobic forces may play the main role in the binding of 1-3 to BSA. In addition to hydrophobic interaction, a possible covalent bonding may be also considered, instead, the ΔH value obtained (78-79 kJ mol⁻¹) is less than the expected value for a covalent bond formation (\geq 120 kJ mol⁻¹) [61].

According to the theory of Miller [62], when $\Delta\lambda$ between excitation wavelength and the emission wavelength is set at 15 or 60 nm, the synchronous fluorescence gives information about the molecular environment in the vicinity of tyrosine and tryptophan residues, respectively. The synchronous fluorescence spectra of BSA with various amounts of 1-3 were recorded at $\Delta\lambda = 15$ nm and $\Delta\lambda = 60$ nm (Figure 3.17). It is apparent that the emission maxima of tyrosine and tryptophan residues have significant blue-shifted (tyrosine: 1, 314-299; 2, 314-308; 3, 314-303 nm and tryptophan: 1, 346-338; 2, 346-343; 3, 346-339 nm). The blue shift expressed that the conformation of BSA was changed, leading to the decrease in polarity and increase in hydrophobicity around the tyrosine and tryptophan residues. For BSA-(1/2/3) system, the synchronous fluorescence quenching ratios (Figure 3.18), RSFQ at $\Delta\lambda = 60$ nm (1, 74.7; 2, 70.3; 3, 72.1%) is greater than the corresponding one for $\Delta\lambda = 15$ nm (1, 55.0; 2, 45.6; 3, 60.1%), indicating that 1-3 reached sub-domain IIA, where the only one Trp 212 residues on BSA was located.

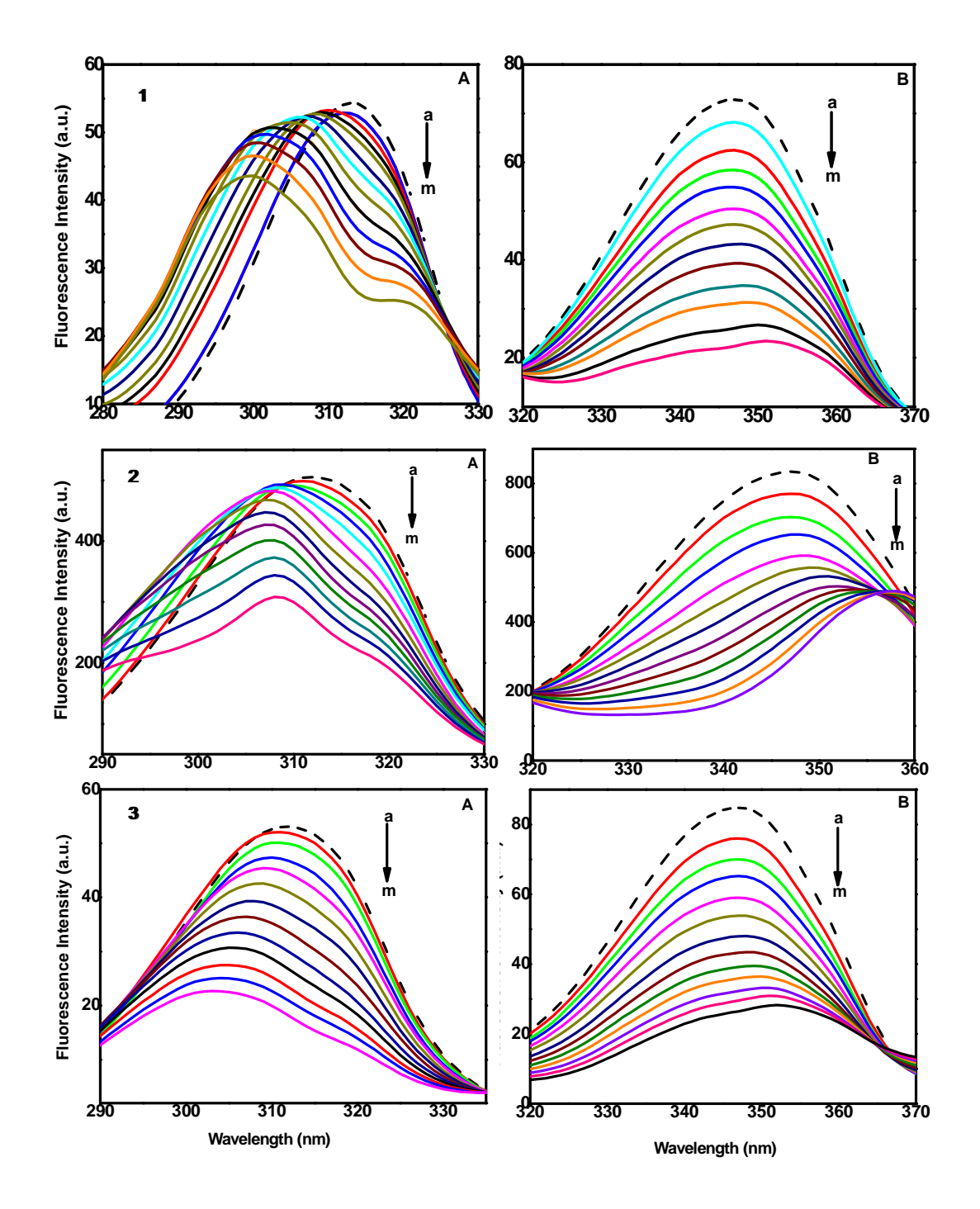


Figure 3.17 Synchronous fluorescence spectra of BSA $(1 \times 10^{-6} \text{ mol } \text{L}^{-1})$ upon addition of **1-3**; $\Delta\lambda = 15$ nm (left, A) and $\Delta\lambda = 60$ nm (right, B). The concentration of **1-3** varied from (a) 0.0 to (j) 4.0×10^{-6} mol L^{-1} .

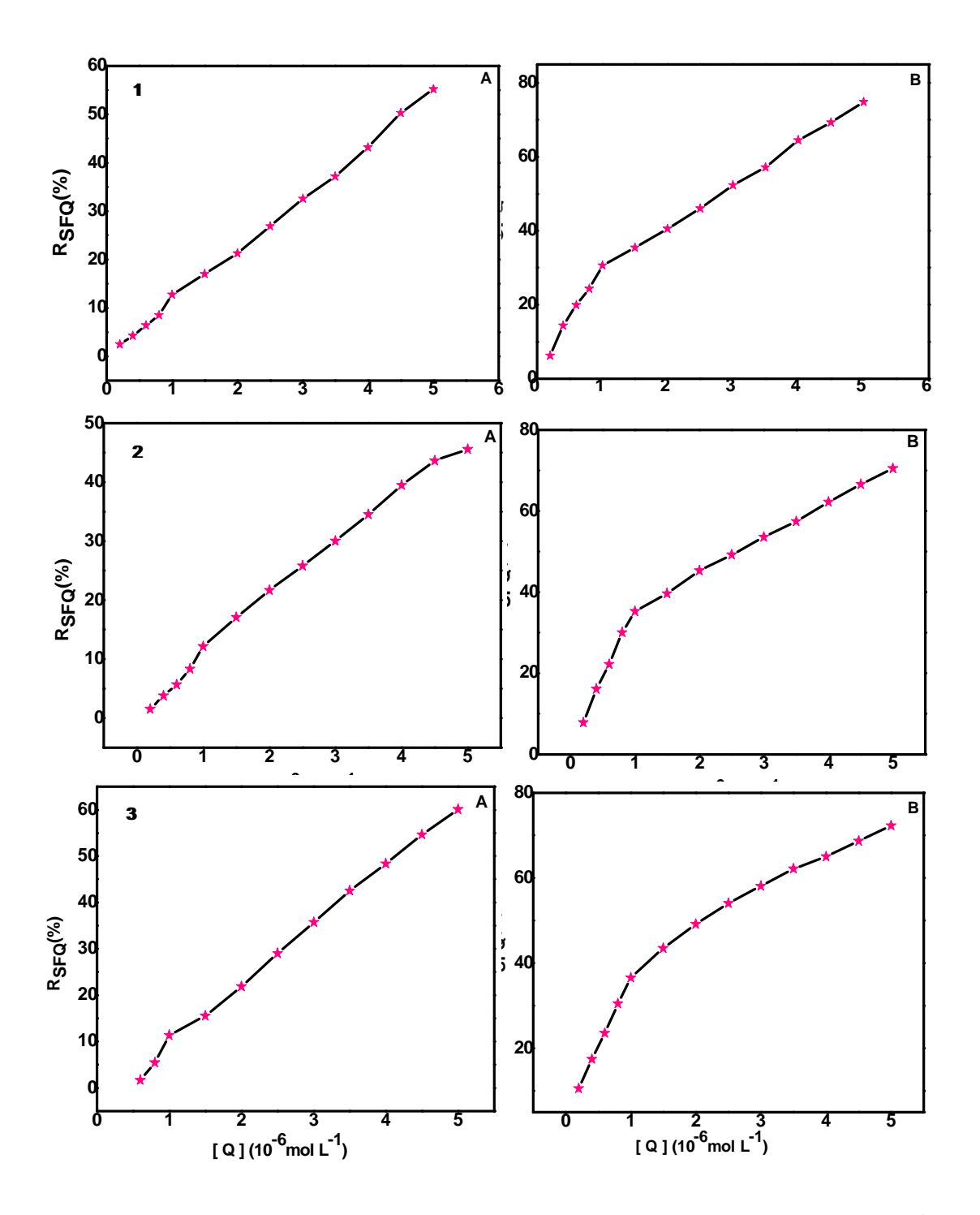


Figure 3.18 Ratios of synchronous fluorescence quenching (R_{SFQ}) of BSA (1×10^{-6} mol L^{-1}) upon addition of **1-3**; $\Delta\lambda = 15$ nm (A) and $\Delta\lambda = 60$ nm (B). The concentration of **1-3** varied from (a) 0.0 to (j) 3.5×10^{-6} mol L^{-1} .

To estimate the distance between the buried Trp-212 (as donor) and the interacted complex (as acceptor), Förster's non-radiative energy transfer theory (FRET) [63] was adopted. The overlap of the UV absorption spectra of Cu(II) complexes with the fluorescence emission spectra of BSA is made (Figure 3.19). The energy transfer efficiency is not only depending on the distance between the donor and acceptor, but also on the critical energy transfer distance (r), which should be less than 8 nm. According to the Förster's equations (Table 3.7), we obtain $J(\lambda)$ (1, 4.33; 2, 8.02; 3, $3.08 \times 10^{15} \,\mathrm{M}^{-1}\mathrm{cm}^{3}$), R_{0} (1, 1.46; 2, 3.18; 3, 2.06 nm), E (1, 0.18; 2, 0.09; 3, 0.08) and r (1, 6.61; 2, 3.80; 3, 2.14 nm). The donor (Trp 212 in BSA) to acceptor (1-3) distance (r) is less than 8 nm [58], indicating that the non-radiative energy transfer from BSA to Cu(II) complexes occurs with high possibility. These accord with the conditions of FRET, indicating again the static quenching interaction between Cu(II) complexes and BSA [64].

Table 3.7Förster's energy transfer parameters of the interaction of Cu(II) complexes with BSA

	E	$J \times 10^{15} (M^{-1} cm^{-1})$	R_0 (nm)	r (nm)
1	0.18	4.33	1.46	6.61
2	0.09	8.02	3.18	3.80
3	0.08	3.08	2.06	2.14

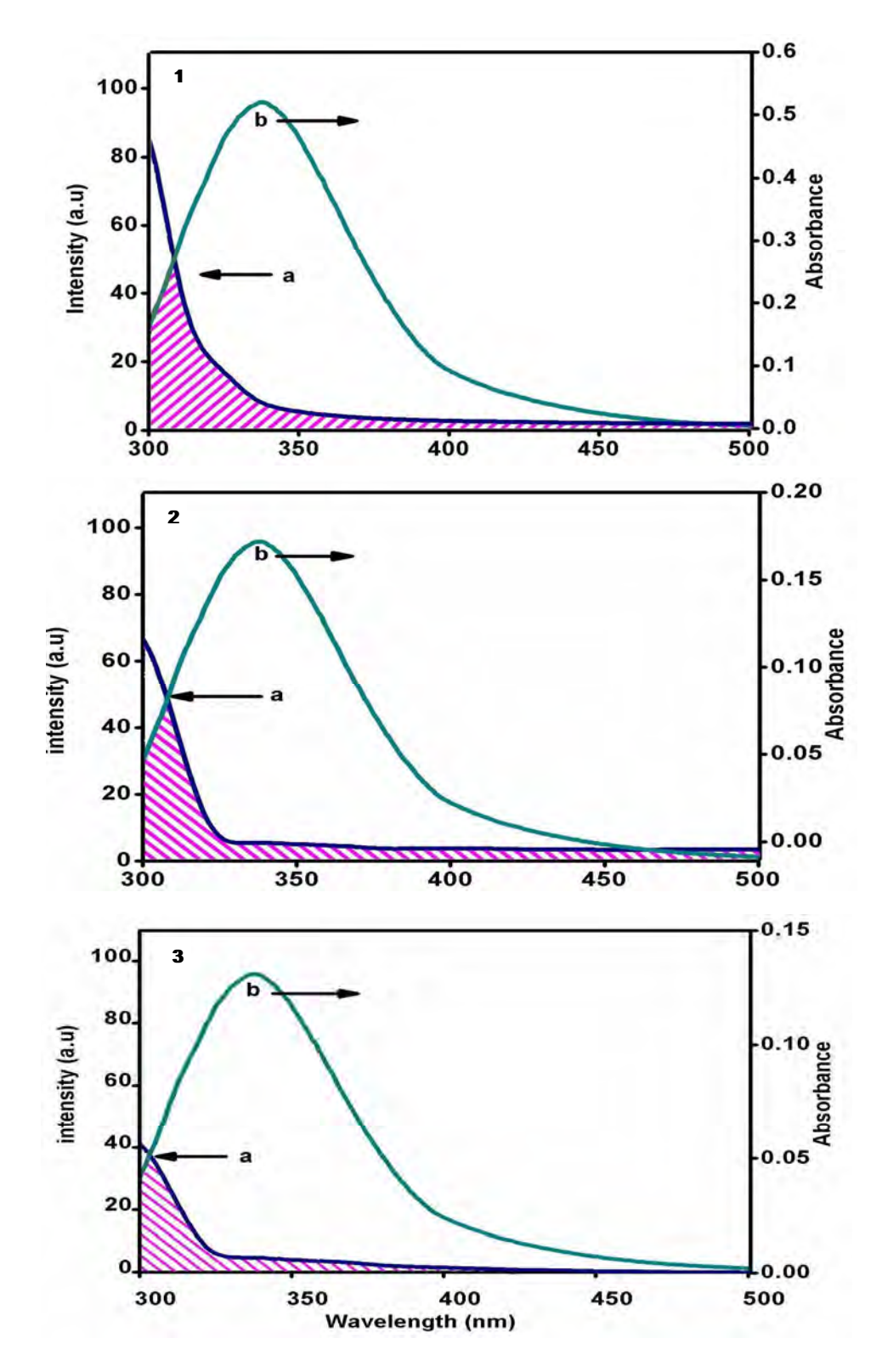


Figure 3.19 Overlap of the fluorescence spectra (b) of BSA and the absorption spectra (a) of 1-3 [BSA] = [Cu complex] = 1×10^{-6} mol L⁻¹.

3.3.7 DNA cleavage studies

The complex concentrations in the range 5-500 µM, 1-3 fail to show any cleavage (Figures 3.20, 3.21 and 3.22) when supercoiled (SC) pUC19 DNA (20 μM) was incubated with them in the absence of an activator in 2% DMF/5 mM Tris-HCl/50 mM NaCl buffer at pH 7.1 for 1 h at 37 °C. Therefore, the ability of 1-3 to cause DNA cleavage was studied in the presence of H₂O₂. In control experiments with DNA alone or DNA with H₂O₂ alone no DNA cleavage is observed. At lower complex concentrations, 1 (20 µM), 2 (12 µM) and 3 (30 µM) convert SC DNA into nicked circular (NC) form and then to linear open circular (LC) form (Figures 3.23, 3.24, and 3.25) revealing the efficient cleavage like activity. As concentrations of 1-3 are increased, the amount of form I decrease while both forms II and III increase. Interestingly, even at 12 µM concentration, the cleavage ability of 2 is found to be more efficient and also exhibits the same percentage of cleavage of DNA from form I to form II as in 1 and 3. The difference in the cleavage activity is due to the binding efficiency of the complexes to DNA (cf. Above). It means that 2 can intercalate into DNA owing to favorable planarity of the ligand phen, and that copper cation may coordinate with the negatively charged oxygen in the phosphodiester backbone of DNA, displacing a water molecule, which enhances the binding affinity between 2 and DNA. In the presence of H₂O₂ as a reducing agent, Cu(II) complex is first reduced to form Cu(I) species and bound to DNA [65], which reacts readily with H₂O₂ to produce a peroxide complex such as DNA-Cu(I)OOH [66]. In the proximity of DNA, furthermore, the reduction of the peroxide complex (DNA-Cu(I)OOH) produces the ROS in abundance, i.e., hydroxyl radical, •OH, which would immediately attack the adjacent deoxyribose ring in the DNA skeleton. The preliminary mechanism of

DNA strand scission by **1-3** has been investigated in the presence of several additives such as DMSO, superoxide dismutase (SOD), NaN₃, and catalase. Remarkably, SOD, NaN₃, and catalase are ineffective, rule out the possibility of DNA cleavage by $^{1}O_{2}$ or O_{2}^{-} or $H_{2}O_{2}$ and imply that •OH radicals are playing a role in the DNA cleavage reaction (**Figures 3.26, 3.27, and 3.28**). The strongly DNA bound complex **2** (through partial intercalation via planar phen moiety) is located near the cleavage site is stabilized more in the Cu(I) state and so shows higher DNA cleavage compared to **1** and **3** (through partial intercalation via bzim moiety) using the availability of $H_{2}O_{2}$ since $H_{2}O_{2}$ is needed for both oxidation and reduction steps.

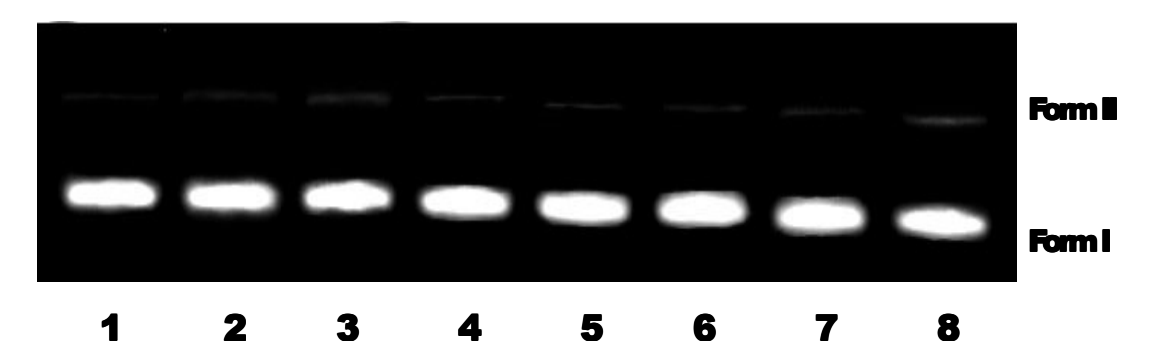


Figure 3.20 Agarose gel showing cleavage of 20 μM SC pUC19 DNA incubated with 1 in 2% DMF/5 mM Tris-HCl/50 mM NaCl buffer at pH 7.1 and 37 °C for 1 h. Lane 1, DNA control; lanes 2-8, DNA + 1 (5, 10, 50, 100, 200, 300, 500 μM respectively). Forms I and II are supercoiled and nicked circular forms of DNA respectively.

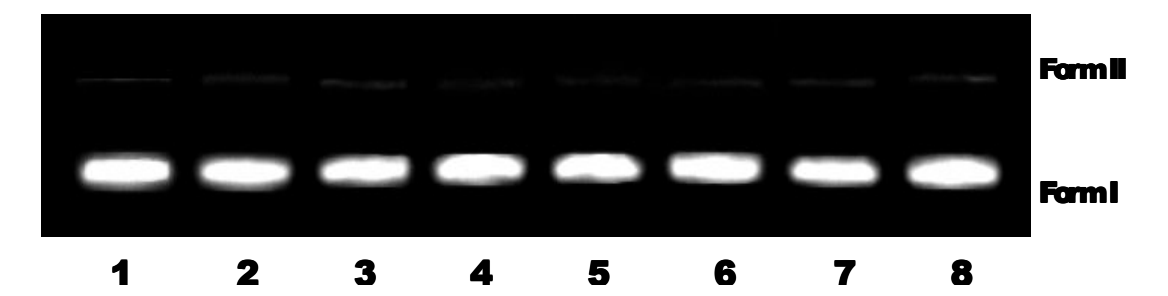


Figure 3.21 Agarose gel showing cleavage of 20 μM SC pUC19 DNA incubated with 2 in 2% DMF/5 mM Tris-HCl/50 mM NaCl buffer at pH 7.1 and 37 °C for 1 h. Lane 1, DNA control; lanes 2-8, DNA + 2 (5, 10, 50, 100, 200, 300, 500 μM respectively). Forms I and II are supercoiled and nicked circular forms of DNA respectively.

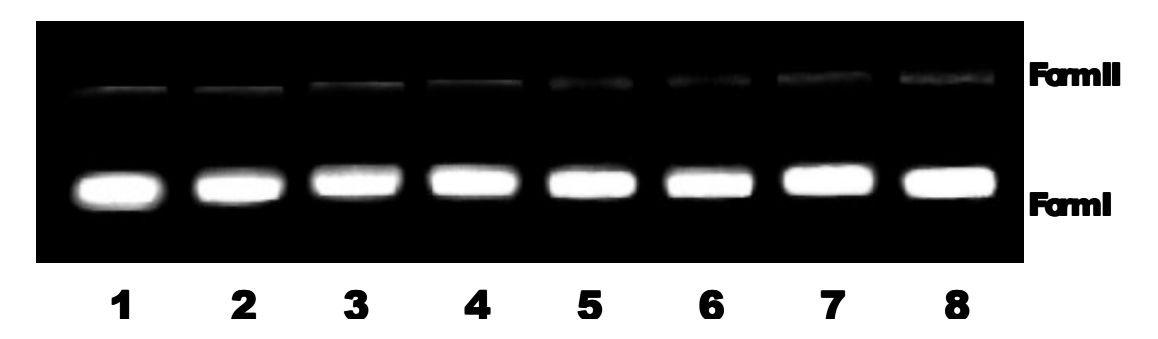


Figure 3.22 Agarose gel showing cleavage of 20 μM SC pUC19 DNA incubated with 3 in 2% DMF/5 mM Tris-HCl/50 mM NaCl buffer at pH 7.1 and 37 °C for 1 h. Lane 1, DNA control; lanes 2-8, DNA + 3 (5, 10, 50, 100, 200, 300, 500 μM respectively). Forms I and II are supercoiled and nicked circular forms of DNA respectively.

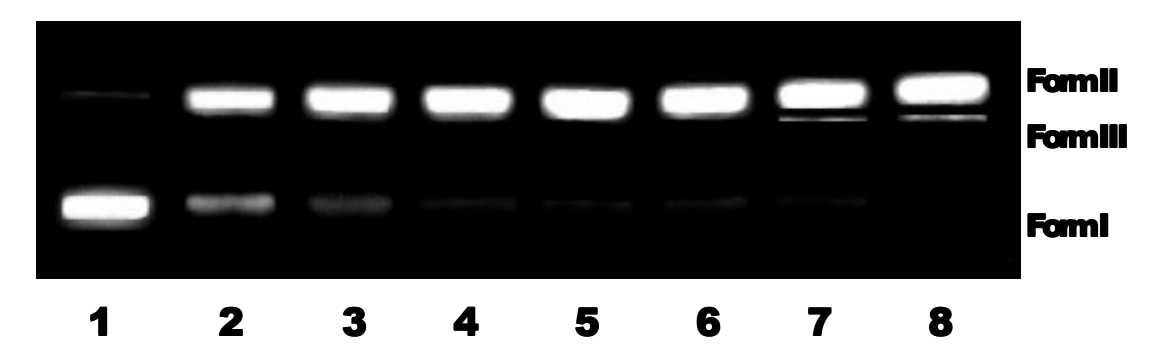


Figure 3.23 Agarose gel showing cleavage of 20 μM SC pUC19 DNA incubated with **1** in 2% DMF/5 mM Tris-HCl/50 mM NaCl buffer at pH 7.1 and 37 °C in the presence of H₂O₂ (200 μM). Lane 1, DNA + H₂O₂; lanes 2-8, DNA + H₂O₂+ **1** (1, 2, 3, 5, 10, 15, 20 μM respectively). Forms I, II and III are supercoiled, nicked circular and linear forms of DNA respectively.

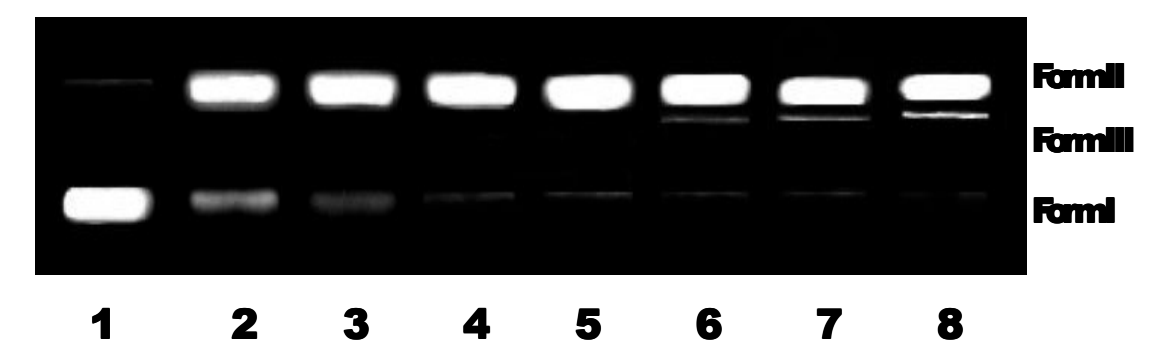


Figure 3.24 Agarose gel showing cleavage of 20 μM SC pUC19 DNA incubated with 2 in 2% DMF/5 mM Tris-HCl/50 mM NaCl buffer at pH 7.1 and 37 °C in the presence of H₂O₂ (200 μM). Lane 1, DNA + H₂O₂; lanes 2-8, DNA + H₂O₂+ 2 (1, 2, 4, 6, 8, 10, 12 μM respectively). Forms I, II and III are supercoiled, nicked circular and linear forms of DNA respectively.

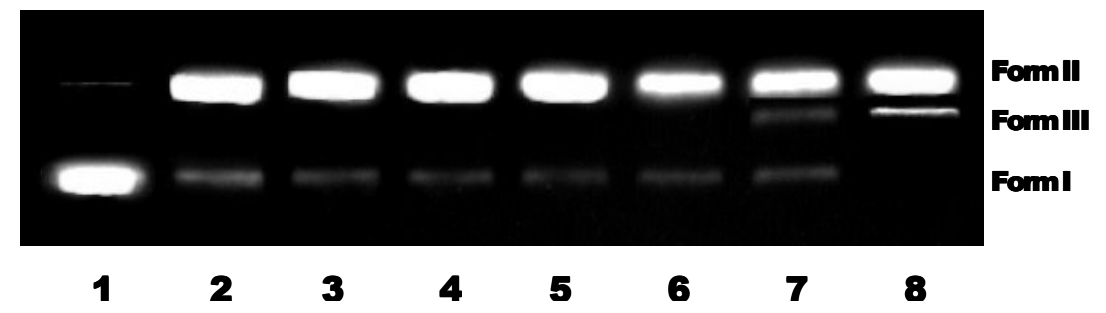


Figure 3.25 Agarose gel showing cleavage of 20 μ M SC pUC19 DNA incubated with **3** in 2% DMF/5 mM Tris-HCl/50 mM NaCl buffer at pH 7.1 and 37 °C in the presence of H₂O₂ (200 μ M). Lane 1, DNA + H₂O₂; lanes 2-8, DNA + H₂O₂ + **3** (1, 2, 4, 6, 8, 10, 12 μ M respectively). Forms I, II and III are supercoiled, nicked circular and linear forms of DNA respectively.

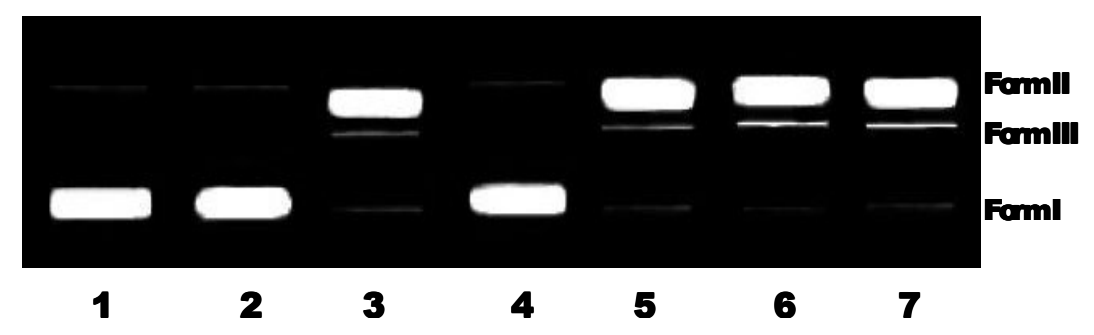


Figure 3.26 Gel electrophoresis diagram showing the cleavage of 20 μ M SC pUC19 DNA by **1** (20 μ M) in a 2% DMF/5 mM Tris-HCl/50 mM NaCl buffer at pH 7.1 and 37 °C in the presence of H₂O₂ (200 μ M). with an incubation time of 2 h: lane 1, DNA control; lane 2, DNA + **1**; lane 3, DNA + **1** + H₂O₂; lane 4, DNA + **1** + H₂O₂ + DMSO (20 μ M); lane 5, DNA + **1** + H₂O₂ + SOD (0.5 units); lane 6, DNA + **1** + H₂O₂ + NaN₃ (100 μ M); lane 7, DNA + **1** + H₂O₂ + Catalase (6 unit).

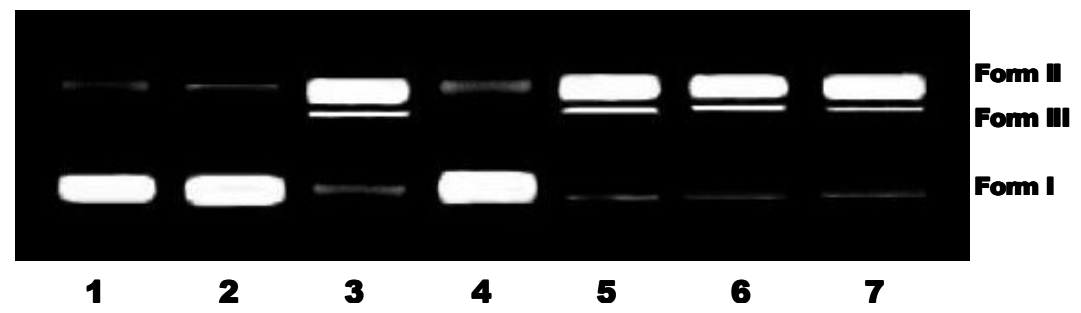


Figure 3.27 Gel electrophoresis diagram showing the cleavage of 20 μ M SC pUC19 DNA by 2 (12 μ M) in a 2% DMF/5 mM Tris-HCl/50 mM NaCl buffer at pH 7.1 and 37 °C in the presence of H₂O₂ (200 μ M) with an incubation time of 2 h: lane 1, DNA control; lane 2, DNA + 2; lane 3, DNA + 2 + H₂O₂; lane 4, DNA + 2 + H₂O₂+DMSO (20 μ M); lane 5, DNA + 2 + H₂O₂ + SOD (0.5 units); lane 6, DNA + 2 + H₂O₂ + NaN₃ (100 μ M); lane 7, DNA + 2 + H₂O₂ + Catalase (6 unit).

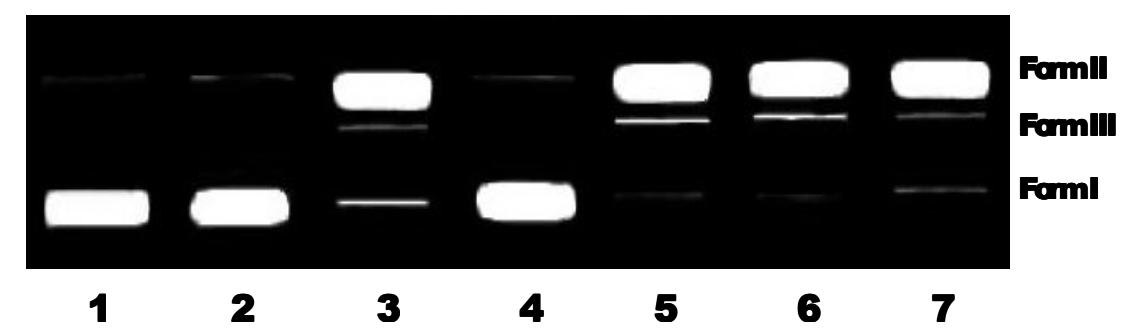


Figure 3.28 Gel electrophoresis diagram showing the cleavage of 20 μ M SC pUC19 DNA by 3 (30 μ M) in a 2% DMF/5 mM Tris-HCl/50 mM NaCl buffer at pH 7.1 and 37 °C in the presence of H₂O₂ (200 μ M). with an incubation time of 2 h: lane 1, DNA control; lane 2, DNA + 3; lane 3, DNA + 3 + H₂O₂; lane 4, DNA + 3 + H₂O₂ + DMSO (20 μ M); lane 5, DNA + 3 + H₂O₂ + SOD (0.5 units); lane 6, DNA + 3 + H₂O₂ + NaN₃ (100 μ M); lane 7, DNA + 3 + H₂O₂ + Catalase (6 unit).

3.3.8 *In Vitro* cytotoxicity studies

Many copper(II) complexes display efficient cytotoxic action and anticancer properties due to the higher DNA binding affinity and prominent DNA cleavage activity [67,68]. Thus, as all the complexes strongly bind to DNA and induce efficient DNA cleavage, their cytotoxicity against the human cervical carcinoma (HeLa) cell line has been investigated in comparison with the widely used drug cisplatin under identical conditions by using MTT assay. Their cytotoxicity was found to be concentration-dependent (0.25 to 100 μ M) for 48 h incubation, which increases the percentage of cell inhibition (Figure 3.29 CC). The IC₅₀ values obtained reveal that the potency of the complexes to kill the cancer cells follows the order 2 > 1 > 3, disclosing that the mode and extent of interaction of complexes with DNA dictate the cell killing ability (cf. above). The cell killing ability with 2 and 1 is remarkable in displaying cytotoxicity (IC₅₀: 2, 2.17 (0.26); 1, 8.33 (0.16) μ M), approximately 8 and 2 times more potent respectively than cisplatin (IC₅₀, 16.41 (0.21) μ M)^[3] whereas 3 (IC₅₀, 20.82 (0.09) μ M) show relatively lower cytotoxicity. Notably, the highly remarkable

cytotoxicity of **2** compared to **1** and **3** is attributed to the stronger binding of the complex through the partial intercalative insertion of planar phen ring between the base pairs and its higher cleavage activity is responsible for its potency to induce cell death. As a measure of therapeutic potential, we further determined the cytotoxicity of **1-3** against normal mouse embryonic fibroblasts cell line NIH 3T3 (**Figure 3.29 NC**). In general, they do not cause any damage toward NIH 3T3 ($IC_{50} > 100 \mu M$), indicating that they are non-toxic to healthy cells, which is expected for a better drug.

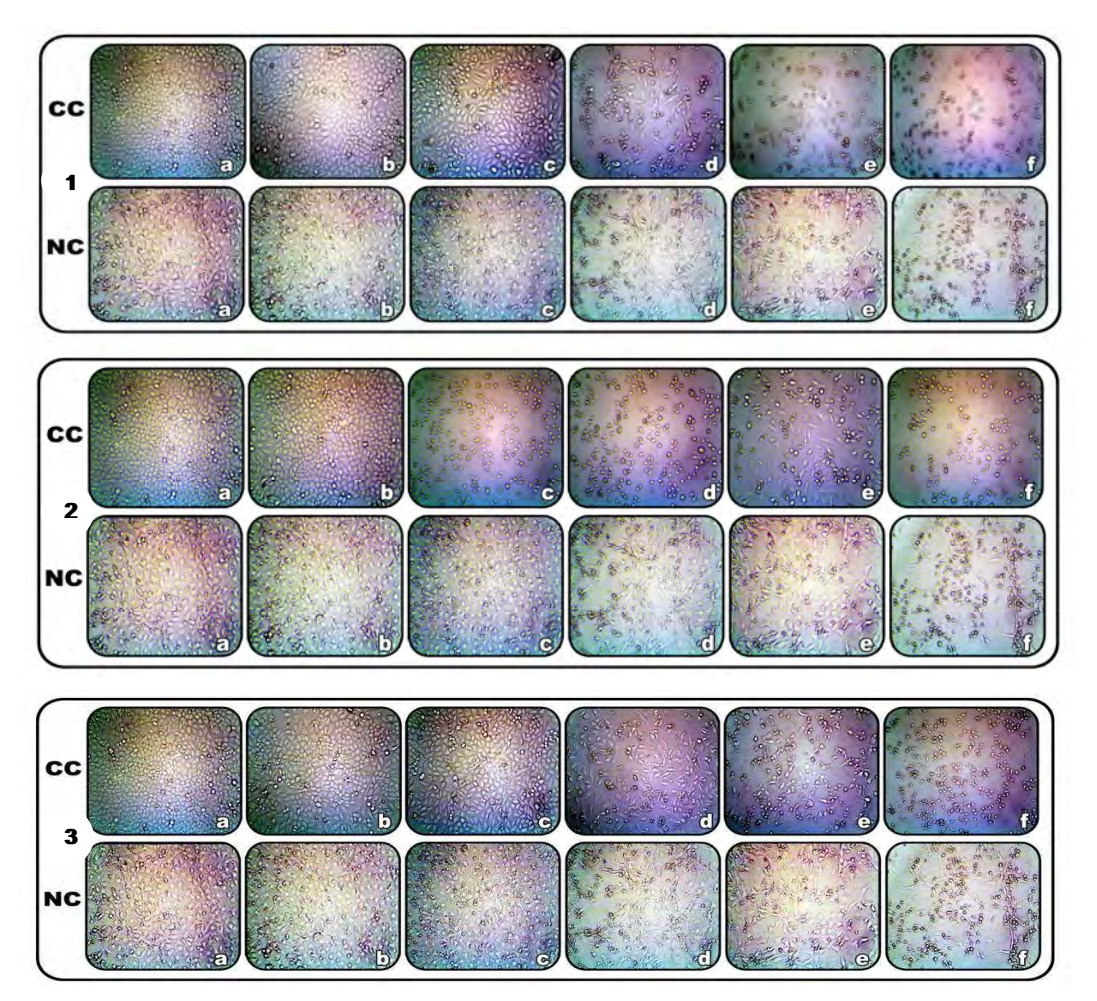


Figure 3.29 Photomicrograph of human cervical carcinoma cell line (HeLa; CC) and normal mouse embryonic fibroblasts cell line (NIH 3T3; NC) after 48 h exposure with **1-3**. CC (a, control; b, 0.25 μM; c, 2.5 μM; d, 25 μM; e, 50 μM; f, 100 μM). NC (a, control; b, 0.1 μM; c, 1.0 μM; d, 10 μM; e, 50 μM; f, 100 μM).

3.4 Conclusion

The copper(II) complexes of the type $[Cu(bba)(diimine)](ClO_4)_2$ are involved in two types of partial intercalative mode of interactions with CT DNA, (i) via planar phen moiety in $[Cu(bba)(phen)](ClO_4)_2$ (2, stronger) and (ii) via bzim moiety in $[Cu(bba)(bpy)](ClO_4)_2$ (1, moderate) and $[Cu(bba)(dpa)](ClO_4)_2$ (3, weak). The findings of the interaction mechanism of 1-3 with BSA are as follows: (a) strong quencher and interact with BSA through static quenching procedure; (b) the binding reaction is spontaneous; (c) hydrophobic interactions play a major role in the reaction; (d) affects the conformation of tryptophan residues micro-region and (e) the energy transfer occurs with high probability. These results support the fact that the Cu(II) complexes can bind to BSA and transport in the body. Further, the DNA binding, DNA cleavage, and *in vitro* cytotoxicity studies show that the binding propensity, cleavage ability, and cell killing activity follow the order 2 > 1 > 3. Overall, these studies demonstrate that 2 is a promising chemotherapeutic scaffold, with well-defined biological interactions and activity derived from the redox-active copper center.

References

[1] R.A. Alderden, M.D. Hall, T.W. Hambley, J. Chem. Educ. 83 (2006) 728-734.

- [2] Y.W. Jung, S.J. Lippard, Chem. Rev. 107 (2007) 1387-1407.
- [3] S. Sangeetha, M. Murali, Inorg. Chem. Commun. 59 (2015) 46-49.
- [4] S. Sangeetha, M. Murali, Int. J. Biol. Macromol. 107 (2018) 2501-2511
- [5] A. Nori, J. Kopecek, Adv. Drug Delivery Rev. 57 (2005) 609-636.
- [6] Y. Xie, G.G. Miller, S.A. Cubitt, K.J. Soderlind, M.J. Allalunis-Turner, J.W. Lown, Anti-Cancer Drug Des. 12 (1997) 169-179.
- [7] M. Shi, K. Ho, A. Keating, M.S. Shoichet, Adv. Funct. Mater. 19 (2009) 1689-1696.
- [8] W.O. Foye, Cancer Chemotherapeutic Agents, American Chemical Society, Washington DC, 1995.
- [9] B. Rosenberg, L. VamCamp, J.E. Trosko, V.H. Mansour, Nature 222 (1969) 385-386.
- [10] D. Senthil Raja, N.S.P. Bhuvanesh, K. Natarajan, Dalton Trans. 41 (2012)4365-4377.
- [11] P.J. Bednarski, F.S. Mackay, P.J. Sadler, Anticancer Agents Med. Chem. 7 (2007) 75-93.
- [12] X. Qiao, Z.Y. Ma, C.Z. Xie, F. Xue, Y.W. Zhang, J.Y. Xu, Z.Y. Qiang,J.S. Lou, G.J. Chen, S.P. Yan, J. Biol. Inorg. Chem. 105 (2011) 728-737.
- [13] F. Kratz, In Metal Complexes in Cancer Chemotherapy; Keppler, B. K., Ed.; VCH: Weinheim, Germany (1993) p 391.
- [14] M.J. McKeage, Drug Safety 13 (1995) 228-244.

[15] A.A. Spasov, I.N. Yozhitsa, L.I. Bugaeva, V.A. Anisimova, Phar. Chen. J. 33 (1999) 232-243.

- [16] R.A. Bucknall, S.B. Carter, Nature (1967) 1099-1101.
- [17] F. Gumus, O. Algul, G. Eren, H. Eroglu, N. Diril, S. Gur, A. Ozkul, Eur.J. Med. Chem. 38 (2003) 473-480.
- [18] M. Gocke, S. Utku, S. Gur, A. Rozkul, F. Gumus, Eur. J. Med. Chem. 40 (2005) 135-141.
- [19] N. Bharti, M.T. Shailendra, Bioorg. Med. Chem. Lett. 12 (2002) 869-871.
- [20] V.G. Vaidyanathan, B.U. Nair, J. Inorg. Biochem. 91 (2002) 404-412.
- [21] J. Wang, L. Shuai, X. Xiao, Y. Zeng, Z. Li, T. Matsumura-Ione, J. Inorg. Biochem. 99 (2005) 883-885.
- [22] F. Ssczewski, E. Dziemidowicz-Borys, P.J. Bednarski, R. Grünert, M. Gdaniec,P. Tabin, J. Inorg. Biochem. 100 (2006) 1389-1398.
- [23] B. Coyle, P. Kiusella, M. McCann, D. Devereux, R. O'Connor, M. Clynes,K. Kavanagh, Toxicol. In Vitro 18 (2004) 63-70.
- [24] D. Devereux, M. McCann, D. O'Shea, R. Kelly, D. Egan, C. Deegan,K. Kavanagh, V. McKee, G. Finn, J. Inorg. Biochem. 98 (2004) 1023-1031.
- [25] F. Gumus, G. Eren, L. Acik, A. Celebi, F. Ozturk, S. Yilmaz, R.I. Sagkan,S. Gur, A. Ozkul, A. Elmali, Y. Elerman, J. Med. Chem. 52 (2009) 1345-1357.
- [26] SMART & SAINT Software References manuals, version 5.0; Bruker AXS Inc.: Madison, WI, 1998.
- [27] G.M. Sheldrick, SAINT 5.1; Siemens Industrial Automation Inc.: Madison, WI, 1995.
- [28] SADABS, Empirical Absorption Correction Program; University of Göttingen:G ottingen, Germany, 1997.

[29] G.M. Sheldrick, SHELXTL Reference Manual, Version 5.1; Bruker AXS:Madison, WI, 1997.

- [30] G.M. Sheldrick, SHELXS-97: Program for the Solution of Crystal Structure; University of G ottingen: Göttingen, Germany, 1997.
- [31] G.M. Sheldrick, Acta Crystallogr. A64 (2008) 112-122.
- [32] A.T. Chaviara, E.E. Kioseoglou, A.A. Pantazaki, A.C. Tsipis, P.A. Karipidis,D.A. Kyriakidis, C.A. Bolos, J. Inorg. Biochem. 102 (2008) 1749-1764.
- [33] J.E. Huheey, E.A. Keiter, R.L. Keiter, O.K. Medhu, Inorganic Chemistry, Principles of Structure and Reactivity; Pearson Education, Upper Saddle River, NJ, 2006, 425-426.
- [34] A.W. Addison, T.N. Rao, J. Reedijk, J. van Rijn, G.C. Verschoor, J. Chem. Soc. Dalton Trans. (1984) 149-1356.
- [35] G. Murphy, C. Murphy, B. Murphy, B. J. Hathway, Dalton Trans. (1997) 2653-2660.
- [36] P. Tamil Selvi, M. Murali, M. Palaniandavar, M. Kockerling, G. Henkel, Inorg. Chim. Acta B 340 (2002) 139-146.
- [37] Z.R. Liao, D.F. Xiang, D.F. Li, F. Sheng, F.S. Mei, Synth. React. Inorg. Met.-Org. Chem. 30 (2000) 683-693.
- [38] M. Palaniandavar, T. Pandiyan, M. Lakshminarayanan, H. Manohar, J. Chem. Soc., Dalton Trans. 3 (1995) 455-461.
- [39] K. Pijus, S. Saha, R. Majumdar, R.R. Dighe, A.R. Chakravarty, Inorg. Chem.49 (2010) 849-859.
- [40] T.-H. Huang, H. Yang, G. Yang, S.-I. Zhu, C.-L. Zhang, Inorg. Chim. Acta 455 (2017) 1-8.

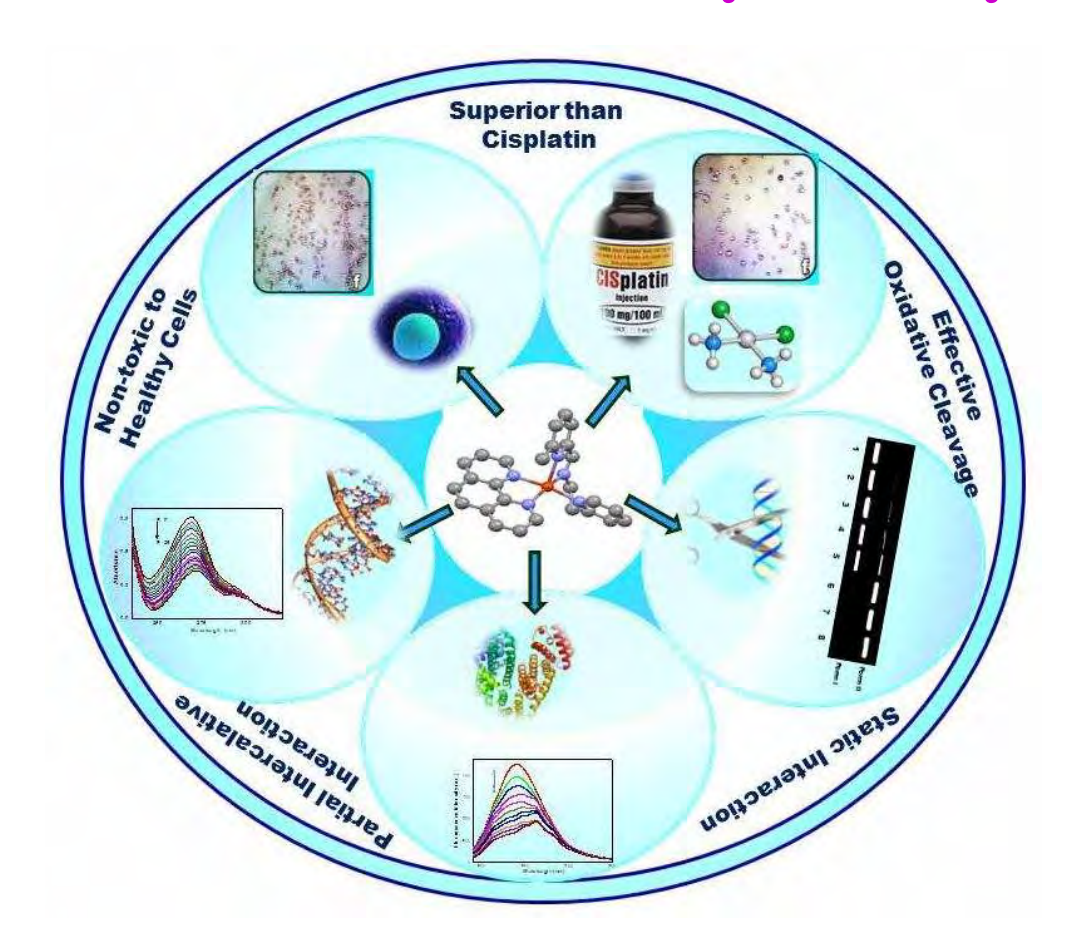
[41] T.-H. Huang, M.-H. Zhang, C.-Y. Gao, L.-T. Wang, Inorg. Chim. Acta 408 (2013) 91-95.

- [42] A.B.P. Lever, Inorganic Electronic Spectroscopy, Elsevier, Amsterdam, 1984.
- [43] V. Sathya, M. Murali, Inorg. Chem. Commun. 92 (2018) 55-59.
- [44] U. Sakaguchi, A.W. Addison, J. Chem. Soc., Dalton Trans. (1979) 600-608.
- [45] M. Palaniandavar, I. Somasundaram, M. Lakshminarayanan, H. Manohar, Dalton Trans. (1996) 1333–1340.
- [46] M. Murali, M. Palaniandavar, T. Pandiyan, Inorg. Chim. Acta 224 (1994) 19-25.
- [47] C. Rajarajeswari, R. Loganathan, M. Palaniandavar, E. Suresh, A. Riyasdeen,M.A.Akbarsha, Dalton Trans. 42 (2013) 8347–8363.
- [48] E. Turkkan, U. Sayin, N. Erbilen, S. Pehlivanoglu, G. Erdogan, H.U. Tasdemir, A.O. Saf, L. Guler, E.G. Akgemci, J. Organomet. Chem. 2017, 831, 23-25.
- [49] B.J. Hathaway, Copper in: Comprehensive Coordination Chemistry, vol. 5, Pergamon Press, Oxford, 1987, pp. 533-774.
- [50] R. Balamurugan, M. Palaniandavar, H. Stoeckli-Evans, M. Neuburger, Inorg.Chim. Acta 359 (2006) 1103-1113.
- [51] B.D. Wang, Z.D.Y. Yang, T.R. Li, Bioorg. Med. Chem. 14(2006) 6012-6021.
- [52] J.B. Le Pecq, C. Paoletti, J. Mol. Biol. 27 (1967) 87-106.
- [53] S. Ramakrishnan, V. Rajendiran, M. Palaniandavar, V.S. Periasamy, B.S. Srinag,H. Krishnamurthy, M.A. Akbarsha, Inorg. Chem. 48 (2009) 1309-1322.
- [54] Y.B. Zeng, N. Yang, W.S. Liu, N. Tang, J. Inorg. Biochem. 97 (2003) 258-264.
- [55] T. Hirohama, Y. Kuranuki, E. Ebina, T. Sugizaki, H. Arii, M. Chikira,P. Tamil Selvi, M. Palaniandavar, J. Inorg. Biochem. 99 (2005) 1205-1219.

- [56] M.R. Eftink, C.A. Ghiron, Anal. Biochem. 114 (1981) 199-227.
- [57] X. Zhao, R. Liu, Z. Chi, Y. Teng, P. Qin, J. Phys. Chem. B 114 (2010) 5625-5631.
- [58] W. He, Y. Li, C. Xue, Z. Hu, X. Chen, F. Sheng, Bioorg. Med. Chem. 13 (2005) 1837-1845.
- [59] A. Sulkowska, J. Równicka, B. Bojko, W. Sułkowski, J. Mol. Struct. 651 (2003)133-140.
- [60] P.D. Ross, S. Subramanian, Biochemistry 20 (1981) 3096-3102.
- [61] C. Nain Lunardi, A. Claudio Tedesco, T.L. Kurth, I.M. Brinn, Photochem. Photobiol. Sci. 2 (2003) 954-959.
- [62] J.N. Miller, Proc. Anal. Div. Chem. Soc. 16 (1979) 203-208.
- [63] T. Förster, O. Sinanoglu (Eds.), Modern Quantum Chemistry, vol. 3, Acdemic Press, New York, 1966.
- [64] Y. Wang, Y. Wei, C. Dong, J. Photochem. Photobiol. 17 (2006) 6-11.
- [65] B. Saha, M. Md. Islam, S. Paul, S. Samanta, S. Ray, C.R. Santra, S.R. Choudhury, B. Dey, A. Das, S. Ghosh, S. Mukhopadhyay, G.S. Kumar, P. Karmakar, J. Phys. Chem. B 114 (2010) 5851-5861.
- [66] J. Tan, B. Wang, L. Zhu, J. Biol. Inorg. Chem. 14 (2009) 727-739.
- [67] M. Ganesh Pandian, R. Loganathan, S. Ramakrishnan, E. Suresh, A. Riyasdeen,M.A. Akbarsha, M. Palaniandavar, Polyhedron 52 (2013) 924–938.
- [68] Y. Gou, J. Li, B. Fan, B. Xu, M. Zhou, F. Yang, Eur. J. Med. Chem. 134 (2017) 207-217.

Chapter 4

Mixed Ligand Copper(II) Complexes with CuN₅ Chromophore: Synthesis, Structure, DNA binding and Cleavage, BSA interaction and Cytotoxicity



Copper(II) complexes possess a distorted square pyramidal coordination geometry that allows them to bind to CT DNA via partial intercalative interaction, efficient oxidative cleavage of supercoiled plasmid DNA, and a static quenching process with BSA. They have better cytotoxicity to cisplatin while being non-toxic to healthy cells.

4 Mixed Ligand Copper(II) Complexes with CuN₅ Chromophore: Synthesis, Structure, DNA binding and Cleavage, BSA interaction and Cytotoxicity

4.1 Introduction

Many transition metal complexes were found to be potential chemotherapeutic drugs and some of the complexes were under various stages of clinical trials. Among which certain dinuclear platinum complexes were found to be better anticancer drugs than cisplatin [1,2]. However, the widespread use of platinum-based drugs in medical applications has resulted in a variety of side effects, including nephrotoxicity, ototoxicity, and neurotoxicity, as well as inborn or acquired drug resistance [3-5]. As a result, the recent research community has been inspired to develop new low-toxicity compounds capable of producing a variety of DNA adducts with improved pharmacological properties [1,2,6]. The major intracellular target for an anticancer complex is DNA, and their feasible interaction might cause DNA damage in cancer cells, inhibiting them and causing cell death. These complexes may also interact with protein (BSA) [7-9]. Many of the metal complexes apply their anticancer activities by DNA interaction upon intercalation. Thus, DNA cleavage activity possesses a momentous role in improving the excellence of anticancer drugs [10,11]. Among them, the metal ion chosen was also playing an outstanding role in chemotherapeutic drug development. Here, we have opted for one of the most abundant transition metals, specifically less toxic and biocompatible copper. Copper is a bio-essential metal ion that is involved in a variety of biological activities, most notably the regular function of cells. Copper(II) complexes with well-defined redox activity could be effective antioxidants, antimicrobials, antiparasitics, and anticancer agents [10-13]. Some families of copper complexes have been studied as prospective anticancer agents in recent years [14], and our new copper complexes are being considered as better alternatives to platinum complexes. While there is little evidence of mechanistic action on the molecular level, copper complexes have attracted a lot of attention and have given rise to optimistic expectations based on modes of action that differ from those of other metal complexes, particularly platinum drugs [15-19]. Due to their powerful DNA binding/cleaving ability, mixed ligand copper(II) complexes have recently been discovered to be good anticancer agents via inducing apoptosis [20-22]. The biological activity of the 3N Schiff base is related to its ability to chelate transition metal ions; coordinating to the metal ion through nitrogen atoms could be an effective cytotoxic molecule, enhancing biological activity [23,24]. The ability of copper complexes to function as anticancer compounds is influenced by their ligand design, copper ion oxidation states, and potential interactions with biomolecules. The coordination structure of the copper complexes obtained may have additionally increased DNA interactions, enhancing their chemotherapeutic efficacy [25].

From 1970 onwards, diimine copper(II) complexes, specifically those containing 1,10-phenanthroline (phen), have been studied for their various biological functions. It has been reported that combining a single diimine (one phen moiety) can increase activity; however combining two diimine in the same complex can retard biological processes, especially under physiological conditions. [26]. As shown, these types of mixed-ligand complexes exhibit similar DNA binding/cleaving, cytotoxic actions, and, as a result, induce apoptosis. The physicochemical properties of copper complexes, such as planarity, hydrophobicity, the size of the diimine moiety, the nature of the co-ligands, and the coordination geometry of the metal complexes, have all been confirmed to play an important role in their interactions with DNA. As an extension

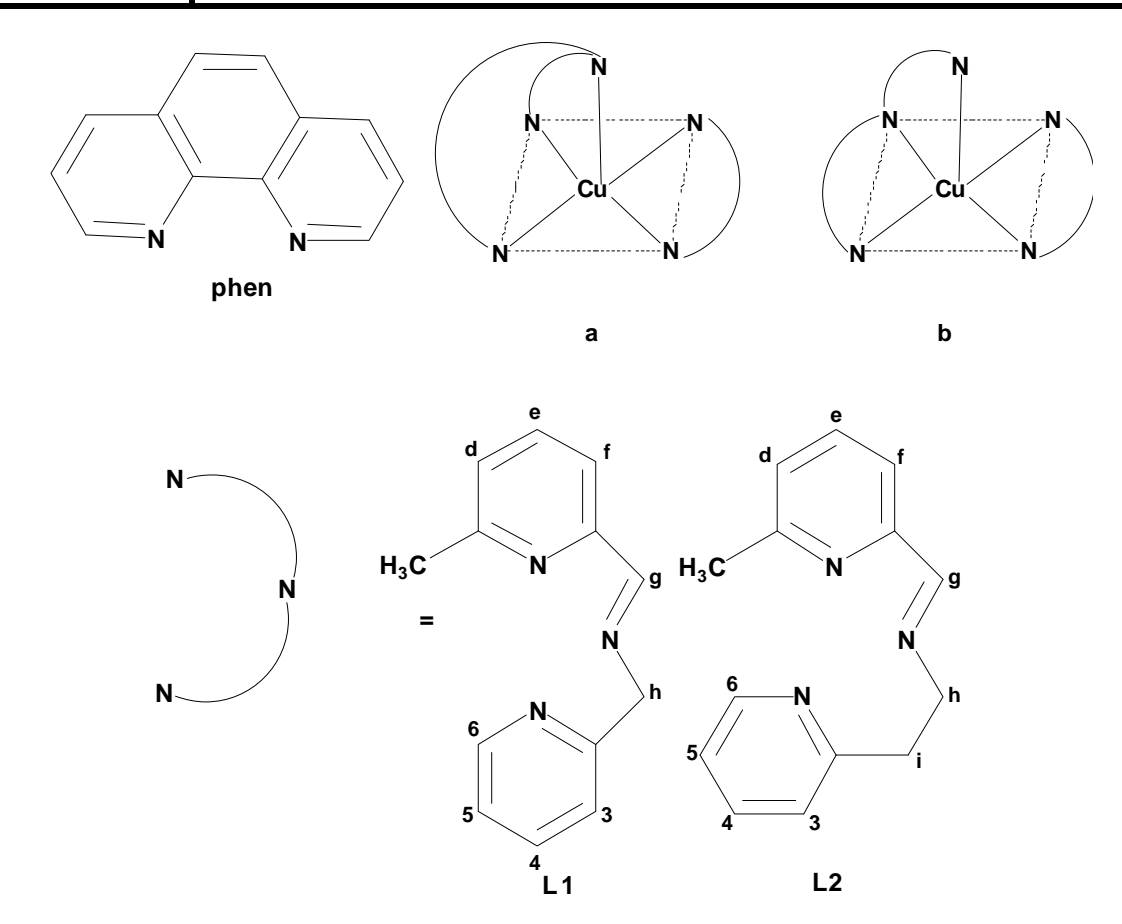
to these prior findings, this study looks into how the use of diimine co-ligands in copper(II) complexes resulted in a synergistic impact, which could indicate a promising strategy for the design and development of promising chemotherapeutic drugs.

Therefore, we have synthesized and characterized two mixed ligand copper(II) complexes of the type [Cu(L1/L2)(phen)](ClO₄)₂ where L1 or L2 is a tridentate Schiff base ligand derived from the condensation of 6-methylpyridine-2-carbaldehyde with 2-aminomethylpyridine (L1) or 2-aminoethylpyridine (L2) (Scheme 4.1). The interactions of these complexes with CT DNA and BSA were studied using various spectral and electrochemical techniques and intend to explore binding properties. Besides the cleavage activities with pUC19 supercoiled plasmid DNA was also investigated. The chemotherapeutic efficacy was studied in terms of cytotoxicity activities of the complexes against human cervical carcinoma (HeLa). Interestingly, the present mixed ligand copper(II) complexes of tridentate 3N ligands with phen are involved in partial intercalative binding with DNA and display potent DNA cleavage and anticancer activities.

4.2 Experimental

4.2.1 Synthesis of (6-methylpyridin-2-ylmethylene)-(pyridin-2-ylmethyl)amine, L1

2-Aminomethylpyridine (0.55 g, 5 mmol) in ethanol (15 mL) was added drop wise to 6-methyl-pyridine-2-carboxaldehyde (0.60 g, 5 mmol) in ethanol (15 mL). The mixture was refluxed for 3 h with constant stirring. After the solvent was removed under reduced pressure, 20 mL of CH₂Cl₂ was then added, and it was rotaevaporated to get (6-methylpyridin-2-ylmethylene)-(pyridin-2-ylmethyl)amine as bright yellow oil.



Scheme 4.1 Schematic representation of the copper(II) complex (a and b) and structure of ligands (L1, L2, phen) and proton numbering scheme (L1, L2).

Yield: ~ 0.76 g, 72%. Anal. Calcd. for $C_{13}H_{13}N_3$: C, 73.91; H, 6.20; N, 19.89. Found: C, 73.99; H, 6.15; N, 19.83%. Selected FT-IR (cm⁻¹) bands in KBr: 1610 v_{imine} (C=N), 1525 v(C=C), 982 v_{C-H} (H-C=N), 726 and 782 v(C-H). HRMS value in CH₂Cl₂: m/z, 211.98 (M+H)⁺. ¹H NMR (300 MHz, DMSO-d₆) δ/ppm: 7.45 (d, 1H, H_d), 7.06 (t, 1H, H_e), 7.21 (d, 1H, H_f), 8.91 (s, 1H, H_g), 3.79 (s, 2H, H_h), 7.36 (d, 1H, H₃), 7.56 (t, 1H, H₄), 7.14 (t, 1H, H₅), 8.53 (d, 1H, H₆), 2.46 (s, 3H, Py-CH₃).

4.2.2 Synthesis of (6-methylpyridin-2-ylmethylene)-(pyridin-2-ylethyl)amine, L2

The ligand L2 was prepared by the method adopted for the preparation of L1, except that 2-aminoethylpyridine (0.11 g, 1 mmol) was used instead of 2-aminomethylpyridine.

Yield: ~ 0.90 g, 78%. Anal. Calcd. for $C_{14}H_{15}N_3$: C, 74.64; H, 6.71; N, 18.65. Found: C, 74.61; H, 6.79; N, 18.71%. Selected FT-IR (cm⁻¹) bands in KBr: 1611 v_{imine} (C=N), 1529 v(C=C), 981 v_{C-H} (H-C=N), 730 and 783 v(C-H). HRMS value in CH_2CI_2 : m/z, 226.22 (M+H)⁺. ¹H NMR (300 MHz, DMSO-d₆) δ /ppm: 7.43 (d, 1H, H_d), 7.07 (t, 1H, H_e), 7.25 (d, 1H, H_f), 8.95 (s, 1H, H_g), 3.81 (t, 2H, H_h), 3.62 (t, 2H, H_i), 7.41 (d, 1H, H₃), 7.63 (t, 1H, H₄), 6.98 (t, 1H, H₅), 8.62 (d, 1H, H₆), 2.48 (s, 3H, Py-CH₃).

4.2.3 Synthesis of copper(II) complexes

The copper(II) complexes were prepared using the general procedure as follows: Copper(II) acetate monohydrate (0.2 g, 1 mmol) taken in ethanol (15 mL) was slowly added to 1,10-phenanthroline monohydrate (0.20 g, 1 mmol) in ethanol (15 mL) and stirred for 1 h up to dissolution. To this mixture, the ligand L1 (0.21 g, 1 mmol) or L2 (0.23 g, 1 mmol) was added with stirring to the reaction mixture. The resulting green solution was refluxed at 70 °C for 3 h. After the complexation, it was filtered while hot and added ethanolic solution of NaClO₄ (0.12 g, 1 mmol). The solution was cooled to room temperature, and green colored crystalline solids of 1 or 2 were formed after three days. They were filtered off, washed with a small amount of cold ethanol, and dried under vacuum over P₄O₁₀.

[Cu(L1)(phen)](ClO₄)₂ 1: Yield: ~ 0.37 g (63%). Found, C, 50.84; H, 3.55; N, 11.91%. C₂₅H₂₁N₅O₈Cl₂Cu requires C, 50.86; H, 3.59; N, 11.86%. Λ_M in DMF solution, 203 Ω^{-1} cm⁻¹mol⁻¹. ESI-MS m/z = 391.25 [Cu(L1)(phen)]²⁺ (calcd 391.48). μ_{eff} , 1.86 μ B (27 °C). Selected FT-IR (cm⁻¹) bands in KBr: 1585 ν_{imine} (C=N), 1519 ν (C=C), 852 ν _{C-H}(H-C=N), 724, 778 ν (C-H), 1090, 622 ν (ClO₄⁻), 530, 562 ν (Cu–N). UV-Visible data in DMF [λ_{max} /nm (ε_{max} /dm³ mol⁻¹ cm⁻¹)]: 684 (100), 896 sh, 323

(4485), 294 (24670), 268 (46420). EPR data: in solid (RT) $g_{iso} = 2.147$; in DMF solution (77 K), $g_{\parallel} = 2.233$, $g_{\perp} = 2.045$, $A_{\parallel} = 188 \times 10^{-4}$ cm⁻¹, $g_{\parallel}/A_{\parallel} = 119$ cm, G = 5.2. Electrochemical data (methanol, 0.1 M TBAP): cyclic voltammetry, $E_{1/2} = -0.077$ V, $\Delta E_{\rm p} = 100$ mV, $i_{\rm pa}/i_{\rm pc} = 0.7$, $D = 7.7 \times 10^{-6}$ cm² s⁻¹ and differential pulse voltammetry, $E_{1/2} = -0.063$ V.

[Cu(L2)(phen)](ClO₄)₂ 2: Yield: ~ 0.39 g (65%). Found, C, 51.71; H, 3.89; N, 11.64%. C₂₆H₂₃N₅O₈Cl₂Cu requires C, 51.67; H, 3.84; N, 11.59%. $\Lambda_{\rm M}$ in DMF solution, 205 Ω^{-1} cm⁻¹mol⁻¹. ESI-MS m/z = 405.27 [Cu(L2)(phen)]²⁺ (calcd 405.50). $\mu_{\rm eff}$, 1.88 μB (27 °C). Selected FT-IR (cm⁻¹) bands in KBr: 1585 $\nu_{\rm imine}$ (C=N), 1519 ν (C=C), 852 $\nu_{\rm C-H}$ (H-C=N), 724, 779 ν (C-H), 1090, 622 ν (ClO₄⁻) 538, 571 ν (Cu–N). UV-Visible data in DMF [$\lambda_{\rm max}$ /nm ($\varepsilon_{\rm max}$ /dm³ mol⁻¹ cm⁻¹)]: 675 (280), 856 sh, 321 (7895), 293 (32420), 268 (49330). EPR data: in solid (RT) $g_{\rm iso}$ = 2.172; in DMF solution (77 K), g_{\parallel} = 2.233, g_{\perp} = 2.042, A_{\parallel} = 189 × 10⁻⁴ cm⁻¹, g_{\parallel} / A_{\parallel} = 118 cm, G = 5.5. Electrochemical data (methanol, 0.1 M TBAP): cyclic voltammetry, $E_{1/2}$ = -0.072 V, $\Delta E_{\rm p}$ = 86 mV, $i_{\rm pa}/i_{\rm pc}$ = 0.9, D = 8.2 × 10⁻⁶ cm² s⁻¹ and differential pulse voltammetry, $E_{1/2}$ = -0.059 V.

4.2.4 X-ray structure determination

The single crystal of [Cu(L)(phen)](ClO₄)₂ (**2**) in a green color appropriate for the determination of X-ray structural was acquired upon slow evaporation at 5 °C after a couple of weeks in MeOH:MeCN (2:1 v/v) mixture. A single crystal of the size $0.350 \times 0.320 \times 0.210 \text{ mm}^3$ was chosen under the polarizing microscope and then mounted on the glass fiber. Diffraction data for the complex were collected at 298 K on a Bruker AXS-KAPPA APEX II diffractometer (Mo-K_{α} radiation, λ = 0.71073 Å) in

the θ range 2-25°. Unit cell parameters were determined by the least-squares method based on all reflections with $F^2 > 2\sigma(F^2)$ using Bruker SMART software. Cell refinement, correction for Lorentz and polarization effects, integration of the intensities, and absorption corrections were carried out using packages Bruker SAINT and SADABS. The structure was solved by the direct method (SIR-92) [27] and refined by a full-matrix least-squares method (SHELXL-2014) [28]. All the calculations were carried out using the programs in the WinGX module [29]. Non-hydrogen atoms were refined anisotropically. The Cl1 and O1, O2, O3, and O4 was found to be disordered over two positions and the occupancy factors were assigned as 0.775(10) and 0.225(10) while O5, O6, O7, and O8 were also disordered over two positions and the occupancy factors were given as 0.506(8) and 0.494(8). All the hydrogen atoms were placed geometrically and refined with the use of a riding model. The final difference Fourier maps displayed no peaks of chemical importance. The graphic representation of the molecule was done using the program ORTEP3 for Windows [30] with 40% probability displacement ellipsoids. Crystallographic data for the structural analysis of [Cu(L2)(phen)](ClO₄)₂ have been deposited with Cambridge Crystallographic Data Center, CCDC No. 2143125.

4.3 Results and discussion

4.3.1 Synthesis and general properties

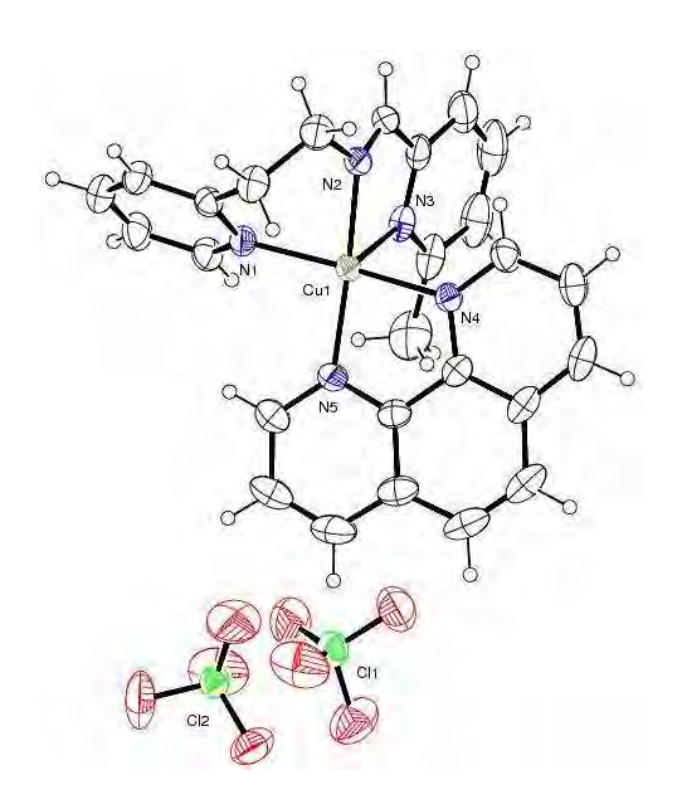
The Schiff base ligands L1 and L2 were synthesized by condensing 2-aminomethylpyridine or 2-aminoethylpyridine and 5-methylpyridine-2-carboxaldehyde. The copper(II) complexes of the ligands were prepared by the reaction of copper(II) acetate monohydrate, 1,10-phenanthroline, and L1 or L2 in equimolar quantities using

ethanol as solvent. Both complexes **1** and **2** were isolated as green colored crystalline compounds in good yields. Based on the elemental analysis the complexes were formulated as $[Cu(L1/L2)(phen)](ClO_4)_2$, which was confirmed by a single crystal X-ray structure determination of **2**. The ESI mass spectral data of **1** and **2** display base peaks at m/z 391.25 and 405.27 respectively, which can be attributed to the complex cations $[Cu(L1)(phen)]^{2+}$ and $[Cu(L2)(phen)]^{2+}$ respectively. This is supported by values of molar conductivity in DMF $(\Lambda_M/\Omega^{-1} \text{ cm}^2 \text{ mol}^{-1}: \mathbf{1}, 203; \mathbf{2}, 205)$, which falls in the range [31] for 1:2 electrolytes. The formation of the dicationic complexes was evidenced by the presence of an intense absorption for the ClO_4^{-1} stretches at 1090, 622 cm⁻¹ in the IR spectrum of the complexes. As expected, the band belonging to V_{imine} (C=N) (L1, 1610; L2, 1611 cm⁻¹) was shifted to 1585 cm⁻¹ due to the coordination of imine nitrogen to copper(II). The sharp bands observed at 530-571 cm⁻¹ can be assigned to V(Cu-N), probably originating from the coordination of the L1 (1) or L2 (2) and phen (1 and 2) ligands.

4.3.2 Description of crystal structure

The ORTEP representation of the complex dication of $[Cu(L2)(phen)](ClO_4)_2$ **2,** including coordinated atom numbering scheme is shown in **Figure 4.1A** and the crystal structure refinement data and selected bond lengths and bond angles are listed in **Tables 4.1 and 4.2** respectively. The asymmetric unit of **2** contains one dicationic complex molecule and two perchlorate anions. The copper atom in the complex is coordinated by all the three nitrogen atoms (N1, N2, N3) of the tridentate ligands L2 and both the nitrogen atoms (N4, N5) of phen. The value of the structural index τ of $0.06 \ [\tau = (\beta-\alpha)/60$, where $\alpha = N2-Cu1-N5 = 165.67^{\circ}$ and $\beta = N1-Cu1-N4 = 169.43^{\circ}$]

(A)



(B)

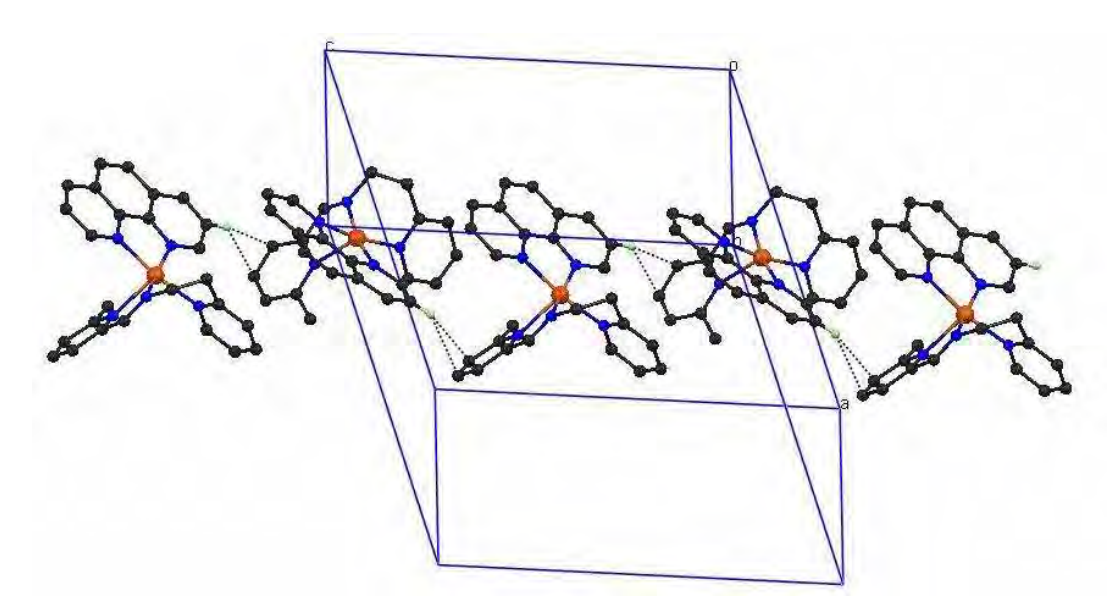


Figure 4.1 (A) An ORTEP view of $[Cu(L2)(phen)](ClO_4)_2$ **2** with atom numbering of complex and thermal ellipsoids at 40% probability. (B) The interpair C-H··· π interaction in $[Cu(L2)(phen)]^{2+}$ **2** involving the π -ring of the methyl pyridyl ring of L2 and the hydrogen atom [C(23)-H] of the pyridyl moiety of phen.

Table 4.1
Selected crystal data and structure refinement parameters for 2

Formula C ₂₆ H ₂₃ Cl ₂ N ₅ O ₈ Cu
Formula maight
Formula weight 667.93
Temperature (K) 296(2)
Wavelength (Å) 0.71073
Crystal system Monoclinic
Space group P2 ₁ /c
a (Å) 16.2038(10)
b (Å) 11.7856(8)
c (Å) 15.4244(10)
α (°) 90
β(°) 108.735(2)
γ(°) 90
$V(\text{Å})^3, Z$ 2789.5(3), 4
$D_{\rm calc} ({\rm mg \ m}^{-3})$ 1.590
$\mu (\text{mm}^{-1})$ 1.033
F(000) 1364
Crystal size (mm ³) $0.350 \times 0.320 \times 0.210$
θ (°) 2.179 to 24.998
Index ranges $-19 \le h \le 19$
$-13 \le k \le 14$
-18 ≤ 1 ≤ 16
Reflections collected 19061
Independent reflections 4879
Reflections observed $[I > 2\sigma(I)]$ 4069
$R_{\rm int}$ 0.0300
GOOF 1.048
$R_1 [I > 2\sigma(I)] \qquad 0.0397$
$wR_2 [I > 2\sigma(I)] $ 0.0994
R_1 , w R_2 all data 0.0507/0.1087

Table 4.2Selected bond lengths (Å) and bond angles (°) for **2**

N(1)-Cu(1)	2.007(2)	N(2)-Cu(1)	1.991(3)
N(3)-Cu(1)	2.250(3)	N(4)-Cu(1)	2.022(2)
N(5)-Cu(1)	2.012(3)		
N(2)-Cu(1)-N(1)	83.26(10)	N(2)-Cu(1)-N(5)	165.67(12)
N(1)-Cu(1)-N(5)	96.15(11)	N(2)-Cu(1)-N(4)	96.30(10)
N(1)-Cu(1)-N(4)	169.43(11)	N(5)-Cu(1)-N(4)	81.64(11)
N(2)-Cu(1)-N(3)	77.82(11)	N(1)-Cu(1)-N(3)	101.57(10)
N(5)-Cu(1)-N(3)	116.18(11)	N(4)-Cu(1)-N(3)	88.62(10)

reveals that the coordination geometry around copper(II) is best described as distorted square pyramidal [32-34]. The corners of the square plane of the geometry are occupied by N1 and N2 nitrogen atoms of the facially coordinated L2 and N4 and N5 nitrogen of phen. The N3 nitrogen atom of L2 occupies the apical position at a distance (2.250(3) Å) longer than the equatorial nitrogen atoms (1.991 - 2.022Å), as a consequence of the presence of two electrons in the d_{z^2} orbital of copper(II). It is interesting to note that the τ value of **2** is very much lower than that of its dipica analogue [Cu(dipica)(phen)]²⁺ (τ , 0.77) [35] indicating that both the apical coordination of 6-methypyridine (mpy) nitrogen atom (N3) of L2 at longer distance and the six-membered chelate ring formed by L2 decrease the steric congestion at copper(II) and change (i) the meridional fashion to facial and (ii) coordination geometry from trigonal bipyramidal towards square pyramidal. Also, the incorporation of the six-membered chelate ring and axial coordination of mpy facilitates stronger coordination of pyridyl N1 nitrogen atom (Cu-N_{py}: **2**, 2.007(2); [Cu(dipica)(phen)]²⁺, 2.058(5) Å) and phen N4 and N5 nitrogen atoms (Cu-N_{phen}: **2**, 2.022(2) and 2.012; [Cu(dipica)(phen)]²⁺, 2.157(5) Å).

Notably, the incorporation of phen in the coordination sphere of **2** displaces the axially coordinated imine nitrogen of L2 (**Scheme 4.1a**) to a more strongly bound equatorial position (**Scheme 4.1b**; 1.991(3) Å) and decreases the steric congestion at copper(II) resulting in the distorted square pyramidal geometry, as revealed by the increase in trans bond angles (N1-Cu1-N4 = 169.43° and N2-Cu1-N5 = 165.67°). Another important structural observation is the inter-pair C-H··· π anti-parallel non-covalent interactions (**Figure 4.1B**) involving C(23)-H of the pyridine ring of phen and the centroid (C_g) of mpy ring of L2 (C(23)-H···C_g(mpy) = 2.942 Å), which is probably responsible for the stabilization of the distorted square pyramidal geometry [36].

4.3.3 Electronic and EPR spectral properties

The electronic spectra (**Figures 4.2 and 4.3**) of **1** and **2** are very similar to each other and show a broad low energy ligand field (LF) band (λ_{max} : **1**, 684; **2**, 675 nm) followed by a shoulder (λ_{max} : **1**, 896; 2, 856) in the visible region revealing a square-derived coordination geometry around Cu(II) with slight distortion [37]. The observed molar absorptivity of **2** (ε_{max} , 280 M⁻¹ cm⁻¹) is higher than that of **1** (ε_{max} , 100 M⁻¹ cm⁻¹) due to the presence of a flexible six-membered chelate ring, which increases the distortion in square-based Cu(II) coordination geometry of **2**. The intense absorption bands observed in the range 268-323 nm are attributed to the intraligand $\pi \rightarrow \pi^*$ transitions. Both the complexes are soluble in 2% DMF/5 mM Tris-HCl/50 mM NaCl buffer (pH 7.1), stable in air, and non-hygroscopic. The UV-visible spectral studies of the complexes in buffer solutions reveal no change in the coordination sphere, thus, the complexes retain their identity in buffer solution (24 h of incubation at 37 °C).

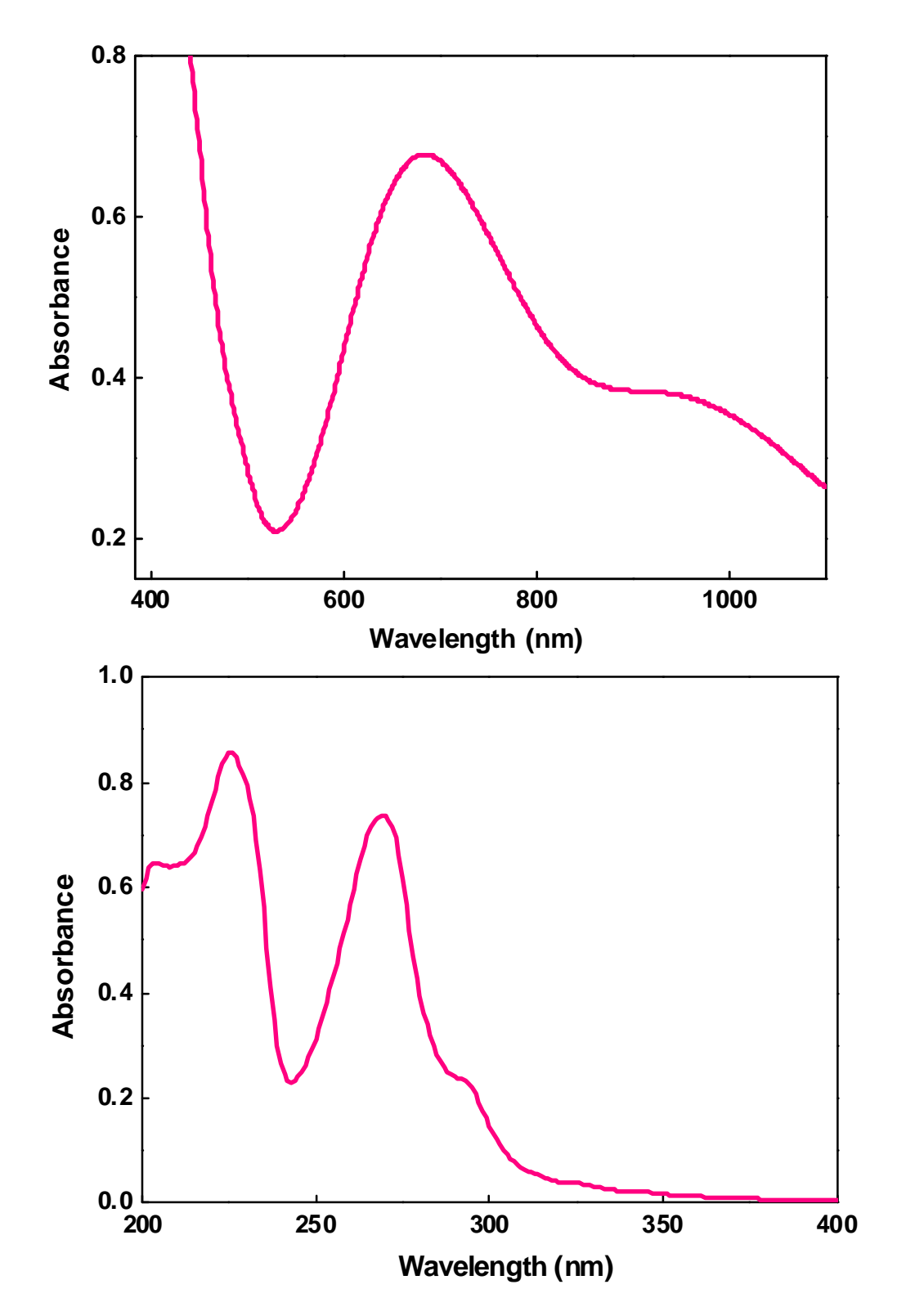


Figure 4.2 Electronic spectra of [Cu(L1)(phen)](ClO₄)₂ 1 in DMF.

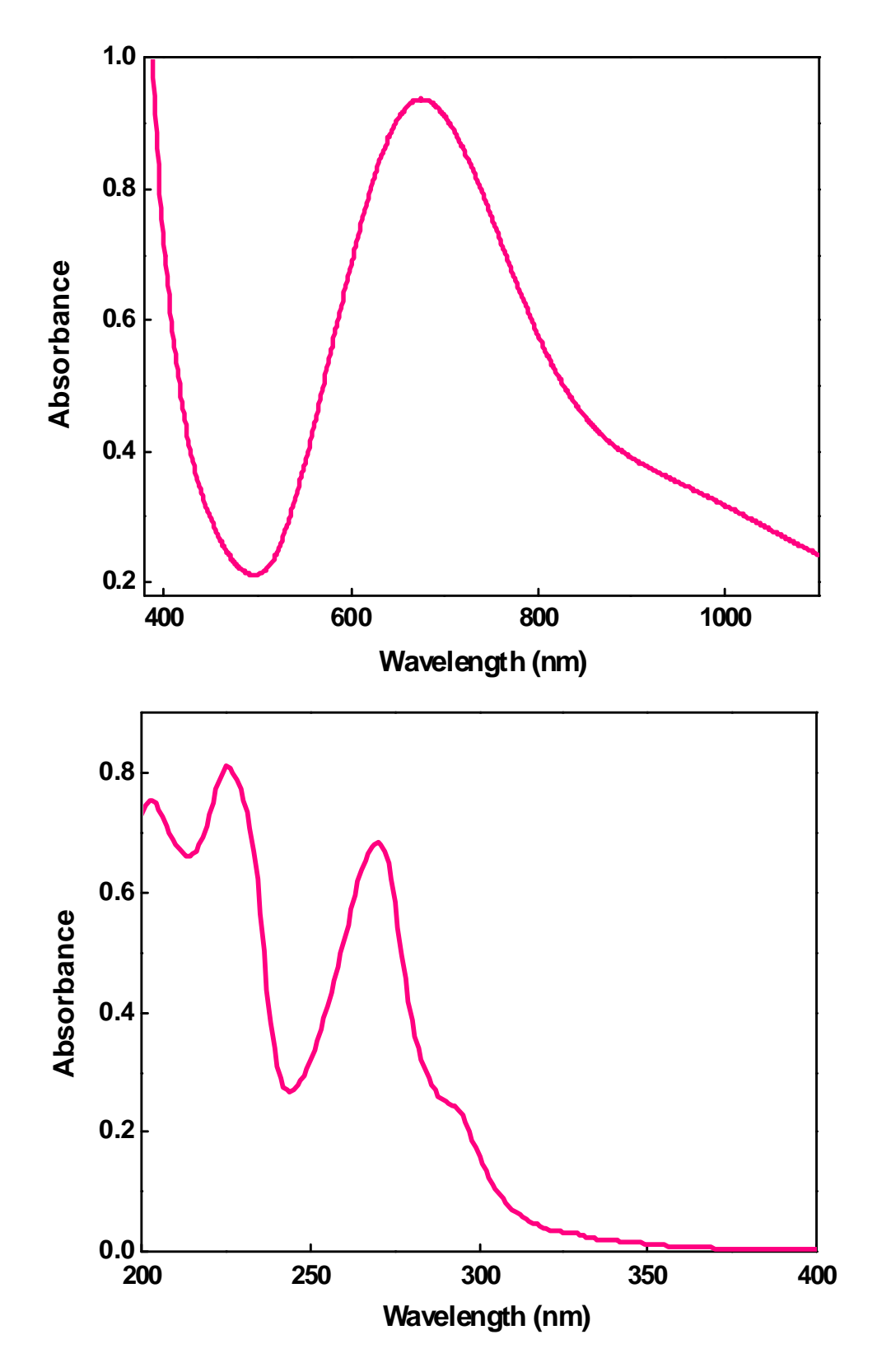


Figure 4.3 Electronic spectra of [Cu(L2)(phen)](ClO₄)₂ 2 in DMF.

The polycrystalline EPR spectra of **1** and **2** are isotropic (**Figures 4.4** and **4.5**). The frozen solution EPR spectra of both the complexes exhibit spectral features typical of mononuclear Cu(II) species (**Figures 4.6** and **4.7**). They are axial with $g_{\parallel} > g_{\perp} > 2.0$ and $G = [(g_{\parallel} - 2)/(g_{\perp} - 2)] = 5.2-5.5$ suggesting the presence of a $d_{x^2-y^2}$ ground state in copper(II) located in square-based geometries [38,39]. A square-based CuN₄ chromophore is expected [40-44] to show a g_{\parallel} value of 2.200 and A_{\parallel} value in the range $180 - 200 \times 10^{-4}$ cm⁻¹, and the distortion or incorporation of strong axial interaction is expected to enhance the g_{\parallel} value and decrease the A_{\parallel} value [40-44]. So the observed values of g_{\parallel} (2.233) and A_{\parallel} (188 - 189 × 10⁻⁴ cm⁻¹) are consistent with the CuN₅ chromophore of the complexes in solution. The $g_{\parallel}/A_{\parallel}$ values (118-119 cm) fall within the range (105-135 cm) expected for complexes with square planar geometry [45] suggesting that there is a slight distortion from planarity, which is evident from the X-ray crystal structure of **2**.

4.3.4 Electrochemical properties

The cyclic (CV) and differential pulse voltammetric (DPV) techniques were employed to investigate the redox behavior of **1** and **2** in DMF solution on stationary glassy carbon electrodes. It displays well-defined cathodic and anodic waves revealing the reversible Cu^{II}/Cu^I redox couple (**Figures 4.8 and 4.9**), owing to the linearity of the plots of i_{pc} versus $v^{1/2}$ (D: **1**, 7.7; **2**, 8.2 × 10⁻⁶ cm² s⁻¹) and the value of peak current ratio (i_{pa}/i_{pc} : **1**, 0.7; **2**, 0.9). On the other hand, the value of the difference in peak potentials (ΔE_p : **1**, 100; **2**, 86 mV) is close to Fc/Fc⁺ couple (ΔE_p , 86 mV; $E_{1/2}$, 0.406 V vs SCE) in a similar experimental condition. Interestingly, the less negative redox potential, $E_{1/2}$ of **2** is higher and peak potential separation, ΔE_p is lower than that of **1** ($E_{1/2}$ and ΔE_p : **1**, -0.077 V and 100 mV; **2**, -0.072 V and 87 mV) for Cu^{II}/Cu^I couple.

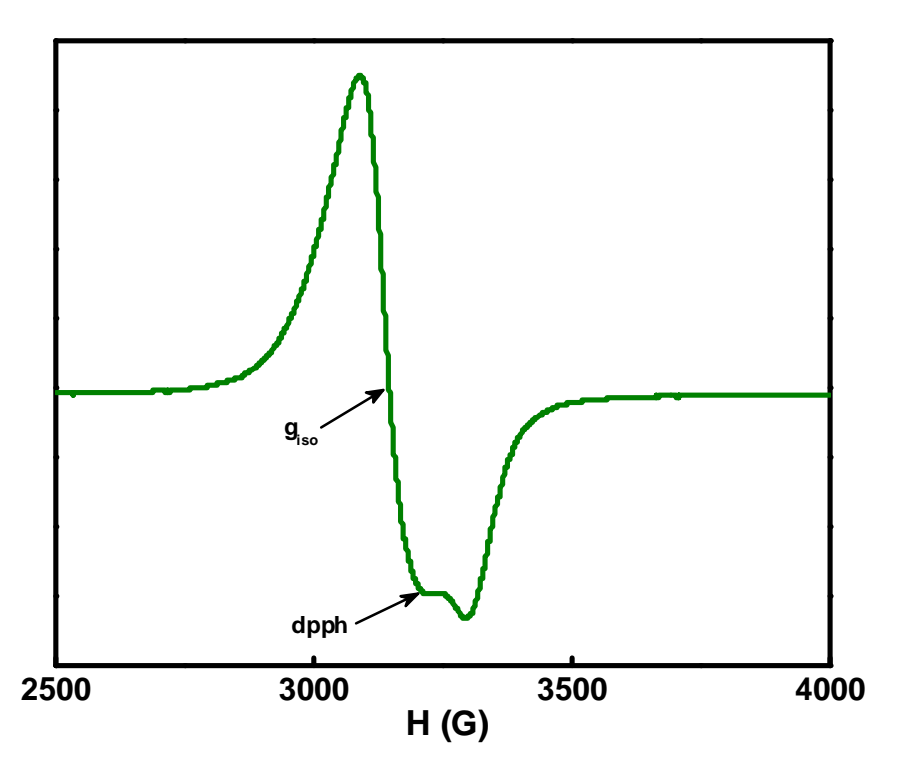


Figure 4.4 Polycrystalline EPR spectrum of $[Cu(L1)(phen)](ClO_4)_2$ 1 at RT.

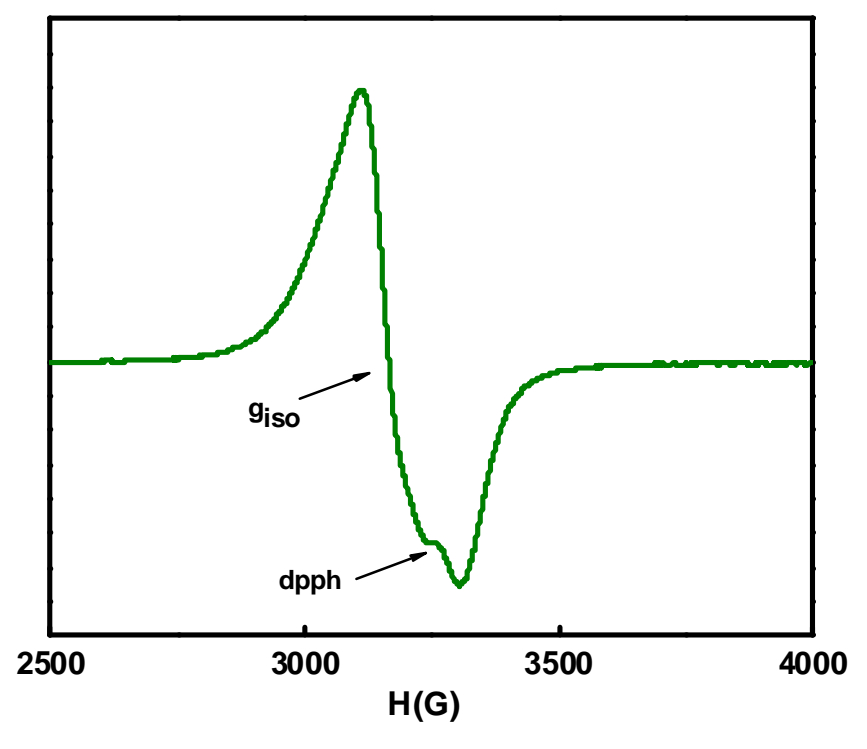


Figure 4.5 Polycrystalline EPR spectrum of [Cu(L2)(phen)](ClO₄)₂ 2 at RT.

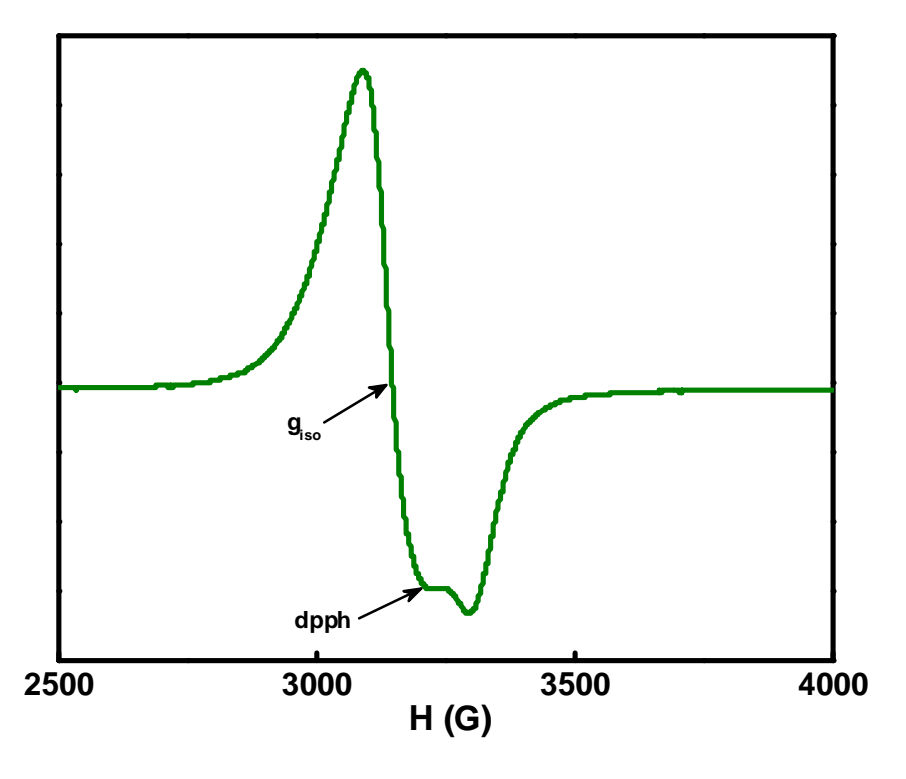


Figure 4.6 EPR spectrum of [Cu(L1)(phen)](ClO₄)₂ 1 in DMF at 77 K.

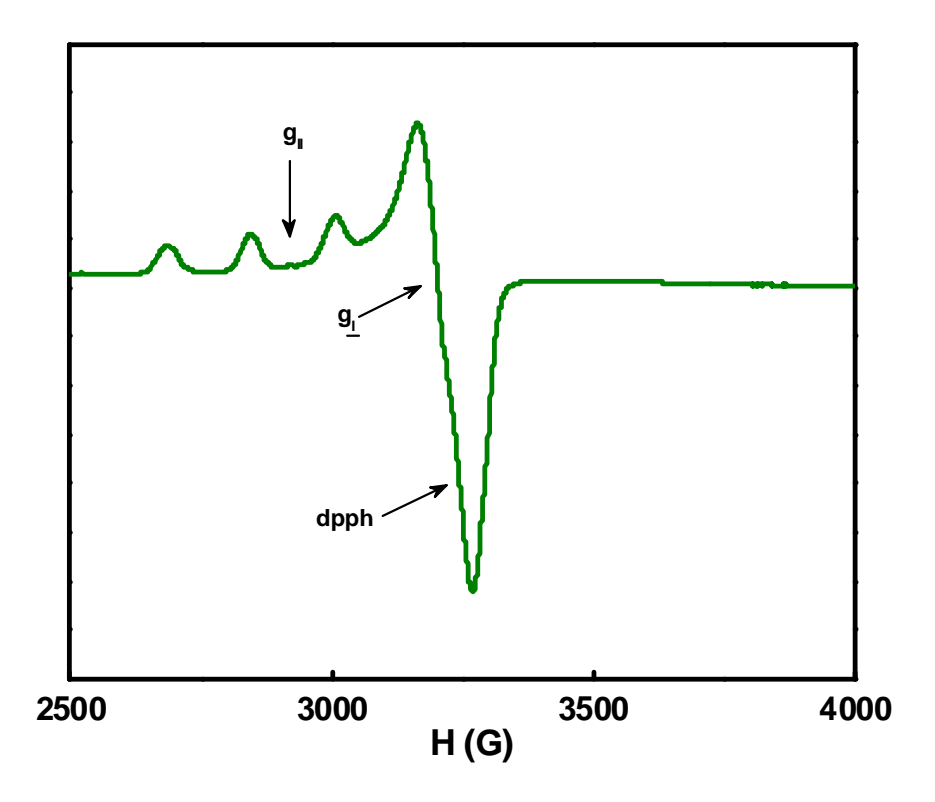


Figure 4.7 EPR spectrum of [Cu(L2)(phen)](ClO₄)₂ 2 in DMF at 77 K.

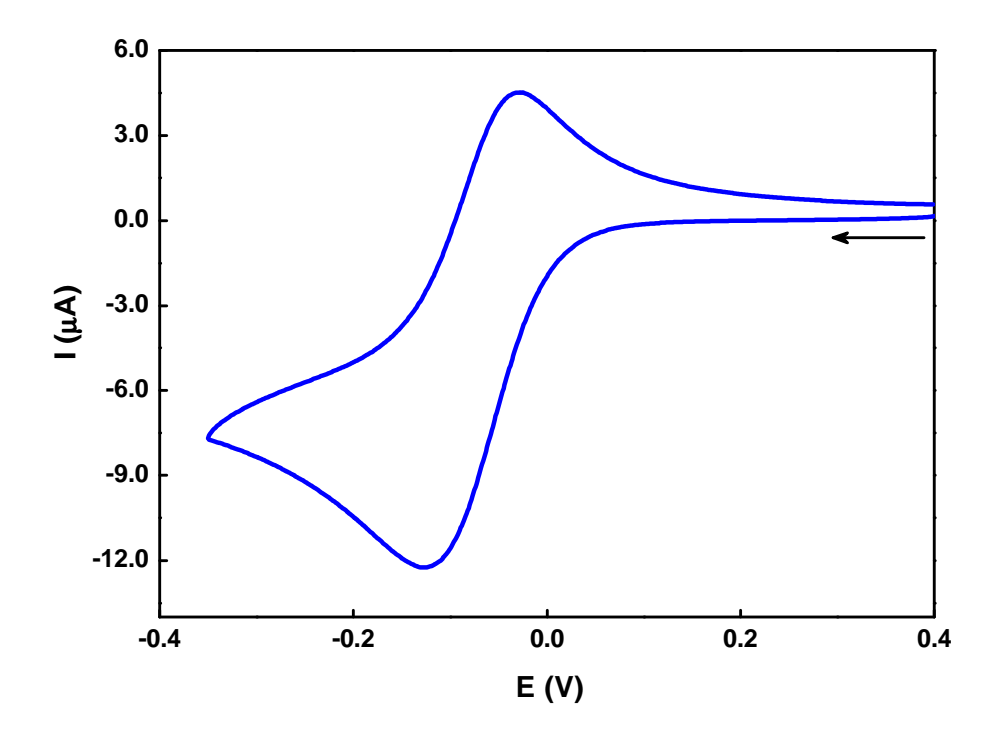


Figure 4.8 Cyclic voltammogram of $[Cu(L1)(phen)](ClO_4)_2$ **1** at 50 mV s⁻¹ scan rate in DMF.

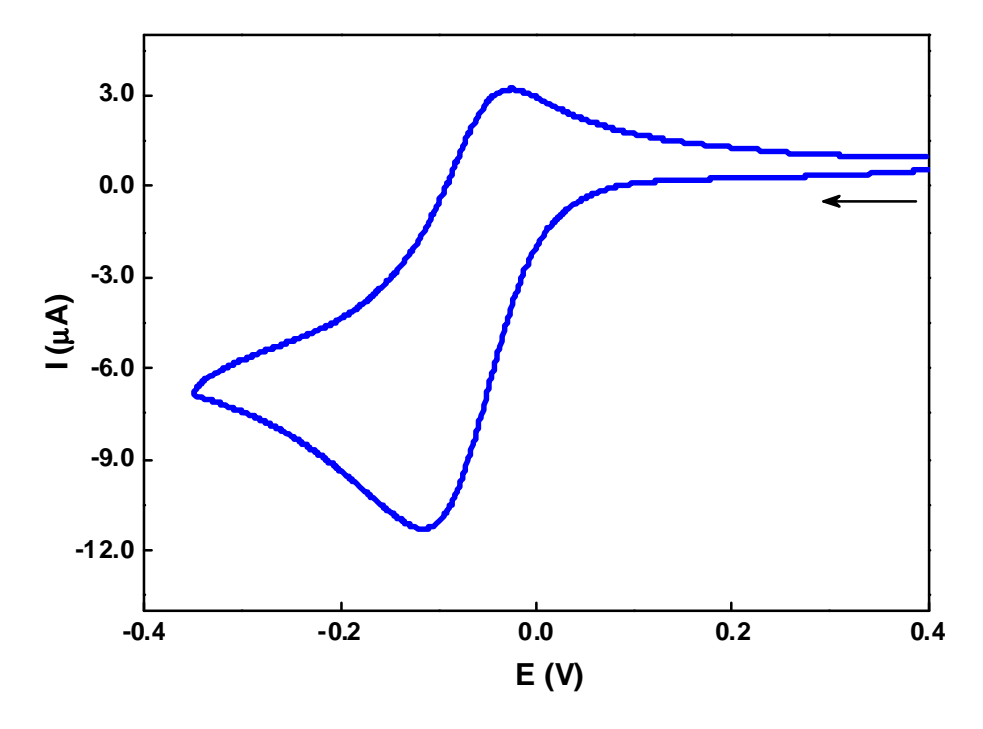


Figure 4.9 Cyclic voltammogram of [Cu(L2)(phen)](ClO₄)₂ **2** at 50 mV s⁻¹ scan rate in DMF.

It indicates the smallest structural reorganization between copper(II) and copper(I) species, renders the Cu(II) to Cu(I) electron transfer more facile. It is due to the existence of flexible six-membered chelate ring forming boat conformation, attracted by the steric hindrance between the 6-metyl group in pyridine moiety of L2 and phen ligands, distort the Cu(II) coordination geometry [46,47]. The redox potential of the Cu^{II}/Cu^I couple from the DPV is -0.063 V (1) and -0.059 V (2) vs SCE (Figures 4.10 and 4.11).

4.3.5 DNA binding studies

The binding mode of the metal complexes with CT DNA is usually characterized using the electronic absorption spectral titration by following the changes in absorbance and shift in wavelength upon varying the concentration of DNA. Upon incremental addition of DNA to 1 and 2 (Figures 4.12 and 4.13), the ligand centered band (268 nm) shows a decrease in molar absorptivity (hypochromism: 1, ~60; 2, ~32%) with red shift (1, 3; 2, 2 nm) at R = 25 (R=[DNA]/[Cu]). Hypochromism with red or no shift is associated with the intercalative mode of interaction with CT DNA, due to strong stacking interactions between the electronic states of the intercalating chromophore and the nucleobases [48]. The observed hypochromic effect with a slight red shift strongly indicates the binding mode of 1 and 2 to CT DNA through partial intercalative interaction. The binding propensities of the complexes are usually expressed with the intrinsic binding constant (K_b) value (Table 4.3). The K_b value was determined by monitoring the changes in the absorption intensity of the complexes with the addition of CT DNA (Figures 4.12 and 4.13, inset).

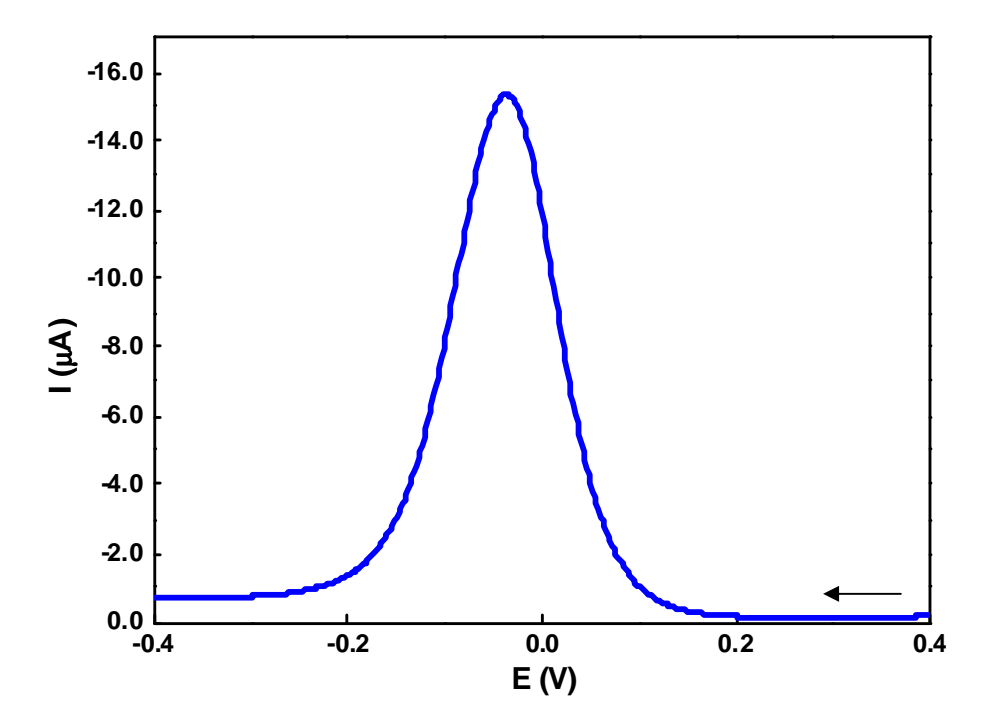


Figure 4.10 Differential pulse voltammogram of [Cu(L1)(phen)](ClO₄)₂ **1** at 2 mV s⁻¹ scan rate in DMF.

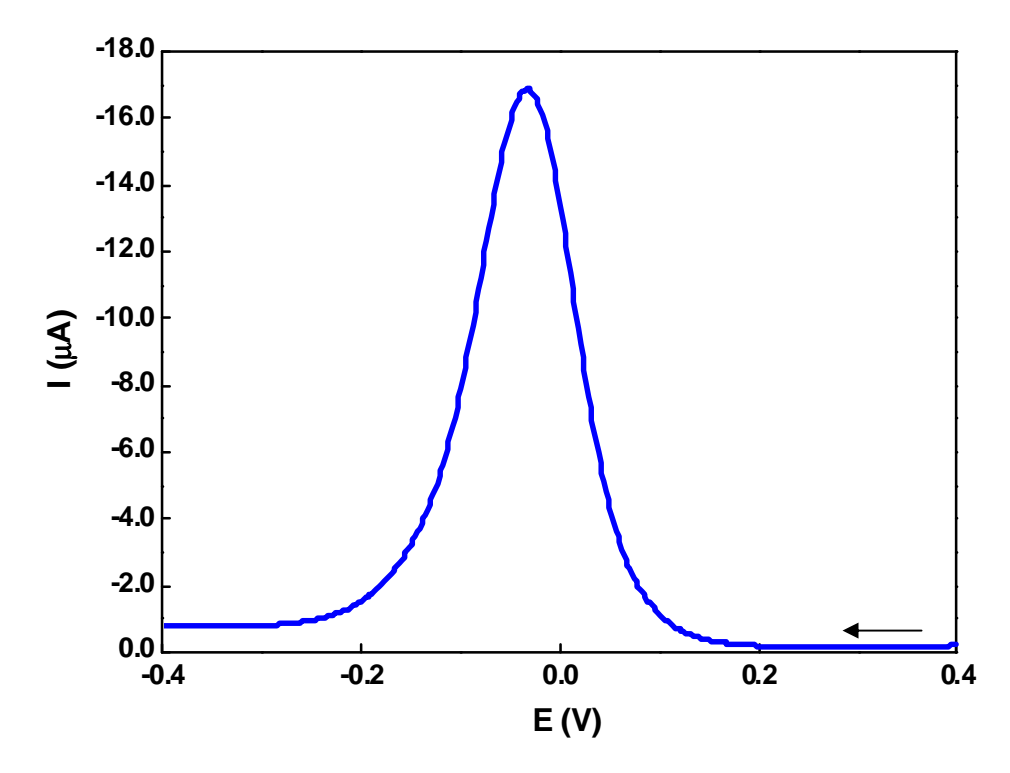


Figure 4.11 Differential pulse voltammogram of [Cu(L2)(phen)](ClO₄)₂ **2** at 2 mV s⁻¹ scan rate in DMF.

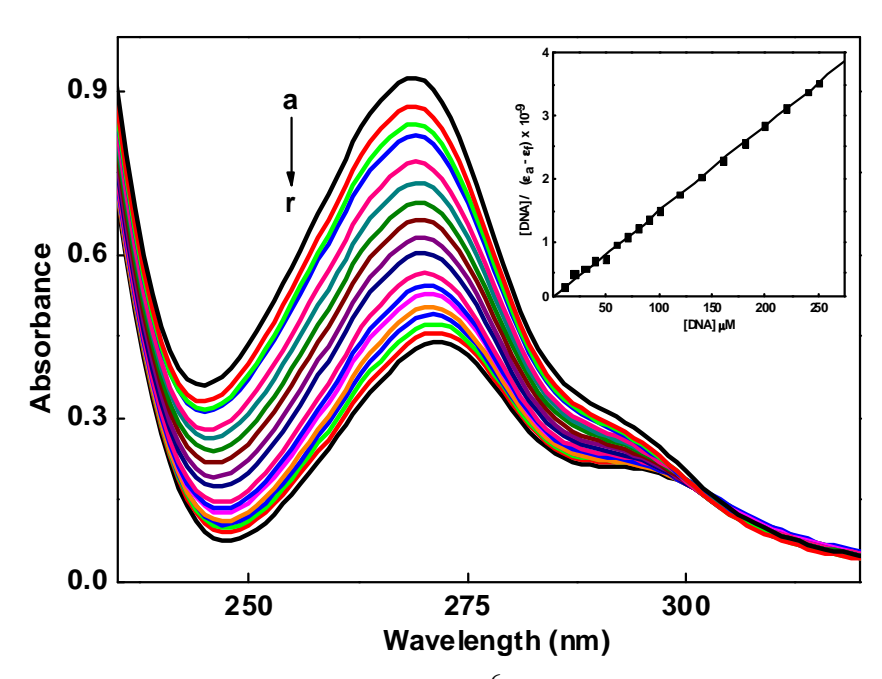


Figure 4.12 Absorption spectra of 1 (10×10^{-6} M) in 2% DMF/5 mM Tris-HCl/50 mM NaCl buffer at pH 7.1 in the absence (R = 0) and presence (R = 25) of increasing amounts of CT DNA. Inset: Plot of [DNA] vs [DNA]/(ϵ_a - ϵ_f) at R = 25 of 1.

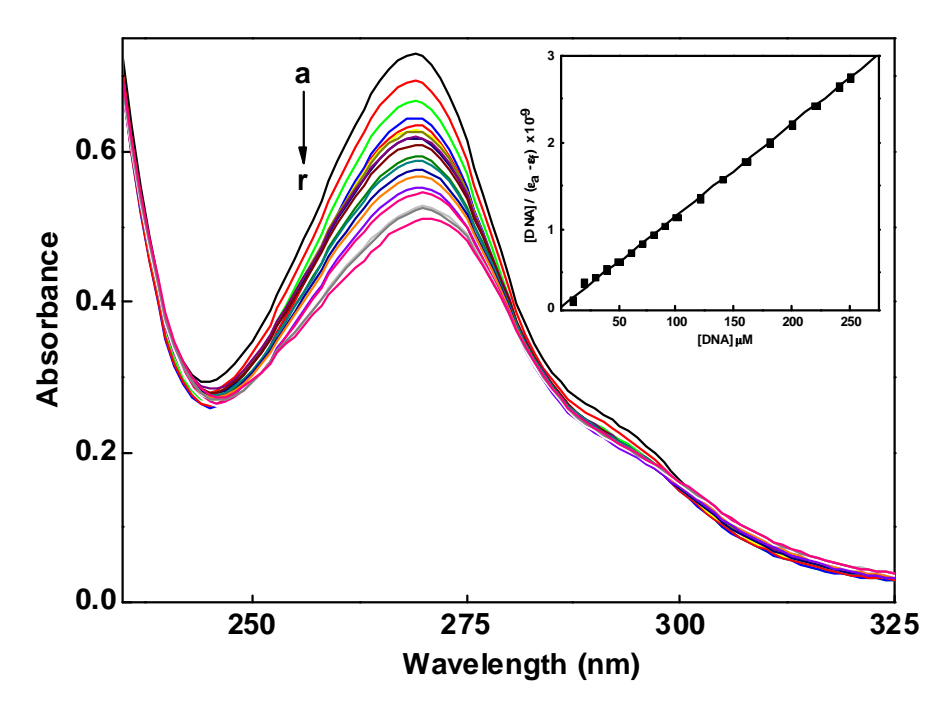


Figure 4.13 Absorption spectra of 2 (10×10^{-6} M) in 2% DMF/5 mM Tris-HCl/50 mM NaCl buffer at pH 7.1 in the absence (R = 0) and presence (R = 25) of increasing amounts of CT DNA. Inset: Plot of [DNA] vs [DNA]/(ϵ_a - ϵ_f) at R = 25 of 2.

Table 4.3Ligand-based absorption spectral properties^a and fluorescence spectral properties^b of copper(II) complexes (1 and 2) bound to CT DNA

		Ligand-based					
Complex	λ_{max} (nm)	R	Change in absorbance	Δε (%)	Red- shift (nm)	$K_{\rm b}$ (× 10^5 M ⁻¹)	K_{app}^{b} (× $10^6 M^{-1}$)
$\left[Cu(L1)(phen) \right]^{2+} 1$	268	25	Hypochromism	60	3	1.355± 0.001	5.2
[Cu(L2)(phen)] ²⁺ 2	268	25	Hypochromism	32	2	1.056± 0.001	5.0

^aMeasurements were made at R = 25, where R = [DNA]/[complex]; the concentration of solutions of Cu(II) complexes = 10×10^{-6} M (1 and 2).

The strong DNA binding affinity (K_b in the order of $10^5 \,\mathrm{M}^{-1}$) of the complexes follows the order 1 (1.36) > 2 (1.06). The higher binding strength in 1 is attributed to the presence of a rigid five-membered chelate ring. The rigidity enhances the partial intercalative interaction of phen ligand between the base pairs of DNA. The hydrophobic interaction of the 6-methyl group with the hydrophobic DNA surface further supports to increase in the DNA binding affinity [49] in 1. The lower binding affinity of 2 is due to the presence of a flexible six-membered chelate ring. The flexibility reduces the efficiency of partial intercalative interaction of phen ligand followed by the decrease in the hydrophobic interaction of the 6-methyl group in 2. Thus, the greater hypochromism and red shift along with a higher K_b value for 1 in comparison to that for 2, indicates the better DNA binding propensity of 1 through partial intercalative interaction.

^bApparent DNA binding constant from the ethidium bromide displacement assay using increasing concentrations (0-10 μ M) of **1** and **2**

To provide further evidence for the interaction mode, the binding of 1 and 2 to CT DNA has been studied by a competitive binding fluorescence assay using EthBr. The fluorescence intensity of EthBr bound to DNA at 594 nm (λ_{ex} , 520 nm) shows a remarkable decrease (Figures 4.14 and 4.15) with the addition of 1 (78%) or 2 (77%), indicating DNA-bound EthBr molecules are released into solution [50]. Such fluorescence quenching may be caused by the strong partial intercalative interaction of 1 or 2 (cf. above), leading to the displacement of DNA-bound EthBr. The slope of the plot of I₀/I versus [complex] gives K_{SV} (Figures 4.14 and 4.15, inset) [51]. It is seen that the fluorescence quenching follows Stern-Volmer behavior and the calculated values of K_{SV} are 4.26×10^5 M⁻¹ (1) and 4.12×10^5 M⁻¹ (2). The apparent DNA binding constant (K_{app}) is calculated [52] using the equation, $K_{EthBr}[EthBr] = K_{app}[complex]$, where K_{EthBr} is 4.94×10^5 M⁻¹ [53], the concentration of EthBr is 1.25×10^{-6} M, and the concentration of the complex is that used to obtain a 50% reduction of fluorescence intensity of EthBr (**Table 4.3**). The calculated K_{app} values are 5.20×10^6 M^{-1} (1) and $5.00 \times 10^6 M^{-1}$ (2) and the results suggest that 1 intercalated more strongly than 2. These values are consistent with the K_b value obtained by electronic absorption spectral study.

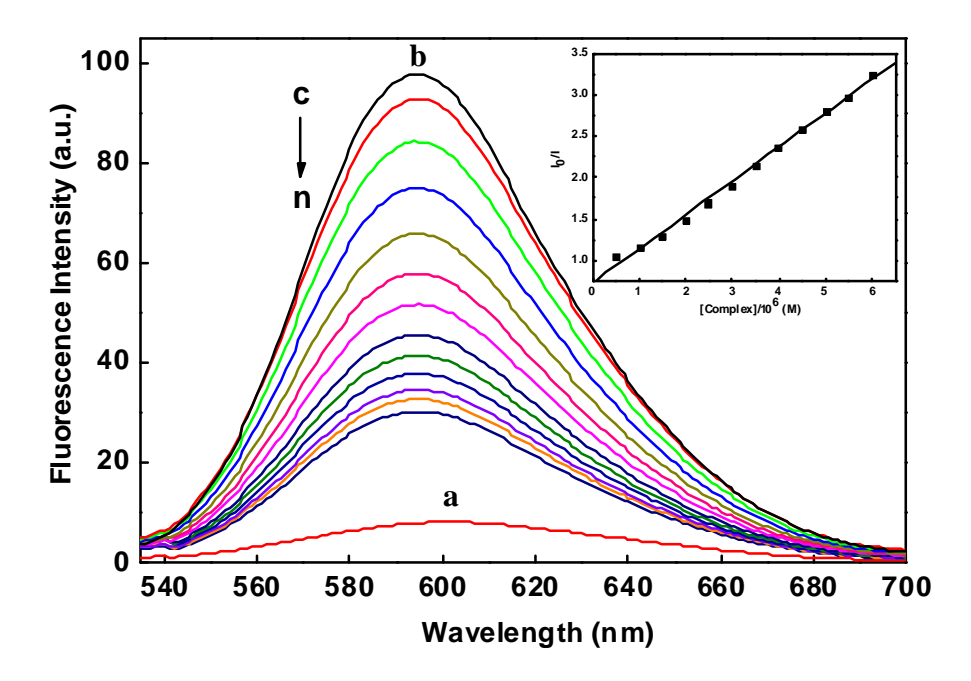


Figure 4.14 Fluorescence quenching curves of ethidium bromide bound to DNA in 2% DMF/5 mM Tris-HCl/50 mM NaCl buffer at pH 7.1: (a) EthBr (1.25 μM); (b) EthBr + DNA (125 μM); (c-m) EthBr + DNA + 1 (0-10 μM). Inset: Plot of I₀/I versus [complex].

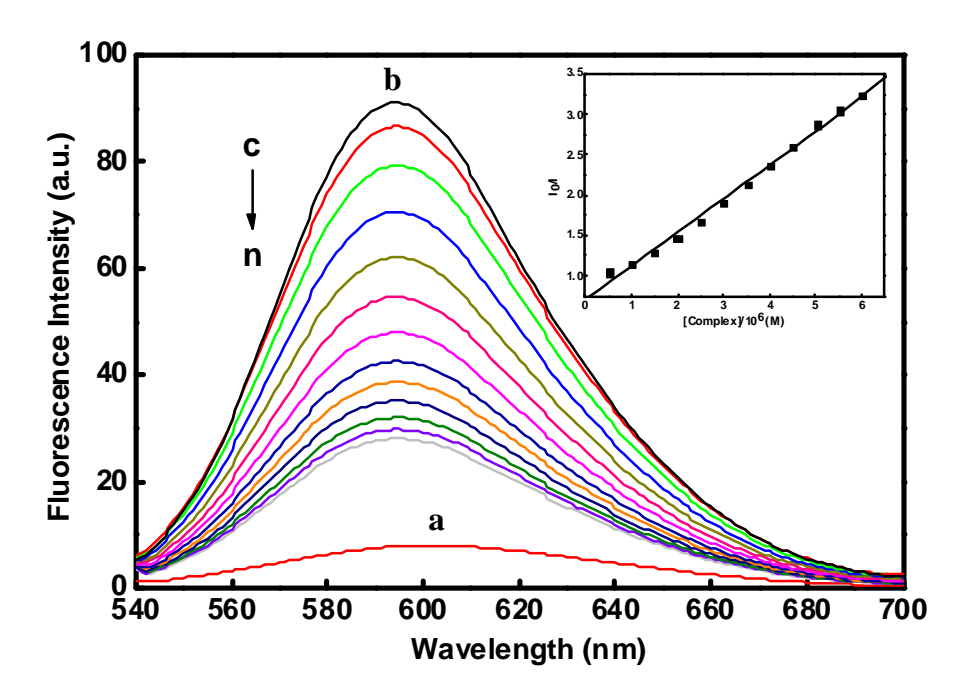


Figure 4.15 Fluorescence quenching curves of ethidium bromide bound to DNA in 2% DMF/5 mM Tris-HCl/50 mM NaCl buffer at pH 7.1: (a) EthBr (1.25 μ M); (b) EthBr + DNA (125 μ M); (c-m) EthBr + DNA + 2 (0-10 μ M). Inset: Plot of I₀/I versus [complex].

The observed circular dichroic (CD) spectrum of CT DNA (2 × 10⁻⁵ M) consists of a positive band (270 nm) due to base stacking and a negative band (240 nm) due to helicity (**Figures 4.16a and 4.17a**), which is characteristic of DNA in the right-handed B form [54]. The simple groove binding and electrostatic interaction of small molecules with DNA show less or no perturbations on the base stacking and helicity bands, while intercalation enhances the intensities of both the bands stabilizing the right-handed B conformation of DNA [55]. When **1** or **2** is incubated with DNA at 1/R (=[Cu complex]/[DNA]) value of 3, the CD spectrum of DNA (**Figures 4.16b and 4.17b**) changes both positive (vast increase in intensity; red-shift: **1** and **2**, 3nm) and negative bands (slight decrease in intensity; red-shift: **1** and **2**, 4 nm), which is consistent with partial intercalative interaction of phen ring, supporting the results from electronic absorption spectroscopy.

Knowledge of DNA interaction of the reduced and/or the oxidized form of a metal can also be complemented by studying the electrochemical behavior of metal complexes with DNA [56]. For studying the binding mode of complexes with DNA using cyclic voltammetry (CV), the redox potential was measured for a fixed concentration of the complex with increases in the concentration of CT DNA. Both the complexes display well-defined cathodic and anodic waves (Figures 4.18a and 4.19a) within the time scale of the CV experiments (2% DMF/5 mM Tris-HCl/50 mM NaCl buffer; pH 7.1). The redox-active complexes 1 and 2 show the reversible Cu(II)/Cu(I) couple ($E_{1/2}$: 1, -0.079; 2, -0.073 V/ ΔE_p : 1, 99; 2, 89 mV/ i_{pa}/i_{pc} : 1, 0.8; 2, 0.6). Upon the addition of CT DNA (R = [DNA]/[Cu] = 5) a significant reduction in cathodic and a slight decrease in anodic peak currents are observed due to slow diffusion of DNA bound complex to the electrode surface.

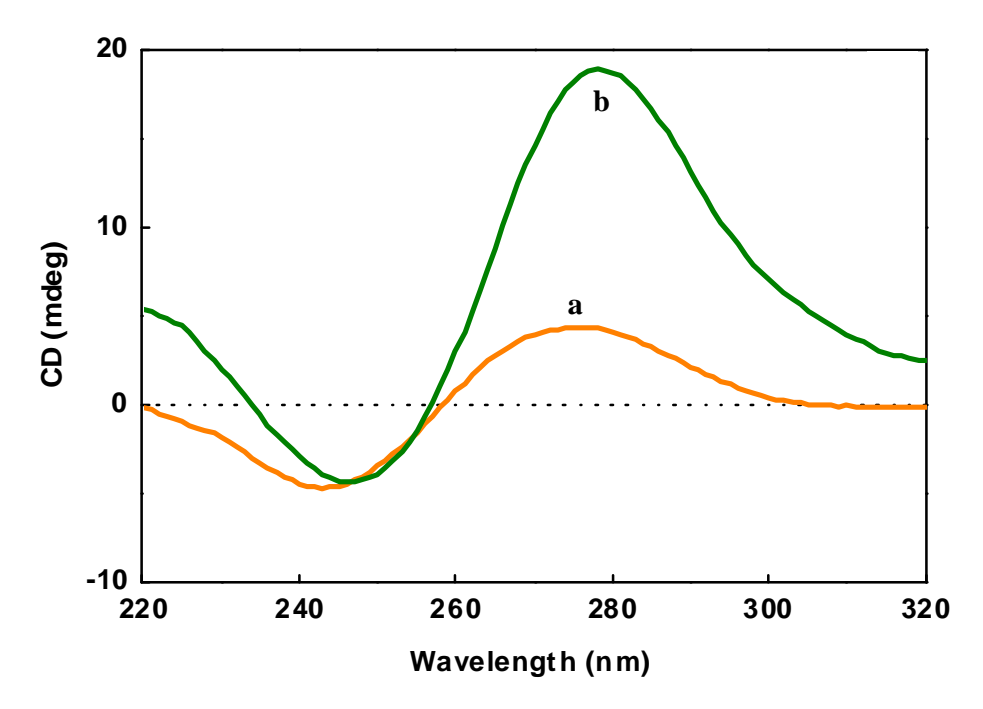


Figure 4.16 Circular dichroism spectra of CT DNA in 2% DMF/5 mM Tris-HCl/50 mM NaCl buffer at pH 7.1 and 25 °C in the absence (a) and presence (b) of 1 at 1/R value of 3.

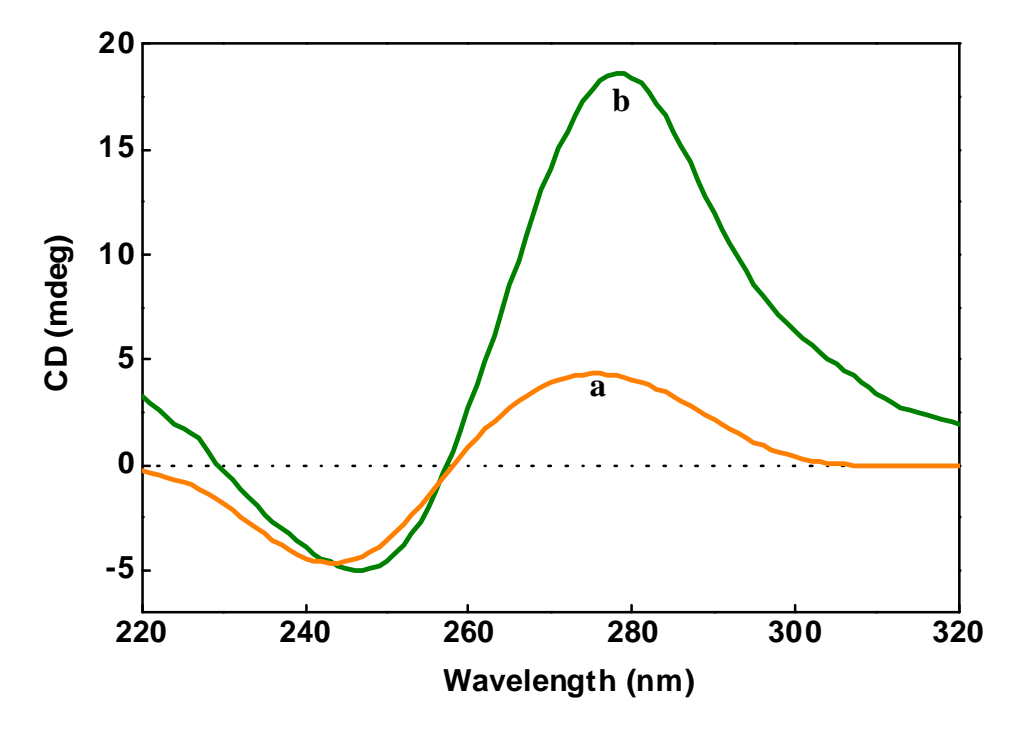


Figure 4.17 Circular dichroism spectra of CT DNA in 2% DMF/5 mM Tris-HCl/50 mM NaCl buffer at pH 7.1 and 25 °C in the absence (a) and presence (b) of 2 at 1/R value of 3.

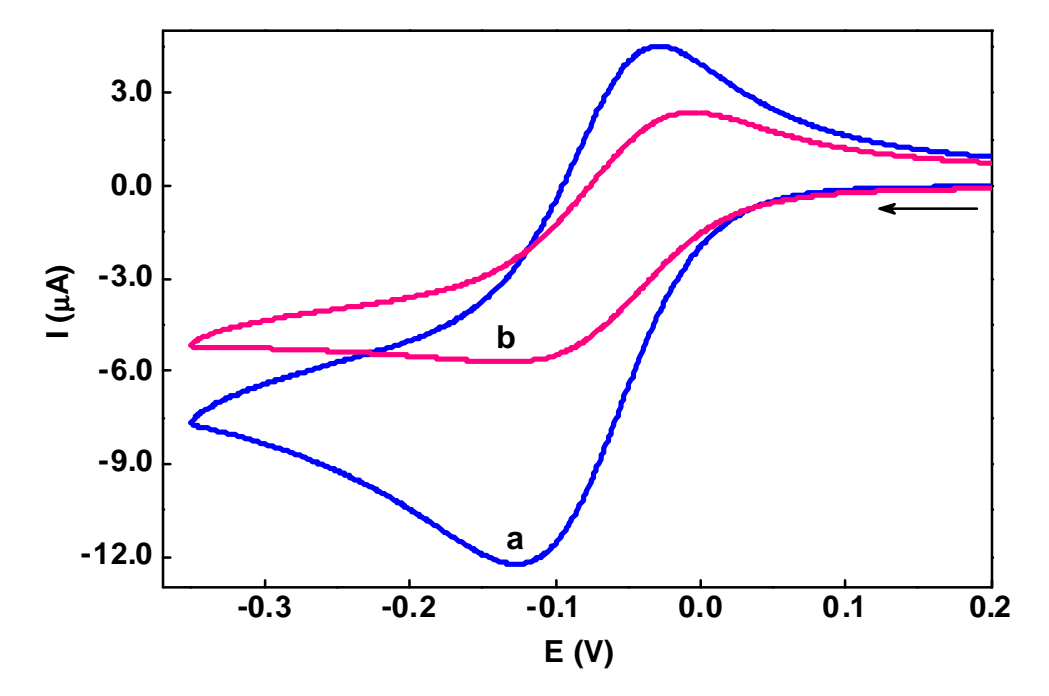


Figure 4.18 Cyclic voltammograms of **1** (0.5 mM) in the absence (a) and presence (b) of CT DNA (R = 5) at 25.0±0.2 °C at 50 mV s⁻¹ scan rate in 2% DMF/5 mM Tris-HCl/50 mM NaCl buffer at pH 7.1.

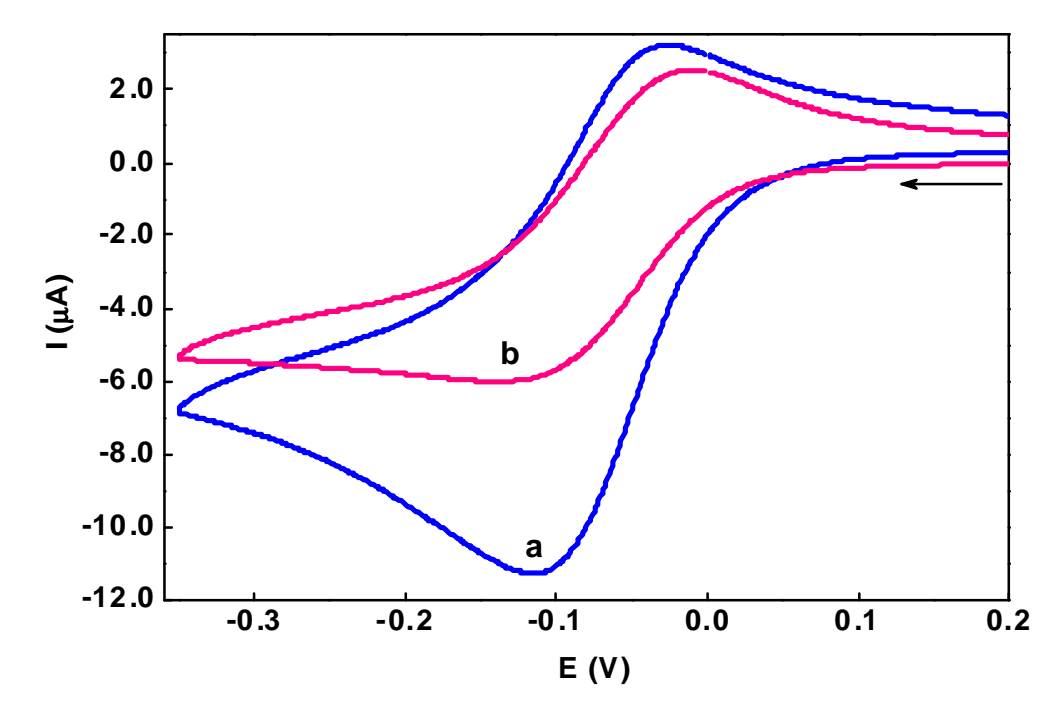


Figure 4.19 Cyclic voltammograms of 2 (0.5 mM) in the absence (a) and presence (b) of CT DNA (R = 5) at 25.0 ± 0.2 °C at 50 mV s⁻¹ scan rate in 2% DMF/5 mM Tris-HCl/50 mM NaCl buffer at pH 7.1.

The decrease in current is more significant for 1 than for 2 (Figures 4.18b and **4.19b**). The cathodic peak potential undergoes a positive shift for 2 and a negative shift for 1 while the anodic peak potential experiences a negative shift for both 1 and 2 [57]. Usually, a positive shift in potential is observed for the intercalation mode of binding, whereas a negative shift is observed for electrostatic interaction. Thus, the observed redox potential ($E_{1/2}$) shift for **1** is less positive (+2 mV) and for **2** is less negative (-4 mV). It implies that the binding of 1 and 2 to DNA is through partial intercalative interaction. For a Nernstian electron-transfer system, in which both oxidized (Cu²⁺) and reduced forms (Cu⁺) associate with a third species in solution (DNA), differential pulse voltammetry (DPV) can be used to calculate the ratio of corresponding equilibrium constants for each oxidation state binding to DNA [56]. The $E_{1/2}$ values (DPV: 1, -0.063; 2, -0.058 V) for the Cu(II)-Cu(I) redox couple of the complexes (Figures 4.20 and 4.21) are shifted (1, +1; 2, -6 mV) revealing the stronger DNA binding affinity of 1 compared to that of 2 (cf. above). The shift in the value of the formal potential (ΔE^{0}) can be used to estimate the ratio of the equilibrium binding constant (K^+/K^{2+}) values of the Cu(I) and Cu(II) form to DNA, which is calculated to be 1.0 (1) and 1.3 (2), suggesting their stabilization in the Cu(I) oxidation state upon binding to CT DNA [58].

4.3.6 DNA cleavage

In the absence of external additives, the ability of **1** and **2** to cleave DNA was tested using gel electrophoresis on supercoiled (SC) pUC19 plasmid DNA as the substrate in a medium of 2% DMF/5 mM Tris-HCl/50 mM NaCl buffer (pH = 7.1).

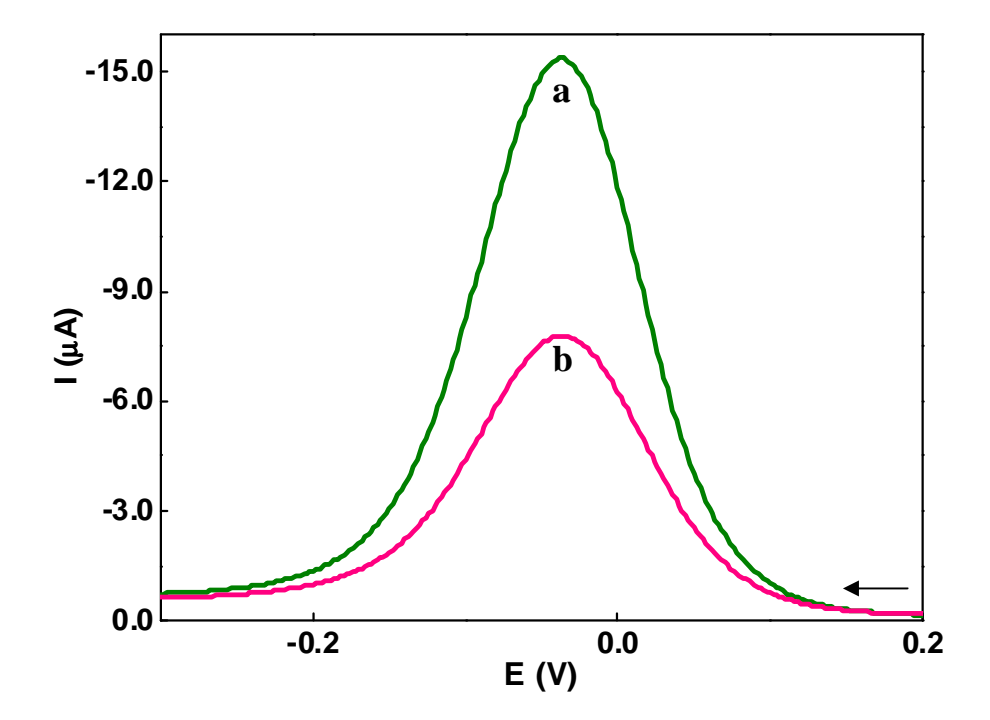


Figure 4.20 Differential pulse voltammograms of 1 (0.5 mM) in the absence (a) and presence (b) of CT DNA (R = 5) at 25.0 ± 0.2 °C at 2 mV s⁻¹ scan rate in 2% DMF/5mM Tris-HCl/50 mM NaCl buffer at pH 7.1.

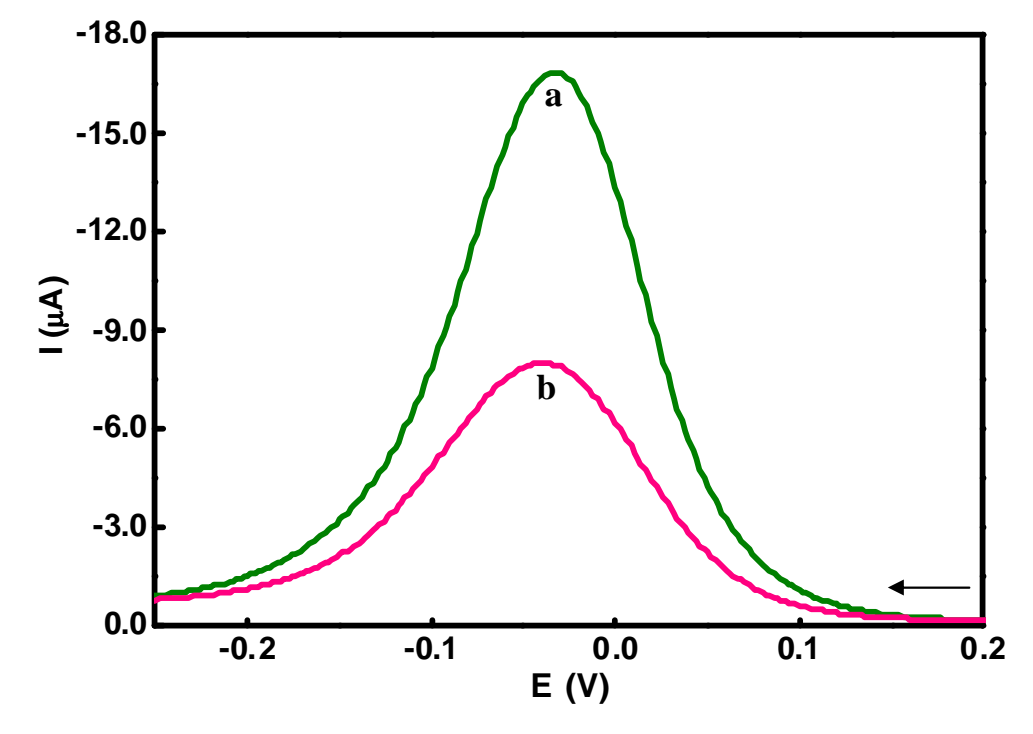


Figure 4.21 Differential pulse voltammograms of 2 (0.5 mM) in the absence (a) and presence (b) of CT DNA (R = 5) at 25.0 ± 0.2 °C at 2 mV s⁻¹ scan rate in 2% DMF/5mM Tris-HCl/50 mM NaCl buffer at pH 7.1.

Upon incubation of the plasmid DNA (20 µM in base pairs) with 1 and 2 (100 μM) for 1 h at 37 °C followed by electrophoresis, the fastest migration is observed for the SC DNA (Form I). A single strand of SC DNA relaxes upon cleavage, resulting in the slower-moving nicked circular (NC) DNA (Form II). As no linear DNA (LC, Form III) is discernible between Forms I and II, it is clear that both the DNA strands are not cleaved by 1 or 2 (Figures 4.22 and 4.23). Both complexes convert SC DNA to NC DNA to a nearly identical level (43%) while control studies with DNA alone reveal no cleavage. The partial intercalation of the phen ring and the hydrophobic interaction of the 6-methyl moiety present in the L1/L2 ligand with the DNA surface result in moderate nuclease activity, which is compatible with the changes in DNA binding affinity (cf. above). The amount of Form I decrease while that of Form II increases when the concentrations of 1 or 2 are increased (25-200 µM) while keeping the DNA concentration constant (20 µM). They cause complete conversion of SC DNA to NC DNA (97%) at a complex concentration of 200 µM, demonstrating that the cleavage of pUC19 DNA is extremely concentration-dependent. Thus, the partial intercalation of 1 and 2, supported by the strong hydrophobic interaction of the 6-methyl moiety, leads to increased DNA-binding of the complexes and larger DNA double-helix distortions, resulting in significant DNA cleavage activity even in the absence of an activator [59].

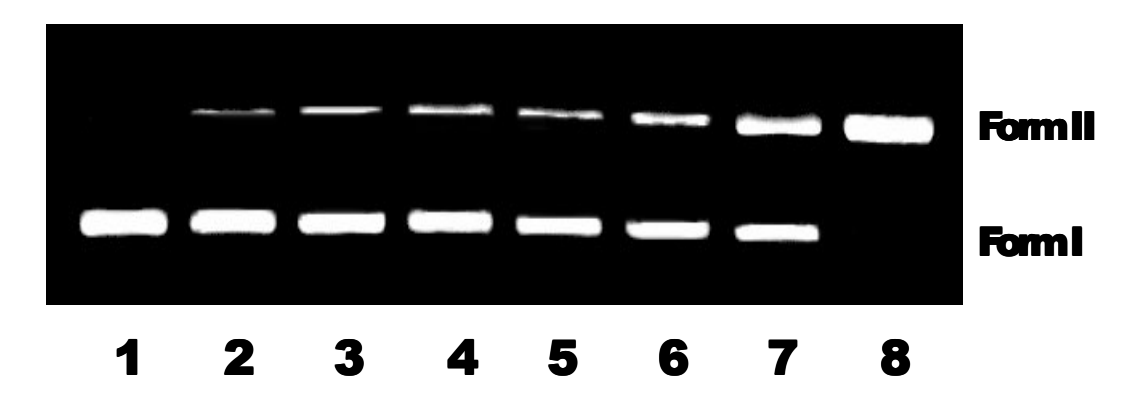


Figure 4.22 Agarose gel showing cleavage of 20 μM SC pUC19 DNA incubated with 1 in 2% DMF 50 mM Tris-HCl/NaCl buffer (pH 7.1) at 37 °C for 1 h. Lane 1, DNA; lanes 2-8, DNA + 1 (25, 50, 100, 125, 150, 175, 200 μM respectively). Forms I and II are supercoiled and nicked circular forms of DNA respectively.

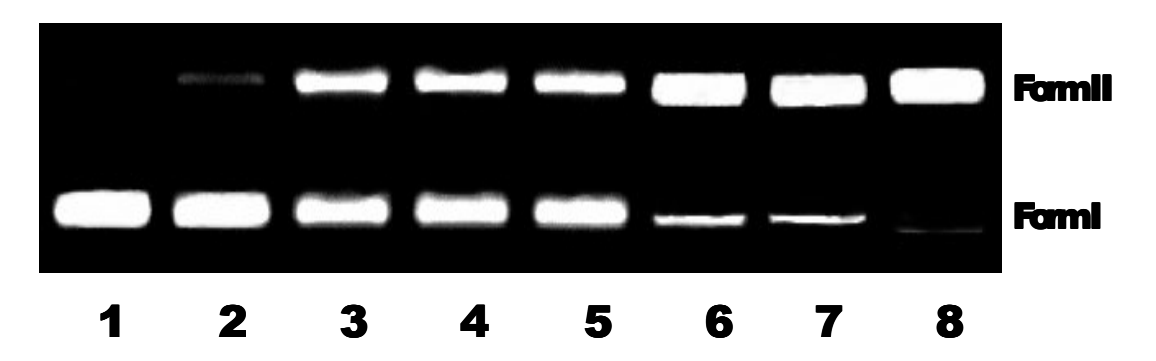


Figure 4.23 Agarose gel showing cleavage of 20 μM SC pUC19 DNA incubated with 2 in 2% DMF 50 mM Tris-HCl/NaCl buffer (pH 7.1) at 37 °C for 1 h. Lane 1, DNA; lanes 2-8, DNA + 2 (25, 50, 100, 125, 150, 175, 200 μM respectively). Forms I and II are supercoiled and nicked circular forms of DNA respectively.

On the other hand, incubation of 1 and 2 (25 µM) with supercoiled pUC19 DNA (20 µM) in 2% DMF/5 mM Tris-HCl/50 mM NaCl buffer (pH 7.1) in the presence of an external activator, H₂O₂ (50 μM), was used to test the ability of the present complexes to effect oxidative DNA cleavage (Figures 4.24 and 4.25). There is no DNA cleavage activity in the control experiments with DNA or H₂O₂ alone. Both complexes convert Form I to Form II (1, 97; 2, 93%) with substantial oxidative DNA cleavage. The ability of copper(II) complexes to induce oxidative DNA cleavage follows the order 1 > 2, which is consistent with their DNA binding affinity. At a concentration of 15 µM, complex 1 induces more than 50% DNA cleavage, whereas 2 causes the same proportion of DNA cleavage but at a slightly higher (20 µM) concentration. It suggests that complexes capable of a higher non-covalent interaction with DNA have higher DNA cleavage activity. Complex 1 with stronger DNA binding affinity exhibits oxidative DNA cleavage activity slightly higher than that of 2. The higher stability of Cu(I) species of 1 and 2 (cf. above, less negative Cu(II)/Cu(I) redox potential) causes more generation of ROS. As the concentration of 1 or 2 is increased, the amount of Form I decreases, while the concentration of H₂O₂ (50 µM) and DNA (20 µM) remains constant. Moreover, 1 achieves maximum DNA degradation at a concentration of 20 µM (Figure 4.24, lane 6), but 2 completes at a concentration of 30 µM (Figure 4.25, lane 8). It confirms the efficient DNA cleavage activity of complexes containing phen, which position themselves near the site of DNA cleavage through non-covalent interaction of the phen ligand and generate more ROS, resulting in higher cleavage efficiency (cf. above).

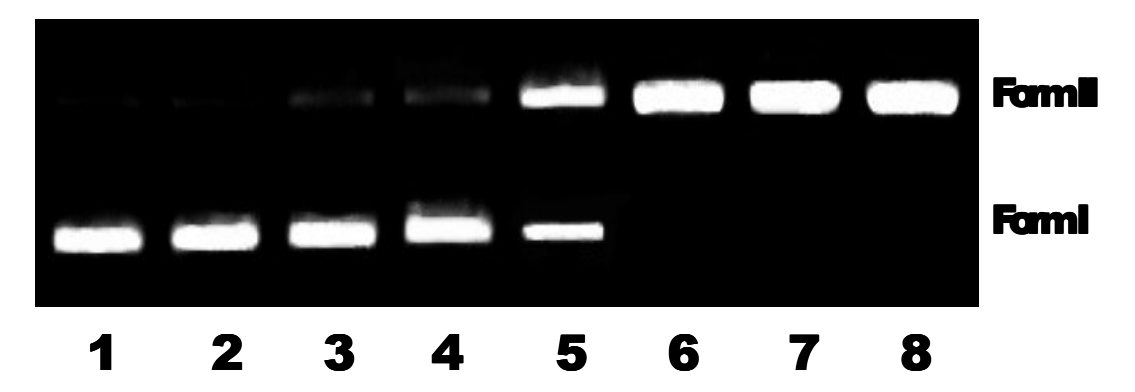


Figure 4.24 Agarose gel showing cleavage of 20 μM SC pUC19 DNA incubated with 1 in 2% DMF 50 mM Tris-HCl/NaCl buffer (pH 7.1) at 37 °C for 1 h in the presence of H₂O₂ (50 μM). Lane 1, DNA; Lane 2, DNA + H₂O₂; lanes 3-8, DNA + H₂O₂ + 1 (5, 10, 15, 20, 25, 30 μM respectively). Forms I and II are supercoiled and nicked circular forms of DNA respectively.

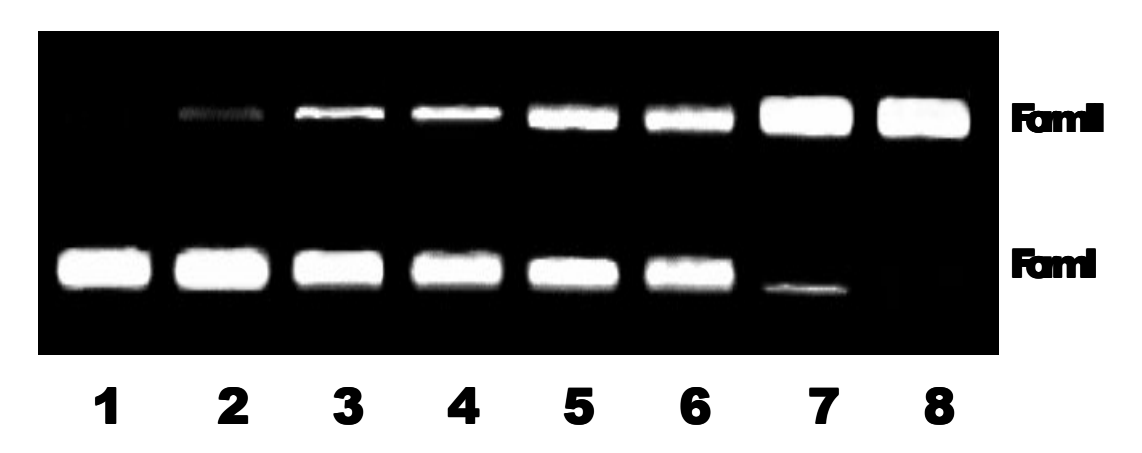


Figure 4.25 Agarose gel showing cleavage of 20 μM SC pUC19 DNA incubated with 2 in 2% DMF 50 mM Tris-HCl/NaCl buffer (pH 7.1) at 37 °C for 1 h in the presence of H₂O₂ (50 μM). Lane 1, DNA; Lane 2, DNA + H₂O₂; lanes 3-8, DNA + H₂O₂ + 2 (5, 10 , 15, 20, 25, 30 μM respectively). Forms I and II are supercoiled and nicked circular forms of DNA respectively.

Alternatively, the supercoiled pUC19 DNA (20 µM in base pairs) and 1 or 2 (5-30 μM) are incubated for 1 h at 37 °C in a medium 2% DMF/5 mM Tris-HCl/50 mM NaCl buffer (pH = 7.1), with ascorbic acid (H_2A ; 20 μ M) as an activating agent. Under identical conditions, no cleavage of pUC19 DNA occurred for H₂A or copper(II) complex alone. It was discovered that at a complex concentration of 20 µM (1) and 25 μ M (2), SC DNA is converted into >90% NC DNA (Figures 4.26 and 4.27). When the complex concentration is increased in the presence of H₂A, the amount of Form I gradually decrease while that of Form II gradually increases. It was revealed that 1 and 2 can convert SC DNA into NC DNA but not LC DNA. They cause complete conversion of Form I to Form II (97%) at a complex concentration of 25 µM (1) or 30 µM (2), demonstrating that the cleavage of pUC19 DNA is concentrationdependent. Under identical conditions, the time-dependent cleavage of DNA by 1 or 2 in the presence of H_2A was investigated ([complex] = 25 μ M and [DNA] = 20 μM in bp) as a function of time (0-60 minutes). The amount of NC DNA increases as the reaction time is extended, while the amount of SC DNA steadily decreases (Figures 4.28 and 4.30). Also, the appearance of NC DNA as well as the disappearance of SC DNA follow pseudo-first-order kinetic profiles and fit well into a single-exponential decay curve (Figures 4.29 and 4.31). Also, it is noted that 50% of DNA cleavage reached within 35 minutes; the rate of DNA cleavage reaches the maximum within 55 minutes and then remains constant.



Figure 4.26 Agarose gel showing cleavage of 20 μM SC pUC19 DNA incubated with 1 in 2% DMF 50 mM Tris-HCl/NaCl buffer (pH 7.1) at 37 °C for 1 h in the presence of ascorbic acid (H₂A, 20 μM). Lane 1, DNA; Lane 2, DNA + H₂A; lanes 3-8, DNA + H₂A + 1 (5, 10, 15, 20, 25, 30 μM respectively). Forms I and II are supercoiled and nicked circular forms of DNA respectively.

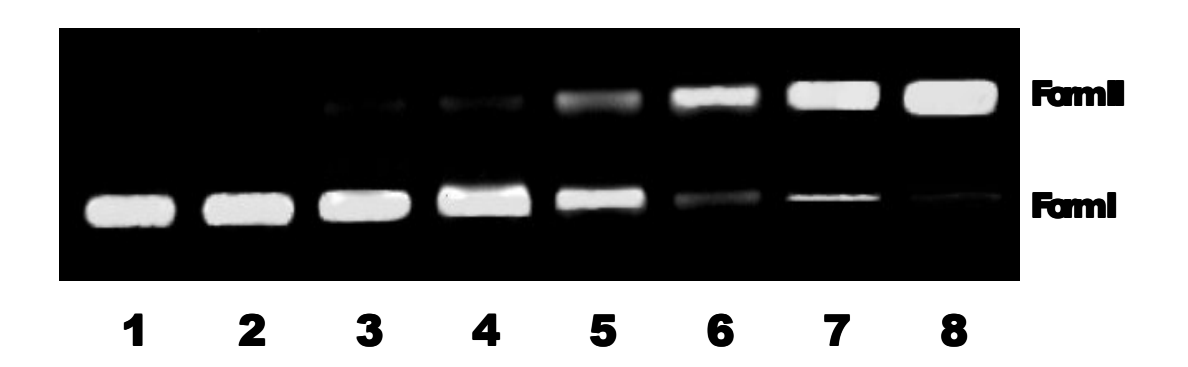


Figure 4.27 Agarose gel showing cleavage of 20 μM SC pUC19 DNA incubated with 2 in 2% DMF 50 mM Tris-HCl/NaCl buffer (pH 7.1) at 37 °C for 1 h in the presence of ascorbic acid (H₂A, 20 μM). Lane 1, DNA; Lane 2, DNA + H₂A; lanes 3-8, DNA + H₂A + 2 (5, 10, 15, 20, 25, 30 μM respectively). Forms I and II are supercoiled and nicked circular forms of DNA respectively



Figure 4.28 Agarose gel showing cleavage of 20 μM SC pUC19 DNA incubated with 1 (25 μM) in 2% DMF 50mM Tris-HCl/NaCl buffer (pH 7.1) at 37 °C for 1 h in the presence of ascorbic acid (H₂A, 20 μM). Lane C, DNA; Lane C+R, DNA + H₂A; lanes 1-13, DNA + H₂A + 1 (0, 5, 10, 15, 20, 25, 30, 35, 40, 45, 50, 55, 60 min respectively). Forms I and II are supercoiled and nicked circular forms of DNA respectively.

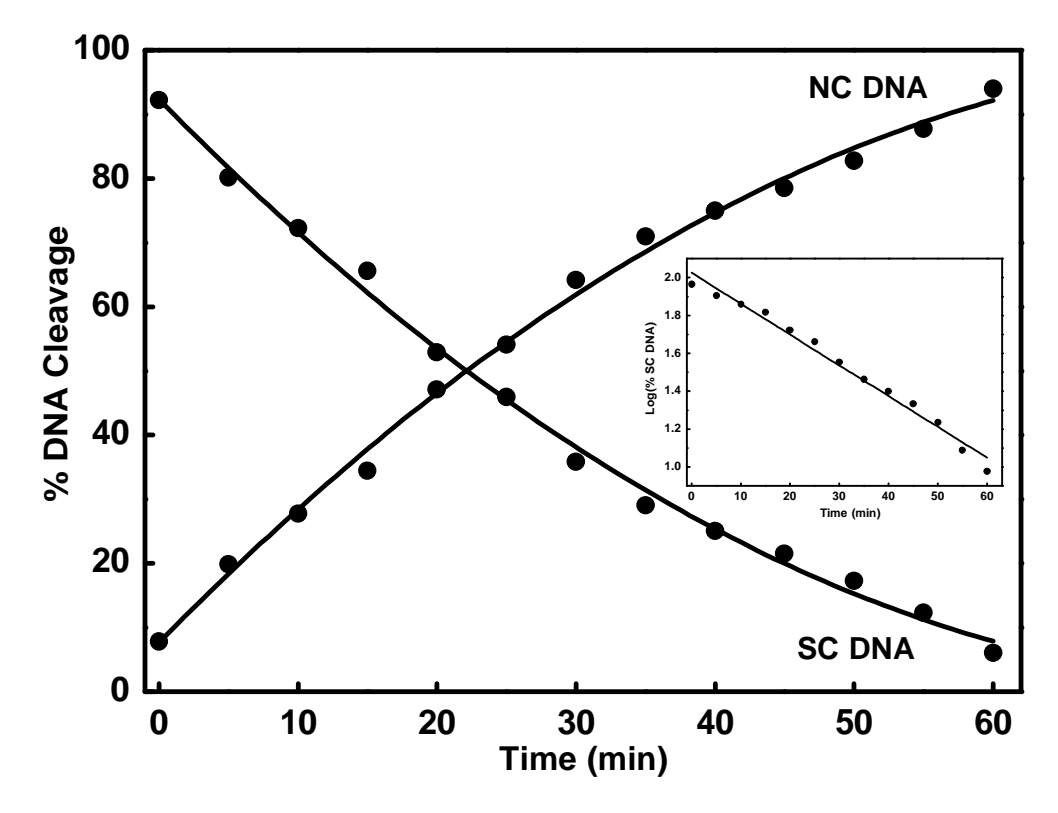


Figure 4.29 Disappearance of the supercoiled form (SC DNA) and formation of the nicked circular form (NC DNA) of pUC19 DNA in the presence of the 1 (25 μ M) with the incubation time (0, 5, 10, 15, 20, 25, 30, 35, 40, 45, 50, 55, 60 min respectively). Inset: (% SC DNA) versus time for a complex concentration of 25 μ M.

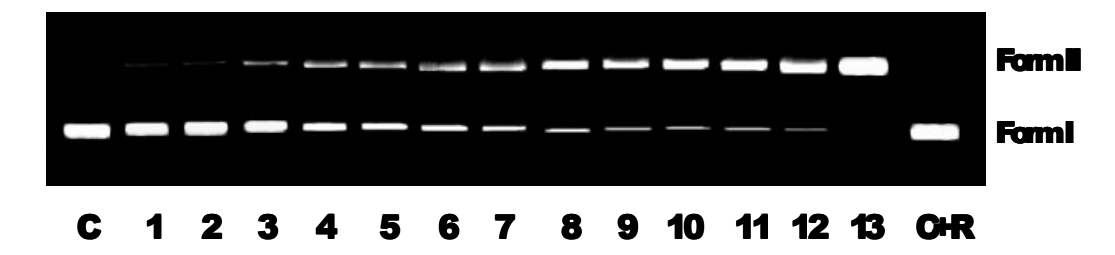


Figure 4.30 Agarose gel showing cleavage of 20 μM SC pUC19 DNA incubated with 2 (30 μM) in 2% DMF 50mM Tris-HCl/NaCl buffer (pH 7.1) at 37 °C for 1 h in the presence of ascorbic acid (H₂A, 20 μM). Lane C, DNA; Lane C+R, DNA + H₂A; lanes 1-13, DNA + H₂A + 2 (0, 5, 10, 15, 20, 25, 30, 35, 40, 45, 50, 55, 60 min respectively). Forms I and II are supercoiled and nicked circular forms of DNA respectively.

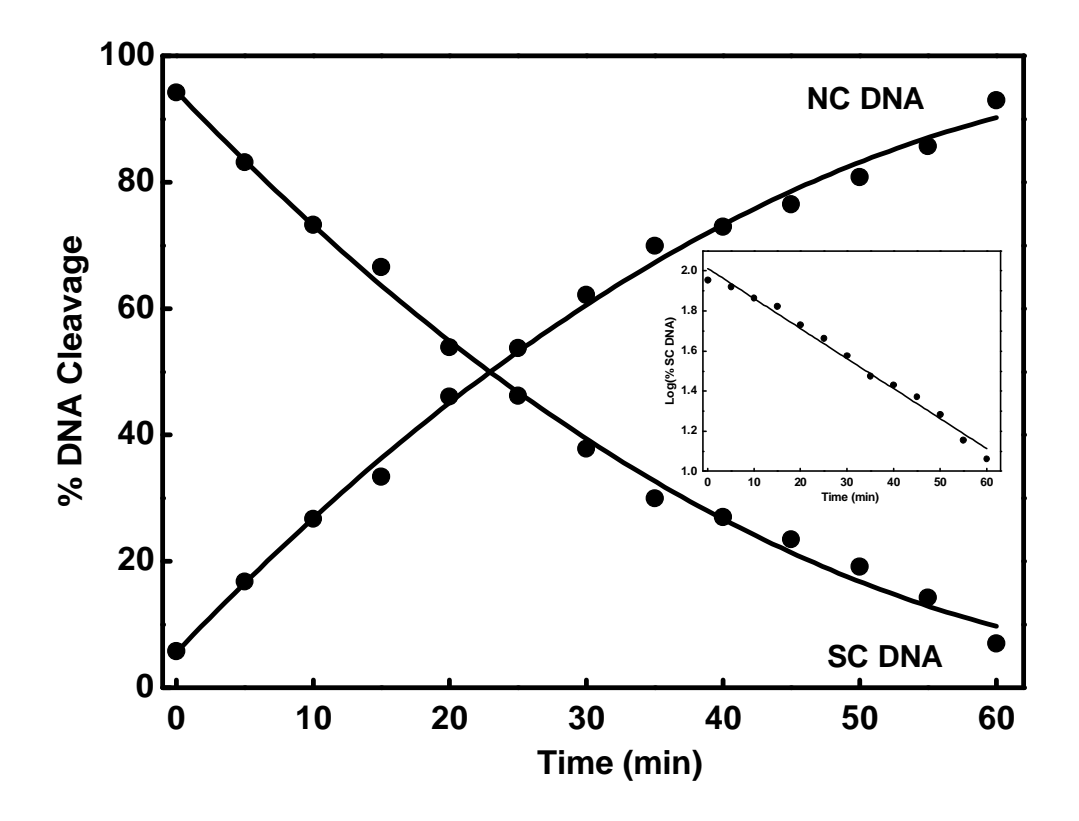


Figure 4.31 Disappearance of the supercoiled form (SC DNA) and formation of the nicked circular form (NC DNA) of pUC19 DNA in the presence of the 2 (25 μ M) with the incubation time (0, 5, 10, 15, 20, 25, 30, 35, 40, 45, 50, 55, 60 min respectively). Inset: (% SC DNA) versus time for a complex concentration of 25 μ M.

The cleavage reactions were carried out by the treatment of several radical scavengers with 1 or 2 for 5 minutes, including DMSO (hydroxyl radical), NaN₃ (singlet oxygen), SOD (superoxide anion), and catalase (H₂O₂), and then incubated. The oxidative DNA cleavage of 1 is suppressed by NaN₃ and catalase (Figure 4.32), whereas 2 is inhibited by NaN₃ and SOD (Figure 4.33). It implies that singlet oxygen, ${}^{1}O_{2}$, and $H_{2}O_{2}$ and singlet oxygen, ${}^{1}O_{2}$ and superoxide anion, O_{2} are involved in the oxidative DNA cleavage of 1 and 2. The greater stability of its Cu(I)-phen species upon binding to DNA appears to be a cause of higher nuclease activity of 1 or 2. The DNA cleavage activity is carried out by the Cu(I) species, which is stabilized by partial interactive binding with DNA close to the deoxyribose rings [60], and the free hydroxyl radicals generated by the interaction of Cu(I) species with molecular oxygen are then involved in DNA cleavage to produce deoxyribose centered radical by C-1 hydrogen abstraction. On the other hand, 1 or 2, with a high K^+/K^{2+} value, stabilizes the Cu(I) species, functions as a better DNA cleaving agent, and has higher cytotoxicity. Groove binding agent methyl green was used to probe the potential interacting mode of 1 and 2 with plasmid pUC19 DNA. When supercoiled pUC19 DNA was treated with methyl green, the cleavage reaction mediated by the complexes was not quenched (Figures 4.32 and 4.33, lane 6) whereas it was completely cleaved to Form II. This suggests that the complexes prefer to bind through partial intercalation rather than groove binding (cf. above) [61].

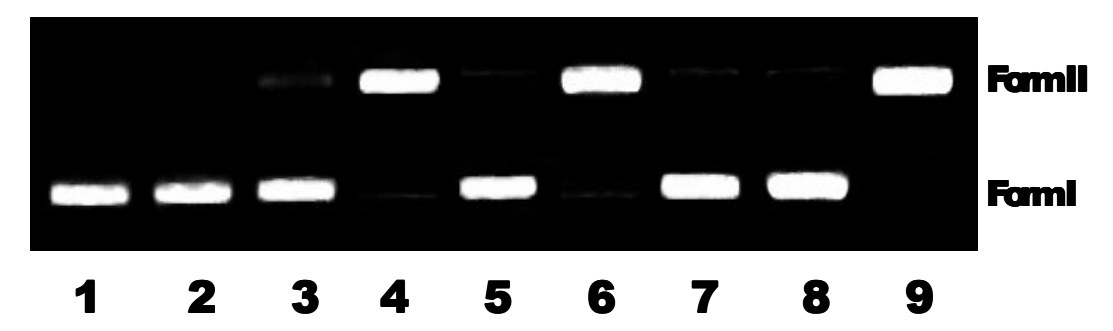


Figure 4.32 Agarose gel showing cleavage of 20 μ M SC pUC19 DNA incubated with 1 (25 μ M) in 2% DMF 50 mM Tris-HCl/NaCl buffer (pH 7.1) at 37 °C for 1 h in the presence of ascorbic acid (H₂A, 20 μ M). Lane 1, DNA; Lane 2, DNA + H₂A; Lane 3: DNA + 1, Lane 4: DNA + 1 + H₂A, Lane 5: DNA + 1 + H₂A + NaN₃ (100 μ M), Lane 6: DNA + 1 + H₂A + Methyl Green (100 μ M), Lane 7: DNA + 1 + H₂A + DMSO (20 μ M), Lane 8: DNA + 1 + H₂A + SOD (0.5 units), Lane 9: DNA + 1 + H₂A + Catalase (0.5 units).



Figure 4.33 Agarose gel showing cleavage of 20 μ M SC pUC19 DNA incubated with 2 (30 μ M) in 2% DMF 50mM Tris-HCl/NaCl buffer (pH 7.1) at 37 °C for 1 h in the presence of ascorbic acid (H₂A, 20 μ M). Lane 1, DNA; Lane 2, DNA + H₂A; Lane 3: DNA + 2, Lane 4: DNA + 2 + H₂A, Lane 5: DNA + 2 + H₂A + NaN₃ (100 μ M), Lane 6: DNA + 2 + H₂A + Methyl Green (100 μ M), Lane 7: DNA + 2 + H₂A + DMSO (20 μ M), Lane 8: DNA + 2 + H₂A + SOD (0.5 units), Lane 9: DNA + 2 + H₂A + Catalase (0.5 units).

4.3.7 BSA binding

Tryptophan residues alone produce the majority of intrinsic fluorescence of BSA at 340 nm when excited at 280 nm, with other amino acid residues like tyrosine and phenylalanine contributing quite slightly [62,63]. Tryptophan emission quenching experiments were carried out to measure the protein binding affinity of complexes by adding increasing concentrations (0-4 mM) of complexes to BSA (1 mM) at 300 and 310 K and monitoring the decrease in fluorescence intensity. At 300 K, the fluorescence intensity of BSA decreases to 63 (1), 62% (2), and at 310 K, it decreases to 69% (1, 2), with a red shift of 4-10 nm (Figures 4.34 and 4.35). The observed Stern-Volmer plots (Figure 4.36) show a good linear relationship [64] in which K_{SV} (**Table 4.4**) increases as temperature rises (300 K: **1**, 5.33; **2**, $4.94 \times 10^5 \text{ M}^{-1}$ and 310 K: 1, 6.59; 2, 6.55×10^5 M⁻¹), indicating that fluorescence quenching is most likely caused by a dynamic quenching mechanism. The obtained bimolecular quenching rate constant (k₀) is in the order of 10¹³ M⁻¹ s⁻¹, which is 1000 times greater than the diffusion-controlled quenching maximum limit $(2.0 \times 10^{10} \text{ M}^{-1} \text{ s}^{-1})$ [65]. Also, when the temperature is raised (300 K, 1, 3.14; 2, 4.58×10^5 M⁻¹ and 310 K, 1, 4.62; 2, $4.92 \times 10^5 \text{ M}^{-1}$), the effective quenching constant, K_a (**Table 4.4**) derived using the modified Stern-Volmer equation (Figure 4.37) [66], increases.

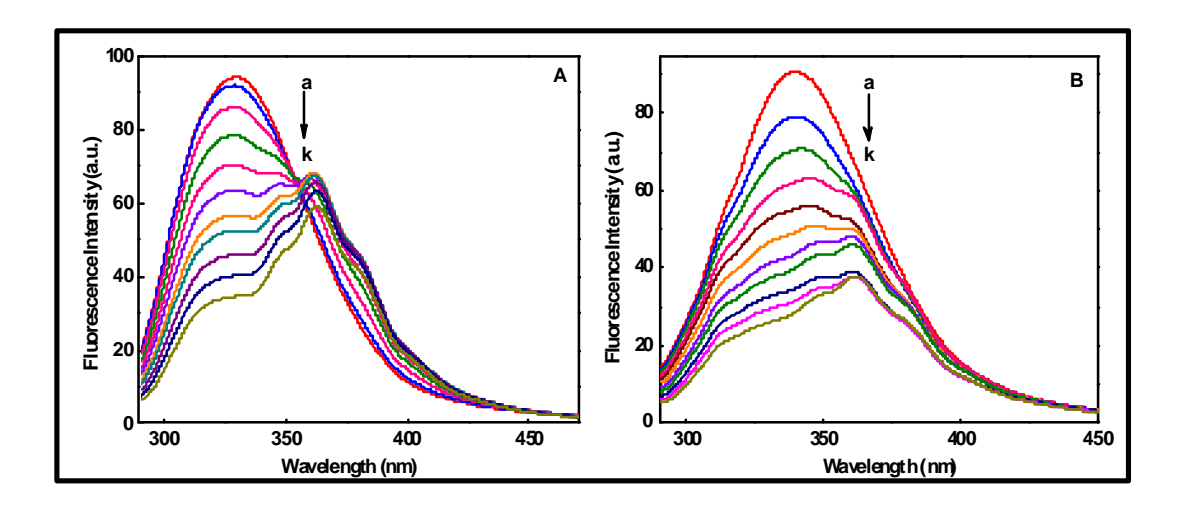


Figure 4.34 Changes in the fluorescence spectra of BSA through the titration with 1 at 300 K (left, A) and 310 K (right, B). The concentration of BSA is 1×10^{-6} mol L^{-1} , and the concentration of 1 was varied from (a) 0.0 to (k) 4.0×10^{-6} mol L^{-1} ; pH 7.4 and λ_{ex} 280 nm.

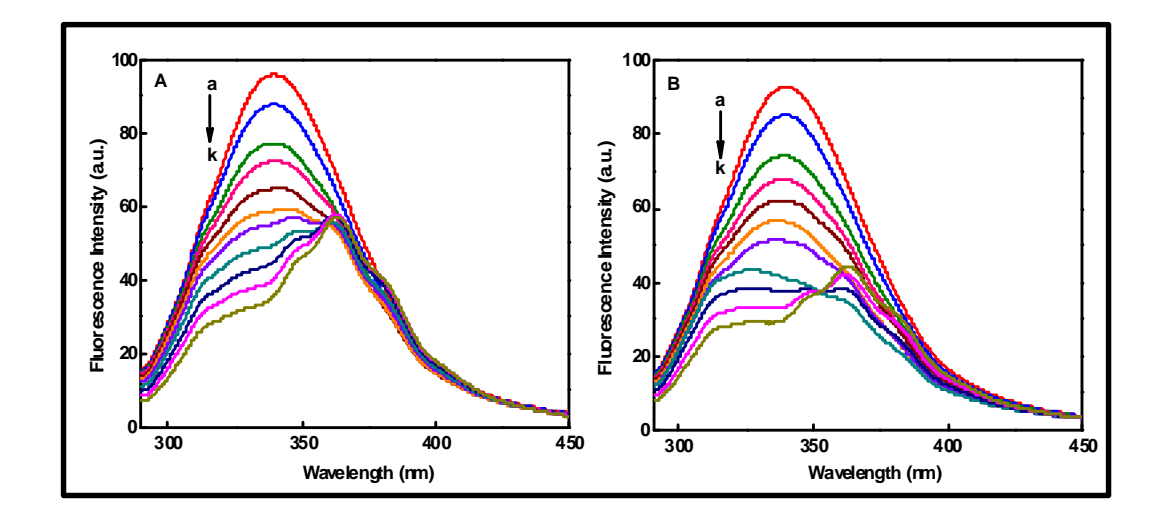


Figure 4.35 Changes in the fluorescence spectra of BSA through the titration with 2 at 300 K (left, A) and 310 K (right, B). The concentration of BSA is 1×10^{-6} mol L^{-1} , and the concentration of 2 was varied from (a) 0.0 to (k) 4.0×10^{-6} mol L^{-1} ; pH 7.4 and λ_{ex} 280 nm.

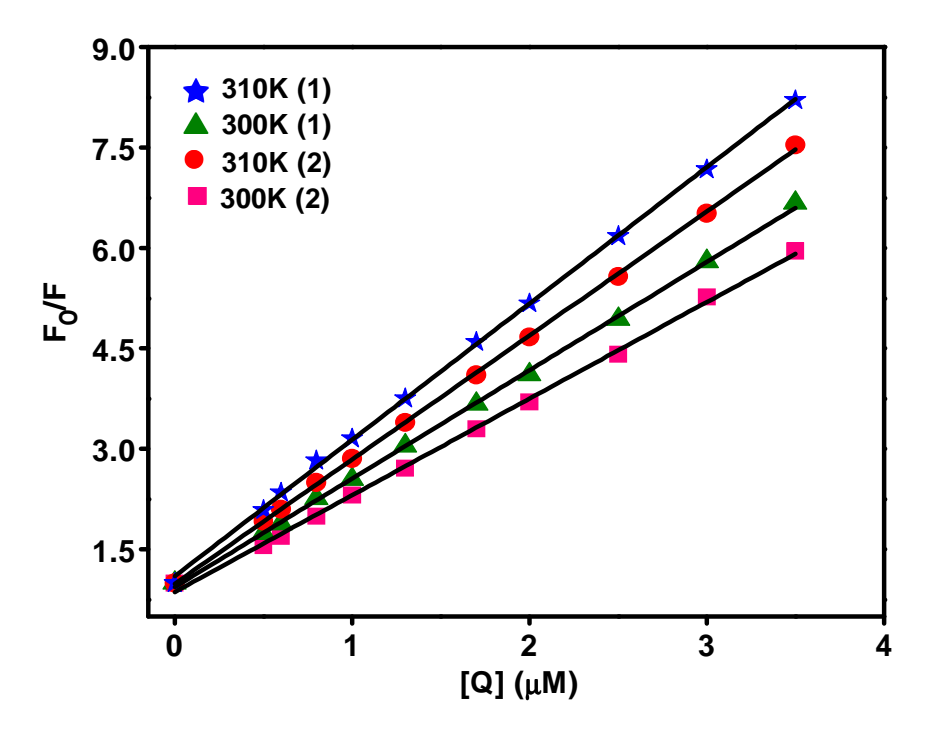


Figure 4.36 The Stern-Volmer plots of BSA at different temperatures for addition of 1 and 2. $\lambda_{ex} = 280$ nm; pH = 7.4.

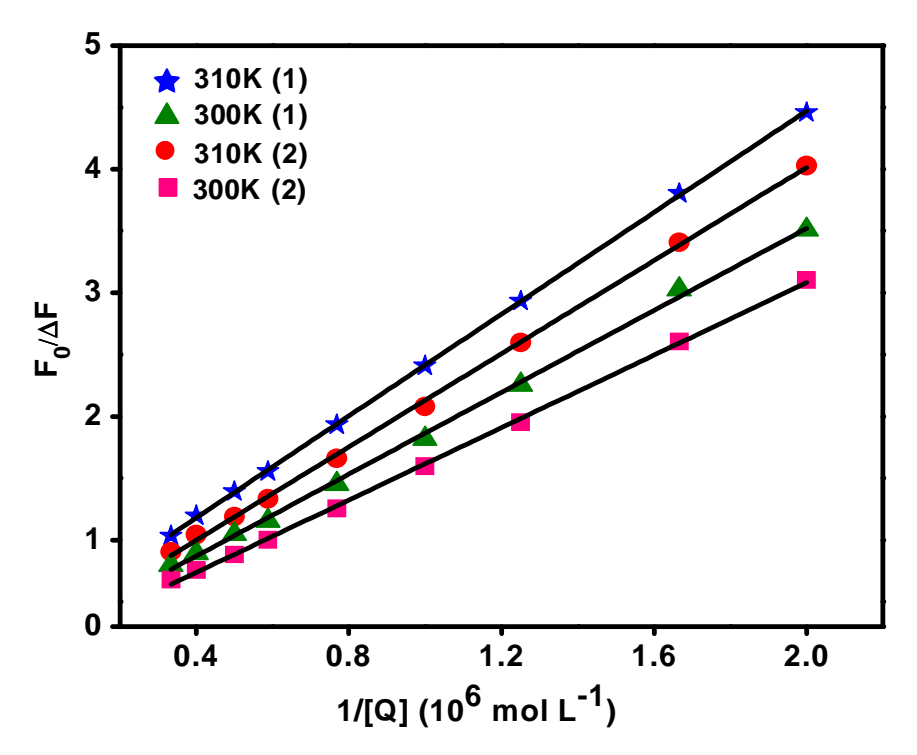


Figure 4.37 The modified Stern-Volmer plots of BSA at different temperatures for addition of 1 and 2. $\lambda_{ex} = 280$ nm; pH = 7.4.

Table 4.4

Quenching, association, binding and thermodynamic parameters of the interaction of 1 and 2 with BSA at different temperatures

Parameters	300 K	R	310 K	R	
[Cu(L1)(phen)](ClO ₄) ₂ 1					
$K_{SV} (10^5 \mathrm{M}^{-1}) \pm \mathrm{SD}$	5.329 ± 0.013	0.9977	6.592 ± 0.018	0.9932	
$k_q (10^{13} M^{-1} s^{-1})$	5.329		6.592		
$K_a (10^5 M^{-1}) \pm SD$	3.137 ± 0.006	0.9992	4.623 ± 0.001	0.9995	
$K_b (10^6 M^{-1}) \pm SD$	1.002 ± 0.011	0.9993	1.211 ± 0.036	0.9997	
$n \pm SD$	1.001 ± 0.006		0.999 ± 0.004		
$\Delta H^{\circ} (kJ \text{ mol}^{-1})$	76.379				
$\Delta S^{\circ} (J \text{ mol}^{-1} K^{-1})$	108.898		110.236		
ΔG° (kJ mol ⁻¹)	-32.593 -3-		-34.096	-34.096	
[Cu(L2)(phen)](ClO ₄) ₂ 2					
$K_{SV} (10^5 \mathrm{M}^{-1}) \pm \mathrm{SD}$	4.938 ± 0.014	0.9926	6.551 ± 0.021	0.9906	
$k_q (10^{13} \text{M}^{\text{-}1} \text{s}^{\text{-}1})$	4.938		6.551		
$K_a (10^5 M^{-1}) \pm SD$	4.584 ± 0.006	0.9951	4.919 ± 0.008	0.9925	
$K_b (10^6 M^{-1}) \pm SD$	2.710 ± 0.012	0.9934	4.721 ± 0.014	0.9922	
$n \pm SD$	1.004 ± 0.002 0.997 ± 0.006				
$\Delta H^{\circ} (kJ \text{ mol}^{-1})$	76.564				
$\Delta S^{\circ} (J \text{ mol}^{-1} K^{-1})$	109.793		110.873		
ΔG° (kJ mol ⁻¹)	-32.861		-34.294		

The absorption spectra of BSA [64] have two absorption peaks at 210 and 280 nm (Figure 4.38), and 210 nm represent the α -helix content in BSA [67]. When the complexes are added, the 210 nm absorbance peak of BSA is dramatically reduced, with a red-shift (1, from 210 to 220 nm; 2, from 210 to 222 nm). Meanwhile, the absorption intensity at 280 nm has slightly increased (Figure 4.38), which indicates that additional aromatic acid residues have been extended into the aqueous environment and destroy the tertiary structure of BSA [68]. These findings indicate that the interaction between copper(II) complexes and BSA is primarily a static quenching process caused by the formation of a ground-state complex (BSA-1 or BSA-2). The binding constant, K_b (Figure 4.39), increases with temperature (300 K: **1**, 1.00; **2**, 2.71 \times 10⁶ M⁻¹ and 310 K: **1**, 1.21; **2**, 4.72 \times 10⁶ M⁻¹), indicating that a stable BSA-1 or BSA-2 ground-state complex is formed [69] (Table 4.4). Additionally, the value of n, which is close to 1 (**Table 4.4**), shows that the binding site in BSA is unique and that the complexes have easy access to the hydrophobic environment of the tryptophan residue [70]. Since the values of ΔG^0 are negative, it is clear that the binding process is spontaneous, as seen in Table 4.4. The presence of significant hydrophobic forces of interaction between the ligands of copper(II) complexes and BSA is also supported by the positive values reported for both ΔH^0 and ΔS^0 [71,72]. Covalent bonding could be considered in addition to the hydrophobic interaction. However, the obtained value for ΔH^0 (76 kJ mol⁻¹) is significantly lower than what would be predicted for the formation of covalent bonds, which should be ≥120 kJ mol⁻¹ [73].

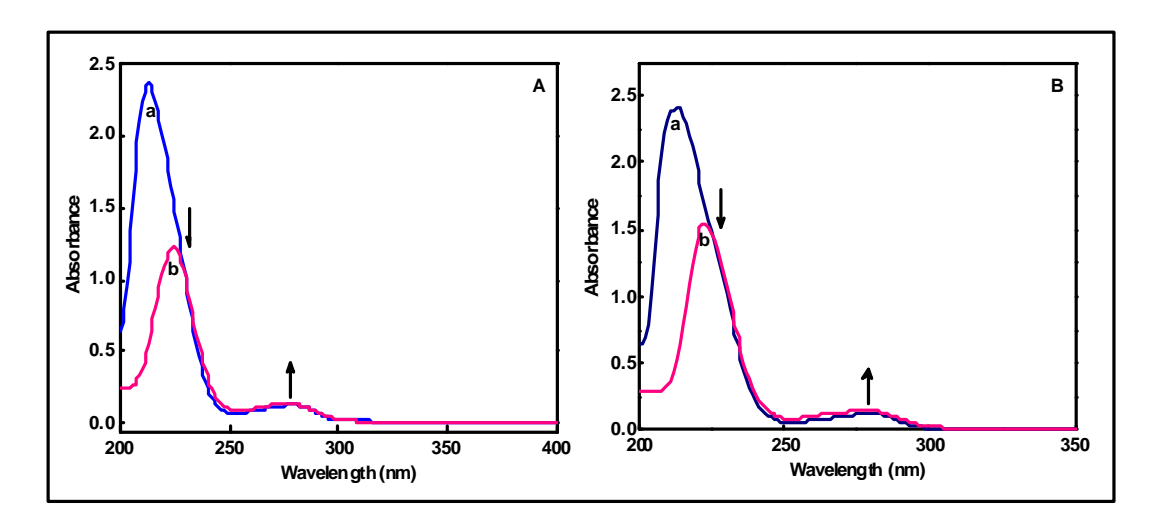


Figure 4.38 UV-Vis absorption spectra of BSA in the absence and presence of **1** (left, A) and **2** (right, B). (a) Absorption spectrum of BSA. (b) Absorption spectrum of BSA in the presence of **1** and **2** at the same concentration, [BSA] = [Cu complex] = 3.5×10^{-6} mol L⁻¹.

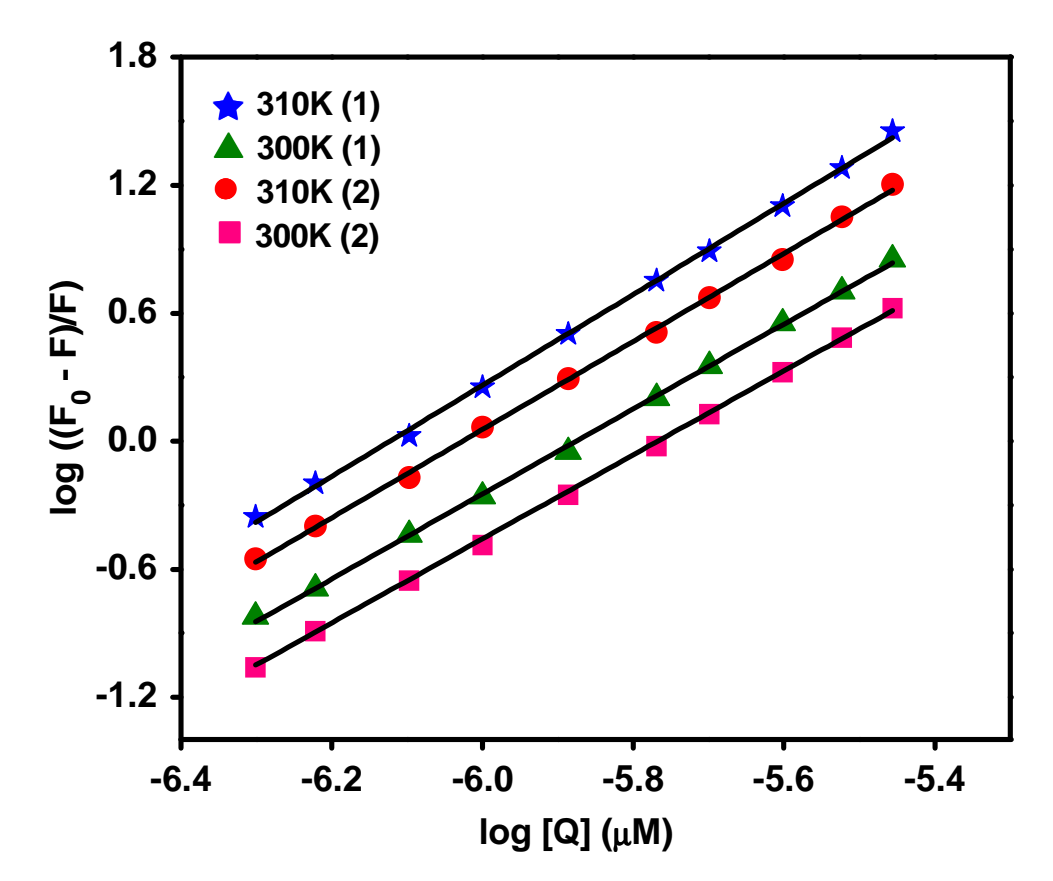


Figure 4.39 Double-log plot of quenching effect of 1 and 2 on BSA fluorescence at pH = 7.4.

4.3.8 Cytotoxic activity

Cytotoxicity is a common limitation in terms of the introduction of new compounds into the pharmaceutical industry. The positive results obtained from DNA binding and DNA cleavage studies for solutions of the new complexes 1 and 2 encouraged us to test their antiproliferative activity in vitro against human cervical carcinoma (HeLa) and mouse embryonic fibroblasts (NIH 3T3) cells by the MTT assay method (48 h incubation time). Complexes were dissolved in DMSO and the blank samples containing the same volume of DMSO were taken as controls to identify the activity of the solvent in this cytotoxicity experiment. Cisplatin was used as a positive control to assess the cytotoxicity of the test complexes. IC₅₀ values obtained for the free ligands and copper-acetate were also obtained for the sake of comparison. The increase in the concentration of 1 or 2 from 0.25 µM to 10 µM increases the percentage of cell inhibition (Figures 4.40 and 4.41) against HeLa cells. The activities of 1 and 2 are very much higher than those of the corresponding free ligands. They have exhibited a significant inhibitory potency against the proliferation of the HeLa cell line at a very low concentration (IC₅₀: 1, 0.85; 2, 1.00 µM) in a dose-dependent manner. Since the phen co-ligand possesses higher lipophilicity [74] to penetrate the cell membrane and act as a recognition element for non-covalent interaction with DNA. Further, the cytotoxicity of 1 and 2 against the HeLa cancer cell line was comparable to that of the prevalent benchmark metallodrug, cisplatin, under the same experimental conditions. The IC₅₀ values of **1** and **2** were ~90 times lower than that of cisplatin (IC₅₀, 16.4 μ M) [75], which is certainly a beneficial factor for considering these complexes as promising candidates for new antitumor agents. However, importantly, 1 showed significantly higher activity against the HeLa cell line than 2. Palaniandavar et al have shown that the mixed ligand Cu(II) complexes of diimine co-ligands exhibit higher cell killing activity [76]. Thus the present complexes containing phen as co-ligand, which involves non-covalent interaction show better cytotoxicity than the related Cu(II) complexes reported in the literature [77]. In addition, **1** and **2** do not cause any damage to the normal mouse embryonic fibroblasts cells (NIH 3T3, $IC_{50} > 500 \mu M$), indicating that they are non-toxic to healthy cells, which is expected for a better drug.

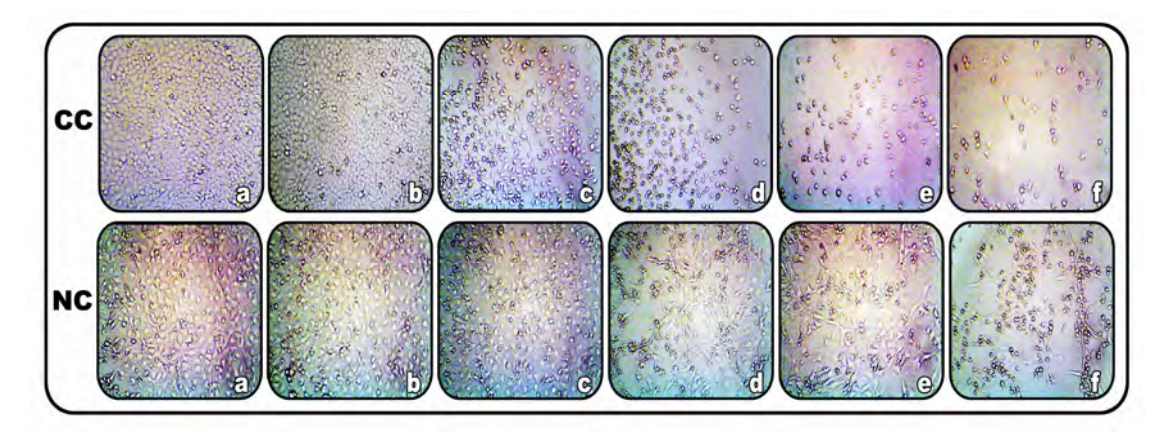


Figure 4.40 Photomicrograph of human cervical carcinoma cells (HeLa; CC) and mouse embryonic fibroblasts cells (NIH 3T3; NC) after 48 h exposure with 1 (CC: a, control; b, 0.25 μM; c, 0.50 μM; d, 1 μM; e, 5 μM; f, 10 μM and NC: a, control; b, 25 μM; c, 50 μM; d, 100 μM; e, 200 μM; f, 500 μM).

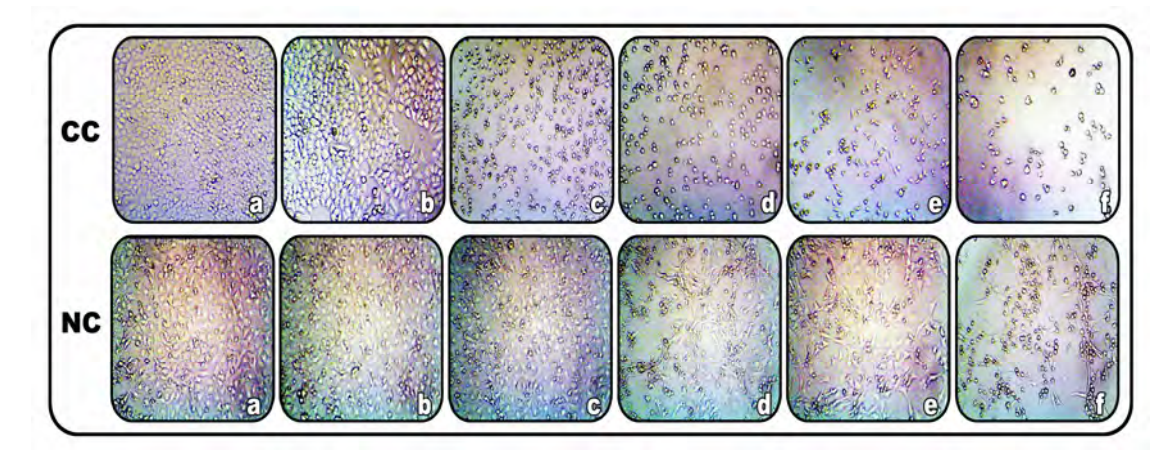


Figure 4.41 Photomicrograph of human cervical carcinoma cells (HeLa; **CC**) and mouse embryonic fibroblasts cells (NIH 3T3; **NC**) after 48 h exposure with **2** (**CC**: a, control; b, 0.25 μM; c, 0.50 μM; d, 1 μM; e, 5 μM; f, 10 μM and **NC**: a, control; b, 25 μM; c, 50 μM; d, 100 μM; e, 200 μM; f, 500 μM).

4.4 Conclusion

Two mixed ligand copper(II) complexes of the type [Cu(L1)/L2) (phen)] (ClO₄)₂ (1-2) have been synthesized and characterized. The geometry of 2 was analyzed through single-crystal X-ray diffraction and shown to have a CuN₅ chromophore. The coordination environment of the Cu(II) atom in 2 can be described as distorted square pyramidal. A three dimensional infinite network is formed and dominated by the interpair C-H··· π anti-parallel non-covalent interactions. Absorption, EPR, and ESI-MS spectral investigations revealed that both complexes preserve their identity in solution. The binding properties of the complexes with CT DNA and BSA have been investigated. The results of electronic absorption and circular dichroic spectroscopy, as well as electrochemistry, indicate that both complexes bind to DNA in a partial intercalative mode with a high affinity for DNA. The competitive binding studies with EthBr have revealed a significant decrease in the fluorescence intensity of the EthBr-DNA system in the presence of both complexes and implying that the complexes can compete for DNA-binding sites with EthBr and displace EthBr from the EthBr-DNA system. Also, both the complexes show significant DNA cleavage activity in the absence of an activator (97%, 200 µM complex concentration), and the cleavage activity is increased in the presence of hydrogen peroxide (97%, 20 µM (1) or 30 µM (2) complex concentration) or ascorbic acid (97%, 25 µM (1) or 30 µM (2) complex concentration). Interestingly, both the complexes show a reversible redox behavior. They cause a considerable decrease in current when they bind to CT DNA, shift to a less negative or less positive Cu(II)/Cu(I) redox potential, and stable the Cu(I) oxidation state, resulting in more evident chemical nuclease activity. The mechanism of quenching in BSA is thought to be through static mode, implying that complexes bind to BSA via hydrophobic interaction, based on protein binding studies. Their affinity for BSA (K_b , 10^6 M⁻¹) shows that the complexes are delivered in the blood by serum albumin. The two copper(II) complexes possess greater cytotoxic activity than cisplatin against HeLa cancer cells and are non-toxic to healthy cells (NIH 3T3), according to MTT experiment data. As a result, this class of complexes has the potential to be a promising alternative to platinum-based anticancer drugs, and more mechanistic and cellular uptake investigations are needed to evaluate the increased efficacy of complexes to kill cancer cells.

References

- [1] H. Prakash, A. Shodal, H. Yasul, H. Sakural, S. Hirota, Inorg. Chem. 47 (2008) 5045-5047.
- [2] D. Li, J. Tian, Y. Kou, F. Huang, G. Chen, W. Gu, X. Liu, D. Liao, P. Cheng,S. Yan, Dalton Trans. 18 (2009) 3574-3583.
- [3] A. Barve, A. Kumbhar, M. Bhat, B. Joshi, R. Butcher, U. Sonawane, R. Joshi, Inorg. Chem. 48 (2009) 9120-9132.
- [4] M.A. Fuertes, C. Alonso, J.M. Perez, Chem. Rev. 103 (2003) 645-662.
- [5] A.I. Matesanz, C. Hernandez, A. Rodriguez, P. Souza, Dalton Trans. 40 (2011) 5738-5745.
- [6] S. Dhar, D. Senapati, P.K. Das, P. Chatopadhyay, M. Nethaji, A.R. Chakravarty,J. Am. Chem. Soc. 125 (2003) 12118-12124.
- [7] M.L.P.D. Santos, A.F. Alario, A.S.A. Mangrich, A.M.C. Ferreira, J. Inorg. Biochem. 71 (1998) 71-78.
- [8] R.S. Kumar, S. Arunachalam, Polyhedron 26 (2007) 3255-3262.
- [9] A. Robert, B. Meunier, Chem. Eur. J. 7 (1998) 1287-1296.
- [10] C.D. Fan, H. Su, J. Zhao, B.X. Zhao, S.L. Zhang J.Y. Miao, Eur. J. Med. Chem. 45 (2010) 1438-1446.
- [11] J.D. Ranford, P.J. Sadler, D.A. Tocher, J. Chem. Soc. Dalton Trans. 22 (1993) 3393-3399.
- [12] C.H. Ng, K.C. Kong, S.T. Von, P. Balraj, P. Jensen, E. Thirthagiri, H. Hamada,M. Chikira, Dalton Trans. 4 (2008) 447-454.
- [13] D. Yoshida, Y. Ikeda, S. Nakazawa, J. Neuro Oncol. 16 (1993) 109-115.

- [14] S. Kathiresan, R. Dhivya, M. Vigneshwar, M. Rajasekaran, J. Ranjani, J. Rajendhran, S. Srinivasan, S. Mugesh, M. Murugan, P.R. Athappan, J. Annaraj, J. Coord. Chem. 68 (2015) 1-15.
- [15] B.C. Bales, T. Kodama, Y.N. Weledji, M. Pitie, B. Meunier, M.M. Greenberg, Nucleic Acids Res. 33 (2005) 5371-5379.
- [16] S. Kathiresan, S. Mugesh, M. Murugan, F. Ahamed, J. Annaraj, RSC Adv. 6 (2016) 1810-1825.
- [17] K. Zheng, L. Jiang, Y.-T. Li, Z.-Y. Wu, C.-W. Yan, RSC Adv. 5 (2015) 51730-51744.
- [18] S. Zhang, Y. Zhu, C. Tu, H. Wei, Z. Yang, L. Lin, J. Ding, J. Zhang, Z. Guo,J. Inorg. Biochem. 98 (2004) 2099-2106.
- [19] V. Gandin, M. Porchia, F. Tisato, A. Zanella, E. Severin, A. Dolmella,C. Marzano, J. Med. Chem. 56 (2013) 7416-7430.
- [20] T.S. Lobana, R. Sharma, G. Bawa, S. Khanna, Coord. Chem. Rev. 253 (2009) 977-1055.
- [21] M. Alagesan, N.S.P. Bhuvanesh, N. Dharmaraj, Dalton Trans. 42 (2013) 7210-7223.
- [22] J.A. Lessa, I.C. Mendes, P.R.O. da Silva, M.A. Soares, R.G. dos Santos, N.L. Spezialic, N.C. Romeiro, E.J. Barreiro, H. Beraldo, Eur. J. Med. Chem. 45 (2010) 5671-5677.
- [23] P. Anitha, N. Chitrapriya, Y.J. Jang, P. Viswanathamurthi, J. Photochem. Photobiol. B. 129 (2013) 17-26.
- [24] A. Basu, D. Thiyagarajan, C. Kar, A. Ramesh, G. Das, RSC Adv. 3 (2013) 14088-14098.

- [25] W.-J. Lian, X.-T. Wang, C.-Z. Xie, H. Tian, X.-Q. Song, H.-T. Pan, X. Qiao, J.-Y. Xu, Dalton Trans. 45 (2016) 9073-9087.
- [26] M. Pitie, B. Donnadieu, B. Meunier, Inorg. Chem. 37 (1998) 3486-3489.
- [27] A. Altomare, G. Cascarano, C. Giacovazzo, A. Guagliardi, J. Appl. Crystallogr.26 (1993) 343-350.
- [28] G.M. Sheldrick, Acta Cryst. Sect. C 71 (2015) 3-8.
- [29] L.J. Farrugia, J. Appl. Cryst. 32 (1999) 837-838.
- [30] L.J. Farrugia, J. Appl. Cryst. 30 (1997) 565.
- [31] J.E. Huheey, E.A. Keiter, R.L. Keiter, O.K. Medhu, Inorganic Chemistry, Principles of Structure and Reactivity, Pearson Education, Upper Saddle River, NJ (2006) p.425.
- [32] G. Murphy, P. Nagle, B. Murphy, B. Hathaway, J. Chem. Soc. Dalton Trans. (1997) 2645-2652.
- [33] G. Murphy, C. Murphy, B. Murphy, B. Hathaway, J. Chem. Soc. Dalton Trans. (1997) 2653-2660.
- [34] P. Nagle, E. Osullivan, B. Hathaway, J. Chem. Soc. Dalton Trans. (1990) 3399-3406.
- [35] G. Huang, C. Su, S. Wang, F. Liao, K. Lin, J. Coord. Chem. 49 (2000) 211-226.
- [36] P.S. Subramanian, E. Suresh, P. Dastidar, Polyhedron 23 (2004) 2515-2522.
- [37] A.W. Addison, M. Carpenter, L.K.-M. Lau, M. Wicholas, Inorg. Chem. 17 (1978) 1545-1552.
- [38] B.J. Hathaway, G. Wilkinsons, R.G. Gillard, J.A. McCleverty (Eds), Comprehensive Coordination Chemistry, vol. 5, Pergamon. Oxford. (1987) pp 861.

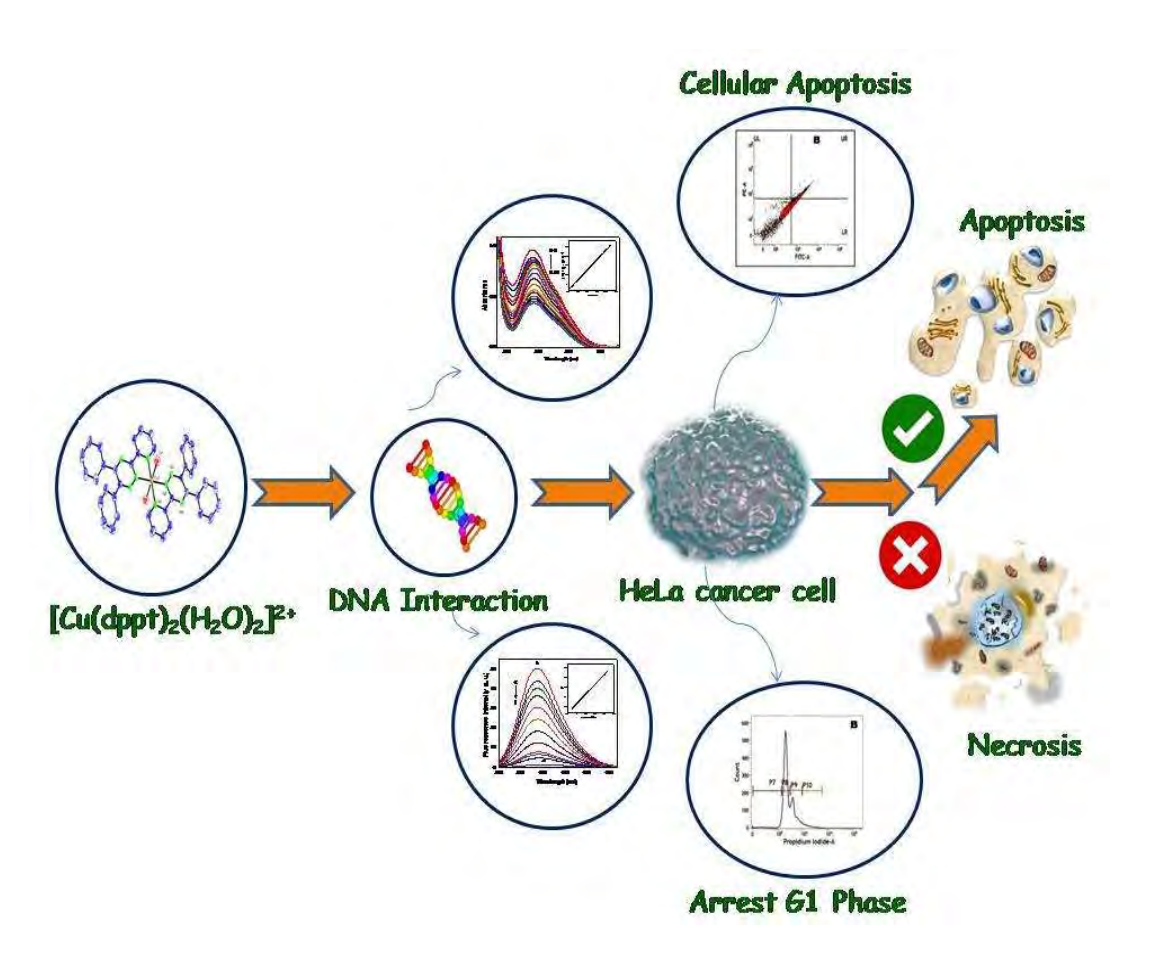
- [39] A.W. Addison, Copper coordination chemistry, in: K.D Karlin, J. Zubieta, Biohemical and Inorganic Perspectives, Adenine, Guilderland, New York. 109 (1983).
- [40] U. Sakaguchi, A.W. Addison, J. Chem. Soc. Dalton Trans. (1979) 600-608.
- [41] D.X. West, M. Palaniandavar, Inorg. Chim. Acta, 76 (1983) L149-L150.
- [42] A.W. Addison, P.J. Burke, K. Henrick, T.N. Rao, E. Sinn, Inorg. Chem. 22 (1983) 3645-3653.
- [43] M. Palaniandavar, I. Somasundaram, M. Lakshminarayanan, H. Manohar, J. Chem. Soc. Dalton Trans. (1996) 1333-1340.
- [44] M. Murali, M. Palaniandavar, T. Pandiyan, Inorg. Chim. Acta. 224 (1994) 19-25.
- [45] C. Rajarajeswari, R. Loganathan, M. Palaniandavar, E. Suresh, A. Riyasdeen,M.A. Akbarsha, Dalton Trans. 42 (2013) 8347-8363.
- [46] A.W. Addison, Inorg. Chim. Acta, 162 (1989) 217-220.
- [47] S. Usha, M. Palaniandavar, J. Chem. Soc. Dalton Trans. (1994) 2277-2283.
- [48] A. Erxleben, Coord. Chem. Rev. 360 (2018) 92-121.
- [49] S. Ramakrishnan, V. Rajendiran, M. Palaniandavar, V.S. Periasamy, B.S. Srinag,H. Krishnamurthy, M.A. Akbarsha, Inorg. Chem. 48 (2009) 1309-1322.
- [50] J.W. Chen, X.Y. Wang, Y. Chao, J.H. Zhu, Y.G. Zhu, Y.Z. Li, Q. Xu, Inorg. Chem. 46 (2007) 3306-3312.
- [51] J.R. Lakowicz, G. Webber, Biochemistry 12 (1973) 4161-4170.
- [52] M. Lee, A.L. Rhodes, M.D. Wyatt, S. Forrow, J.A. Hartley, Biochemistry 32 (1993) 4237-4245.
- [53] M. Ganeshpandian, R. Loganathan, E. Suresh, A. Riyasdeen, M.A. Akbarsha,M. Palaniandavar, Dalton Trans. 43 (2014) 1203-1219.

- [54] V.I. Ivanov, L.E. Minchenkova, A.K. Schyolkina, A.I. Polytayer, Biopolymers 12 (1973) 89-110.
- [55] J.G. Collins, T.P. Shields, J.K. Barton, J. Am. Chem. Soc. 116 (1994) 9840-9846.
- [56] M. T. Carter, M. Rodriguez, A. J. Bard, J. Am. Chem. Soc. 111 (1989) 8901-8911.
- [57] G. Psomas, J. Inorg. Biochem. 102 (2008) 1798-1811.
- [58] S. Ramakrishnan, M. Palaniandavar, Dalton Trans. (2008) 3866-3878.
- [59] E. Lamour, S. Routier, J.L. Bernier, J.P. Catteau, C. Bailly, H. Vezin, J. Am.Chem. Soc. 121 (1999) 1862-1869.
- [60] M. Aharma, M. Ganeshpandian, M. Majumder, A. Tamilarasan, M. Sharma,
 R. Mukhopadhyay, N. S. Islam, M. Palaniandavar, Dalton Trans. 49 (2020)
 8282–8297.
- [61] M.S. Deshpande, S. Junedi, H. Prakash, S. Nagao, M. Yamanaka, S. Hirota, Chem. Commun., 50 (2014) 15034-15036.
- [62] C.V. Dang, R.F. Ebert, W.R. Bell, J. Biol. Chem., 260 (1985)9713-9719.
- [63] C.X. Wang, F.F. Yan, Y.X. Zhang, L. Ye, J. Photochem. Photobiol. A, 192 (2007) 23-28.
- [64] J. R. Lakowicz, Principles of fluorescence spectroscopy, Springer Science + Business Media, New York, 3rd edn, 2006.
- [65] X. Zhao, R. Liu, Z. Chi, Y. Teng, P. Qin, J. Phys. Chem. B 114 (2010) 5625-5631.
- [66] S.S. Lehrer, Biochemistry 10 (1971) 3254-3263.
- [67] M.R. Eftink, C.A. Ghiron, J. Phys. Chem. 80 (1976) 486-493.

- [68] Y. Li, W. Y. He, C.X. Xue, Z.D. Hu, X.G. Chen, F.L. Sheng, Bioorg. Med. Chem. 13 (2005) 1837-1845.
- [69] A. Divsalar, M.J. Bagheri, A.A. Saboury, H. Mansoori-Torshizi, M. Amani,J. Phys. Chem. B 113(2009) 14035-14042.
- [70] H. Gao, L.D. Lei, J.Q. Liu, Q. Kong, X.G. Chen, Z.D. Hu, J. Photochem. Photobiol. A 167 (2004) 213-221.
- [71] P.D. Ross, S. Subramanian, Biochemistry 20 (1981) 3096-3102.
- [72] D.A. Leckband, Biomol. Struct. 29 (2000) 1-26.
- [73] C.N. Lunardi, A.C. Tedesco, T.L. Kurth, I.M. Brinn, Photochem. Photobiol. Sci. 2 (2003) 954-959.
- [74] C.T. Dillon, P.A. Lay, A.M. Bonin, M. Cholewa, G.J.F. Legge, Chem. Res. Toxicol. 13 (2000) 742-748.
- [75] S. Sangeetha, M. Murali, Inorg. Chem. Commun. 59 (2015) 46-49.
- [76] C. Rajarajeswari, R. Loganathan, M. Palaniandavar, E.suresh, A. Riyasdeen,M.A. Akbarsha, Dalton Trans. 42 (2013) 8347-8363.
- [77] C. Rajarajeswari, M. Ganeshpandian, M. Palaniandavar, A. Riyasdeen, M.A. Akbarsha, J. Inorg. Biochem. 140 (2014) 255-268.

Chapter 5

DNA Binding, In Vitro Cytotoxicity and Anticancer Drug Mechanism of Copper(II) Complex Containing Pyridyl-Triazine Ligand



The $[Cu(dppt)_2(H_2O)_2](ClO_4)_2$ exhibits very active inhibitory effect, which was higher than cisplatin. Its biological evaluation provides evidence that it blocked cell cycle at G1 phase and induced apoptosis alone along with the generation of ROS.

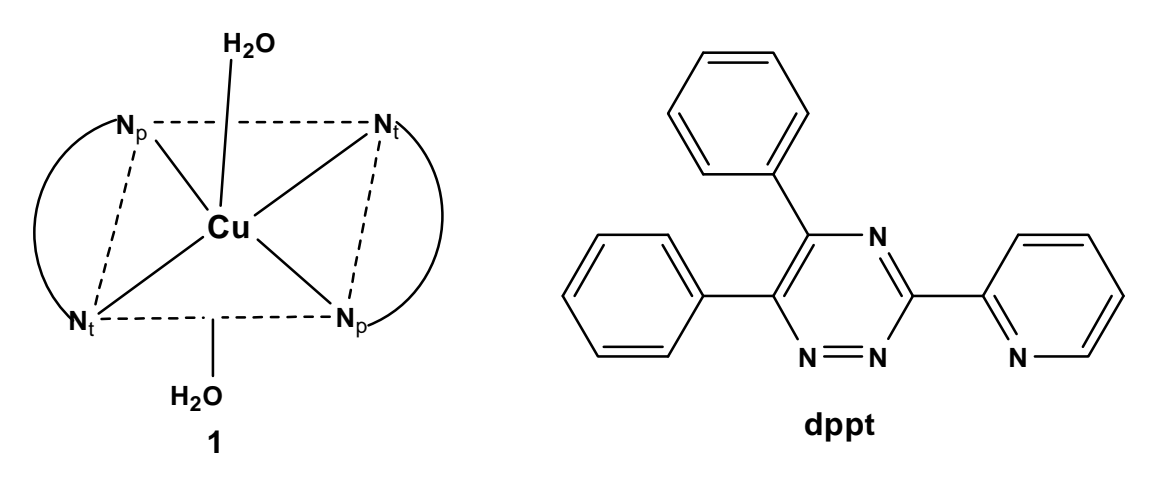
5 DNA Binding, *In Vitro* Cytotoxicity and Anticancer Drug Mechanism of Copper(II) Complex Containing Pyridyl-Triazine Ligand

5.1 Introduction

Recently there have been many reports highlighting the use of transition metal complexes as anticancer agents [1, 2]. Probably the best known of these is cisplatin [cis-di-amminedichloroplatinum(II)]. It has been widely used in the treatment of a variety of cancers such as testicular, brain, ovarian, bladder, and breast cancer [3]. The clinical success of cisplatin is limited by its significant side effects, such as nausea, vomiting, and severe nephrotoxicity [3]. The use of cisplatin and related platinum complexes as anticancer agents has stimulated a search for other active transition metal complexes which are as effective, but with lesser side effects. In nature, many biological systems make extensive use of metal ions such as zinc and copper, which play critical roles in the normal functioning of organisms [4]. Transition metals such as copper, iron, and manganese, among others, are involved in multiple biological processes from electron transfer to catalysis to structural roles and are frequently associated with active sites of proteins and enzymes [4]. However, dysregulation of some of these essential metals during normal biochemical processing has been implicated in the development of various pathological disorders, such as cancer [5]. These cellular functions only require the "trace metals" in minuscule but tightly regulated amounts. By comparison, other metals such as arsenic, cadmium, chromium, and nickel are less beneficial since they produce a wide range of toxic side-effects, including carcinogenesis [4,6].

In particular, copper(II) cation can bind to negatively charged DNA and have been shown to play an important role in the local formation of hydroxy radicals [7,8]. One of the consequences of high copper levels in the body is an increase in the rate of radical formation leading to oxidative damage [8]. This leads to a disruption of lipid bilayers due to oxidation and cleavage of vulnerable unsaturated fatty acid residues of phospholipids. Alterations in protein function are also promoted through the oxidation of thiol and possibly amino groups. Gene expression may also be altered due to oxidation of guanosine and adenosine residues in nucleic acids or altered transcription factor/growth factor activities [9]. More anecdotally, in the human body, Cu binds to N7 of guanine residue of DNA and generates ROS through the oxidation-reduction reaction resulting in DNA damage and cell apoptosis [10-12]. All these findings support that the antitumor agent based on Cu could be promising for the treatment of cancer.

In the present study, a novel, green colored copper(II) complex [Cu(dppt)₂(H₂O)₂](ClO₄)₂ (**1**), where dppt is 3-(2-pyridyl)-5,6-diphenyl-1,2,4-triazine (**Scheme 5.1**) has been synthesized and its ability to bind calf thymus (CT) DNA has been studied. The primary aim of the current study was to determine the cancer chemotherapeutic potential of metal-free dppt, [Cu(dppt)₂(H₂O)₂](ClO₄)₂ using human cervical carcinoma cells (HeLa) and normal mouse embryonic fibroblasts cells (NIH 3T3). To illustrate that the effect observed was due to the complex rather than the free metal ion, the antitumour activity of the simple Cu(II) salt, Cu(OAc)₂·H₂O was also determined. In addition, the relative potency of the test agent was determined by the inclusion of one of the best known and most biologically active metal-based anti-cancer agent, cisplatin. Furthermore, aspects of the anticancer drug mechanisms underlying the cytotoxic response were probed.



Scheme 5.1 Schematic representation of the copper(II) complex (1) and structure of ligand dppt.

5.2 Experimental

5.2.1 Synthesis of complex, $[Cu(dppt)_2(H_2O)_2](ClO_4)_2$ (1)

An ethanolic solution (5 mL) of 5,6-diphenyl-3-(2-pyridyl)-1,2,4-trazine (dppt: 0.62 g, 2 mmol) was added dropwise to an aqueous solution (10 mL) of copper(II) acetate monohydrate (0.20 g, 1 mmol). The resulting green coloured solution was stirred for 8 h at room temperature. The product was precipitated as the perchlorate salt by adding stoichiometric equivalent of NaClO₄ (0.12 g, 1 mmol) in water (3 mL). The bright green product, [Cu(dppt)₂(H₂O)₂](ClO₄)₂, was collected by suction filtration, washed with cold water and ether and then air-dried. Yield: 76%. Selected IR peaks (v, cm⁻¹): 3447 b (v_{O-H}), 1500 m, 1527 s and 1600 w (v_{C=N}) and (v_{N=N}), 1103 and 1064 (v_{ClO4}). Anal. Calcd for C₄₀H₃₂N₈O₁₀Cl₂Cu: C, 52.27; H, 3.51; N, 12.19 %. Found: C, 52.32; H, 3.49; N 12.24 %. $\Lambda_{\rm M}$ (DMF): 165 Ω^{-1} cm² mol⁻¹. $\mu_{\rm eff}$ (27 °C): 1.78 $\mu_{\rm B}$. Electronic spectrum in DMF [$\lambda_{\rm max}$ /nm ($\epsilon_{\rm max}$ /dm³ mol⁻¹ cm⁻¹)]: 278 (8240), 322 (4885), 494 (35) 688 (30). Electronic spectrum in 2% DMF/5 mM Tris-HCl/50 mM NaCl buffer solution [$\lambda_{\rm max}$ /nm ($\epsilon_{\rm max}$ /dm³ mol⁻¹ cm⁻¹)]: 265 (8350),

292 (4900), 482(45), 676 (40). Room temperature polycrystalline EPR spectrum: $g_{iso} = 2.061$. EPR spectrum in DMF solution at 77 K: $g_{\parallel} = 2.292$, $g_{\perp} = 2.060$, $A_{\parallel} = 165 \times 10^{-4}$ cm⁻¹, $g_{\parallel}/A_{\parallel} = 139$ cm, G = 4.9. Redox behavior: $E_{1/2} = 0.243$ V (CV) and 0.242 V (DPV), $\Delta E_p = 81$ mV, $i_{pa}/i_{pc} = 1.1$, $D = 6.2 \times 10^6$ cm²s⁻¹.

5.2.2 X-ray crystallography

The blocks of bright green single crystals of $[Cu(dppt)_2(H_2O)_2](ClO_4)_2$ (1) separated upon cooling a solution of 1 in MeOH:MeCN:Et₂O at 5 °C for seven days. The latter were found suitable for X-ray studies.

A bright green needle-like single crystal of the complex $[Cu(dppt)_2(H_2O)_2]$ ($ClO_4)_2$ **1** with dimensions $0.35 \times 0.30 \times 0.30 \text{ mm}^3$ was selected under the polarizing microscope and then mounted on glass fiber. The crystal data collections were performed on a Bruker AXS-KAPPA APEX II diffractometer equipped with a CCD area detector utilizing Mo- K_α radiation ($\lambda = 0.71073 \text{ Å}$) at 273 K. Data were collected and reduced by SMART and SAINT software in the Bruker packages [13]. The structure was solved by direct methods and subsequently refined by full-matrix least-squares calculations with the SHELXL-2018/3 software package [14]. All non-hydrogen atoms were refined anisotropically while hydrogen atoms were placed in geometrically idealized positions and constrained to ride on their parent atoms. The graphics interface package used was PLATON, and the figures were generated using the ORTEP 3.07 generation package [15].

Also, hydrogens on water oxygen which is connected to Cu are located. The disorder in perchlorate anion is fixed and the ratio of occupancies of disordered moieties is found to be 53:47. Crystallographic data for the structural analysis of

[Cu(dppt)₂(H₂O)₂](ClO₄)₂ (**1**) have been deposited with Cambridge Crystallographic Data Center, CCDC No. 1994856.

5.3 Results and discussion

5.3.1 Synthesis and characterization of [Cu(dppt)₂(H₂O)₂](ClO₄)₂ 1

The bright green complex, $[Cu(dppt)_2(H_2O)_2](ClO_4)_2$ (1) was prepared in good yield (76%) and purity by the reaction of an aqueous solution of $Cu(OAc)_2 \cdot H_2O$, ethanolic solution of 5,6-diphenyl-3-(2-pyridyl)-1,2,4-triazine (dppt) and $NaClO_4$ in a stoichiometric ratio (1:2:1) at room temperature. The selected frequencies observed in the IR spectra of 1, the broad band that appeared at 3447 cm⁻¹ represents the existence of H_2O [16]. The stretching vibrations of the C=N and N=N groups appear at considerably lower values for the $\nu_{C=N}$ and $\nu_{N=N}$ of the free dppt ligand supporting the coordination of the triazine and pyridyl nitrogen donors to copper(II) ion [17]. It displays two well split bands at 1103 and 1064 cm⁻¹ due to perchlorate anion. Such splitting normally arises due to the coordination of or hydrogen bonding [18] of ClO_4 ; however, none of these is present in the crystal structure. Elemental analysis of 1 was entirely consistent with its determined composition by X-ray crystallography. This is substantiated by conductivity measurements in DMF solution, which is expected for a 1:2 electrolyte in solution.

5.3.2 Structure description

It was possible to attain a single-crystal X-ray structure and the copper atom of $[Cu(dppt)_2(H_2O)_2](ClO_4)_2$ (1) is located on the inversion center and occupies special position a of the C2/c space group, thus the asymmetric unit consists of a half of complex cation and one perchlorate anion. The details of data collection and structure

analysis are given in Table 5.1 while selected bond lengths and angles are listed in **Table 5.2**. The structure of **1** at low temperature is almost the same as that already determined by Palaniandavr et al. [19] at room temperature. In the complex, the copper atom is coordinated to two 3-(2-pyridyl)-5,6-diphenyl-1,2,4-triazine (dppt) via one triazine nitrogen, one pyridine nitrogen, and two water molecules (Figure 5.1). The dppt is an asymmetric bidentate ligand using only two donor nitrogen atoms (Ntz and N_{py}), which forms a five-membered chelate ring with envelop conformation. The N(2) atom of triazine ring of dppt is coordinated to copper(II) instead of N(4) atom, due to the steric effect of the phenyl group substituted at C(7) atom adjacent to the N(4) atom. Thus, the coordination number is six with a CuN₄O₂ chromophore and the geometry of the centrosymmetric copper(II) ion in 1 is described as elongated octahedral. The two N_{py} (N(1)) and two N_{tz} (N(2)) nitrogens of the dppt ligands define the best equatorial tetragonal plane while the two oxygen atoms of water molecules occupy the axial position at longer distances (2.424 Å), as a consequence of the Jahn-Teller effect. The two dppt ring systems are strictly coplanar and are bound to Cu^{II} in *trans* configuration. The coordination plane is not a perfect square as shown by the bite angles which are not equal to 90° . The two Cu-N_{py} (2.044(3) Å) and Cu-N_{tz} (2.024(3) Å) bond distances are not appreciably different indicating that the donor strength of two nitrogens is equal. At the same time, all the bond distances are >2 Å [20] signifying that the bonds are weaker. The two phenyl rings at C(7) and C(8) of the triazine ring are not coplanar with the coordination plane (CuN₄), as is evident from the dihedral angles (CuN₄ and phenyl ring plane at C(7), 35.25°; CuN₄ and phenyl ring plane at C(8), 51.98°) formed by the least-squares planes. The phenyl-phenyl repulsion is evidenced by their significant dihedral angle of 59.8°.

Table 5.1
Selected crystal data and structure refinement parameters for 1

Formula $C_{40}H_{28}N_8Cl_2O_{10}Cu$ Formula weight 915.14 Temperature (K) 273(2) Wavelength (Å) 0.71073 Crystal system Monoclinic Space group C^2/c a (Å) 12.1016(8) b (Å) 29.8689(18) $α$ (°) 90 $β$ (°) 92.782(4) $γ$ (°) 90 V (Å) 3 4098.8(5) Z 4 D_{calc} (g cm $^{-3}$) 1.483 $μ$ (mm $^{-1}$) 0.731 F (000) 1868 Crystal size (mm) 0.35 × 0.30 × 0.30 $θ$ (°) 1.365-28.159 Reflections collected 21997 Independent reflections 4942 Reflections observed [I > 2 $σ$ (I)] 3616 R_{int} 0.0324 GOOF 1.081 R_1 [I > 2 $σ$ (I)] 0.0814 w_2 [I > 2 $σ$ (I)] 0.1054 R_1 , w_2 all data 0.2354/0.2629		memoni purumeters 101 1
Temperature (K) 273(2) Wavelength (Å) 0.71073 Crystal system Monoclinic Space group $C2/c$ a (Å) 12.1016(8) b (Å) 11.3529(8) c (Å) 29.8689(18) α (°) 90 β (°) 92.782(4) γ (°) 90 V (Å) ³ 4098.8(5) Z 4 D_{cale} (g cm ⁻³) 1.483 μ (mm ⁻¹) 0.731 F (000) 1868 Crystal size (mm) 0.35 × 0.30 × 0.30 θ (°) 1.365-28.159 Reflections collected 21997 Independent reflections 4942 Reflections observed [I > 2 σ (I)] 3616 R_{int} 0.0324 GOOF 1.081 R_1 [I > 2 σ (I)] 0.0814 w R_2 [I > 2 σ (I)] 0.1054	Formula	$C_{40}H_{28}N_8Cl_2O_{10}Cu$
Wavelength (Å) 0.71073 Crystal system Monoclinic Space group $C2/c$ a (Å) 12.1016(8) b (Å) 11.3529(8) c (Å) 29.8689(18) α (°) 90 β (°) 92.782(4) γ (°) 90 V (Å) ³ 4098.8(5) Z 4 D_{calc} (g cm ⁻³) 1.483 μ (mm ⁻¹) 0.731 F (000) 1868 Crystal size (mm) 0.35 × 0.30 × 0.30 θ (°) 1.365-28.159 Reflections collected 21997 Independent reflections 4942 Reflections observed [I > 2σ (I)] 3616 R_{int} 0.0324 GOOF 1.081 R_1 [I > 2σ (I)] 0.0814 w R_2 [I > 2σ (I)] 0.1054	Formula weight	915.14
Crystal system Monoclinic Space group $C2/c$ a (Å) $12.1016(8)$ b (Å) $11.3529(8)$ c (Å) $29.8689(18)$ α (°) 90 β (°) $92.782(4)$ γ (°) 90 V (Å) 3 $4098.8(5)$ Z 4 D_{calc} (g cm 3) 1.483 μ (mm $^{-1}$) 0.731 $F(000)$ 1868 Crystal size (mm) $0.35 \times 0.30 \times 0.30$ θ (°) $1.365-28.159$ Reflections collected 21997 Independent reflections 4942 Reflections observed [I > 2σ (I)] 3616 R_{int} 0.0324 GOOF 1.081 R_1 [I > 2σ (I)] 0.0814 wR_2 [I > 2σ (I)] 0.1054	Temperature (K)	273(2)
Space group $C2/c$ a (Å) $12.1016(8)$ b (Å) $11.3529(8)$ c (Å) $29.8689(18)$ α (°) 90 β (°) $92.782(4)$ γ (°) 90 V (Å) 3 $4098.8(5)$ Z 4 D_{calc} (g cm $^{-3}$) 1.483 μ (mm $^{-1}$) 0.731 $F(000)$ 1868 Crystal size (mm) $0.35 \times 0.30 \times 0.30$ θ (°) $1.365-28.159$ Reflections collected 21997 Independent reflections 4942 Reflections observed [I > 2σ (I)] 3616 R_{int} 0.0324 GOOF 1.081 R_1 [I > 2σ (I)] 0.0814 wR_2 [I > 2σ (I)] 0.1054	Wavelength (Å)	0.71073
a (Å) $12.1016(8)$ b (Å) $11.3529(8)$ c (Å) $29.8689(18)$ α (°) 90 β (°) $92.782(4)$ γ (°) 90 V (Å) 3 $4098.8(5)$ Z 4 D_{calc} (g cm ⁻³) 1.483 μ (mm ⁻¹) 0.731 $F(000)$ 1868 Crystal size (mm) $0.35 \times 0.30 \times 0.30$ θ (°) $1.365-28.159$ Reflections collected 21997 Independent reflections 4942 Reflections observed [I > 2σ (I)] 3616 R_{int} 0.0324 GOOF 1.081 R_1 [I > 2σ (I)] 0.0814 wR_2 [I > 2σ (I)] 0.1054	Crystal system	Monoclinic
$\begin{array}{lll} b \ (\mathring{\rm A}) & 11.3529(8) \\ c \ (\mathring{\rm A}) & 29.8689(18) \\ \alpha(^{\circ}) & 90 \\ \beta(^{\circ}) & 92.782(4) \\ \gamma(^{\circ}) & 90 \\ V \ (\mathring{\rm A})^3 & 4098.8(5) \\ Z & 4 \\ D_{\rm calc} \ (g \ {\rm cm}^{-3}) & 1.483 \\ \mu \ ({\rm mm}^{-1}) & 0.731 \\ F(000) & 1868 \\ Crystal \ size \ ({\rm mm}) & 0.35 \times 0.30 \times 0.30 \\ \theta(^{\circ}) & 1.365-28.159 \\ Reflections \ collected & 21997 \\ Independent \ reflections & 4942 \\ Reflections \ observed \ [{\rm I} > 2\sigma({\rm I})] & 3616 \\ R_{\rm int} & 0.0324 \\ GOOF & 1.081 \\ R_1 \ [{\rm I} > 2\sigma({\rm I})] & 0.0814 \\ wR_2 \ [{\rm I} > 2\sigma({\rm I})] & 0.1054 \\ \end{array}$	Space group	C2/c
c (Å) $29.8689(18)$ α (°) 90 β (°) $92.782(4)$ γ (°) 90 V (Å) 3 $4098.8(5)$ Z 4 D_{calc} (g cm 3) 1.483 μ (mm $^{-1}$) 0.731 $F(000)$ 1868 Crystal size (mm) $0.35 \times 0.30 \times 0.30$ θ (°) $1.365-28.159$ Reflections collected 21997 Independent reflections 4942 Reflections observed [I > 2σ (I)] 3616 R_{int} 0.0324 GOOF 1.081 R_1 [I > 2σ (I)] 0.0814 wR_2 [I > 2σ (I)] 0.1054	a (Å)	12.1016(8)
$α(°)$ 90 $β(°)$ 92.782(4) $γ(°)$ 90 $V(Å)^3$ 4098.8(5) Z 4 D_{calc} (g cm ⁻³) 1.483 $μ$ (mm ⁻¹) 0.731 $F(000)$ 1868 Crystal size (mm) 0.35 × 0.30 × 0.30 $θ(°)$ 1.365-28.159 Reflections collected 21997 Independent reflections 4942 Reflections observed [I > 2 $σ$ (I)] 3616 R_{int} 0.0324 GOOF 1.081 R_1 [I > 2 $σ$ (I)] 0.0814 w R_2 [I > 2 $σ$ (I)] 0.1054	b (Å)	11.3529(8)
$eta(^\circ)$ 92.782(4) $\gamma(^\circ)$ 90 $V(\mathring{A})^3$ 4098.8(5) Z 4 $D_{\text{calc}} (g \text{ cm}^{-3})$ 1.483 $\mu (\text{mm}^{-1})$ 0.731 F(000) 1868 Crystal size (mm) 0.35 × 0.30 × 0.30 $\theta(^\circ)$ 1.365-28.159 Reflections collected 21997 Independent reflections 4942 Reflections observed [I > 2 σ (I)] 3616 R_{int} 0.0324 GOOF 1.081 R_1 [I > 2 σ (I)] 0.0814 wR_2 [I > 2 σ (I)] 0.1054	c (Å)	29.8689(18)
γ (°) 90 V (Å)³ 4098.8(5) Z 4 D_{calc} (g cm⁻³) 1.483 μ (mm⁻¹) 0.731 $F(000)$ 1868 Crystal size (mm) 0.35 × 0.30 × 0.30 θ (°) 1.365-28.159 Reflections collected 21997 Independent reflections 4942 Reflections observed [I > 2 σ (I)] 3616 R_{int} 0.0324 GOOF 1.081 R_1 [I > 2 σ (I)] 0.0814 w R_2 [I > 2 σ (I)] 0.1054	$lpha(^\circ)$	90
$\begin{array}{llllllllllllllllllllllllllllllllllll$	$oldsymbol{eta}(^{\circ})$	92.782(4)
Z 4 D_{calc} (g cm ⁻³) 1.483 μ (mm ⁻¹) 0.731 $F(000)$ 1868 Crystal size (mm) 0.35 × 0.30 × 0.30 θ (°) 1.365-28.159 Reflections collected 21997 Independent reflections 4942 Reflections observed [I > 2 σ (I)] 3616 R_{int} 0.0324 GOOF 1.081 R_1 [I > 2 σ (I)] 0.0814 w R_2 [I > 2 σ (I)] 0.1054	γ(°)	90
$\begin{array}{lll} D_{\rm calc} ({\rm g cm^{\text -3}}) & 1.483 \\ \mu ({\rm mm^{\text -1}}) & 0.731 \\ F(000) & 1868 \\ Crystal size ({\rm mm}) & 0.35 \times 0.30 \times 0.30 \\ \theta (^{\circ}) & 1.365 - 28.159 \\ Reflections collected & 21997 \\ Independent reflections & 4942 \\ Reflections observed [{\rm I} > 2\sigma ({\rm I})] & 3616 \\ R_{\rm int} & 0.0324 \\ GOOF & 1.081 \\ R_1 [{\rm I} > 2\sigma ({\rm I})] & 0.0814 \\ wR_2 [{\rm I} > 2\sigma ({\rm I})] & 0.1054 \\ \end{array}$	$V(\text{Å})^3$	4098.8(5)
$\begin{array}{lll} \mu \ (\text{mm}^{-1}) & 0.731 \\ F(000) & 1868 \\ \text{Crystal size (mm)} & 0.35 \times 0.30 \times 0.30 \\ \theta \ (^{\circ}) & 1.365 - 28.159 \\ \text{Reflections collected} & 21997 \\ \text{Independent reflections} & 4942 \\ \text{Reflections observed } [\text{I} > 2\sigma(\text{I})] & 3616 \\ R_{\text{int}} & 0.0324 \\ \text{GOOF} & 1.081 \\ R_1 \ [\text{I} > 2\sigma(\text{I})] & 0.0814 \\ wR_2 \ [\text{I} > 2\sigma(\text{I})] & 0.1054 \\ \end{array}$	Z	4
$F(000)$ 1868 Crystal size (mm) $0.35 \times 0.30 \times 0.30$ $\theta(^{\circ})$ $1.365-28.159$ Reflections collected 21997 Independent reflections 4942 Reflections observed $[I > 2\sigma(I)]$ 3616 R_{int} 0.0324 GOOF 1.081 R_1 $[I > 2\sigma(I)]$ 0.0814 w R_2 $[I > 2\sigma(I)]$ 0.1054	$D_{\rm calc}$ (g cm ⁻³)	1.483
Crystal size (mm) $0.35 \times 0.30 \times 0.30$ θ (°) $1.365-28.159$ Reflections collected 21997 Independent reflections 4942 Reflections observed $[I > 2\sigma(I)]$ 3616 R_{int} 0.0324 GOOF 1.081 R_1 $[I > 2\sigma(I)]$ 0.0814 wR_2 $[I > 2\sigma(I)]$ 0.1054	$\mu \text{ (mm}^{-1})$	0.731
θ (°) 1.365-28.159 Reflections collected 21997 Independent reflections 4942 Reflections observed $[I > 2\sigma(I)]$ 3616 R_{int} 0.0324 GOOF 1.081 R_1 $[I > 2\sigma(I)]$ 0.0814 w R_2 $[I > 2\sigma(I)]$ 0.1054	F(000)	1868
Reflections collected 21997 Independent reflections 4942 Reflections observed $[I > 2\sigma(I)]$ 3616 R_{int} 0.0324 GOOF 1.081 $R_1 [I > 2\sigma(I)]$ 0.0814 $wR_2 [I > 2\sigma(I)]$ 0.1054	Crystal size (mm)	$0.35 \times 0.30 \times 0.30$
Independent reflections 4942 Reflections observed $[I > 2\sigma(I)]$ 3616 R_{int} 0.0324 GOOF 1.081 $R_1 [I > 2\sigma(I)]$ 0.0814 $wR_2 [I > 2\sigma(I)]$ 0.1054	$ heta(^\circ)$	1.365-28.159
Reflections observed $[I > 2\sigma(I)]$ 3616 R_{int} 0.0324 GOOF 1.081 $R_1 [I > 2\sigma(I)]$ 0.0814 $wR_2 [I > 2\sigma(I)]$ 0.1054	Reflections collected	21997
R_{int} 0.0324 GOOF 1.081 $R_1 [I > 2\sigma(I)]$ 0.0814 $wR_2 [I > 2\sigma(I)]$ 0.1054	Independent reflections	4942
GOOF 1.081 $R_1 [I > 2\sigma(I)]$ 0.0814 $wR_2 [I > 2\sigma(I)]$ 0.1054	Reflections observed $[I > 2\sigma(I)]$	3616
$R_1 [I > 2\sigma(I)]$ 0.0814 $wR_2 [I > 2\sigma(I)]$ 0.1054	$R_{ m int}$	0.0324
$wR_2 [I > 2\sigma(I)] $ 0.1054	GOOF	1.081
2 2 2 3 3 3 3 3 3 3 3 3 3 3 3 3 3 3 3 3	R_1 [I > 2 σ (I)]	0.0814
R_1 , w R_2 all data 0.2354/0.2629	$wR_2[I > 2\sigma(I)]$	0.1054
	R_1 , w R_2 all data	0.2354/0.2629

Table 5.2
Selected bond lengths (Å) and bond angles (°) for 1

N(2)-Cu(1)	2.024(3)	N(2)-Cu(1)	2.024(3)
N(1)-Cu(1)	2.044(3)	N(1)-Cu(1)	2.044(3)
O(1)-Cu(1)	2.434(4)	O(1)-Cu(1)	2.434(4)
N(2)-Cu(1)-N(2)	180.0(18)	N(2)-Cu(1)-N(1)	100.26(14)
N(2)-Cu(1)-N(1)	79.74(13)	N(2)-Cu(1)-N(1)	79.74(14)
N(2)-Cu(1)-N(1)	100.26(13)	N(1)-Cu(1)-N(1)	180.00(18)
N(2)-Cu(1)-O(1)	89.54(14)	N(2)-Cu(1)-O(1)	90.46(14)
N(1)-Cu(1)-O(1)	91.00(16)	N(1)-Cu(1)-O(1)	89.00(16)
N(2)-Cu(1)-O(1)	90.46(14)	N(2)-Cu(1)-O(1)	89.54(14)
N(1)-Cu(1)-O(1)	89.00(16)	N(1)-Cu(1)-O(1)	91.00(16)
O(1)-Cu(1)-O(1)	180.00(16)		

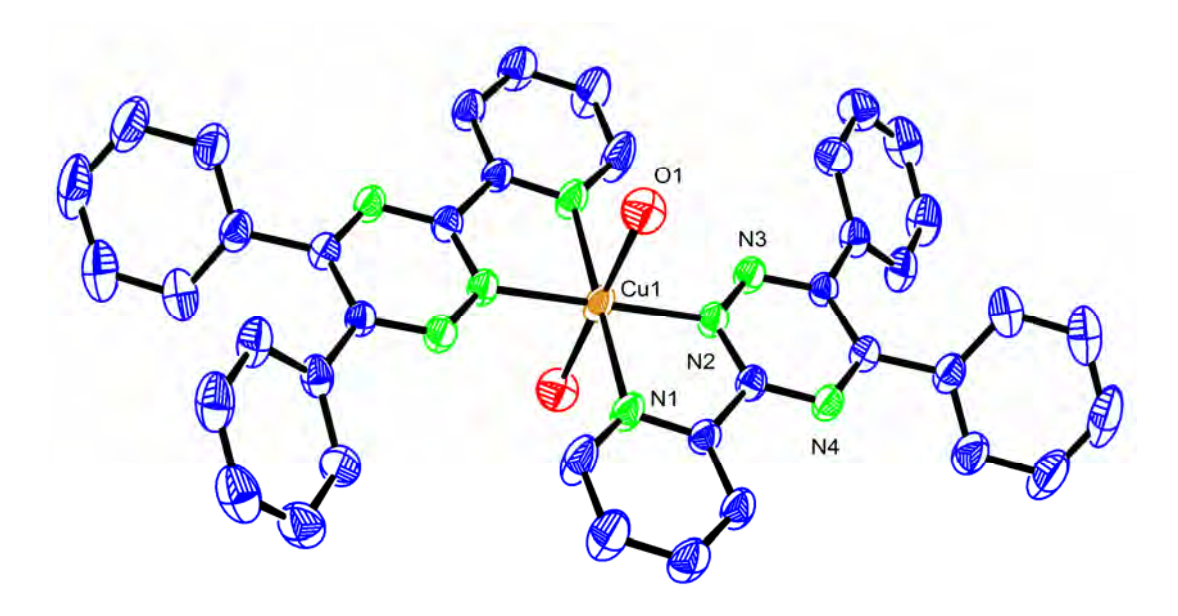


Figure 5.1 An ORTEP drawing of the $[Cu(dppt)_2(H_2O)_2]^{2+}$ cation **1** and hydrogen atoms have been omitted for clarity.

5.3.3 Electronic and EPR spectra

In DMF solution, **1** exhibits only one broad band (λ_{max} , 688 nm) with a very low extinction coefficient (ϵ_{max} , 30 dm³ mol⁻¹ cm⁻¹) value in the visible region (**Figure 5.2**), typical of ligand field (LF) absorption for Cu(II) located in a tetragonal field. The higher energy band observed around 494 nm with low-intensive absorption is assigned to N(π) \rightarrow Cu(II) ligand-to-metal charge transfer (LMCT) transition [21]. The intense absorption band around 322 and 274 nm are attributed to the intraligand $\pi \rightarrow \pi^*$ transitions [22].

The powder EPR spectrum at 298 K of 1 (Figure 5.3) exhibits one broad singlet (g_{iso} , 2.061) arising from dipolar broadening and enhanced spin-lattice relaxation. Its frozen DMF solution EPR spectrum shows axial spectral features (Figure 5.4) consist of four parallel signals (g_{\parallel}) and one perpendicular signal (g_{\perp}), typical of mononuclear Cu(II) species ($g_{\parallel} > g_{\perp} > 2.0$; $G = (g_{\parallel} - 2)/(g_{\perp} - 2) = 4.9$) suggesting the presence of $d_{x^2-y^2}$ ground state in copper(II) located in square-based geometries [23]. Further, a square based CuN₄ chromophore is expected [24,25] to show g_{\parallel} (2.200) and A_{\parallel} (180-200×10⁻⁴ cm⁻¹) values and the strong interaction of two oxygen atoms at the axial position has been found to increase the g_{\parallel} and decrease the A_{\parallel} values [26]. Therefore, the observed g_{\parallel} (2.292) and A_{\parallel} (165×10⁻⁴ cm⁻¹) values are consistent with the presence of a square-based CuN₄ coordination plane with strong axial interaction (cf. above) by two oxygen atoms. The $g_{\parallel}/A_{\parallel}$ quotient (139 cm) is suggestive [26] of negligible distortion from the CuN₄ coordination plane.

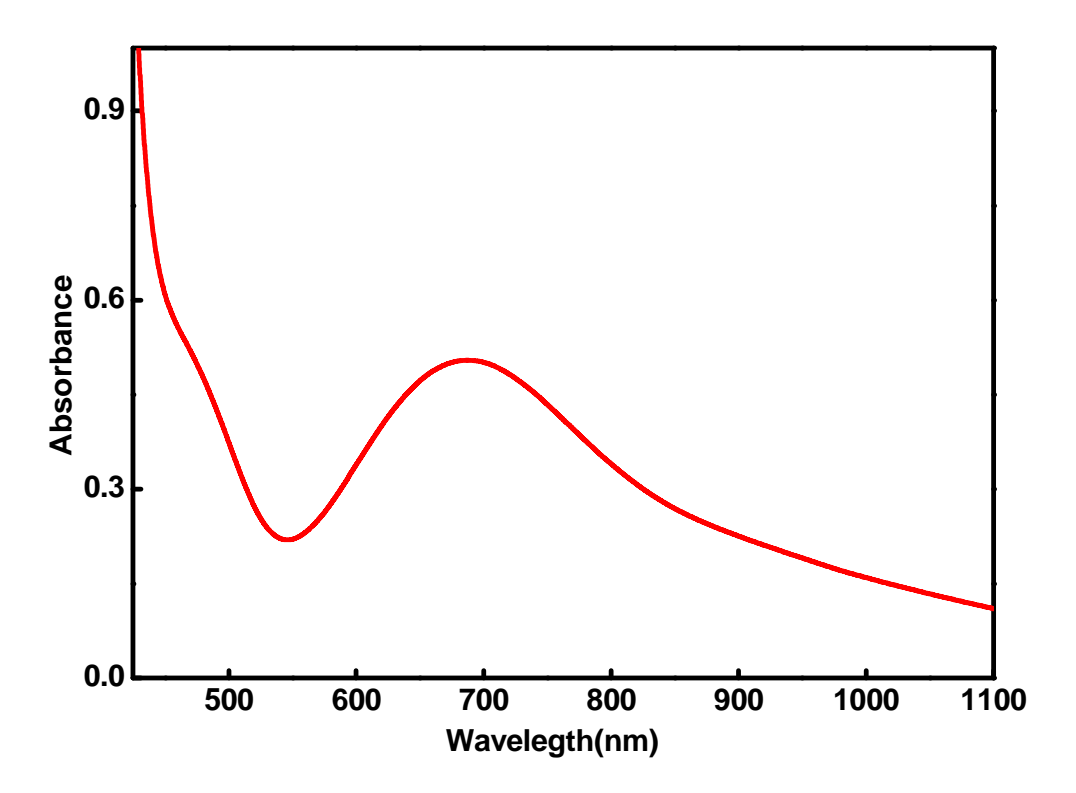


Figure 5.2 Electronic spectrum of [Cu(dppt)₂(H₂O)₂](ClO₄)₂ 1 in DMF.

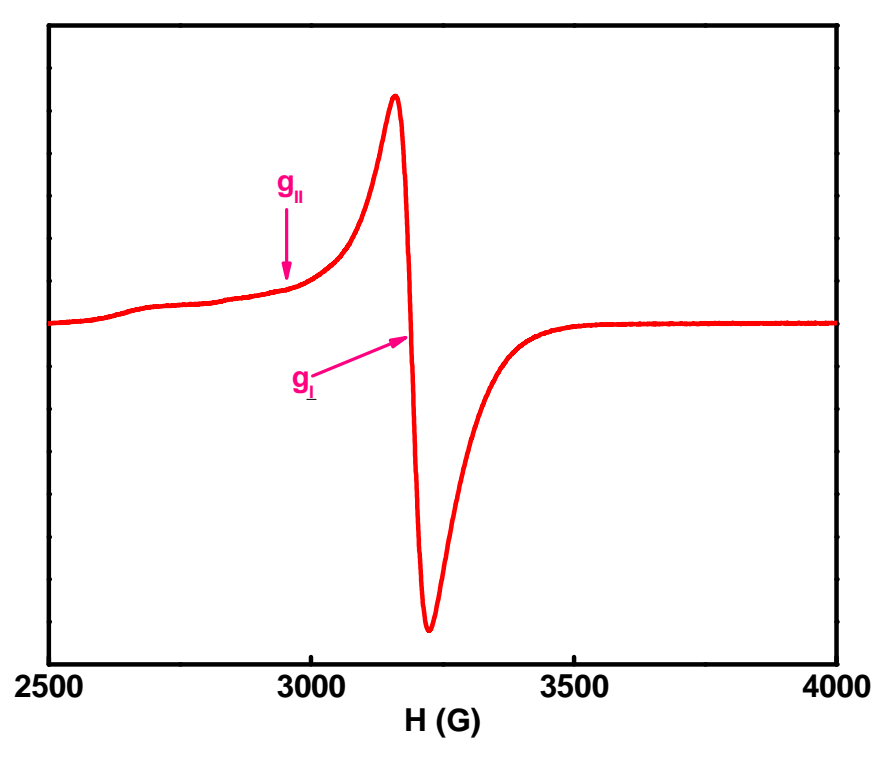


Figure 5.3 Polycrystalline EPR spectrum of $[Cu(dppt)_2(H_2O)_2](ClO_4)_2$ **1** at room temperature.

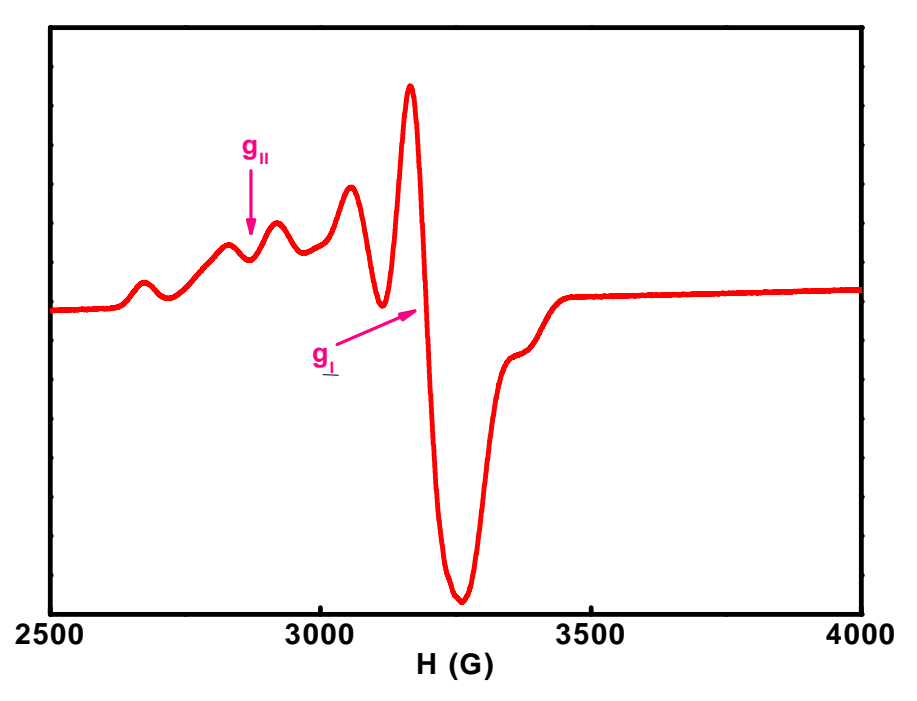


Figure 5.4 EPR spectrum of [Cu(dppt)₂(H₂O)₂](ClO₄)₂ 1 in DMF solution at 77 K.

5.3.4 Redox properties

The electrochemical behavior of **1** has been studied by cyclic voltammetry (CV) in DMF containing 0.1 M TBAP. On the negative scan, one well-defined reduction peak, E_{pc} (0.202 V) is formed whereas, on the reverse sweep, one oxidation peak, E_{pa} (0.283 V) can be observed (**Figure 5.5**). Thus, it shows a quasi-reversible redox couple, $E_{1/2}$ at 0.243 V versus SCE. The reduction process is diffusion controlled with the cathodic current function ($i_{pc}/v^{1/2}$) independent of the scan rate (v) over the range 0.01-0.2 V s⁻¹. The peak potentials separation, ΔE_p is 81 mV and the ratio of cathodic to anodic peak current (i_{pa}/i_{pc}) is close to unity. The weak σ bonding caused by the highly electron-withdrawing phenyl groups as well as strong π back bonding [22] involving the phenyl and pyridine rings, rather than the bulkiness of the ligand molecule, is responsible for the positive $E_{1/2}$ value. The redox potential of the Cu^{II}/Cu^I couple from the differential pulse voltammetry (DPV) is 0.242 V vs SCE (**Figure 5.6**), which is similar to the $E_{1/2}$ value observed from CV.

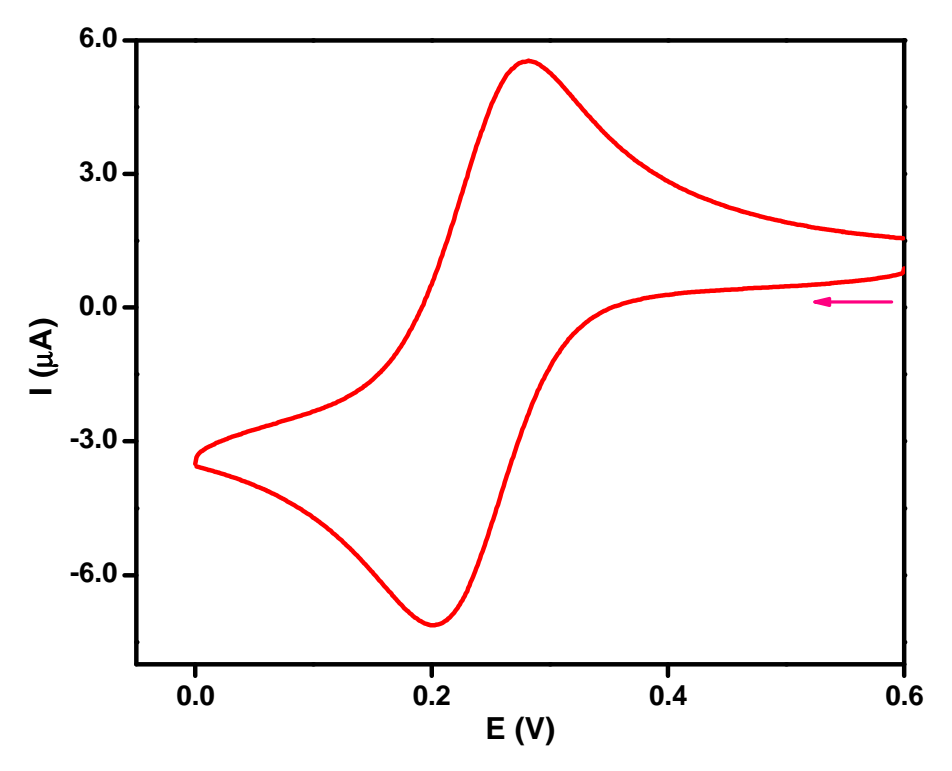


Figure 5.5 Cyclic voltammogram of $[Cu(dppt)_2(H_2O)_2](ClO_4)_2$ **1** at 50 mV s⁻¹ scan rate in DMF.

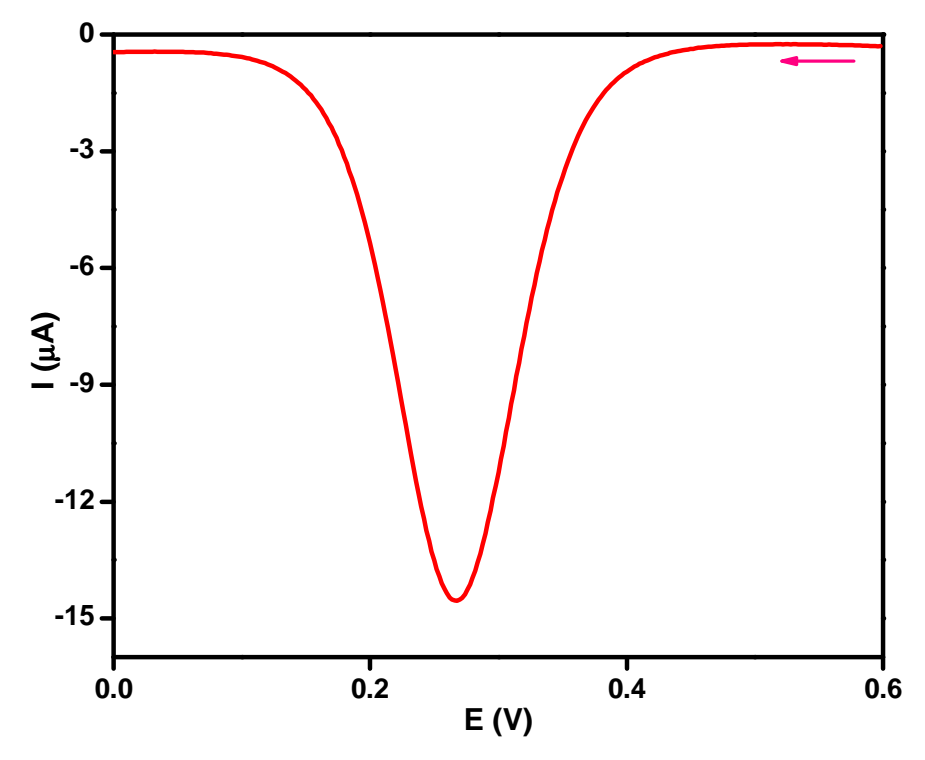


Figure 5.6 Differential pulse voltammogram of [Cu(dppt)₂(H₂O)₂](ClO₄)₂ **1** at 2 mV s⁻¹ scan rate in DMF.

5.3.5 DNA binding studies

In general, hyperchromism were regarded as spectral features for DNA double-helix structural change when DNA reacted with other molecules. The hyperchromism originates from the breakage of the DNA duplex secondary structure; the hypochromism originates from the stabilization of the DNA duplex by either the intercalation binding mode or the electrostatic effect of small molecules. Thus, the absorption spectra of 1 in the absence and presence of DNA at different concentrations (R = [DNA]/[complex] = 1-25) in 2% DMF/5 mM Tris-HCl/50 mM NaCl buffer (pH = 7.1) were recorded (Figure 5.7) at 291 nm (π - π * transition). With an increase in the concentration of CT DNA, the hypochromism of 61.0% and red-shift of 3 nm for 1 were observed indicating the partial intercalative interaction. The extent of binding was calculated using the equation [27] [DNA]/ $(\varepsilon_a - \varepsilon_f)$ = [DNA]/ $(\varepsilon_b - \varepsilon_f) + 1/K_b(\varepsilon_b - \varepsilon_f)$, where [DNA] is the concentration of DNA expressed in base pairs; ε_a , ε_f , and ε_b are the extinction coefficients for the apparent, free and fully bound copper(II) complex, respectively, and K_b is the intrinsic equilibrium DNA binding constant. A plot of [DNA]/(ε_b - ε_f) versus [DNA] gives the intrinsic equilibrium DNA binding constant, K_b, as the ratio of slope to intercept (Figure 5.7, inset). The K_b value has been estimated to be $2.565 \pm 0.001 \times 10^5 \, \text{M}^{-1}$, which suggests the enhanced DNA binding propensity of 1 possibly due to the involvement of partial intercalative interaction of the planar 5,6-diphenyltriazine moiety of coordinated dppt into the DNA base pairs leading to high hypochromism. It suggests that 1 binds with DNA with an affinity less than that of the classical and partial intercalators [28,29] (classical intercalator: EthBr, K_b , ~10⁶ M⁻¹ [30] and partial intercalator: $[Co(phen)_2(dppz)]^{3+}$,

 K_b , 9.09×10^5 M⁻¹ [31]; $[Ru(imp)_2(dppz)]^{2+}$, K_b , 2.19×10^7 M⁻¹ [32]). Again DNA binding interaction is compared with the presence of dppt with CT DNA. From absorption spectra, there is no change in absorption spectral band upon increasing the DNA concentration. This absorbance indicates that there is no involvement of interactions between dppt and the base pairs of DNA.

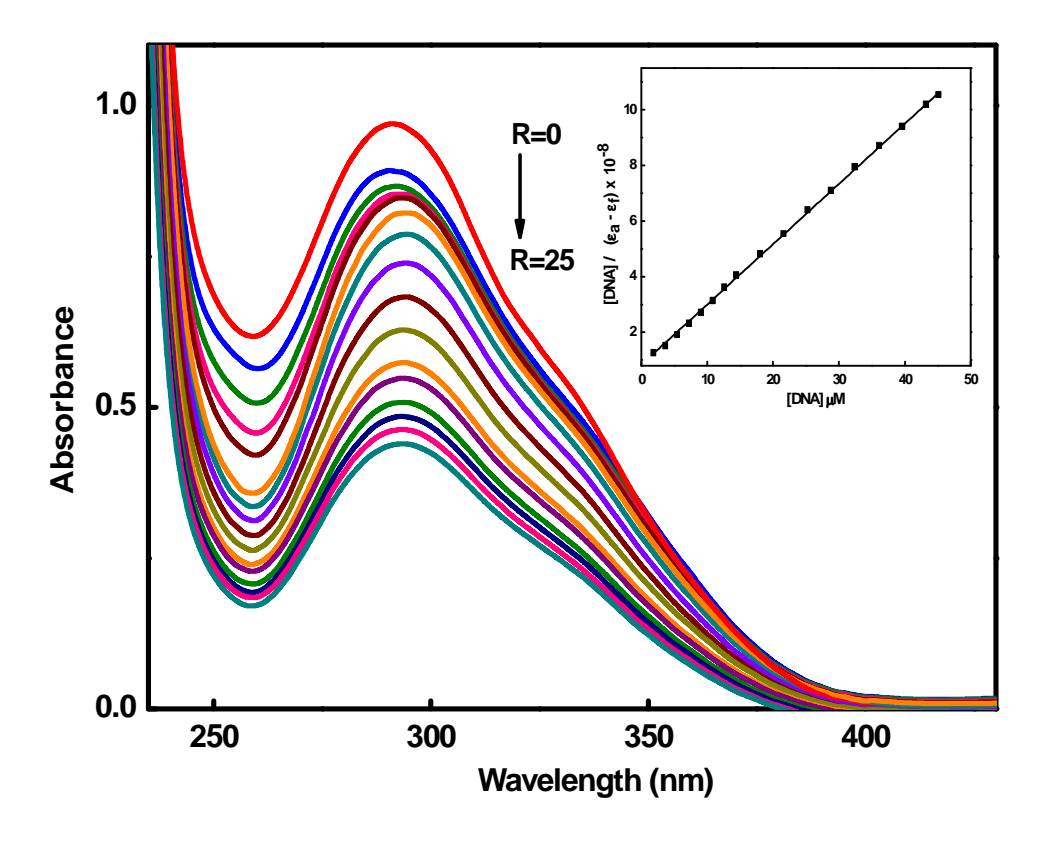


Figure 5.7 Absorption spectra of 1 (25 \times 10⁻⁶ M) in 2% DMF/5mM Tris-HCl/50 mM NaCl buffer at pH 7.1 in the absence (R = 0) and presence (R = 25) of increasing amounts of CT DNA. Inset: Plot of [DNA] vs [DNA]/(ϵ_a - ϵ_f) at R = 25 of 1.

5.3.6 Ethidium Bromide (EthBr) displacement assay

To get more insight into the interaction mode of the ligand or the complexes towards DNA, fluorescence titration experiments have been performed. The fluorescence titrations, especially the EthBr fluorescence displacement experiments, have been

widely used to characterize the interaction of compounds with DNA by following the changes in fluorescence intensity [33]. The method is based on a decrease of fluorescence resulting from the displacement of EthBr from a DNA sequence by a quencher and the quenching is due to the reduction of the number of binding sites in the DNA available to the EthBr [34]. The intrinsic fluorescence intensity of DNA and that of EthBr are low, while the fluorescence intensity of EthBr will be enhanced on the addition of DNA due to its intercalation into the DNA. Therefore, EthBr can be used to probe the interaction of the ligands or complexes with DNA. In our experiment, the fluorescence intensities of the EthBr-DNA system show a decreasing trend with an increasing concentration of 1 (Figure 5.8), indicating that some EthBr molecules are released from EthBr-DNA after an exchange with 1 which results in the fluorescence quenching of EthBr. This may be due to that 1 displaces the EthBr from its DNA-binding sites in a competitive manner. To quantitatively compare this quenching behavior, the classical Stern-Volmer equation was employed [35]. The plot (Figure 5.8, inset) illustrates that the quenching of EthBr bound to DNA is in good agreement with the linear Stern-Volmer equation. The K_{SV} value (1.60 \times $10^5~M^{\text{--}1})$ of $\boldsymbol{1}$ indicates the quenching efficiency and especially significant degree of binding to DNA. The binding strength of 1 (only those samples caused a 50% decrease of fluorescence intensity) with DNA was estimated as apparent binding constant (K_{app}) [36]. The K_{app} value $(2.82 \times 10^5 \text{ M}^{-1})$ supports a strong interaction of 1 with CT DNA and the mode of binding through partial intercalation [37, 38]. The results are consistent with those obtained from electronic absorption titration studies.

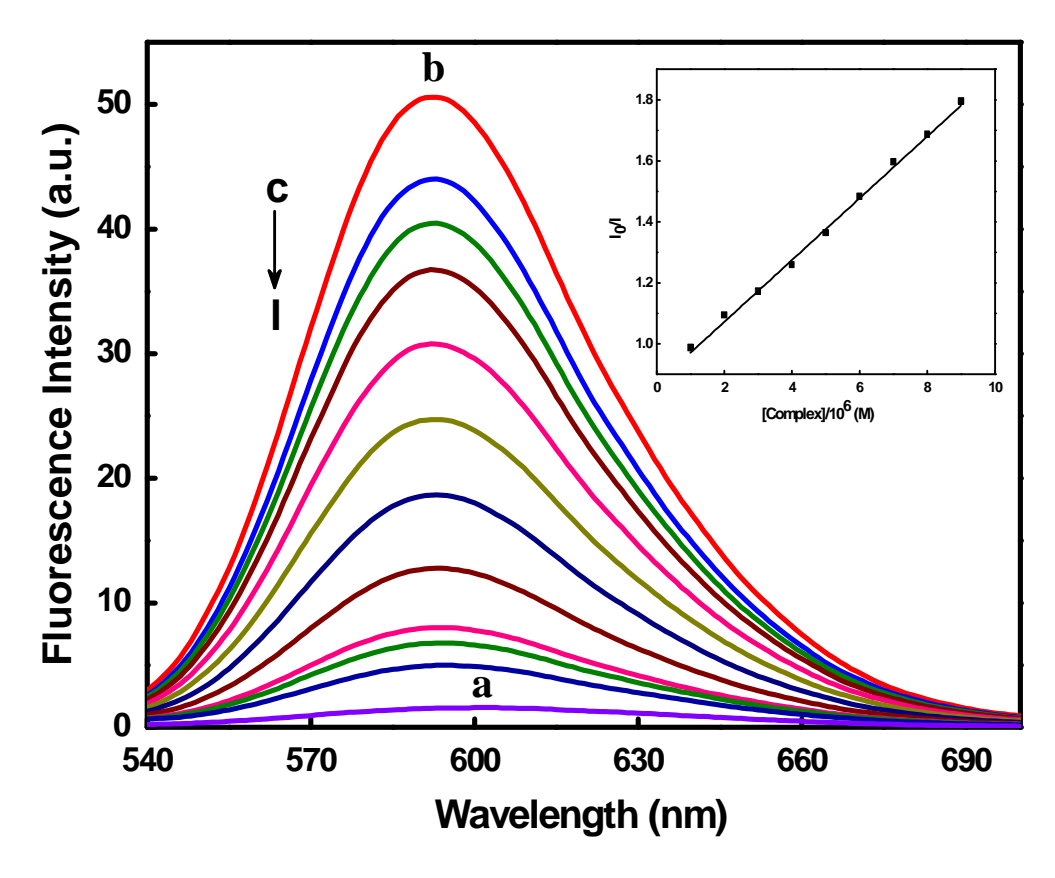


Figure 5.8 Fluorescence quenching curves of ethidium bromide bound to DNA in 2% DMF/5mM Tris-HCl/50 mM NaCl buffer at pH 7.1: (a) EthBr (1.25 μ M); (b) EthBr + DNA (125 μ M); (c-m) EthBr + DNA + **1** (0-9 μ M). Inset: Plot of [complex \times 10⁻⁶] vs I₀/I of **1**.

5.3.7 Voltammetric studies

Electrochemical measurement is a most constructive technique to analyze metal-DNA interactions than spectroscopic methods [39]. The electrochemical investigations of metal-DNA interactions can provide a useful complement to spectroscopic methods, which inform about interactions with both the reduced and oxidized form of the metal. Electrochemical studies of transition-metal complexes have been extensive, and the effect of ligand concentration on potential can be used to determine formation constants. In the absence of DNA, the complexes show sharp waves peaks for both oxidation and reduction states. Upon addition of DNA, both waves' peaks of i_{pc} and

 i_{pa} are decreased, due to large binding of copper(II) complexes to DNA and not to an increase in solution viscosity; we performed voltammetric experiments on a mixture of copper(II) complex, which intercalates between the DNA base pairs. In this study, typical cyclic voltammetric (CV) responses for 1 in 2% DMF-5 mM Tris-HCl-50 mM NaCl buffer (pH = 7.1) in the absence and presence of CT DNA are shown in **Figure 5.9**. The cathodic (0.032 V) and anodic peak potential (0.132 V) values observed for 1 correspond to Cu^{II}/Cu^I redox couple [40]. Upon addition of DNA, both the cathodic and anodic current decreases drastically, which is expected of strong binding of the complex with DNA [41] via partial intercalation. The equilibrium binding constants K_{+}/K_{2+} can be calculated by using the shift value of the formal potential (ΔE_0) of Cu(II)/Cu(I) according to the Bard and Carter equation [42]: $\Delta E^0 = E^0_b - E^0_f = 0.0591$ $\log(K_+/K_{2+})$, where E^0_b and E^0_f are the formal potentials of the bound and free complex forms respectively, and K_{+} and K_{2+} are the corresponding binding constants for the binding of reduction and oxidation species to DNA, respectively. The formal potentials of Cu^{II}/Cu^Icouple (obtained from differential pulse voltammetry (DPV) studies) in the E_f^0 (0.116 V) and E_b^0 (0.032 V) forms shift negatively (-84 mV) after reacting with DNA (Figure 5.10). The ratio of equilibrium binding constants, K_{+}/K_{2+} , is calculated to be 0.04. This suggests that the B form of DNA tends to stabilize the Cu(II) over the Cu(I) state of 1 obviously by partial intercalative interaction and thereby indicating that the species Cu(II) interacts with DNA to a greater extent than Cu(I).

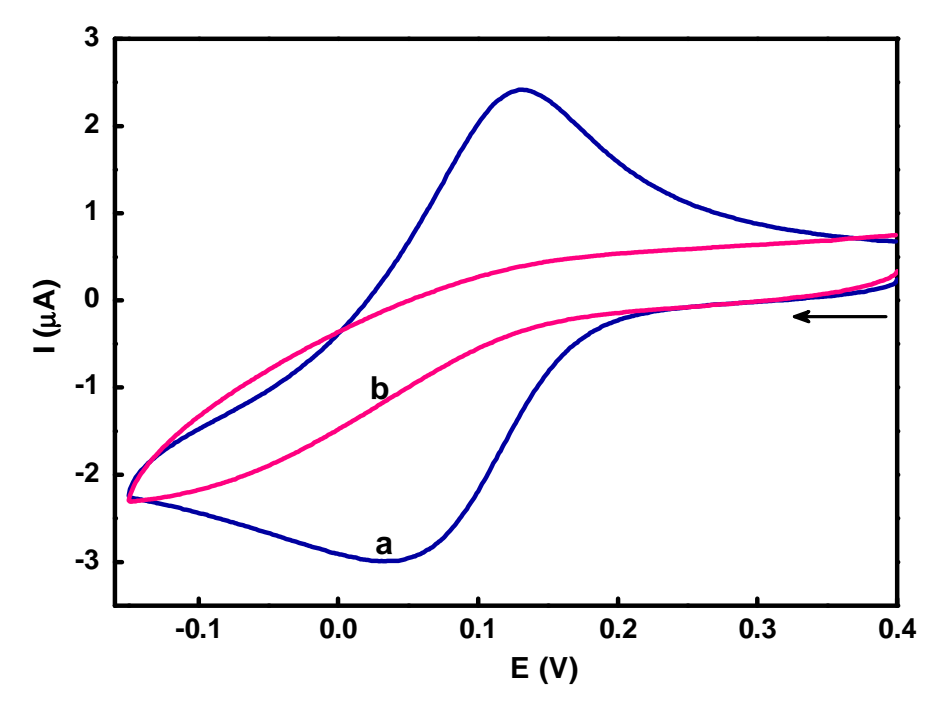


Figure 5.9 Cyclic voltammograms of **1** (0.5 mM) in the absence (a) and presence (b) of CT DNA (R = 5) at 25.0 ± 0.2 °C at 50 mV s⁻¹ scan rate in 2% DMF/5mM Tris-HCl/50 mM NaCl buffer at pH 7.1.

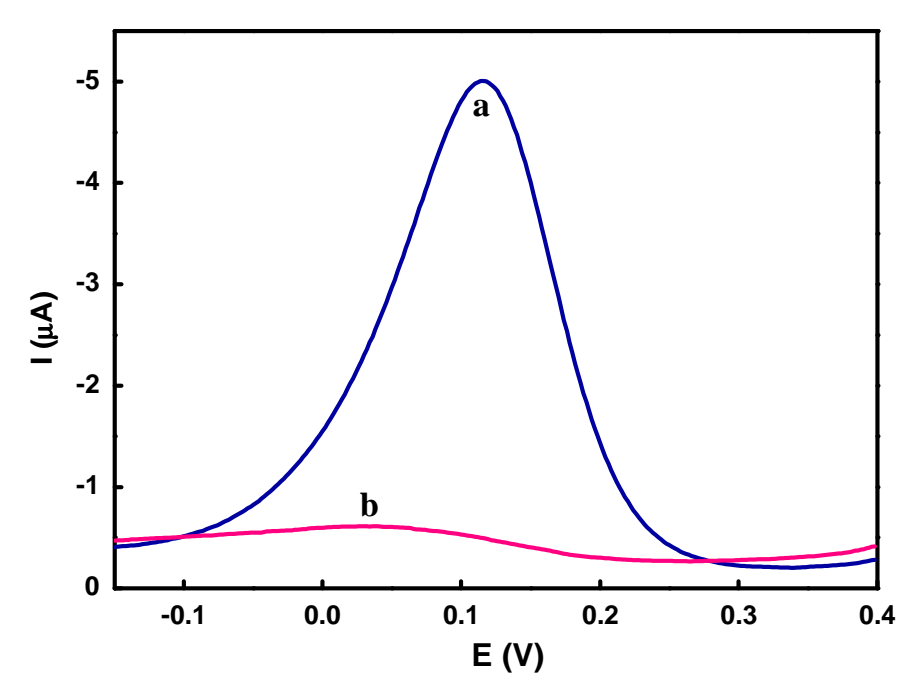


Figure 5.10 Differential pulse voltammograms of 1 (0.5 mM) in the absence (a) and presence (b) of CT DNA (R = 5) at 25.0 ± 0.2 °C at 2 mV s⁻¹ scan rate in 2% DMF/5mM Tris-HCl/50 mM NaCl buffer at pH 7.1.

5.3.8 Cytotoxic activity

The cytotoxicity of the compound against human cervical carcinoma cells HeLa was determined by MTT assay, which serves as an index of cell viability by detecting the reduction of tetrazolium salt to blue formazan by mitochondrial enzyme activity of succinate hydrogenase in living cells. Compounds having IC₅₀ values are considered as highly active ($< 5 \mu M$), moderately active ($5-10 \mu M$), weak ($10-20 \mu M$) and inactive (>20 µM) [R1]. HeLa cells were treated with increasing concentrations (0.1 to 100 µM) of 1 for 48 h, and the viable cells were measured by MTT assay. The copper(II) complex, 1, inhibited the growth of HeLa cells in a dose-dependent manner (IC₅₀, $3.73 \pm 0.57 \mu M$) (Figure 5.11). From the IC₅₀ of 1, we can find that it is found to be highly active against the selected cancer cells [43] and 4.5 times lower than cisplatin (IC₅₀, 16.4 µM). In comparison, free dppt ligand showed no significant growth inhibition activities at a concentration as high as 112.48 µM, which indicated that the chelation of dppt with copper ion was essential for anticancer activities of the copper(II) complex. Because the proliferation of the HeLa cells was not inhibited by incubation of Cu(OAc)₂·H₂O at a concentration up to 705.67 µM, cell growth inhibition activity by copper(II) complex must be derived from the biological activity of 1, not simply from free copper chaperoned into cells by the ligand. In addition, the results of in vitro cytotoxic activity studies have also indicated that the IC₅₀ value of 1 against NIH 3T3 mouse embryonic fibroblasts (normal cells) is found to be above 500 μM (Figure 5.12), which confirmed that 1 is very specific on cancer cells. Finally, the cytotoxic behavior of 1 is consistent with its ability to bind with DNA.

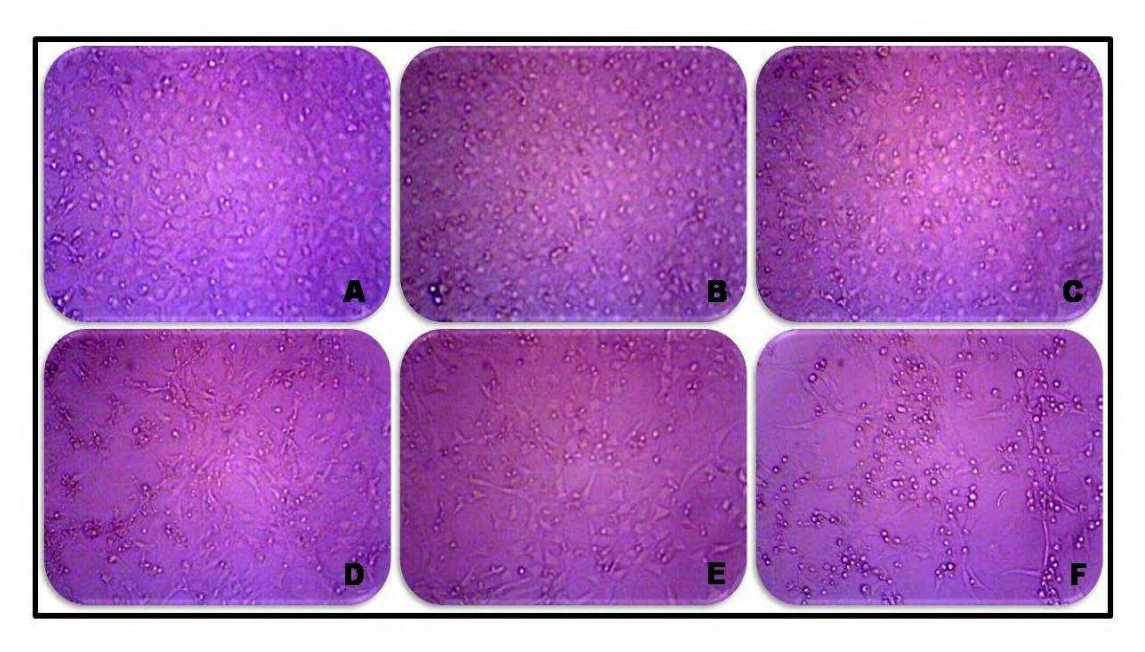


Figure 5.11 Photomicrograph of human cervical carcinoma cells (HeLa) after 48 h exposure with **1** (A, control; B, 0.1 μ M; C, 1 μ M; D, 10 μ M; E, 50 μ M; F, 100 μ M).

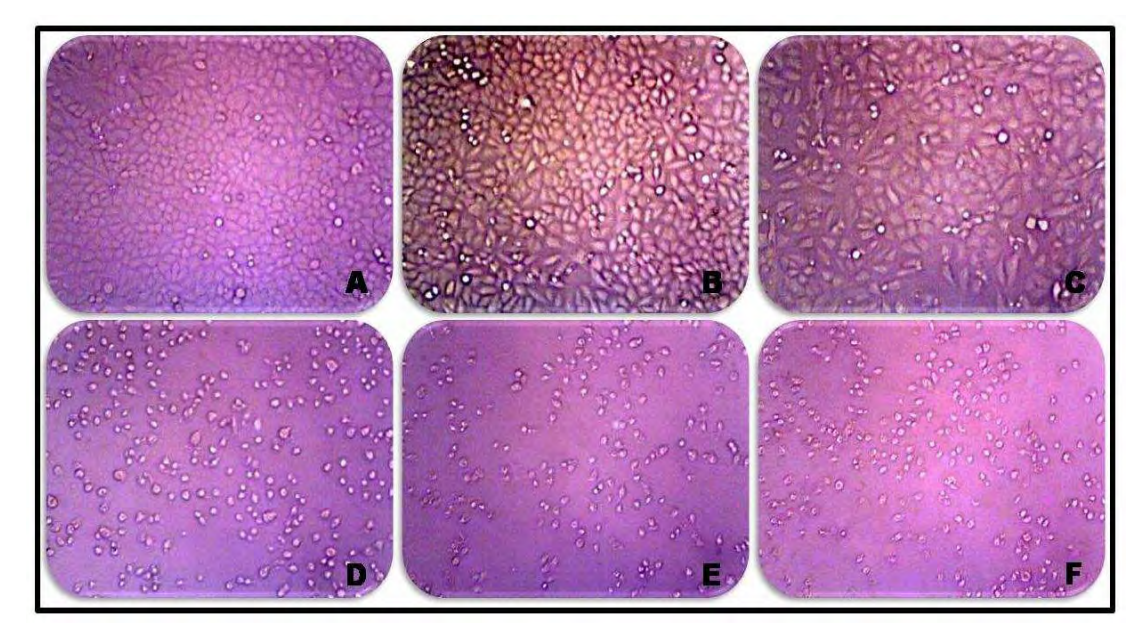


Figure 5.12 Photomicrograph of normal mouse embryonic fibroblasts cells (NIH 3T3) after 48 h exposure with **1** (A, control; B, 25 μ M; C, 50 μ M; D, 100 μ M; E, 200 μ M; F, 500 μ M).

5.3.9 Anticancer drug mechanism

5.3.9a Cell cycle arrest studies

Inhibition of cancer cell proliferation by cytotoxic drugs could be the result of induction of apoptosis, or cell cycle arrest or a combination of these. To elucidate this, profiles of propidium iodide stained HeLa cells treated with IC₅₀ concentration of **1** for 24 h were analyzed by FACS [44]. As shown in the control (**Figure 5.13A**), the percentage in the cell at the G1 phase is 61.94% and a remarkable increase of 17.2% was found (**Figure 5.13B**). The increase in the G1 phase was accompanied by the corresponding reduction in G0, S, and G2/M phases. The data mean that **1** induces cell cycle arrest at the G1 phase in HeLa cells.

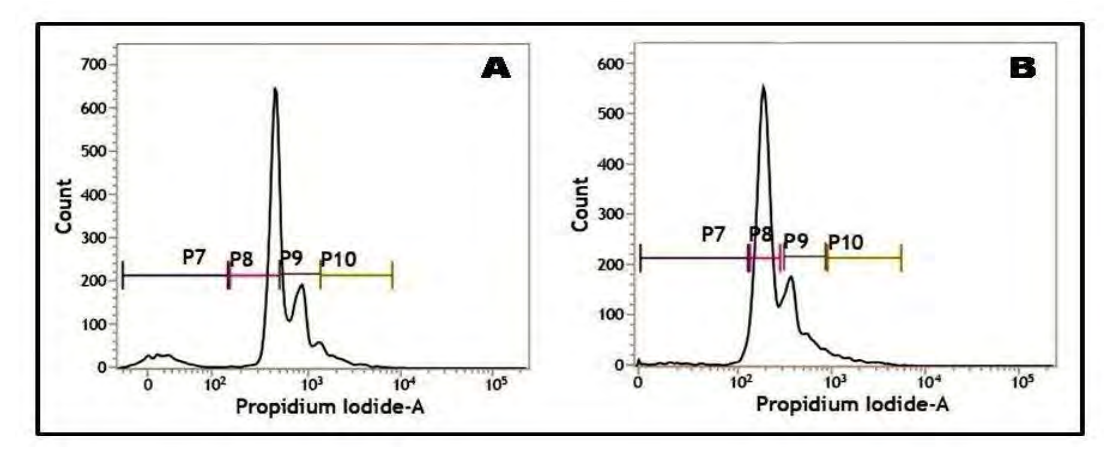


Figure 5.13 Flow cytometric analysis showing the G1 phase cell cycle arrest by 1 in HeLa cells (P7, P8, P9 and P10 corresponds to G0, G1, S and G2/M phases respectively).

5.3.9b DCFDA assay for ROS

It is well known that pharmacological ROS damage might be a potential element to eliminate cancer cells, which suggests that ROS can induce apoptosis in cancer cells [45]. Thus, the mechanistic aspects of the cellular damage were examined by the dichlorofluorescein diacetate (DCFDA) assay in HeLa cells for the generation of ROS using 1 (Figure 5.14). DCFDA, a cell permeable fluorogenic probe, on

oxidation by ROS forms DCF showing an emission maximum at 528 nm [46, 47]. The fluorescence of DCF was observed and quantified by the FACS method in a time-dependent manner. The cells treated with 1 and DCFDA for 1 h show a significant shift of the histogram towards the right, indicating an increase in the intensity of emission resulting from the generation of DCF from DCFDA. As shown in Figure 5.14, in the control, the DCF fluorescence intensity is 100% while the intensity of DCF fluorescence increases to 128% when HeLa cells were incubated with 1. The greater shift implies higher fluorescence intensity resulting from the higher amount of DCF formation and thus greater ROS generation, which is consistent with the apoptotic effect (cf. below) of 1. Moreover, the ROS levels induced by 1 show a time-dependent manner, decreasing the fluorescence intensity for 2 h (119%) and 3 h (116%). The result demonstrates the generation of ROS and this reactive species possibly causing cell apoptosis.

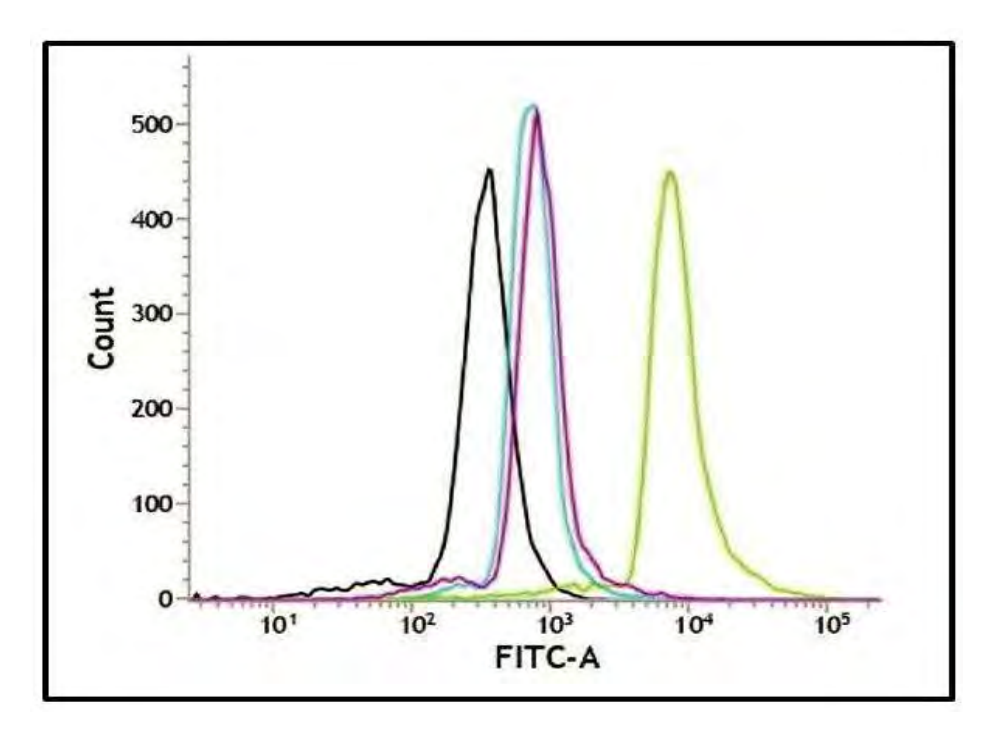


Figure 5.14 DCFDA assay in HeLa cells for generation of ROS using the 1 in a time-dependent manner (control, block; 1 h, red; 2 h, blue; 3 h, green).

5.3.9c Cell death pathway

Cell death occurs mostly through necrosis and apoptosis pathways. Chemotherapy or irradiation can induce apoptosis within cancer cells. We then carried out the apoptosis assay to further evaluate the possible mechanism of cell death induced by 1. To quantify the amount of HeLa cells in different apoptosis stage, flow cytometry analysis of living cells were carried out with an Annexin V and propidium iodide (PI) double staining assay (Figure 5.15). An early feature of apoptotic cells is the loss of plasma membrane asymmetry protein Annexin V has been used widely to detect early stage apoptotic cells [48]. When combined with PI, which stains DNA of cells with permeable membranes, this approach allows a further distinction of living (Annexin V-/PI-, lower left quadrant), early apoptotic (Annexin V+/PI-, lower right quadrant) and late apoptotic/necrotic (Annexin V+/PI+, upper right quadrant) cells [49]. In the control cells (Figure 5.15A), the percentage of living, early apoptotic, late apoptotic and necrosis cells were 99.9, 0.0, 0.1, and 0.0%, respectively. However, 1 treated HeLa cell (Figure 5.15B) displayed a remarkable average of 56.08% of early apoptotic cells and 18.33% of late apoptotic cells. The increased expression of Annexin V positive cells undoubtedly demonstrated the cells were in the apoptosis stage and is consistent with its in vitro cell cytotoxicity. Interestingly, there is no sign of cell death via the necrotic pathway.

To understand the nuclear morphology and the nature of the cell death mechanism, we have carried out DAPI (4',6-diamidino-2-phenylindole) staining with 1, and resulting images of control and treated HeLa cells are shown in Figure 5.16. The control (Figure 5.16A) HeLa cells exhibited an evenly stained nuclei with round

and intact contours whereas the treated cells (**Figure 5.16B**) showed characteristic fragmentation of the nucleus or condensed nuclei which is supportive of the cell toxicity induced by **1** due to apoptotic mode of cell death.

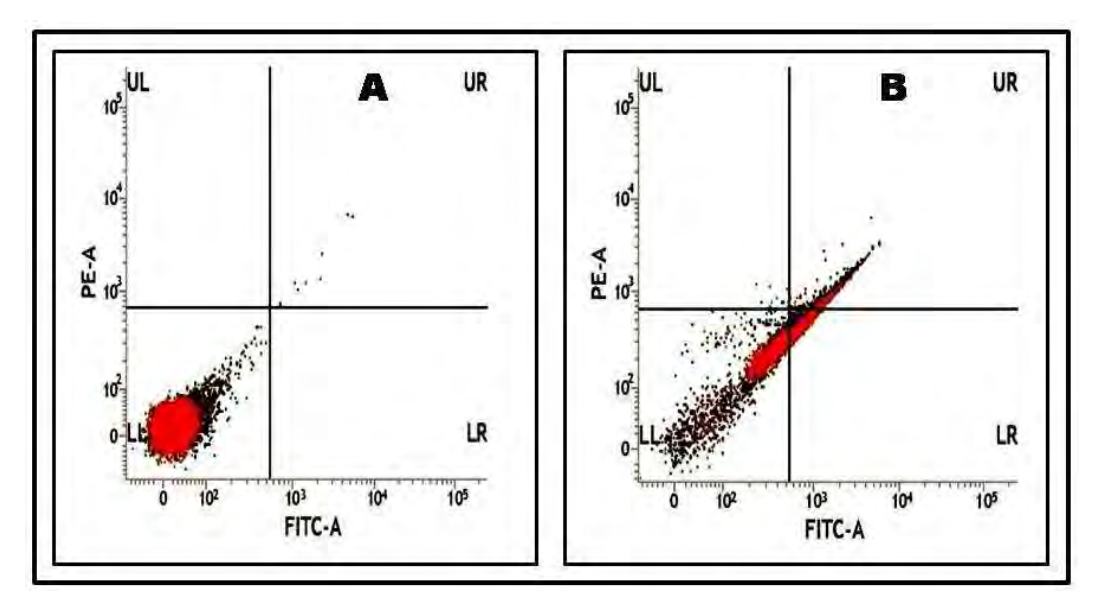


Figure 5.15 Cellular apoptosis induced by 1 as determined from the annexin V-FITC/PI staining assay of the HeLa cells with four distinct phenotypes: viable cells (lower left quadrant, LL); cells at an early stage of apoptosis (lower right quadrant, LR); cells at a late stage of apoptosis (upper right quadrant, UR); and necrosis (upper left quadrant, UL).

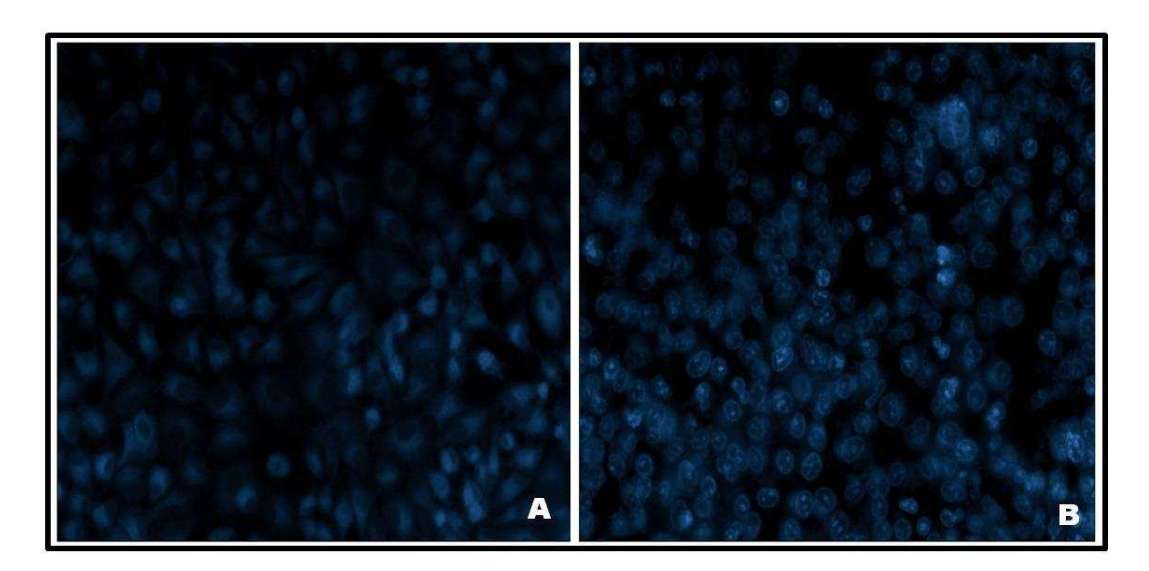


Figure 5.16 HeLa cells stained with DAPI in the presence of 1 and visualized under a fluorescence microscope.

5.4 Conclusion

The copper(II) complex, [Cu(dppt)₂(H₂O)₂](ClO₄)₂, has been synthesized and characterized by different analytical and spectral measurements. The copper(II) complex of dppt has a square-based geometry which is in contrast to those of analogous bpy or phen type diimine complexes. It possesses a quasi-reversible one-electron transfer process with relatively high positive redox potential. The complex binds to CT DNA through partial intercalative mode. It exhibits a highly active inhibitory effect, which was higher than cisplatin and selective to cancer cells while non-toxic to healthy cells. The biological evaluation provides evidence that it blocked the cell cycle at the G1 phase and induced apoptosis alone along with the generation of ROS. The present lead complex is a novel therapeutic agent for the treatment of cervical cancer as well as encourages further exploration of non-platinum anticancer agents. It targets the mitochondria of cancer cells and induces apoptosis by a mechanism involving the formation of ROS.

References

- [1] U. Ndagi, N. Mhlongo, M.E. Soliman, Drug Des. Dev. Ther. 11 (2017) 599-616.
- [2] M. Frezza, S. Hindo, D. Chen, A. Davenport, S. Schmitt, D. Tomco, Q.P. Dou, Curr. Pharm. Des. 16 (2010) 1813-1825.
- [3] C. Marzano, A. Trevisan, L. Giovagnini, D. Fregonal, Toxicol. In Vitro 16 (2002) 413-419.
- [4] C. Orvig, M.J. Abrams, Chem. Rev. 99 (1999) 2201-2204.
- [5] M. Yaman, G. Kaya, H. Yekeler, World J. Gastroenterol. 13 (2007) 612-618.
- [6] K.H. Thompson, C. Orvig, Science 300 (2003) 936-939.
- [7] A. Samuni, M. Chevion, G. Czapski, J. Biol. Chem. 256 (1981) 12632-12635.
- [8] C.A. Wijker, M.V. Lafleur, Mut. Res. 429 (1999) 27-35.
- [9] M.C. Linder, Mut. Res. 475 (2001) 141-152.
- [10] J.J. Knox, S.J. Hotte, C. Kollmannsberger, E. Winquist, B. Fisher, E.A. Eisenhauer, Invest. New. Drugs. 25 (2007) 471-477.
- [11] J. Yuan, D.B. Lovejoy, D.R. Richardson, Blood. 104 (2004) 1450-1458.
- [12] K.J. Barnham, C.L. Masters, A.I. Bush, Nat. Rev. Drug. Discov. 3 (2004) 205-214.
- [13] Bruker AXS Inc., SMART (Version 5.060) and SAINT (Version 6.02),Madison, Wisconsin, USA, 1999.
- [14] SHELXL, G.M. Sheldrick, Acta Cryst. C17 (2015) 3-8.
- [15] L.J. Farrugia, J. Appl. Cryst. 45 (2012) 849-854.
- [16] K. Nakamoto, Infrared and Raman Spectra of Inorganic and Coordination Compounds, 4th ed., Wiley-Interscience, New York, 1986.
- [17] V. Bereau, J. Marrot, CR Chim. 8 (2005) 1087-1092.
- [18] M.R. Rosenthal, J. Chem. Educ. 50 (1973) 331-335.

- [19] R. Uma, M. Palaniandavar, R.J. Butcher, J. Chem. Soc., Dalton Trans. (1996) 2061-2066.
- [20] B. Machura, A. Switlicka, R. Kruszynski, J. Mrozinski, J. Klak, J. Kusz, Polyhedron 27 (2008) 2959-2967.
- [21] R. Liu, M.-M. Huang, X.-X. Yao, H.-H. Li, F.-L. Yang, X.-L. Li, Inorg. Chim. Acta 434 (2015) 172-180.
- [22] A.B.P. Lever, Inorganic Electronic Spectroscopy, Elsevier, Amsterdam, 1984.
- [23] Z. Moradi-Shoeili, Z. Amini, D.M. Boghaei, B. Notash, Polyhedron 53 (2013) 76-82.
- [24] P. Tamil Selvi, M. Murali, M. Palaniandavar, M. Kockerling, G. Henkel, Inorg. Chim. Acta 340 (2002) 139-146.
- [25] C. Rajarajeswari, R. Loganathan, M. Palaniandavar, E. Suresh, A. Riyasdeen,M.A. Akbarsha, Dalton Trans. 42 (2013) 8347-8363.
- [26] R. Loganathan, S. Ramakrishnan, E. Suresh, A. Riyasdeen, M.A. Akbarsha,M. Palaniandavar, Inorg. Chem. 51 (2012) 5512-5532.
- [27] A. Wolfe, G.H. Shimer Jr., T. Meehan, Biochemistry 26 (1987) 6392-6396.
- [28] M. Cory, D.D. McKee, J. Kagan, D.W. Henry, J.A. Miller, J. Am. Chem. Soc. 107 (1985) 2528-2536.
- [29] H.J. Waring, J. Mol. Biol. 13 (1965) 269-282.
- [30] C.-Z. Xie, M.-M. Sun, S.-H. Li, X.-T. Zhang, X. Qiao, Y. Ouyang, J.-Y. Xu. J. Coord. Chem. 66 (2013) 3891-3905.
- [31] S. Arounagiri, B.G. Maiya, Inorg. Chem. 35 (1996) 4267-4270.
- [32] J.G. Liu, B.H. Ye, H. Li, L.N. Ji, R.H. Li, J.Y. Zhou, J. Inorg. Biochem. 73 (1999) 117-122.

- [33] X.W. Li, X.J. Li, Y.T. Li, Z.Y. Wu, C.W. Yan, J. Photochem. Photobiol. B 118 (2013) 22-32.
- [34] R. Indumathy, S. Radhika, M. Kanthimathi, T. Weyhermuller, B.U. Nair, J. Inorg. Biochem. 101 (2007) 434-443.
- [35] J.R. Lakowicz, G. Webber, Biochemistry 12 (1973) 4161-4170.
- [36] M. Lee, A.L. Rhodes, M.D. Wyatt, S. Forrow, J.A. Hartley, Biochemistry 32 (1993) 4237- 4245.
- [37] E. Kahrovic, A. Zahirovic, E. Turkusic, J. Chem. Chem. Eng. 8 (2014) 335–343.
- [38] J. Qian, X. Ma, J. Tian, W. Gu, J. Shang, X. Liu, S. Yan, J. Inorg. Biochem. 104 (2010) 993-999.
- [39] S. Mahadevan, M. Palaniandavar, Inorg. Chem. 37 (1998) 693-700.
- [40] B. Monica, B.F. Marisa, B. Franco, P. Giorgio, P. Silvana, T. Pieralberto, Inorg. Chem. 42 (2003) 2049–2055.
- [41] A.J. Bard, L.R. Faulkner, Electrochemical Methods: Fundamentals and Applications, Wiley, New York, 1980.
- [42] M.T. Carter, A.J. Bard, J. Am. Chem. Soc., 109 (1987) 7528-7530.
- [43] M.T.H. Tarafder, A. Kasbollah, K.A. Crouse, A.M. Ali, B.M. Yamin, H.-K. Fun, Polyhedron 20 (2001) 2363-2370.
- [44] L.C. Crowley, B.J. Marfell, A.P. Scott, N.J. Waterhouse, Cold Spring Harb. Protoc. 11 (2016) 953-956.
- [45] D. Trachootham, J. Alexandre, P. Huang, Nat. Rev. Drug Discovery 8 (2009) 579-591.
- [46] T. Takanashi, Y. Ogura, H. Taguchi, M. Hashizoe, Y. Honda, Investig.Ophthalmol. Vis. Sci. 38 (1997) 2721-2728.

- [47] A.S. Keston, R. Brandt, Anal Biochem 11 (1965) 1-5.
- [48] I. Vermes, C. Haanen, H. Steffens-Nakken, C. Reutelingsperger, J. Immunol.Methods 184 (1995) 39-51.
- [49] R.N. Bhattacharjee, K.S. Park, Y. Kumagai, K. Okada, M. Yamamoto, S. Uematsu, K. Matsui, H. Kumar, T. Kawai, T. Iida, T. Hondo, O. Takeuchi, S. Akira, J. Biol. Chem. 281 (2006) 36897-36904.

Summary

The studies of DNA binding, BSA interaction, and cytotoxicity effects of bisand mixed-ligand copper(II) complexes are presented in this thesis. The DNA binding
and cleaving of the complexes when they interacted with commercially available CT
DNA and supercoiled pUC19 DNA were investigated. BSA was used to test the
ability of the complexes to bind protein. The cytotoxic activity of copper(II) complexes
has been investigated against both human cervical carcinoma cell line (HeLa) and
normal mouse embryonic fibroblasts cells (NIH 3T3). Their interesting aspects of the
anticancer drug mechanisms underlying the cytotoxic response were probed using
FACSverse analysis.

Chapter 1 begins with an introduction of DNA and BSA structures, followed by a general review of the characteristics of metal complex interactions useful in probing DNA and protein. Also included is a brief overview of copper-based anticancer agents. This chapter also discusses the purpose and scope of the current investigation.

Chapter 2 are described the origin of the chemicals used, the purification of solvents, the preparation of stock solutions of DNA samples, and the various spectral, and electrochemical techniques employed in the present investigation.

Studies on the interaction of mononuclear mixed-ligand copper(II) complexes with CT DNA and BSA, DNA cleavage, and cytotoxic activity of the complexes are described in **Chapter 3**. Three mononuclear copper(II) complexes of the type [Cu(bba)(bpy/phen/dpa)](ClO₄)₂ (1-3), where bba (*N*,*N*-bis(benzimidazol-2-ylmethyl)-amine) and bpy (2,2'-bipyridine, 1) or phen (1,10-phenanthroline, 2) or dpa (2,2'-dipyridylamine, 3), have been isolated. The coordination geometry of 1 around

copper(II) is square pyramidal. The electronic absorption (639-667 nm) and EPR spectral parameters (g_{\parallel} , ~2.25; A_{\parallel} , 181-186 × 10⁻⁴ cm⁻¹; $g_{\parallel}/A_{\parallel}$, 122-134 cm) reveal that 1-3 possesses a square pyramidal geometry with CuN₅ chromophore. Different spectral and electrochemical measurements demonstrate partial intercalative interaction of 1-3 to CT DNA viz. (i) via planar phen moiety in 2 (strong) and (ii) via bzim moiety in 1 and 3 (weak). Complexes strongly quench the intrinsic fluorescence of BSA through a static quenching procedure by forming BSA-(1/2/3) adducts, which are stabilized by hydrophobic interactions. The number of binding sites and binding constants were calculated. The energy transfer from BSA to Cu(II) complexes occurs with high probability. Notably, 1-3 exhibit more effective pUC 19 DNA cleavage in the presence of H₂O₂. Complexes 2 and 1 show remarkable cytotoxicity (IC₅₀: 2, 2.17; 1, 8.33 µM) against human cervical carcinoma cells (HeLa) and are more potent than cisplatin (IC₅₀, 16.40 μM) while **3** exhibits less cytotoxicity (IC₅₀, 20.82 μM). The DNA binding propensity, cleavage ability, and cytotoxicity follow the order 2 > 1 > 3. Interestingly, they are non-toxic to healthy cells. Overall, these findings show that 2 is a potential chemotherapeutic scaffold with well-defined biological interactions and activity derived from the redox-active copper center.

In **Chapter 4** are described the mixed-ligand copper(II) complexes of the type $[Cu(L)(phen)](ClO_4)_2$ (1, 2), L is (6-methylpyridin-2-ylmethylene)-(pyridin-2-ylmethyl)-amine (L1) and (6-methylpyridin-2-ylmethy-lene)-(pyridin-2-ylethyl)amine (L2) have been isolated and characterized by elemental analysis, electronic absorption, ESI-MS, and EPR spectral techniques and the electrochemical method. The single crystal X-ray structure of $[Cu(L2)(phen)](ClO_4)_2$ possesses a distorted square pyramidal coordination

geometry. The complexes 1 and 2 bind to calf thymus (CT) DNA through a partial intercalative mode of DNA interaction, according to absorption spectral titration, EthBr displacement assay, and circular dichroic spectral and electrochemical investigations. Both complexes cleave DNA in the absence of an activator, but in the presence of hydrogen peroxide or ascorbic acid as an activator, they show oxidative cleavage of supercoiled (SC) plasmid DNA. It is interesting that 1 and 2 degrade SC DNA into nicked circular (NC) DNA at 20-30 µM concentrations, indicating that they are effective chemical nucleases. With BSA protein, complexes 1 and 2 go through a static mode of quenching. They are notable for exhibiting cytotoxicity against the human cervical carcinoma (HeLa) cell line with a potency greater than the widely used drug cisplatin, demonstrating that they have the potential to be effective anticancer drugs. They are non-toxic to normal mouse embryonic fibroblasts cells (NIH 3T3), signifying that they are selective in their killing of cancer cells. As a result, this family of complexes has the potential to be a promising alternative to platinum-based anticancer drugs, and more mechanistic and cellular uptake studies are needed to assess the enhanced efficacy in killing cancer cells.

The redox-active copper(II) complex with asymmetric bidentate ligand (pyridyl-triazine) has been prepared and characterized by analytical and spectral methods. The DNA Binding, *in vitro* cytotoxicity, and anticancer drug mechanism of bis-copper(II) complex, are dealt with in **Chapter 5**. Mononuclear bis-copper(II) complex, [Cu(dppt)₂(H₂O)₂](ClO₄)₂ (1), where dppt is bidentate N_{tz}N_{py} donor asymmetric ligand has been isolated. The X-ray crystal structure of 1 possesses a CuN₄O₂ chromophore with elongated octahedral geometry. The electronic and EPR spectral

properties demonstrate that the solvent molecules strongly interacted in the axial position thereby weakening the CuN_4 coordination plane. Absorption and emission spectral and electrochemical measurements clearly show the partial intercalative binding of 1 to calf thymus (CT) DNA. Remarkably, it exhibits potent cytotoxicity (IC₅₀, 3.73 μ M) against human cervical carcinoma cells (HeLa), which is 4.5 times better than cisplatin and is non-toxic (IC₅₀, >500 μ M) to normal mouse embryonic fibroblasts cells (NIH 3T3). It blocks the cell cycle progression of HeLa cells in the G1 phase. FACSverse analysis of 1 is suggestive of ROS (reactive oxygen species) generation and induces apoptotic cell death in HeLa cells. The current lead complex is a novel therapeutic agent for cervical cancer treatment that also supports more research into non-platinum anticancer agents. It targets the mitochondria of cancer cells and promotes apoptosis through a process involving the formation of ROS.

Thus in this thesis are described several bis- and mixed-ligand copper(II) complexes containing bi- and tridentate ligands. The structures of the complexes have been determined and the electronic properties of the complexes studied by employing several physical methods. It is disclosed that the present copper(II) complexes have the potential to be developed as an anticancer drug for treating selectively cervical cancer. A few of these complexes have significant potential as substructures for designing newer metal-based anticancer drugs.

In summary, the copper(II) complexes can be taken up in cancer cells and can be transported by BSA in the body. There, the complexes can interact with DNA, this is the probable cause of their ultimate cytotoxic activity.

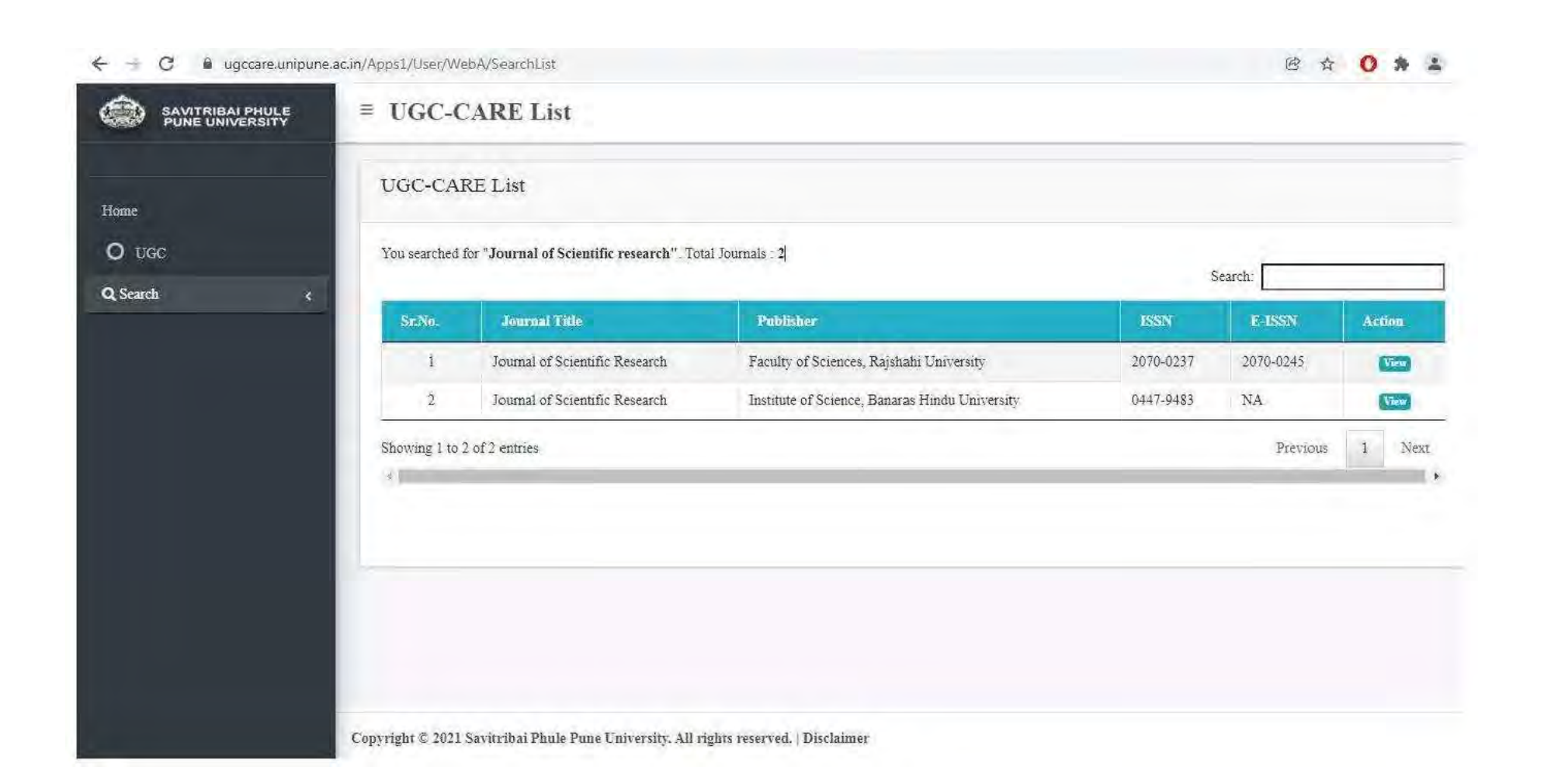
Future work

Although the work in this thesis much has been learned about the design principles and activities through, this new knowledge brings new possibilities of designing anticancer properties of different metal ions such as zinc, ruthenium, iron, nickel, and gold, and also efforts have been focused on other forms of cancers like breast, prostate and testicular cancers, etc. The use of technologies like "Click" chemistry could make it easier to produce ligands and complexes that bind to DNA in many orientations. All of these would be intriguing potential for moving this research ahead to develop more drugs that could be given directly to the site of a specific tumor.

List of Publications

List of Articles Published/Communicated as in the UGC Website

- 1. **J. Manivel**, S. Sangeetha, M. Murali, "DNA and BSA Interaction, DNA Cleavage and *In Vitro* Cytotoxicity of Copper(II) Complexes: [Cu(bba)(phen)](ClO₄)₂ is Promising Chemotherapeutic Scaffold" J. Sci. Res. 12 (2020) 111-133.
- 2. **J. Manivel**, S. Sangeetha, M. Murali, "DNA Binding, In vitro Cytotoxicity and Anticancer Drug Mechanism of Copper(II) Complex Containing Pyridyl-Triazine Ligand", J. Adv. Sci. Res. 12 (2021) 166-175.
- 3. M. Murali, J. Manivel, S. Sangeetha, "Superior Cytotoxic Copper(II) Complexes of Pyridylaldimines and 1,10-Phennathroline: DNA Binding, BSA Interaction and Potent DNA Cleavage Activity", Communicated to J. Biol. Inorg. Chem.



UGC-CARE List

You searched for "chemistry". Total Journals: 39

			Search:		
Sr.No.	Jeurnal Title	Publisher	ISSN	E- ISSN	Action
21	Journal of Applied Biology and Biotechnology	Open Science Publishers	2455- 7005	2347- 212X	Discontinued from Sept. 2019
22	Journal of Applied Geochemistry	Indian Society of Applied Geochemists	0972- 1967	NA	NTerm
23	Journal of Nanostructure in Chemistry	Springer	2008- 9244	2193- 8865	Indexed in Web o
24	Journal of Proteins and Proteomics	Proteomics Society of India	0975- 8151	2524- 4663	(Viet)
25	Journal of Scientific Research	Faculty of Sciences, Rajshahi University	2070- 0237	2070- 0245	Vice
26	Journal of Scientific Research	Institute of Science, Banaras Hindu University	0447- 9483	NA	61pm
27	Journal of Scientific Temper	National Institute of Science Communication and Information Resources	2278- 2788	2278- 2796	5000
28	Journal of Self- Assembly and Molecular Electronics	River Publishers	2245- 4551	2245- 8824	View
29	Journal of Stress Physiology and Biochemistry	Siberian Institute of Plant Physiology and Biochemistry	NA	1997- 0838	(VIew)
30	Journal of Taibah University for Science	Elsevier	NA	1658- 3655	Indexed in Web o

Showing 21 to 30 of 39 entries

Previous 1 2 3 4 Next

Journal Details

Journal Title (in English Language)	Journal of Scientific Research		
Publication Language	English		
Publisher	Faculty of Sciences, Rajshahi University		
ISSN	2070-0237		
E-ISSN	2070-0245		
Discipline	Science		
Subject	Physics and Astronomy (all), Chemistry (all), Mathematics (all)		
Focus Subject	General Physics and Astronomy, General Chemistry, General Mathematics		



Available Online

JOURNAL OF SCIENTIFIC RESEARCH

J. Sci. Res. 12 (1), 111-133 (2020)

www.banglajol.info/index.php/JSR

DNA and BSA Interaction, DNA Cleavage and *In Vitro* Cytotoxicity of Copper(II) Complexes: [Cu(bba)(phen)](ClO₄)₂ is Promising Chemotherapeutic Scaffold

J. Manivel¹, S. Sangeetha^{1,2}, M. Murali^{1*}

¹Coordination and Bioinorganic Chemistry Research Laboratory, Department of Chemistry National College (Autonomous), Tiruchirappalli 620 001Tamil Nadu, India

²Department of Chemistry, Tamilavel Umamaheswaranar Karanthai Arts College, Thanjavur 613 002 Tamil Nadu, India

Received 22 August 2019, accepted in final revised form 18 November 2019

Abstract

Three mononuclear copper(II) complexes of the type [Cu(bba)(bpy/phen/dpa)](ClO₄)₂ (1-3), where bba (N,N-bis(benzimidazol-2-ylmethyl)amine) and bpy (2,2'-bipyridine, 1) or phen (1,10-phenanthroline, 2) or dpa (2,2'-dipyridylamine, 3), have been isolated. The coordination geometry of 1 around copper(II) is square pyramidal. The electronic absorption (639-667 nm) and EPR spectral parameters $(g_{\parallel}, \sim 2.25; A_{\parallel}, 181-186 \times 10^{-4} \text{ cm}^{-1}; g_{\parallel}/A_{\parallel},$ 122-134 cm) reveal that 1-3 possesses a square pyramidal geometry with CuN₅ chromophore. Different spectral and electrochemical measurements clearly demonstrate partial intercalative interaction of 1-3 to CT DNA. Complexes strongly quench the intrinsic fluorescence of BSA through a static quenching procedure by forming BSA-(1/2/3) adducts, which are stabilized by hydrophobic interactions. The number of binding sites and binding constants were calculated. The energy transfer from BSA to Cu(II) complexes occurs with high probability. Notably, 1-3 exhibit more effective pUC 19 DNA cleavage in the presence of H_2O_2 . Complexes 2 and 1 show remarkable cytotoxicity (IC₅₀: 2, 2.17; 1, 8.33 μM) against human cervical carcinoma cells (HeLa) and more potent than cisplatin (IC₅₀, 16.40 μM) while 3 exhibits less cytotoxicity (IC₅₀, 20.82 μM). The DNA binding propensity, cleavage ability and cytotoxicity follow the order 2>1>3. Interestingly, they are non-toxic to healthy cells.

Keywords: Copper(II) complexes; Partial intercalation; Static quenching; DNA cleavage; Cytotoxicity.

1. Introduction

The serendipitous discovery of cisplatin [1] has revolutionized the cancer treatment; however, side-effects associated with the drug restrict its wider use [2]. Copper(II) complexes are regarded as promising and have attracted considerable attention owing to their capability of interacting directly with DNA and BSA [3,4]. Many studies reveal that

^{*}Corresponding author: ma66mu@gmail.com

DNA is the primary intracellular target of anticancer drugs, since the interaction between small molecules and DNA able to cause DNA damage, block DNA synthesis in cancer cells [5-8]. Therefore, under physiological conditions, metal complexes that possess efficient DNA binding and cleavage are regarded as potential candidates for use as therapeutic agents in medicinal applications and for genomic research [9-12]. On the other hand, a vast majority of cytotoxic metal-containing compounds are administered intravenously, special consideration should be given to interactions of the metal drug with macromolecular blood components, which can then be taken up by and accumulate in tumor tissue. In this context, binding toward serum proteins, like albumin or transferrin that may perform a transport function for a metal. Such interactions determine the overall drug distribution and excretion and differences in efficacy, activity, and toxicity [13,14].

Benzimidazole moiety is structurally related to purine bases and is found in a variety of naturally occurring compounds such as vitamin B_{12} . Benzimidazole derivatives display a wide variety of pharmacological properties including antitumor activity [15] and inhibition of nucleic acid synthesis [16]. Transition metal complexes consist of benzimidazole ligands act as cytotoxic [17,18], antiviral [18] and antiamoebic [19] agents. Moreover, ruthenium(I) [20] and zinc(II) [21] complexes of 2,6-bis(benzimidazol-2-yl)pyridine have DNA cleaving properties. Copper(II) complexes with benzimidazole-derived bidentate chelating ligands show most active cytotoxic activity [22] with different human tumor cell lines. There are also many examples in the literature of copper complexes of ligands containing α -diimino (-N=C-C=N-) moiety such as phenanthroline that can induce apoptosis [23] and 2-(4'-thiazolyl)benzimidazole that display antimicrobial activity [24]. In particular, the non-planar nature of benzimidazole ligands, their flexibility, and bulkiness affect the kinetics and cytotoxic properties of the corresponding metal complexes. In addition, benzimidazole-based ligands can possess N-H moiety which can facilitate DNA cleavage in cancer cells [25].

Thus, we have synthesized a series of mixed-ligand copper(II) complexes of the type $[Cu(bba)(diimine)](ClO_4)_2$ [where bba is N,N-bis(benzimidazol-2-ylmethyl)amine and diimine is 2,2'-bipyridine (1, bpy) or 1,10-phenanthroline (2, phen) or 2,2'-dipyridylamine (3, dpa)] and investigated their interaction with calf thymus (CT) DNA and bovine serum albumin (BSA), DNA cleavage activity and *in vitro* cytotoxic properties against human cervical carcinoma cell line (HeLa) and normal mouse embryonic fibroblasts cell line (NIH 3T3).

2. Materials and Methods

Copper(II) perchlorate hexahydrate (Sigma Aldrich), 2,2'-bipyridine, 1,10-phenanthroline (Merck), 2,2'-dipyridylamine (Sigma Aldrich) and *Tetra-N*-butylammonium bromide (Thomas Baker) were used as received. The commercial solvents were distilled and then used for the preparation of ligand and complexes. The ligand *N,N*-bis(benzimidazol-2-ylmethyl)amine (bba) was synthesized according to the published procedure [26,27]. Calf thymus (CT) DNA and bovine serum albumin (BSA) were purchased from Sigma Aldrich and stored at -20 °C. Ultrapure MilliQ water (18.2 m Ω) was used for all the experiments.

The elemental analyses (C, H, N) were carried out using a Perkin-Elmer 2400 series II analyzer. The electrical conductivity was obtained with a Systronic 305 conductivity bridge, using 1×10⁻³ M solution of the complex in dimethylformamide (DMF). Finnigan MAT TSQ-700 equipped with a custom-made electrospray interface (ESI) was used to perform mass spectrometry experiments. Spectra were collected by constant fusion of the analyte dissolved in DMF. Magnetic susceptibility value at 298 K was obtained using Model 300 Lewis-coil-force magnetometer of George Associate Inc. (Berkley, USA) make. The electronic spectra were recorded using Perkin-Elmer Lambda 35 UV-Visible spectrophotometer. The room temperature (RT) solid and liquid-nitrogen temperature (LNT) DMF solution electron paramagnetic resonance spectra were obtained on a JEOL JES-FA200 ESR spectrometer. All fluorescence measurements were performed using a Shimadzu RF-5301PC spectrofluorophotometer equipped with a thermostatic bath and a 10 mm quartz cuvette. The pH was potentiometrically measured using an Elico LI 120 pH meter equipped with a combined glass electrode. Cyclic voltammetry (CV) and differential pulse voltammetry (DPV) on glassy carbon disc electrode were performed in a CHI 620C electrochemical analyzer at 27 ± 0.5 °C. The working electrode was a glassy carbon disk (0.0707 cm²), the reference electrode a saturated calomel electrode and the counter electrode a platinum wire. In DMF solution 0.1 M Tetra-N-butylammonium perchlorate and in buffer solution (pH 7.1) 2% DMF - 5 mMTris-HCl/50 mMNaCl buffer was used as supporting electrolytes. Solutions were deoxygenated by purging with nitrogen gas for 15 min prior to measurements; during measurements, a stream of N2 gas was passed over them. The redox potential $E_{1/2}$ was calculated from the anodic (E_{pa}) and cathodic (E_{pc}) peak potentials of CV traces as (E_{pa} + E_{pc})/2 and as E_p + Δ E/2 (Δ E is the pulse height) from the peak potential (E_{pa}) of DPV response.

2.1. Synthesis of copper(II) complexes

[Cu(bba)(bpy)](ClO₄)₂ (1): The complex 1 was prepared by adding a solution of copper(II) perchlorate hexahydrate (0.370 g, 1 mmol) in methanol (10 mL) to a 15 mL methanolic solution of 2,2'-bipyridine (bpy; 0.156 g, 1 mmol) and N,N-bis(benzimidazol-2-ylmethyl)amine (bba; 0.277 g, 1 mmol) and then stirring the solution for 2 h. The blue precipitate obtained was collected by suction filtration, washed with small amounts of cold methanol and diethyl ether and then dried in vacuum over P_4O_{10} . Yield: 0.45 g (65%). Λ_M (Ω^{-1} cm² mol⁻¹) in DMF at 25 °C: 160. μ_{eff} (solid, 298 K): 1.81 μ_B . ESI-MS (CH₃CN) displays a peak at m/z 248.35 [Cu(bba)(bpy)]²⁺. Anal. Calc. for $C_{26}H_{23}N_7O_8Cl_2Cu$. C, 44.87; H, 3.33; N, 14.09. Found: C, 44.82; H, 3.37; N, 14.14%. FT-IR (KBr, cm⁻¹) selected bands: 1528 v_{bzim} (C=N), 1638 v_{bzim} (-C=N-C=C-), 1040, 1094 v_{bzim} (C-N), 3245 v_{amine} (N-H), 1556 v_{py} (C=N), 1091, 625 v(ClO₄). Electronic spectrum in 2% DMF - 5 mM Tris-HCl/50 mM NaCl buffer solution, λ_{max}/mm (ε_{max}/M^{-1} cm⁻¹): 271 (22680), 278 (24600), 311 sh, 635 (90). Molecular orbital coefficients such as α^2 (0.83), β^2 (0.70) and γ^2 (0.58) and orbital reduction factors viz. K_{\parallel} (0.76) and K_{\perp} (0.69).

The blue-colored crystals of **1** suitable for X-ray diffraction studies were obtained by dissolving the complex in DMF:MeCN mixture (1:5 v/v) and allowing it to crystallize at 5 °C for 12 days.

[Cu(bba)(phen)](ClO₄)₂ (**2**): The complex **2** was prepared by adopting the procedure used for obtaining **1** by using 1,10-phenanthroline (phen; 0.180 g, 1 mmol) instead of bpy. Yield: 0.43 g (60%). $\Lambda_{\rm M}$ (Ω^{-1} cm² mol⁻¹) in DMF at 25 °C: 161. $\mu_{\rm eff}$ (solid, 298 K): 1.79 $\mu_{\rm B}$. ESI-MS (CH₃CN) displays a peak at m/z 260.43 [Cu(bba)(phen)]²⁺. Anal. Calc. for C₂₈H₂₃N₇O₈Cl₂Cu. C, 46.71; H, 3.22; N, 13.62. Found: C, 46.79; H, 3.24; N, 13.69%. FT-IR (KBr, cm⁻¹) selected bands: 1546 $\nu_{\rm bzim}$ (C=N), 1623 $\nu_{\rm bzim}$ (-C=N-C=C-), 1044, 1081 $\nu_{\rm bzim}$ (C-N), 3241 $\nu_{\rm amine}$ (N-H), 1543 $\nu_{\rm py}$ (C=N), 1084, 623 ν (ClO₄). Electronic spectrum in 2% DMF - 5 mM Tris-HCl/50 mM NaCl buffer solution, $\lambda_{\rm max}$ /nm ($\varepsilon_{\rm max}$ /M⁻¹ cm⁻¹): 271 (33440), 278 (35900), 311 sh, 638 (130). Molecular orbital coefficients such as α^2 (0.82), β^2 (0.72) and γ^2 (0.60) and orbital reduction factors viz. K_{\parallel} (0.77) and K_{\perp} (0.70).

[Cu(bba)(dpa)](ClO₄)₂ (**3**): The complex **3** was prepared by adopting the procedure used for obtaining **1** by using 2,2'-dipyridylamine (dpa; 0.171 g, 1 mmol) instead of bpy. Yield: 0.47 g (66%). $\Lambda_{\rm M}$ (Ω^{-1} cm² mol⁻¹) in DMF at 25 °C: 165. $\mu_{\rm eff}$ (solid, 298 K): 1.83 $\mu_{\rm B}$. ESI-MS (CH₃CN) displays a peak at m/z 255.92 [Cu(bba)(dpa)]²⁺. Anal. Calc. for C₂₆H₂₄N₈O₈Cl₂Cu. C, 43.92; H, 3.40; N, 15.76. Found: C, 43.98; H, 3.49; N, 15.88%. FT-IR (KBr, cm⁻¹) selected bands: 1534 $\nu_{\rm bzim}$ (C=N), 1632 $\nu_{\rm bzim}$ (-C=N-C=C-), 1042, 1090 $\nu_{\rm bzim}$ (C-N), 3218 $\nu_{\rm amine}$ (N-H), 1549 $\nu_{\rm py}$ (C=N), 1105, 621 ν (ClO₄). Electronic spectrum in 2% DMF - 5 mM Tris-HCl/50 mM NaCl buffer solution, $\lambda_{\rm max}$ /nm ($\varepsilon_{\rm max}$ /M⁻¹ cm⁻¹): 254 (26930), 271 (25480), 312 (15050), 658 (125). Molecular orbital coefficients such as α^2 (0.81), β^2 (0.67) and γ^2 (0.52) and orbital reduction factors viz. K_{\parallel} (0.73) and K_{\perp} (0.65).

2.2. X-ray crystallography

The crystal of 1 with dimensions $0.42\times0.28\times0.12~\text{mm}^3$ was selected under the polarizing microscope and then mounted on the tip of glass fiber and cemented using epoxy resin. Intensity data for 1 was collected using Mo-K $_{\alpha}$ ($\lambda=0.71073~\text{Å}$) radiation on a Bruker SMART Apex diffractometer equipped with a CCD area detector at 296 K. The SMART program [28] was used for collecting frames of data, indexing the reflections, and determining the lattice parameters. The data integration and reduction were processed with SAINT [29] software. Empirical absorption correction was applied to the collected reflections with SADABS [30]. The structure was solved by direct methods using SHELXS-97 [31-33] and was refined on F² by the full-matrix least-squares technique using the SHELXL-97 [31-33] program package. All the non-hydrogen atoms in 1 were refined anisotropically until convergence is reached. Hydrogen atoms attached to the ligand moieties were stereochemically fixed. The crystallographic data and details of data collection for 1 are given in Table 1.

empirical formula	C ₂₆ H ₂₃ Cl ₂ CuN ₇ O ₈	Formula weight	695.95
crystal system	triclinic	space group	P-1
a, Å	9.120(3)	b, Å	10.506(4)
c, Å	16.767(6)	α, deg	83.346(6)
β, deg	74.488(6)	γ, deg	64.483(5)
V, Å	1396.9(9)	Z	2
λ, Å (Mo Kα)	0.71073	D _{calc} , g cm ⁻³	1.655
goodness-of-fit on F2	1.054	θ for data collection (deg)	1.26-25.00
final R indices $[I > 2\sigma(I)]$	$R_1 = 0.0696$, $wR_2 = 0.1656$	$R_1^{\ a}$	0.0871
$\mathrm{wR_2}^\mathrm{a}$	0.1776		

Table 1. Crystal data and structure refinement details for [Cu(bba)(bpy)](ClO₄)₂ (1).

2.3. DNA binding experiments

Solutions of DNA in the 2% DMF - 5 mM TrisHCl/50 mM NaCl buffer gave a ratio of UV absorbances at 260 and 280 nm, A_{260}/A_{280} , of 1.9, representing that the DNA was free from protein [34]. Concentrated stock solutions of DNA (13.5 mol dm³) were prepared in the buffer and sonicated for 25 cycles, where each cycle consisted of 30 s with 1 min intervals. After 1:100 dilutions, the UV absorbance at 260 nm (ϵ_{260} , 6600 dm³ mol⁻¹ cm⁻¹) was used to estimate the concentration of DNA in nucleotide phosphate (NP). Stock solutions of DNA were kept at 4 °C and used within 4 days. Concentrated stock solutions of copper(II) complexes were prepared by dissolving calculated amounts of the complexes in respective amounts of DMF and diluted suitably with the corresponding buffer to the required concentrations for all experiments. For absorption and emission spectral experiments, the DNA solutions were pretreated with solutions of copper(II) complex to ensure no change in concentrations of the copper(II) complex.

Absorption spectral titration experiments were performed by maintaining a constant concentration of the complex and varying the nucleic acid concentration. This was achieved by dissolving an appropriate amount of the metal complex and DNA stock solutions while maintaining the total volume constant (1 mL). This results in a series of solutions with varying concentrations of DNA but with a constant concentration of the complex. The absorbance (A) of the UV band of the complex was recorded after successive additions of CT DNA.

Emission intensity measurements were carried out using a Shimadzu RF-5301PC spectrofluorophotometer. The 2% DMF - 5 mM Tris-HCl/50 mM NaCl buffer was used as a blank to make preliminary adjustments. Before measurements, the excitation wavelength was fixed and the emission range was adjusted. DNA was pretreated with ethidium bromide in the ratio [NP]: [EthBr] = 1:1 for 30 min at 27 °C. The metal complex was then added to this mixture and their effect on the emission intensity was measured.

 $^{^{}a}R_{1}=\Sigma \; ||F_{o}|-|F_{c}||/\Sigma |F_{o}|, \; wR_{2}=\{\Sigma w[(F_{o}^{\;2}-F_{c}^{\;2})^{2}/\Sigma w[(F_{o}^{\;2})^{2}]\}^{1/2}.$

2.4. Protein binding experiments

The UV-Visible absorption spectra of 1.0 μ M free BSA as well as BSA/copper(II) complex (equal molar ratio) in 0.5 M phosphate buffer of pH 7.4 were recorded from 200-500 nm

Quantitative analyses of the interaction between copper(II) complex and BSA was performed by fluorimetric titration (0.5 M phosphate buffer, pH 7.4). A 3.0 mL portion of the aqueous solution of BSA ($1.0 \times 10^{-6} \text{mol L}^{-1}$) was titrated by successive additions of complex (to give a final concentration of $8.0 \times 10^{-6} \text{mol L}^{-1}$). Titrations were done manually by using an Eppendorf micropipette. For every addition, the mixture solution was shaken and allowed to stand for 20 min at the corresponding temperature (300 and 310 K), and then the fluorescence intensities were measured with an excitation wavelength of 280 nm and emission wavelengths in the interval 290-500 nm. No correction for inner filter effect was applied since copper(II) complex represented very low absorbance (less than 0.1) at excitation and emission wavelengths. The excitation and emission slit width (each 5.0 nm), scan rate (fast) were constantly maintained for all the experiments. In the meantime, the synchronous fluorescence intensity of the mixture solution was measured at $\Delta\lambda = 15$ nm and $\Delta\lambda = 60$ nm, respectively.

2.5. DNA cleavage experiments

The interaction of complexes with supercoiled pUC19 DNA was monitored using agarose gel electrophoresis. In reactions using supercoiled pUC19 DNA, the plasmid DNA (SC form, 20 µM) in 2% DMF - 5 mMTris-HCl/50 mMNaCl buffer solution at pH 7.2 was treated with copper complexes in the same buffer. In each experiment supercoiled pUC19 DNA was treated with different concentrations of complexes and also the cleavage of plasmid DNA in the absence and presence of the activating agent H₂O₂ was monitored using agarose gel electrophoresis. The samples were then incubated for 2 h at 37 °C and analyzed for the cleaved products using gel electrophoresis as discussed below. A loading buffer containing 22% bromophenol blue, 0.22% xylene cyanol and 30% glycerol (3 μL) was added and electrophoresis was performed at 40 V for 6 h in Tris-acetate-EDTA (TAE) buffer (40 mM Tris base, 20 mM acetic acid, 1 mM EDTA) using 1% agarose gel containing 1.0 µg mL⁻¹ EthBr. The gels were viewed in a Gel doc system and photographed using a CCD camera (Alpha Innotech Corporation). The cleavage efficiency was measured by determining the ability of complexes to convert the supercoiled DNA (SC) to nicked circular form (NC) and linear form (LC). In order to identify the reactive oxygen species (ROS) involved in the cleavage reaction the radical scavengers such as hydroxyl radical (DMSO, 6 μL), singlet oxygen (NaN₃, 100 μM), superoxide (SOD, 4 unit), and H₂O₂ (catalase, 6 units) were introduced.

2.6. Cell line

The human cervical cancer cell line (HeLa) was acquired from National Centre for Cell Science (NCCS), Pune. It was grown in Eagles Minimum Essential Medium containing 10% fetal bovine serum (FBS). The cells were preserved at 37 °C, 5% CO₂, 95% air and 100% relative humidity. Maintenance cultures were channelized weekly and the culture medium was altered twice a week.

2.7. Cell culture

To make single cell suspensions, the monolayer cells were detached with trypsinethylenediaminetetraacetic acid (EDTA) and viable cells were counted using a hemocytometer. They were diluted with medium containing 5% FBS to give a final density of 1×10^5 cells/mL. The cell suspension of one hundred microlitres per well were seeded into 96-well plates at a plating density of 10,000 cells/well. They were incubated to allow for cell attachment at 37 °C, 5% CO₂, 95% air and 100% relative humidity. The cells were treated with serial concentrations of the test samples after 24 h. They were dissolved in dimethylsulfoxide (DMSO) and an aliquot of the sample solution was diluted twice to the desired final maximum test concentration with serum-free medium. Also, four serial dilutions were made to give a total of five sample concentrations. Aliquots of 100 μ L of different sample dilutions were added to the suitable wells already containing 100 μ L of the medium, resulting in the required final sample concentrations. The plates were incubated followed by sample addition at 37 °C, 5% CO₂, 95% air and 100% relative humidity for an additional 48 h. The medium alone was served as control and triplicate was maintained for all concentrations.

2.8. Cell viability assay

The cell viability was carried out by using the MTT assay. Complex 1-3 in the concentration range 0.25-100 μ M dissolved in 2% DMF: 5 mMTris-HCl/50 mMNaCl buffer at pH 7.1 were added to the wells 24 h after seeding of 1×10^5 cells per well in 100 μ L of fresh culture medium. After 48 h, 15 μ L of 3-[4,5-dimethylthiazol-2-yl]2,5-diphenyltetrazolium bromide (MTT, 5 mg/mL) in phosphate buffered saline (PBS) was added to each well and incubated at 37 °C for 4 h. The formed formazan crystals were solubilized in 100 μ L of DMSO after the medium with MTT was flicked off. The microplate reader was used to measure the absorbance at 570 nm. Data were collected for three replicates each and the percentage cell viability and percentage cell inhibition was calculated using the following formulas:

% Cell viability = $[A_s]$ / $[A_c]$ \times 100 (where A_s is absorbance of sample and A_c is absorbance of control).

% Cell inhibition = $[100 - ([A_s] / [A_c])] \times 100$

Nonlinear regression graph was plotted between % Cell inhibition and Log concentration and IC_{50} was calculated using GraphPad Prism software.

3. Results and Discussion

3.1. Synthesis and general properties

The mixed ligand copper(II) complexes have been isolated in good yield (60-66%) by the reaction of bba and bpy or phen or dpa and copper(II) perchlorate hexahydrate in methanol at room temperature. All the complexes have been obtained as blue crystalline solids. Based on the elemental analysis the complexes were formulated as [(Cu(bba)(diimine)](ClO₄)₂ and the stoichiometry of 1 was confirmed by single crystal Xray structure determination. They show strong infrared spectral bands in the range 1528-1546 cm⁻¹ and 1623-1638 cm⁻¹ are assigned to $v_{bzim}(C=N)$ and $v_{bzim}(-C=N-C=C-)$ stretching vibrations respectively of the benzimidazole ring. The very strong band (1040-1048 cm⁻¹) and a medium band (1081-1094 cm⁻¹) are assigned to v_{bzim} (C-N) stretching vibrations. The band in the range 3218-3245 cm⁻¹ is due to $v_{amine}(N-H)$ stretching mode of bba ligand while the sharp and strong band (1543-1556 cm⁻¹) is assigned to $v_{pv}(C=N)$ stretching vibration of diimine ligands. The shift in the vibrational bands to lower energy implies the coordination of amine, benzimidazole, and pyridine nitrogens. A broad intense band (1084-1105 cm⁻¹) and a strong sharp band (623-625 cm⁻¹) are observed, which are characteristics of non-coordinated perchlorate ions. The μ_{eff} values (1.79-1.83 μB) are typical of paramagnetic, mononuclear copper(II) species with d⁹ configuration [35]. The ESI-MS data in MeCN (m/z [Cu(bba)(diimine)]²⁺: 1, 248.35; 2, 260.43; 3, 255.92) reveal that the complexes maintain their identity in solution and this is substantiated by values of molar conductivity in DMF ($\Lambda_{\rm M}/\Omega^{-1}~{\rm cm}^2~{\rm mol}^{-1}$: 160-165), characteristics of 1:2 electrolytes [36].

3.2. Description of the crystal structure

The ORTEP view (Fig. 1a) of **1** shows a discrete monomeric copper(II) complex dication and two perchlorate anions. The selected bond distances and bond angles relevant to the copper coordination sphere are given in Table 2.

Table 2.Selected interatomic distances [Å] and bond angles [°] for [Cu(bba)(bpy)](ClO₄)₂ (1).

Cu(1)-N(1)	1.997(4)	Cu(1)-N(2)	1.994(4)	Cu(1)-N(3)	1.987(4)
Cu(1)-N(4)	1.985(4)	Cu(1)-N(7)	2.412(5)		
N(4)-Cu(1)-N(3)	87.03(17)	N(4)- $Cu(1)$ - $N(2)$	170.66(16)	N(3)-Cu(1)-N(2)	96.22(17)
N(4)-Cu(1)-N(1)	95.15(17)	N(3)-Cu(1)-N(1)	176.82(16)	N(2)-Cu(1)-N(1)	81.28(17)
N(4)-Cu(1)-N(7)	77.50(17)	N(3)-Cu(1)-N(7)	78.90(18)	N(2)-Cu(1)-N(7)	111.69(17)
N(1)-Cu(1)-N(7)	103.82(17)				

The value of the structural index [37] τ of 0.10 reveals that the coordination geometry around copper(II) is best described as square pyramidal [38,39] with no significant distortion toward trigonalbipyramidal. The tridentate ligand bba is bound facially to Cu(II) with the two bzim nitrogens (Cu-N_{bzim}, 1.987(4), 1.985(4) Å) located in the basal plane and the two imine nitrogens of bpy (Cu-N_{imine}, 1.997(4), 1.994(4) Å) occupying the remaining corners of the basal plane. The strongly bound bpynitrogens occupy the equatorial sites around Cu(II) with the sterically hindered N7 amine nitrogen atom of bba defaulting to the more weakly bound z-axial position (Cu(1)-N(7), 2.412(5) Å) [27]. The displacement of copper atom above the N1N2N3N4 plane is 0.094 Å illustrating the importance of the steric effect of the bulky bzim moieties. The Cu-N_{bzim} bond distances are similar to those observed for [Cu(bba)Cl₂] [40,41] and [Cu(bba)₂]²⁺ [27]. The axial Cu-N_{amine} bond is longer than the equatorial Cu-N_{bpy} bonds, which is expected of the presence of two electrons in the d_{z²} orbital of Cu(II).

Interestingly, the molecular packing of 1 show two different self-assembled molecular associations between different adjacent molecules, viz. interactions between the molecules I and II and III (Fig. 1b).

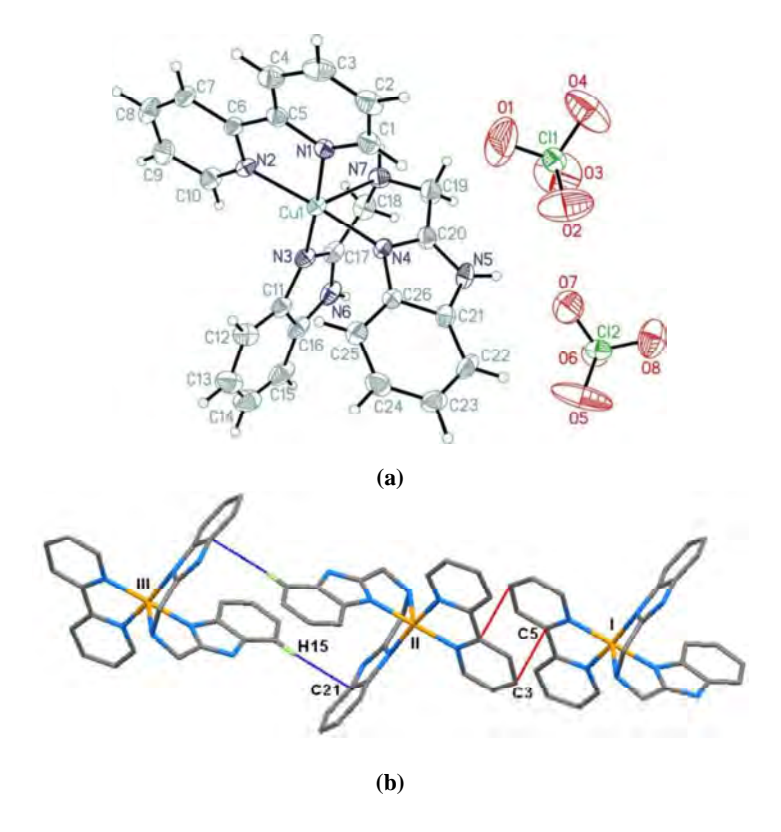


Fig. 1. (a) An ORTEP view of $[Cu(bba)(bpy)](ClO_4)_2$ **1** with atom numbering of complex and thermal ellipsoids at 40% probability. (b) Molecular packing viewed down the a-axis showing intermolecular interactions of $[Cu(bba)(bpy)]^{2+}$ (1) (Blue, C-H··· π ; Red, π ··· π stacking).

The noticeable features are the presence of (i) inter-pair π - π interactions between bpy ligands (I and II) and (ii) C-H··· π non-covalent interactions (II and III). The π - π stacking between C(3) of py and C(5) of py (C(3)···C(5), 3.393 Å) rings of adjacent coordinated bpy ligands giving an average spacing of $C_g(p)$ ···C $_g(p)$ ($C_g(p)$, the centroid of the pyridine ring; 3.546 Å). Such an interaction is expected to stabilize the complex in the solid state [42]. Also, benzene rings of benzimidazole moiety of neighboring molecules display an attractive C-H··· π non-covalent interaction. It gives C(15)-H(15)···C(21) distance of 3.654 Å and the C(15)-H(15)···C $_g$ (benzene) distance of 3.856 Å and \angle C(15)-H(15)···C $_g$ (benzene) angle of 160.02° (C_g (benzene) is the centroid of the benzene in benzimidazole moiety) showing the closure approach and orientation of the neighbouring molecules [43]. Thus, the separation of Cu···Cu between the adjacent molecules is 8.15 (I and II) and 10.69 Å (II and III).

3.3. Electronic and EPR spectral properties

The complexes (1-3) exhibit only one broad band (λ_{max} , 639-667 nm) in the visible region with very low ε_{max} value (70-120 M⁻¹ cm⁻¹), which is typical of a distorted square-based coordination geometry around copper(II). The strong absorption band is observed in the UV region (λ_{max} , 269-315 nm), which is attributing to the intraligand $\pi \rightarrow \pi^*$ transitions [44] from the coordinated diimines. The EPR spectra of 1-3 display one broad singlet (g_{iso} , 2.053-2.066) in the polycrystalline state at 298 K arising from dipolar broadening and enhanced spin-lattice relaxation. The frozen DMF solution EPR spectra of the complexes are axial $[g_{\parallel} > g_{\perp} > 2.0$; G = $[(g_{\parallel} - 2)/(g_{\perp} - 2)] = 4.9-5.1$] suggesting the presence of $d_{x^2-y^2}$ ground state in copper(II) located in square-based geometries [45]. A square-based CuN₄ chromophore is expected [46-48] to show a g_{\parallel} value of 2.200 and A_{\parallel} value in the range 180-200 × 10⁻⁴ cm⁻¹ and a tetrahedral distortion from square planar coordination geometry or axial interaction would increase both the ligand field band position (cf. above) and g_{\parallel} value and decrease the A_{\parallel} value [46-48]. So, the observed values of g_{\parallel} (~2.25) and A_{\parallel} $(181-186 \times 10^{-4} \text{ cm}^{-1})$ for 1-3 are consistent with the presence of a square-based CuN₄ chromophore with no significant distortion from planarity, as evident from the crystal structure of 1 (cf. above). This is supported by the values of $g_{\parallel}/A_{\parallel}$ quotient (122–124 cm) falls in the range of 105–135 cm [49]. Molecular orbital coefficients [50], α^2 (covalent inplane σ -bonding: 1, 0.83; 2, 0.82; 3, 0.81) and β^2 (covalent in-plane π -bonding; 1, 0.70; 2, 0.72; 3, 0.67) values show that there is a considerable interaction in the in-plane σbonding while the in-plane π -bonding is nearly covalent. For complexes 1-3, it is observed that $K_{\parallel} > K_{\perp}$ [51] (K_{\parallel} (1, 0.76; 2, 0.77; 3, 0.73) and K_{\perp} (1, 0.69; 2, 0.70; 3, 0.65) are orbital reduction factors), illustrating the significant out-of-plane π -bonding.

3.4. Electrochemical properties

The complexes are redox-active and show a one-electron quasi-reversible ($\Delta E_{\rm p}$: 1, 198; 2, 128; 3, 206 mV) cyclic voltammetric responses in DMF for the Cu(II)/Cu(I) couple ($E_{1/2}$: 1, -0.074; 2, -0.074; 3, -0.072 V vs SCE) with an $i_{\rm pa}/i_{\rm pc}$ ratio (1, 0.9; 2, 1.0; 3, 0.9) of

unity. Though the $E_{1/2}$ values are similar, the E_{pa} (1, -0.173; 2, -0.138; 3, -0.175 V) and E_{pc} (1, 0.025; 2, -0.010; 3, 0.031 V) values suggest the stability order for the copper(I) species as 2 (phen) >1 (bpy) >3 (dpa). A greater stabilization of the Cu(I) species for the phen complex is related to the planar phenyl moiety enhancing the π -acidity of the ligand. Notably, 2 shows very low ΔE_p value compared to 1 and 3, demonstrating the minimal structural reorganization between copper(II) and copper(I) species. It leads to a facile heterogeneous electron transfer [52] possibly due to the equatorial coordination of planar phen and bulky benzimidazoles of bba.

3.5. DNA binding studies

DNA is an important cellular target of many metallodrugs for the treatment of multiple pathologies including cancer. Thus, the binding ability of the complexes 1-3 with calf thymus (CT) DNA is characterized by measuring the effects on absorption, emission, and circular dichroism spectral and electrochemical techniques. The absorption spectra of 1-3 in the absence and presence of CT DNA at different concentrations R=25 (R=[DNA] / [Cu complex]; Fig. 2) show interesting changes in the intensity of intraligand absorption band (268 nm). This suggests the hypochromism for 1-3, typical of metal complex's association with the DNA helix. The strong hypochromic effect (61%) along with the 3 nm red shift for 2 reveals the partial intercalative [53] interaction through the active participation of planar phen moiety with DNA. However, the lack of red shift suggests that the binding mode of 1 and 3 (hypochromic effect: 1, 56; 3, 48%) was not intercalative. Because of the bulky structure of the complexes as well as the co-lignad is non-planar bpy (1) or dpa (3), the bzim rings cannot completely intercalate. When one of the two bzim rings inserts into the helix, the other ring extends away from the plane due to the stereochemistry effect and hence decreasing the effective area of overlap. Therefore, the observed spectral changes were rationalized in terms of feeble intercalation via bzim moiety in 1 and 3. To further illustrate the DNA binding strength, the intrinsic binding constant K_b was determined for **1-3** which were found to be $3.26 \times 10^4 \,\mathrm{M}^{-1}$ (1), $3.49 \times 10^4 \,\mathrm{M}^{-1}$ (2), $3.11 \times 10^4 \,\mathrm{M}^{-1}$ (3). The binding constants were lower compared to classical intercalators (EthBr-DNA, 1.4×10^6 M⁻¹) [54], the diminution could be explained by the steric constraints imposed by the ligand framework and thus encouraging a partial intercalative binding mode for these complexes and it was found for many other compounds with the same order of K_b values [55].

The observed circular dichroic (CD) spectrum of CT DNA consists of a positive band at 273 nm owing to base stacking and a negative band at 243 nm owing to helicity which is typical of DNA in right-handed B-form. Upon incubation of CT DNA with 1-3, shows conformational changes: (i) the intensity of both the bands of CT DNA increases (1 and 3) with the red shift of 2-3 nm in the positive band and (ii) the intensity of positive band increases while the intensity of the negative band decreases (2) with the red shift of 3 nm in the positive band (Fig. 3). These observations are consistent with the partial

intercalative interaction through planar phen moiety (2) or bzim moiety (1 and 3) supporting the results from UV-vis spectroscopy.

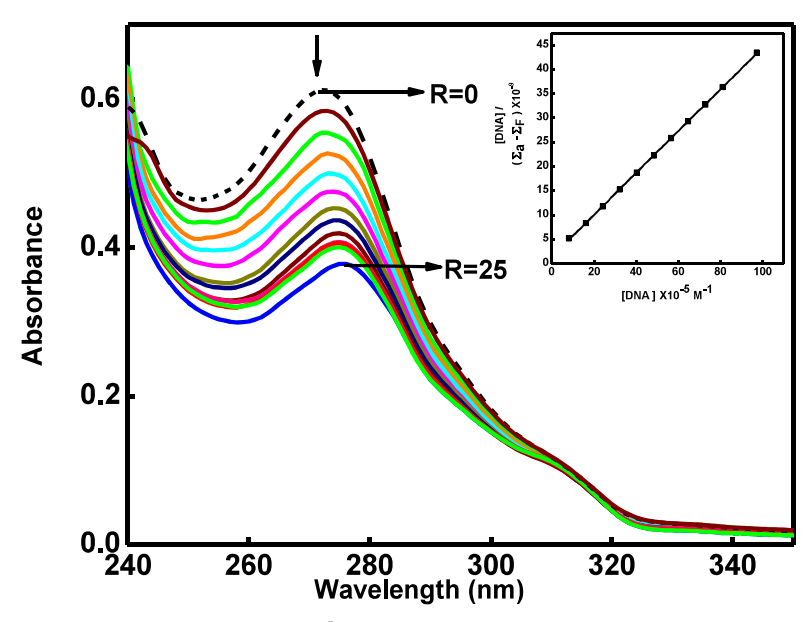


Fig. 2. Absorption spectra of 2 (2.7 \times $10^{\text{-5}}$ M) in 2% DMF/5mM Tris-HCl/50 mMNaCl buffer at pH 7.1 in the absence (R = 0) and presence (R = 25) of increasing amounts of CT DNA. Inset: Plot of [DNA] vs [DNA]/ $(\varepsilon_a - \varepsilon_f)$ at R = 25 of 2.

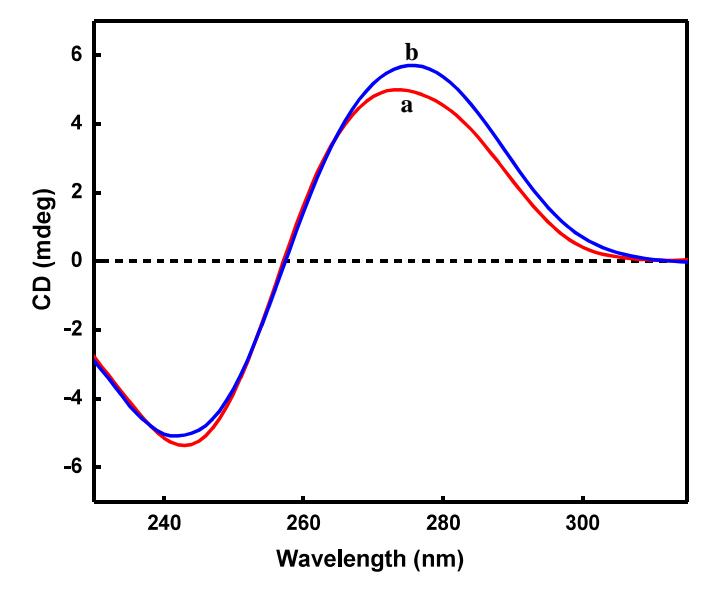


Fig. 3. Circular dichroism spectra of CT DNA in 2% DMF/5mM Tris-HCl/50 mMNaCl buffer at pH 7.1 and 25 $^{\circ}$ C in absence (a) and presence (b) of 2 at 1/R value of 3.

In competitive DNA binding experiment, with increasing amounts of 1-3, the fluorescence intensity of CT DNA-EthBr system (594 nm) was quenched (1, 89; 2, 96; 3, 76%) with the red shift of 5 nm (2) or 1 nm (1) or no shift (3), which was due to the partial intercalation of copper(II) complexes to DNA base pairs displacing some EthBr from CT DNA-EthBr system (Fig. 4) [56]. The quenching data (K_{sv}) were analyzed according to the Stern-Volmer equation and the binding constant (K_{app}) value obtained using the equation, $K_{EthBr}[EthBr] = K_{app}[Cu(II) Complex]$. The K_{sv} (1, 1.55 × 10⁴; 2, 5.40 × 10⁴; 3, 1.01 × 10⁴ M⁻¹) and K_{app} (1, 1.54 × 10⁵; 2, 2.06 × 10⁵; 3, 1.03 × 10⁵ M⁻¹) values indicate that the complex 2 binds more strongly (via planar phen moiety) than the complexes 1 and 3 (via bzim moiety) through partial intercalative mode.

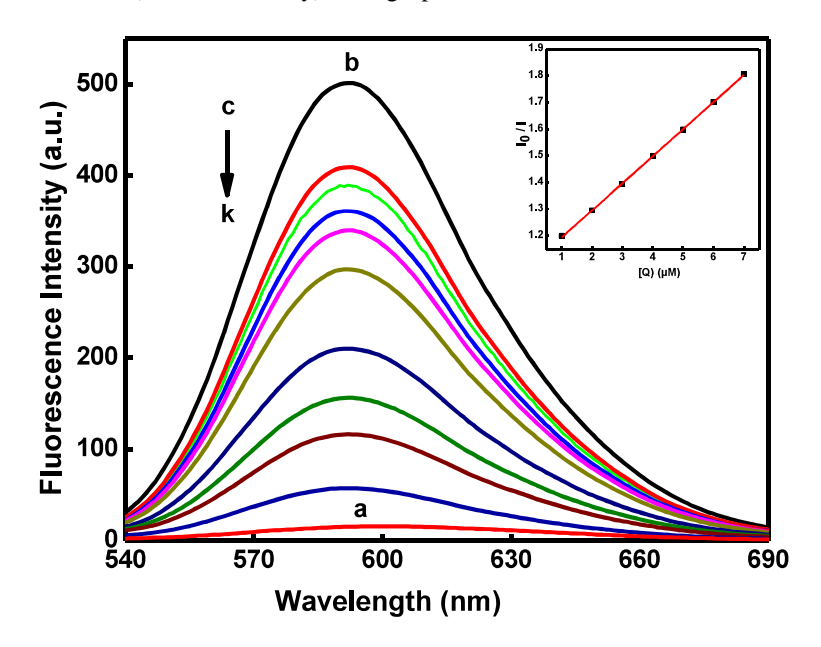


Fig. 4. Fluorescence quenching curves of ethidium bromide bound to DNA in 2% DMF/5mM Tris-HCl/50 mMNaCl buffer at pH 7.1: (a) EthBr (1.25 μ M); (b) EthBr+DNA (125 μ M); (c-k) EthBr+DNA+ **2** (0-10 μ M). Inset: Plot of I_0/I vs [complex] of **2**.

The cyclic voltammograms of the complexes in the absence of DNA reveal a non-Nernstian but a fairly quasi-reversible ($\Delta E_{\rm p}$: 1, 110; 2, 128; 3, 111 mV) one electron redox process ($i_{\rm pa}/i_{\rm pc}$: 1, 1.0; 2, 1.2; 3, 1.0) involving the Cu(II)/Cu(I) couple ($E_{\rm 1/2}$: 1, -0.089; 2, -0.091; 3, -0.085 V vs SCE). Upon the addition of excess DNA (R = 5), the complexes show a significant reduction in both cathodic and anodic peak currents and reveal quasi-reversible ($\Delta E_{\rm p}$: 1, 156; 2, 129; 3, 116 mV) one electron ($i_{\rm pa}/i_{\rm pc}$: 1, 1.0; 2, 1.1; 3, 1.2) electrochemical behavior for Cu(II)/Cu(I) couple ($E_{\rm 1/2}$: 1, -0.193; 2, -0.191; 3, -0.198 V vs SCE). Interestingly, the reduction in both the peak currents indicates that the complexes bind through the partial intercalative mode and causes slow diffusion of an equilibrium mixture of the free and DNA-bound complexes to the electrode surface.

Further, the observed shifts (104-127 mV) in $E_{1/2}$ values (DPV) to more negative potentials (Fig. 5) suggest that both Cu(II) and Cu(I) forms of the present complexes bind to DNA but with Cu(II) displaying higher DNA binding affinity than Cu(I) form, which is substantiated by the ratio of the equilibrium constants (K_+/K_{2+}) [57]. The K_+/K_{2+} values (1, 0.02; 2, 0.02; 3, 0.01) are far less than unity suggesting preferential stabilization of Cu(II) form over Cu(I) form on binding to DNA.

3.6. Protein binding studies

Three intrinsic flours present in the protein, such as tryptophan, tyrosine and phenylalanine residues are responsible for the fluorescence of protein. Actually, the intrinsic fluorescence of many proteins is caused mainly by tryptophan alone. Fluorescence quenching corresponds to any process, which is a reduction of the fluorescence intensity from a fluorophore due to a variety of molecular interactions such as molecular rearrangements, reactions at excited-state, energy transfer ground-state complex formation and collisional quenching. Thus, the emission spectra of BSA ($\lambda_{\rm em}$, 340 nm; $\lambda_{\rm ex}$, 280 nm) in the presence of increasing concentrations of 1-3 were recorded at 300 K and 310 K.

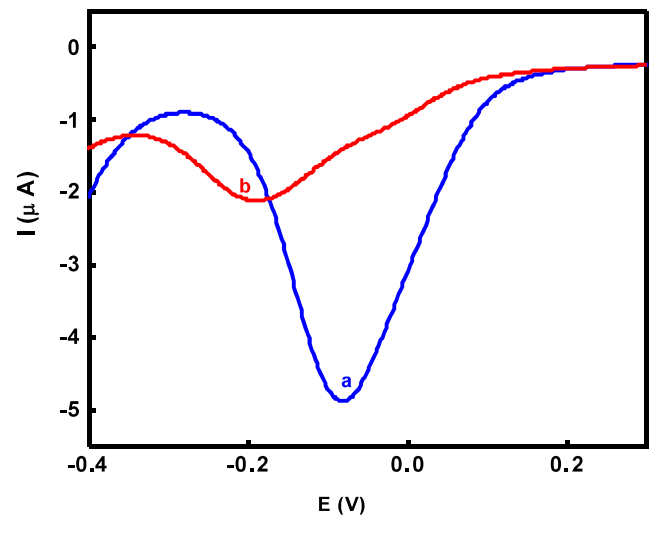


Fig. 5. Differential pulse voltammograms of **2** (0.5 mM) in the absence (a) and presence (b) of CT DNA (R = 5) at 25.0 ± 0.2 °C at 2 mV s⁻¹ scan rate in 2% DMF/5mM Tris-HCl/50 mMNaCl buffer at pH 7.1.

The fluorescence intensity of BSA decreased regularly (Fig. 6), up to 61.6-74.4% (300 K) and 67.2-71.0% (310 K), accompanied by a hypsochromic shift of 3-14 nm (1 and 2) and bathochromic shift of 4-9 nm (3). The Stern-Volmer plots are linear [K_{SV} : 300 K, 3.16 (1); 2.45 (2); 2.01 × 10⁵ M⁻¹ (3) and 310 K, 3.58 (1); 2.79 (2); 2.15 × 10⁵ M⁻¹ (3)] and suggest that a single quenching mechanism, either static or dynamic is occurred at these concentrations [58]. The quenching rate constant (K_q) is on the order of 10¹³ M⁻¹s⁻¹, which

is 1000-fold higher than the maximum limit $(2.0 \times 10^{10} \, M^{\text{-l}} \, s^{\text{-l}})$ [59], which indicates that the quenching is not initiated by dynamic collision but from the formation of the complex. On the other hand, upon addition of **1-3** to BSA, a significant decrease in 210 nm absorbance peak of BSA is observed (Fig. 7), which is attributed, to the induced perturbation of α -helix of BSA.

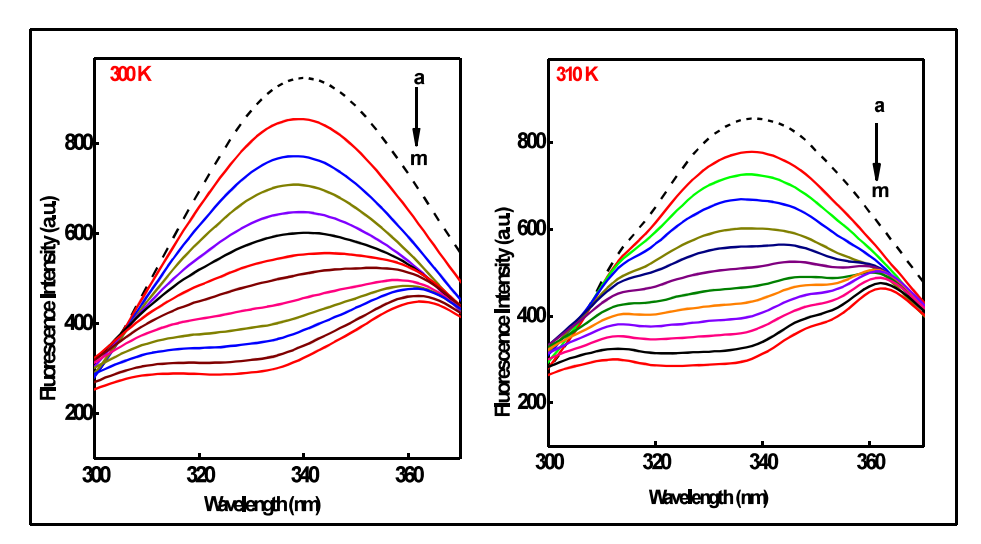


Fig. 6. Changes in the fluorescence spectra of BSA through the titration with **2** at 300 K (left), and 310 K (right). The concentration of BSA is $1\times10^{\text{-6}}$ mol $L^{\text{-1}}$, and the concentration of **2** was varied from (a) 0.0 to (k) $4.0\times10^{\text{-6}}$ mol $L^{\text{-1}}$; pH 7.4 and λ_{ex} 280 nm.

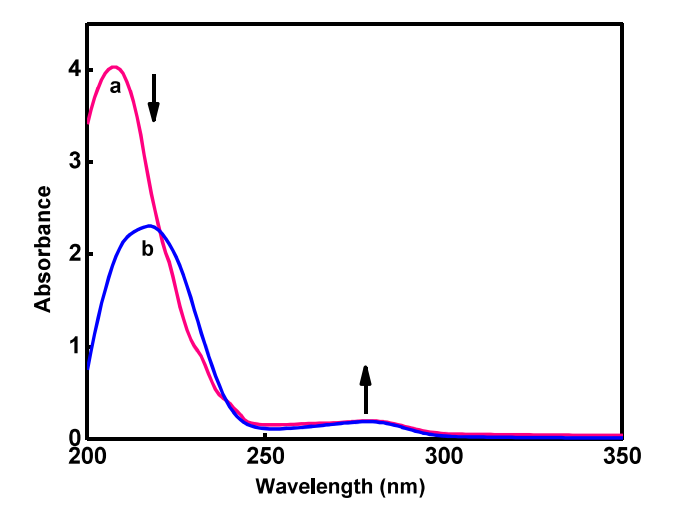


Fig. 7. UV-Vis absorption spectra of BSA in the absence and presence of **2**. (a) Absorption spectrum of BSA. (b) Absorption spectrum of BSA in the presence of **2** at the concentration, [BSA] = [Cu complex] = 3.5×10^{-6} mol L⁻¹.

Meanwhile, the absorption intensity of the 280 nm band is increased due to the alteration in the microenvironment of three amino acid residues followed by the disturbance of the tertiary structure of BSA. Therefore the interaction between 1-3 and BSA leads to an adduct species which undergoes mainly a static quenching process [60]. The binding constant K_b is decreased with increasing temperature [300 K, 0.83 (1); 0.73 (2); $1.42 \times 10^5 \text{ M}^{-1}$ (3) and 310 K, 0.42 (1); 0.60 (2); $0.78 \times 10^5 \text{ M}^{-1}$ (3)], which indicates the formation of stable BSA-(1/2/3) adduct and the number of binding site n is equal to 0.9 corresponds to the existence of a single binding site. So, the results suggest that the complex binds to the hydrophobic pocket located in subdomain IIA [61]. In order to elucidate the interaction forces of 1-3 with BSA, the thermodynamic parameters were calculated. The spontaneity of the interaction is revealed by negative ΔG value. The positive values obtained for both ΔH and ΔS indicates that a hydrophobic association is the major binding force and that the interaction is entropy driven process [62]. Therefore, hydrophobic forces may play the main role in binding of 1-3 to BSA. In addition to hydrophobic interaction, a possible covalent bonding may be also considered, instead, the ΔH value obtained (78-79 kJ mol⁻¹) is less than the expected value for a covalent bond formation ($\ge 120 \text{ kJ mol}^{-1}$) [63].

According to the theory of Miller [64], when $\Delta\lambda$ between excitation wavelength and the emission wavelength is set at 15 or 60 nm, the synchronous fluorescence gives information about the molecular environment in a vicinity of tyrosine and tryptophan residues, respectively. The synchronous fluorescence spectra of BSA with various amounts of 1-3 were recorded at $\Delta\lambda=15$ nm and $\Delta\lambda=60$ nm (Fig. 8). It is apparent that the emission maxima of tyrosine and tryptophan residues have significant blue-shifted (tyrosine: 1, 314-299; 2, 314-308; 3, 314-303 nm and tryptophan: 1, 346-338; 2, 346-343; 3, 346-339 nm). The blue-shift expressed that the conformation of BSA was changed, leading to the decrease in polarity and increase in hydrophobicity around the tyrosine and tryptophan residues. For BSA-(1/2/3) system, the synchronous fluorescence quenching ratios, RSFQ at $\Delta\lambda=60$ nm (1, 74.7; 2, 70.3; 3, 72.1%) is greater than the corresponding one for $\Delta\lambda=15$ nm (1, 55.0; 2, 45.6; 3, 60.1%), indicating that 1-3 reached sub-domain IIA, where the only one Trp 212 residues on BSA was located.

In order to estimate the distance between the buried Trp-212 (as donor) and the interacted complex (as acceptor), Förster's non-radiative energy transfer theory (FRET) [65] was adopted. The overlap of the UV absorption spectra of Cu(II) complexes with the fluorescence emission spectra of BSA is made. The energy transfer efficiency is not only depending on the distance between the donor and acceptor, but also to the critical energy transfer distance (r), which should be less than 8 nm. According to the Förster's equations, we obtain $J(\lambda)$ (1, 4.33; 2, 8.02; 3, 3.08 × 10¹⁵ M⁻¹cm³), R_0 (1, 1.46; 2, 3.18; 3, 2.06 nm), E (1, 0.18; 2, 0.09; 3, 0.08) and r (1, 6.61; 2, 3.80; 3, 2.14 nm). The donor (Trp 212 in BSA) to acceptor (1-3) distance (r) is less than 8 nm [60], indicates that the non-radiative energy transfer from BSA to Cu(II) complexes occurs with high possibility. These accord with the conditions of FRET, indicating again the static quenching interaction between Cu(II) complexes and BSA [66].

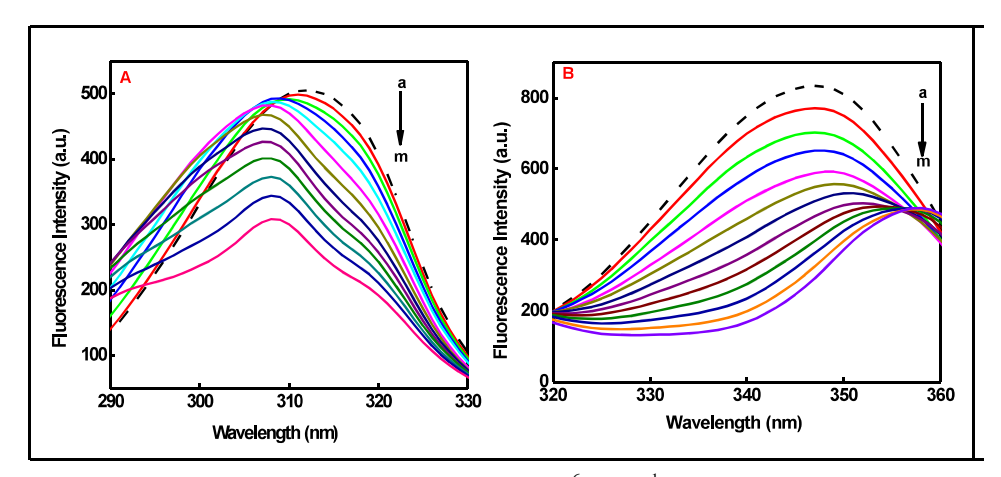


Fig. 8.Synchronous fluorescence spectra of BSA (1 \times 10⁻⁶ mol L⁻¹) upon addition of 2; $\Delta\lambda=15$ nm (left, **A**) and $\Delta\lambda=60$ nm (right, **B**). The concentration of 2 varied from (a) 0.0 to (j) 4.0×10^{-6} mol L⁻¹.

3.7. DNA cleavage studies

The complex concentrations in the range 5-500 µM, 1-3 fail to show any cleavage (Fig. 9) when supercoiled (SC) pUC19 DNA (20 μM) was incubated with them in the absence of an activator in 2% DMF/5 mMTris-HCl/50 mMNaCl buffer at pH 7.1 for 1 h at 37 °C. Therefore, the ability of 1-3 to cause DNA cleavage was studied in the presence of H₂O₂. In control experiments with DNA alone or DNA with H2O2 alone no DNA cleavage is observed. At lower complex concentrations, 1 (20 μM), 2 (12 μM) and 3 (30 μM) convert SC DNA into nicked circular (NC) form and then to linear open circular (LC) form (Fig. 10) revealing the efficient cleavage like activity. As concentrations of 1-3 are increased, the amount of form I decrease while both forms II and III increase. Interestingly, even at 12 μM concentration, the cleavage ability of 2 is found to be more efficient and also exhibits the same percentage of cleavage of DNA from the form I to form II as in 1 and 3. The difference in the cleavage activity is due to the binding efficiency of the complexes to DNA (cf. Above). It means that 2 can intercalate into DNA owing to favorable planarity of the ligand phen, and that copper cation may coordinate with the negatively charged oxygen in the phosphodiester backbone of DNA, displacing a water molecule, which enhances the binding affinity between 2 and DNA. In the presence of H₂O₂ as a reducing agent, Cu(II) complex is first reduced to form Cu(I) species and bound to DNA [67], which reacts readily with H₂O₂ to produce a peroxide complex such as DNA-Cu(I)OOH [68]. In the proximity of DNA, furthermore, the reduction of the peroxide complex (DNA-Cu(I)OOH) produces the ROS in abundance, i.e., hydroxyl radical, •OH, which would immediately attack the adjacent deoxyribose ring in the DNA skeleton. The preliminary mechanism of DNA strand scission by 1-3 has been investigated in the presence of several additives such as DMSO, superoxide dismutase (SOD), NaN3, and catalase. It is

remarkable that SOD, NaN₃ and catalase are ineffective, rule out the possibility of DNA cleavage by ${}^{1}O_{2}$ or O_{2} or O_{2} or $H_{2}O_{2}$ and imply that •OH radicals are playing a role in the DNA cleavage reaction (Fig. 11). The strongly DNA bound complex 2 (through partial intercalation via planar phen moiety) is located near the cleavage site is stabilized more in the Cu(I) state and so shows higher DNA cleavage compared to 1 and 3 (through partial intercalation via bzim moiety) using the availability of H₂O₂ since H₂O₂ is needed for both oxidation and reduction steps.

3.8. In Vitro cytotoxicity studies

Several copper(II) complexes display efficient cytotoxic action and anticancer properties due to the higher DNA binding affinity and prominent DNA cleavage activity [69,70]. Thus, as all the complexes strongly bind to DNA and induce efficient DNA cleavage, their cytotoxicity against human cervical carcinoma (HeLa) cell line has been investigated in comparison with the widely used drug cisplatin under identical conditions by using MTT assay. Their cytotoxicity was found to be concentration-dependent (0.25 to 100 µM) for 48 h incubation, which results in an increase in the percentage of cell inhibition (Fig. 12 CC).

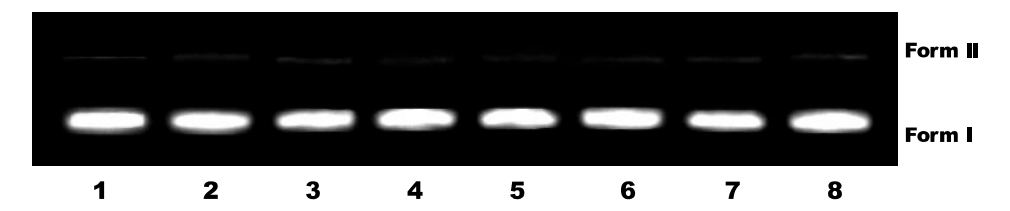


Fig. 9. Agarose gel showing cleavage of 20 µM SC pUC19 DNA incubated with 2 in 2% DMF/5 mMTris-HCl/50 mMNaCl buffer at pH 7.1 and 37 °C for 1 h. Lane 1, DNA control; lanes 2-8, DNA+2 (5, 10, 50, 100, 200, 300, 500 μM respectively). Forms I and II are supercoiled and nicked circular forms of DNA respectively.

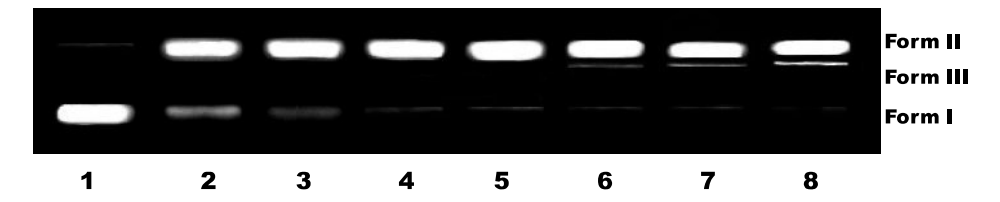


Fig. 10. Agarose gel showing cleavage of 20 μM SC pUC19 DNA incubated with 2 in 2% DMF/5 mMTris-HCl/50 mMNaCl buffer at pH 7.1 and 37 °C in the presence of H₂O₂ (200 μM). Lane 1, DNA+ H_2O_2 ; lanes 2-8, DNA+ H_2O_2 +2 (1, 2, 4, 6, 8, 10, 12 μ M respectively). Forms I, II and III are supercoiled, nicked circular and linear forms of DNA respectively.



Fig. 11. Gel electrophoresis diagram showing the cleavage of 20 μ M SC pUC19 DNA by **2** (12 μ M) in a 2% DMF/5 mMTris-HCl/50 mMNaCl buffer at pH 7.1 and 37 °C in the presence of H₂O₂ (200 μ M) with an incubation time of 2 h: lane 1, DNA control; lane 2, DNA+**2**; lane 3, DNA+**2**+H₂O₂; lane 4, DNA+**2**+H₂O₂+DMSO (20 μ M); lane 5, DNA+**2**+H₂O₂+SOD (0.5 units); lane 6, DNA+**2**+H₂O₂+NaN₃ (100 μ M); lane 7, DNA+**2**+H₂O₂+Catalase (6 unit).

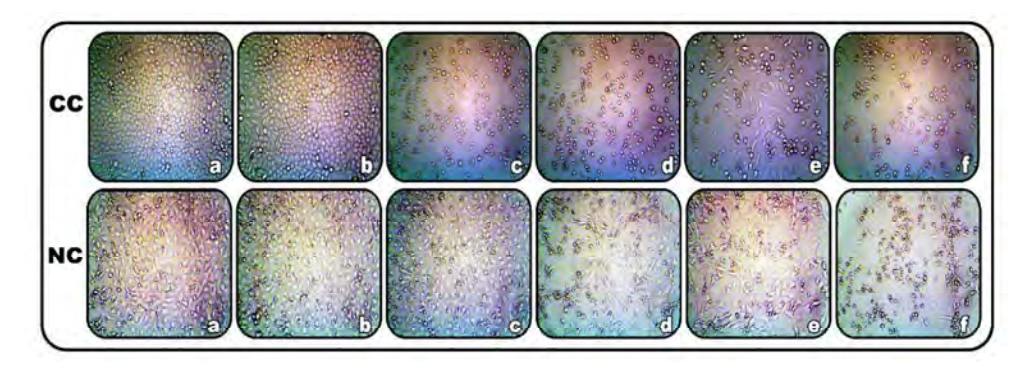


Fig. 12. Photomicrograph of human cervical carcinoma cell line (HeLa; CC) and normal mouse embryonic fibroblasts cell line (NIH 3T3; NC) after 48 h exposure with 2. CC (a, control; b, 0.25 μ M; c, 2.5 μ M; d, 25 μ M; e, 50 μ M; f, 100 μ M). NC (a, control; b, 0.1 μ M; c, 1.0 μ M; d, 10 μ M; e, 50 μ M; f, 100 μ M).

The IC₅₀ values obtained reveal that the potency of the complexes to kill the cancer cells follows the order 2>1>>3, disclosing that the mode and extent of interaction of complexes with DNA dictate the cell killing ability (cf. above). The cell killing ability with 2 and 1 is remarkable in displaying cytotoxicity (IC₅₀: 2, 2.17 (0.26); 1, 8.33 (0.16) μ M), approximately 8 and 2 times more potent respectively than cisplatin (IC₅₀, 16.41 (0.21) μ M) [3] whereas 3 (IC₅₀, 20.82 (0.09) μ M) show relatively lower cytotoxicity. Notably, the highly remarkable cytotoxicity of 2 compares to 1 and 3 is attributed to the stronger binding of the complex through the partial intercalative insertion of planar phen ring between the base pairs and its higher cleavage activity is responsible for its potency to induce cell death. As a measure of therapeutic potential, we further determined the cytotoxicity of 1-3 against normal mouse embryonic fibroblasts cell line NIH 3T3 (Fig. 12 NC). In general, they do not cause any damage toward NIH 3T3 (IC₅₀> 100 μ M), indicating that they are non-toxic to healthy cells, which is expected for a better drug.

4. Conclusion

The copper(II) complexes of the type [Cu(bba)(diimine)](ClO₄)₂ are involved in two types of partial intercalative mode of interactions with CT DNA, (i) *via* planar phen moiety in [Cu(bba)(phen)](ClO₄)₂ (2, stronger) and (ii) *via* bzim moiety in [Cu(bba)(bpy)](ClO₄)₂ (1, moderate) and [Cu(bba)(dpa)](ClO₄)₂ (3, weak). The findings of the interaction mechanism of 1-3 with BSA are as follows: (a) strong quencher and interact with BSA through static quenching procedure; (b) the binding reaction is spontaneous; (c) hydrophobic interactions play a major role in the reaction; (d) affects the conformation of tryptophan residues micro-region and (e) the energy transfer occurs with high probability. These results support the fact that the Cu(II) complexes can bind to BSA and transport in the body. Further, the DNA binding, DNA cleavage and *in vitro* cytotoxicity studies show that the binding propensity, cleavage ability, and cell killing activity follow the order 2>1>3. Overall, these studies demonstrate that 2 is promising chemotherapeutic scaffold, with well-defined biological interactions and activity derived from the redox-active copper center.

Acknowledgments

We are grateful to the DST-FIST programme of the National College (Autonomous), Tiruchirappalli. Thanks are due to SAIF, Indian Institute of Technology Madras for X-ray crystal structure data, solution, and refinement and for recording EPR spectra. Authors thank Professor A. Ramu, School of Chemistry, Madurai Kamaraj University for CD spectral measurements.

Supporting information

Crystallographic data for the structural analysis of the copper(II) complex (1) have been deposited with Cambridge Crystallographic Data Center, CCDC No. 1865376. Copies of this information may be obtained free of charge from http://www.ccdc.ac.uk/const/retrieving.html or from the CCDC, 12 Union Road, Cambridge CB2 1EZ, UK (email: deposit@ccdc.cam.ac.uk). Supplementary data associated with this article can be found online in the Supporting Information section at the end of the article.

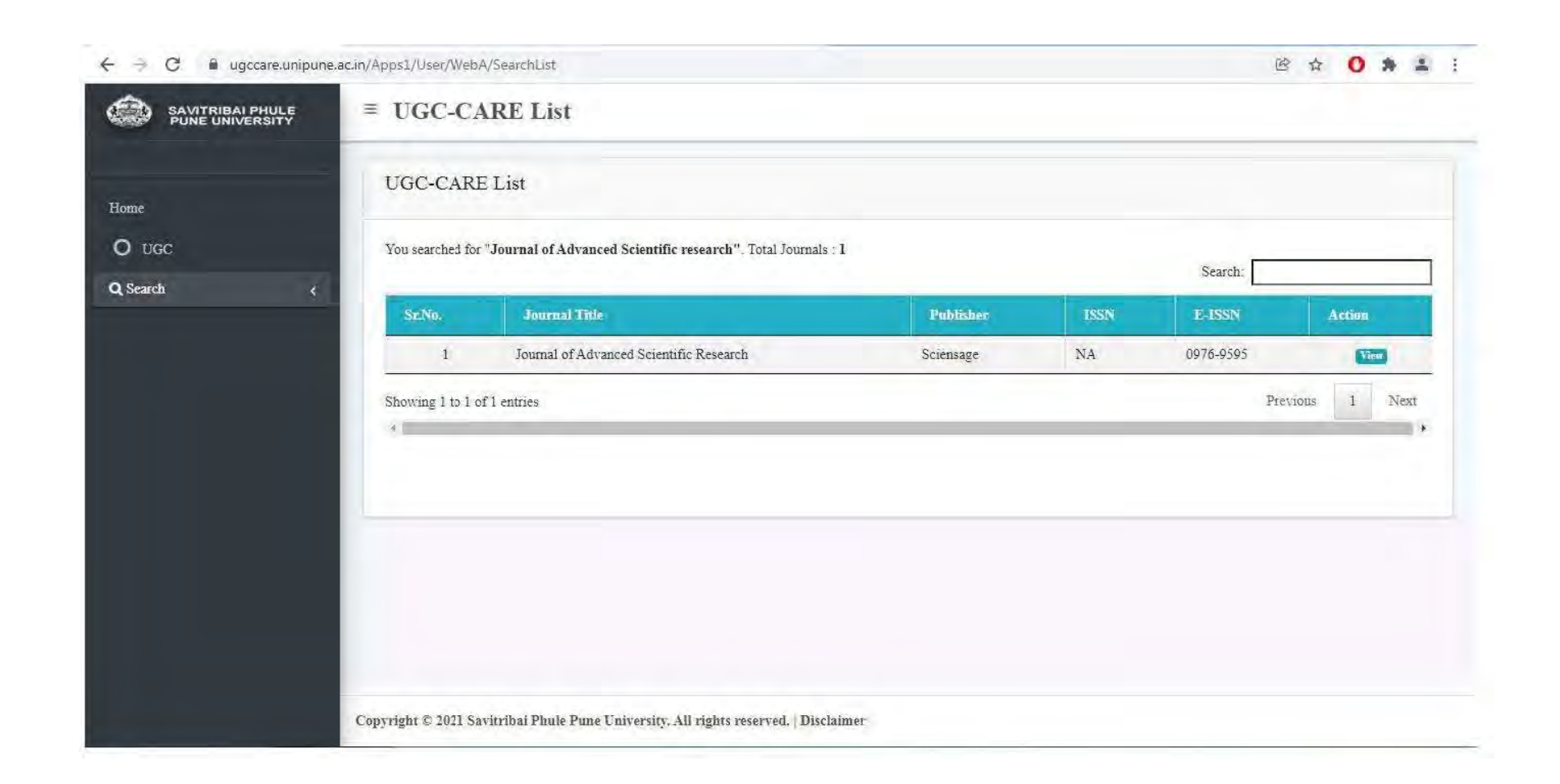
References

- R. A. Alderden, M. D. Hall, and T. W. Hambley, J. Chem. Educ. 83, 728 (2006). https://doi.org/10.1021/ed083p728
- 2. Y. W. Jung and S. J. Lippard, Chem. Rev. 107, 1387 (2007). https://doi.org/10.1021/cr068207j
- S. Sangeetha and M. Murali, Inorg. Chem. Commun. 59, 46 (2015). https://doi.org/10.1016/j.inoche.2015.06.032
- S. Sangeetha and M. Murali, Int. J. Biol. Macromol. 107, 2501 (2018). https://doi.org/10.1016/j.ijbiomac.2017.10.131
- A. Nori and J. Kopecek, Adv. Drug Delivery Rev. 57, 609 (2005). https://doi.org/10.1016/j.addr.2004.10.006

- Y. Xie, G. G. Miller, S. A. Cubitt, K. J. Soderlind, M. J. Allalunis-Turner, and J. W. Lown, Anti-Cancer Drug Des. 12, 169 (1997).
- M. Shi, K. Ho, A. Keating, and M. S. Shoichet, Adv. Funct. Mater. 19, 1689 (2009). https://doi.org/10.1002/adfm.200801271
- W. O. Foye, Cancer Chemotherapeutic Agents (American Chemical Society, Washington DC, 1995).
- B. Rosenberg, L. VamCamp, J. E. Trosko, and V. H. Mansour, Nature 222, 385 (1969). https://doi.org/10.1038/222385a0
- D. Senthil Raja, N. S. P. Bhuvanesh, and K. Natarajan, Dalton Trans. 41, 4365 (2012). https://doi.org/10.1039/c2dt12274j
- P. J. Bednarski, F. S. Mackay, and P. J. Sadler, Anticancer Agents Med. Chem. 7, 75 (2007). https://doi.org/10.2174/187152007779314053
- X. Qiao, Z. Y. Ma, C. Z. Xie, F. Xue, Y. W. Zhang, J. Y. Xu, Z. Y. Qiang, J. S. Lou, G. J. Chen, and S. P. Yan, J. Inorg. Biochem. 105, 728 (2011). https://doi.org/10.1016/j.jinorgbio.2011.01.004
- F. Kratz, in Metal Complexes in Cancer Chemotherapy, ed. B. K. Keppler (VCH: Weinheim, Germany, 1993) pp. 391.
- M. J. McKeage, Drug Safety, 13, 228 (1995). https://doi.org/10.2165/00002018-199513040-00003
- A. A. Spasov, I. N. Yozhitsa, L. I. Bugaeva, and V. A. Anisimova, Pharm. Chem. J. 33, 232 (1999). https://doi.org/10.1007/BF02510042
- 16. R. A. Bucknall and S. B. Carter, Nature 213, 1099 (1967). https://doi.org/10.1038/2131099a0
- 17. F. Gumus, O. Algul, G. Eren, H. Eroglu, N. Diril, S. Gur, and A. Ozkul, Eur. J. Med. Chem. **38**, 473 (2003). https://doi.org/10.1016/S0223-5234(03)00058-8
- M. Gocke, S. Utku, S. Gur, A. Rozkul, and F. Gumus, Eur. J. Med. Chem. 40, 135 (2005). https://doi.org/10.1016/j.ejmech.2004.09.017
- N. Bharti, M. T. Shailendra, G. Garza, E. Delia, C-. Vega, J. Castro-Garza, K. Saleem, F. Naqvi, M. R. Maurya, and A. Azam, Bioorg. Med. Chem. Lett. 12, 869 (2002). https://doi.org/10.1016/S0960-894X(02)00034-3
- V. G. Vaidyanathan and B. U. Nair, J. Inorg. Biochem. 91, 405 (2002). https://doi.org/10.1016/S0162-0134(02)00448-8
- J. Wang, L. Shuai, X. Xiao, Y. Zeng, Z. Li, and T. Matsumura-Ione, J. Inorg. Biochem. 99, 883 (2005). https://doi.org/10.1016/j.jinorgbio.2004.12.018
- 22. F. Ssczewski, E. Dziemidowicz-Borys, P. J. Bednarski, R. Grünert, M. Gdaniec, and P. Tabin, J. Inorg. Biochem. **100**, 1389 (2006). https://doi.org/10.1016/j.jinorgbio.2006.04.002
- B. Coyle, P. Kiusella, M. McCann, D. Devereux, R. O'Connor, M. Clynes, and K. Kavanagh, Toxicol. In Vitro 18, 63 (2004). https://doi.org/10.1016/j.tiv.2003.08.011
- D. Devereux, M. McCann, D. O'Shea, R. Kelly, D. Egan, C. Deegan, K. Kavanagh, V. McKee, and G. Finn, J. Inorg. Biochem. 98, 1023 (2004). https://doi.org/10.1016/j.jinorgbio.2004.02.020
- F. Gumus, G. Eren, L. Acik, A. Celebi, F. Ozturk, S. Yilmaz, R.I. Sagkan, S. Gur, A. Ozkul, A. Elmali, and Y. Elerman, J. Med. Chem. 52, 1345 (2009). https://doi.org/10.1021/jm8000983
- D. Wahnon, R. C. Hynes, and J. Chin, J. Chem. Soc. Chem. Commun. 1441 (1994). https://doi.org/10.1039/c39940001441
- Z. Liao , D. Xiang , D. Li , F. Sheng , F. Mei , B. Luo, and L. Shen, Synth. React. Inorg. Met.-Org. Chem. 30, 683 (2000). https://doi.org/10.1080/00945710009351791
- SMART & SAINT Software References Manuals, version 5.0 (Bruker AXS Inc.: Madison, WI, 1998).
- 29. G. M. Sheldrick, SAINT 5.1 (Siemens Industrial Automation Inc.: Madison, WI, 1995).
- 30. SADABS, Empirical Absorption Correction Program (University of Göttingen: Gottingen, Germany, 1997).
- G. M. Sheldrick, SHELXTL Reference Manual, Version 5.1 (Bruker AXS: Madison, WI, 1997).

- G. M. Sheldrick, ActaCrystallogr. A64, 112 (2008). https://doi.org/10.1107/S0108767307043930
- C. Merill, D. Goldman, S. A. Sedman, and M. H. Ebert, Science 211, 1437 (1980). https://doi.org/10.1126/science.6162199
- A. T. Chaviara, E. E. Kioseoglou, A. A. Pantazaki, A. C. Tsipis, P. A. Karipidis, D. A. Kyriakidis, and C. A. Bolos, J. Inorg. Biochem. 102, 1749 (2008). https://doi.org/10.1016/j.jinorgbio.2008.05.005
- 36. J. E. Huheey, E. A. Keiter, R. L. Keiter, and O. K. Medhu, Inorganic Chemistry, Principles of Structure and Reactivity (Pearson Education, Upper Saddle River, NJ, 2006) pp. 425-426.
- A. W. Addison, T. N. Rao, J. Reedijk, J. van Rijn, and G. C. Verschoor, J. Chem. Soc. Dalton Trans. 1349 (1984). https://doi.org/10.1039/DT9840001349
- G. Murphy, C. Murphy, B. Murphy, and B. J. Hathway, Dalton Trans. 2653 (1997). https://doi.org/10.1039/a702293j
- 39. P. T. Selvi, M. Murali, M. Palaniandavar, M. Kockerling, and G. Henkel, Inorg. Chim. Acta **340**, 139 (2002). https://doi.org/10.1016/S0020-1693(02)01091-5
- M. Palaniandavar, T. Pandiyan, M. Lakshminarayanan, and H. Manohar, J. Chem. Soc. Dalton Trans. 3, 455 (1995). https://doi.org/10.1039/dt9950000455
- K. Pijus, S. Saha, R. Majumdar, R. R. Dighe, and A. R. Chakravarty, Inorg. Chem. 49, 849 (2010). https://doi.org/10.1021/ic900701s
- 42. T.-H. Huang, H. Yang, G. Yang, S.-I. Zhu, and C.-L. Zhang, Inorg. Chim. Acta **455**, 1 (2017). https://doi.org/10.1016/j.ica.2016.10.012
- T. -H. Huang, M. -H. Zhang, C. -Y. Gao, and L. -T. Wang, Inorg. Chim. Acta 408, 91 (2013). https://doi.org/10.1016/j.ica.2013.08.024
- 44. A. B. P. Lever, Inorganic Electronic Spectroscopy (Elsevier, Amsterdam, 1984).
- V. Sathya and M. Murali, Inorg. Chem. Commun. 92, 55 (2018). https://doi.org/10.1016/j.inoche.2018.04.003
- U. Sakaguchiand A.W. Addison, J. Chem. Soc. Dalton Trans. 600 (1979). https://doi.org/10.1039/dt9790000600
- 47. M. Palaniandavar, I. Somasundaram, M. Lakshminarayanan, and H. Manohar, Dalton Trans. 1333 (1996). https://doi.org/10.1039/dt9960001333
- M. Murali, M. Palaniandavar and T. Pandiyan, Inorg. Chim. Acta 224, 19 (1994). https://doi.org/10.1016/0020-1693(94)04009-5
- C. Rajarajeswari, R. Loganathan, M. Palaniandavar, E. Suresh, A. Riyasdeen, and M. A. Akbarsha, Dalton Trans. 42, 8347 (2013). https://doi.org/10.1039/c3dt32992e
- E. Turkkan, U. Sayin, N. Erbilen, S. Pehlivanoglu, G. Erdogan, H. U. Tasdemir, A. O. Saf, L. Guler, and E. G. Akgemci, J. Organomet. Chem. 831, 23 (2017). https://doi.org/10.1016/j.jorganchem.2016.12.020
- 51. B. J. Hathaway, Copper in: Comprehensive Coordination Chemistry (Pergamon Press, Oxford, 1987) 5, pp. 533-774.
- 52. R. Balamurugan, M. Palaniandavar, H. Stoeckli-Evans, and M. Neuburger, Inorg. Chim. Acta 359, 1103 (2006). https://doi.org/10.1016/j.ica.2005.09.062
- B. D. Wang, Z. D. Y. Yang and T. R. Li, Bioorg. Med. Chem. 14, 6012 (2006). https://doi.org/10.1016/j.bmc.2006.05.015
- J. B. Le Pecq and C. Paoletti, J. Mol. Biol. 27, 87 (1967). https://doi.org/10.1016/0022-2836(67)90353-1
- S. Ramakrishnan, V. Rajendiran, M. Palaniandavar, V. S. Periasamy, B. S. Srinag, H. Krishnamurthy, and M. A. Akbarsha, Inorg. Chem. 48, 1309 (2009). https://doi.org/10.1021/ic801144x
- Y. B. Zeng, N. Yang, W. S. Liu, and N. Tang, J. Inorg. Biochem. 97, 258 (2003). https://doi.org/10.1016/S0162-0134(03)00313-1

- 57. T. Hirohama, Y. Kuranuki, E. Ebina, T. Sugizaki, H. Arii, M. Chikira, P. T. Selvi, and M. Palaniandavar, J. Inorg.Biochem. 99, 1205 (2005). https://doi.org/10.1016/j.jinorgbio.2005.02.020
- M. R. Eftink and C. A. Ghiron, Anal. Biochem. 114, 199 (1981). https://doi.org/10.1016/0003-2697(81)90474-7
- X. Zhao, R. Liu, Z. Chi, Y. Teng, and P. Qin, J. Phys. Chem. B 114, 5625 (2010). https://doi.org/10.1021/jp100903x
- W. He, Y. Li, C. Xue, Z. Hu, X. Chen, and F. Sheng, Bioorg. Med. Chem. 13, 1837 (2005). https://doi.org/10.1016/j.bmc.2004.11.038
- 61. A. Sulkowska, J. Równicka, B. Bojko, and W. Sułkowski, J. Mol. Struct. **651**, 133 (2003). https://doi.org/10.1016/S0022-2860(02)00642-7
- P. D. Ross and S. Subramanian, Biochemistry 20, 3096 (1981). https://doi.org/10.1021/bi00514a017
- C. N. Lunardi, A. C. Tedesco, T. L. Kurth, and I. M. Brinn, Photochem. Photobiol. Sci. 2, 954 (2003). https://doi.org/10.1039/B301789C
- J. N. Miller, Proc. Anal. Div. Chem. Soc. 16, 203 (1979). https://doi.org/10.1039/ad9791600199
- 65. T. Förster and O. Sinanoglu, Modern Quantum Chemistry (Acdemic Press, New York, 1966) 3.
- Y. Wang, Y. Wei, and C. Dong, J. Photochem. Photobiol. 177, 6 (2006). https://doi.org/10.1016/j.jphotochem.2005.04.040
- 67. B. Saha, M. M. Islam, S. Paul, S. Samanta, S. Ray, C. R. Santra, S. R. Choudhury, B. Dey, A. Das, S. Ghosh, S. Mukhopadhyay, G. S. Kumar, and P. Karmakar, J. Phys. Chem. B **114**, 5851 (2010). https://doi.org/10.1021/jp909127a
- J. Tan, B. Wang, and L. Zhu, J. Biol. Inorg. Chem. 14, 727 (2009). https://doi.org/10.1007/s00775-009-0486-8
- M. G. Pandian, R. Loganathan, S. Ramakrishnan, E. Suresh, A. Riyasdeen, M. A. Akbarsha, and M. Palaniandavar, Polyhedron 52, 924 (2013). https://doi.org/10.1016/j.poly.2012.07.021
- 70. Y. Gou, J. Li, B. Fan, B. Xu, M. Zhou, and F. Yang, Eur. J. Med. Chem. **134**, 207 (2017). https://doi.org/10.1016/j.ejmech.2017.04.026



UGC-CARE List

				Search:	
r.No.	Journal Title	Publisher	ISSN	E- ISSN	Action
11	Current Microwave Chemistry	Bentham Science Publishers	2213- 3356	2213- 3364	Whose
12	Current Physical Chemistry	Bentham Science Publishers	1877- 9468	1877- 9476	(Villates)
13	Current Traditional Medicine	Bentham Science Publishers	2215- 0838	2215- 0846	Indexed in Scopus
14	Defence Life Science Journal	Defence Scientific Information and Documentation Centre	2456- 379X	2456- 0537	Indexed in Scopus
15	Entomon	Association for Advancement of Entomology	0377- 9335	NA	Wiew)
16	Environmental and Experimental Biology	University of Latvia	1691- 8088	2255- 9582	
17	Genomics and Computational Biology	Johannes Gutenberg University	NA	2365- 7154	Discontinued from Oct 2020
18	International Journal of Electrochemistry	Hindawi Limited	2090- 3529	2090- 3537	Wew
19	Iranian Journal of Mathematical Chemistry	University of Kashan	2226- 6489	2008- 9015	Discontinued from Sep 2019
20	Journal of Advanced Scientific Research	Sciensage	NA	0976- 9595	(1000)

Showing 11 to 20 of 39 entries

Previous

0

1.

1

Journal Details

Journal Title (in English Language)	Journal of Advanced Scientific Research		
Publication Language	English		
Publisher	Sciensage		
ISSN	NA		
E-ISSN	0976-9595		
Discipline	Science		
Subject	Chemistry (all), Medicine (all), Pharmacology, Toxicology and Pharmaceutics (all)		
Focus Subject	General Chemistry, General Medicine, General Pharmacology, Toxicology and Pharmaceutics		



Journal of Advanced Scientific Research

ISSN
0976-9595
Research Article

Available online through http://www.sciensage.info

DNA BINDING, IN VITRO CYTOTOXICITY AND ANTICANCER DRUG MECHANISM OF COPPER(II) COMPLEX CONTAINING PYRIDYL-TRIAZINE LIGAND

Jeyaraman Manivel¹, Somasundaram Sangeetha^{1, 2}, Mariappan Murali*¹

¹Coordination and Bioinorganic Chemistry Research Laboratory, Department of Chemistry, National College (Autonomous), Tiruchirappalli, Tamil Nadu, India

²Department of Chemistry, Tamilavel Umamaheswaranar Karanthai Arts College, Thanjavur, Tamil Nadu, India *Corresponding author: murali@nct.ac.in

ABSTRACT

Mononuclear copper(II) complex $[Cu(dppt)_2(H_2O)_2](ClO_4)_2$ (1), where dppt is bidentate $N_{py}N_{tz}$ donor asymmetric ligand (pyridyl-triazine) has been isolated. The X-ray crystal structure of 1 possesses a CuN_4O_2 chromophore with elongated octahedral geometry. The electronic and EPR spectral properties demonstrate that the solvent molecules strongly interacted in the axial position thereby weakens the CuN_4 coordination plane. Absorption and emission spectral and electrochemical measurements clearly show the partial intercalative binding of 1 to calf thymus (CT) DNA. Remarkably, it exhibits potent cytotoxicity (IC₅₀, 3.73 μ M) against human cervical carcinoma cells (HeLa), which is 4.5 times better than cisplatin and is non-toxic (IC₅₀, >500 μ M) to normal mouse embryonic fibroblasts cells (NIH 3T3). It blocks cell cycle progression of HeLa cells in G1 phase. FACSverse analysis of 1 is suggestive of ROS (reactive oxygen species) generation and absolutely induces apoptotic cell death in HeLa cells.

Keywords: Copper(II) complex, DNA Binding, ROS, Apoptosis, Cytotoxicity.

1. INTRODUCTION

Currently, several reports were highlighting the use of transition metal complexes as anticancer agents [1, 2]. Probably the exception known of those is cisplatin [cisdiamminedichloroplatinum(II)]. It has been extensively used to treat a diffusion of cancers which include testicular, brain, ovarian, bladder, and breast cancer [3]. The scientific success of cisplatin is constrained by its considerable side effects, consisting of nausea, vomiting, and intense nephrotoxicity [3]. Using cisplatin and associated platinum complexes as anticancer agents have inspired a search for other energetic transition metal complexes which can be as powerful, but with lesser side effects. Many biological systems in nature make massive use of metal ions, inclusive of zinc and copper, which play essential roles within the regular functioning of organisms. Transition metals including copper, iron, and manganese, amongst others, are involved in a couple of biological processes from electron transfer to catalysis to structural roles and are often related to active sites of proteins and enzymes [4]. However, dysregulation of some of these vital metals in the course of normal biochemical processing has been implicated in the development of many pathological disorders, together with cancer [5]. These cellular roles simply need the "trace metals" in miniscule however firmly regulated quantities. Through assessment, different metals including arsenic, cadmium, chromium, and nickel are much less useful in view that they produce an extensive variety of toxic facet consequences, which includes carcinogenesis [4,6]. Particularly, copper(II) cation can bind to negatively charged DNA and had been proven to play a crucial function within the nearby formation of hydroxyl radicals [7, 8]. One of the results of excessive copper levels inside the body is a growth within the rate of radical formation mainly to oxidative damage [8]. This results in a disruption of lipid bilayers because of oxidation and cleavage of inclined unsaturated fatty acid residues of phospholipids. Changes in protein features also are promoted via oxidation of thiol and probably amino groups. Gene expression may also be altered because of the oxidation of guanosine and adenosine residues in nucleic acids or altered transcription factor or growth factor activities [9, 10]. More anecdotally, in the human body, Cu binds to N7 of guanine residue of DNA and generates ROS through the oxidation-reduction reaction resulting in DNA damage and cell apoptosis [11-13]. All these findings aid that the antitumor agent primarily based on Cu could be promising for the treatment of cancer. Therefore, a novel, green coloured copper(II) complex [Cu(dppt)₂(H₂O)₂](ClO₄)₂ (1), where dppt is 3-(2-pyridyl)-5,6-diphenyl-1,2,4-triazine has been synthesized. Its ability to bind calf thymus (CT) DNA and cancer chemotherapeutic potential against human cervical carcinoma cells (HeLa) and normal mouse embryonic fibroblasts cells (NIH 3T3) has been studied. Also, interesting aspects of the anticancer drug mechanisms underlying the cytotoxic response were probed.

2. EXPERIMENTAL

2.1. Material and methods

Copper(II) acetate monohydrate, 5,6-diphenyl-3-(2-pyridyl)-1,2,4-triazine, $NaClO_4$, tetra-N-butylammonium perchlorate (TBAP), ethanol, N,N-dimethyl formamide (DMF), anhydrous ether were of analytical grade and used as received from commercial sources. Calf thymus (CT) DNA was commercially purchased from Sigma Aldrich and stored at -20 $^{\circ}$ C while tris (hydroxymethyl) aminomethane and ethidium bromide (EthBr) were obtained from Merck.

The cell lines HeLa and NIH 3T3 were procured from the NCCS, Pune, India. Cell culture media and reagents were purchased from Hi Media, India. 3-(4,5-Dimethylthiazolyl-2)-2,5-diphenyltetrazolium bromide (MTT) and Annexin V and Apoptosis Detection Kit were purchased from Sigma Aldrich, USA. All antibodies used in this study were procured from Cell Signaling Technology, USA. Ultra-pure Milli-Q water (18.2 $\mu\Omega$) was used for all experiments.

The elemental analyses (C, H, N) were carried out using a Perkin-Elmer 2400 series II analyzer. The electrical conductivity was obtained with a Systronic 305 conductivity bridge, using 1×10^{-3} M solution of complex in N,N-dimethyl formamide (DMF). FTIR spectra were recorded using a Perkin Elmer Spectrum RX1 FTIR spectrophotometer in the range 400-4000 cm⁻¹ with a sample prepared at KBr disc. The electronic spectra were recorded using Perkin Elmer Lambda 365 UV-VIS spectrophotometer using cuvettes of 1 cm length. X-band electron paramagnetic resonance (EPR) measurements were performed at room temperature in the solid state and at 77 K in the DMF solution on JEOL JES-FA200 ESR spectrometer. Emission intensity

measurements were carried out using a Shimadzu RF-5301PC spectrofluorophotometer equipped with a thermostatic bath. Solutions of DNA in the 5 mM Tris HCl/50 mM NaCl buffer gave a ratio of UV absorbances at 260 and 280 nm, A_{260}/A_{280} , of 1.9 [14], indicating that the DNA was sufficiently free of protein. Concentrated stock solutions of DNA (13.5 mol dm³) were prepared in buffer and sonicated for 25 cycles, where each cycle consisted of 30 s with 1 min intervals. The concentration of DNA in nucleotide phosphate (NP) was determined by UV absorbance at 260 nm after 1:100 dilutions. The extinction coefficient, ε_{260} , was taken as 6600 dm³ mol⁻¹cm⁻¹. Stock solutions were stored at 4°C and used after no more than 4 days. Concentrated stock solutions of copper(II) complex was prepared by dissolving in 2% DMF 5 mM Tris-HCl/50 mM NaCl buffer at pH 7.1 and diluting suitably with the corresponding buffer to required concentrations for all the experiments. For absorption and emission spectral experiments, the DNA solutions were pretreated with solutions of copper(II) complex to ensure no change in concentrations of the copper(II) complex. Cyclic voltammetry (CV) and differential pulse voltammetry (DPV) were performed in a CHI 620C electrochemical analyzer at 25 ± 0.2 °C. The working electrode was a glassy carbon disk (0.0707 cm²) and the reference electrode a saturated calomel electrode. A platinum wire was used as the counter electrode. The supporting electrolyte was tetra-Nbutylammonium perchlorate (TBAP) or 2% DMF 5 mM Tris-HCl/50 mM NaCl buffer (pH 7.1). Solutions were deoxygenated by purging with nitrogen gas for 15 min prior to measurements; during measurements a stream of N, gas was passed over them. The redox potential $E_{1/2}$ was calculated from the anodic (E_{na}) and cathodic (E_{pc}) peak potentials of CV traces as (E_{pa} + E_{pc})/2 and also from the peak potential (E_{pa}) of DPV response as $E_p + \Delta E/2$ (ΔE is the pulse height).

2.2. Synthesis of complex, $[Cu(dppt)_2(H_2O)_2]$ (ClO₄)₂(1)

An ethanolic solution (5 mL) of 5,6-diphenyl-3-(2-pyridyl)-1,2,4-trazine (dppt: 0.62 g, 2 mmol) was added dropwise to an aqueous solution (10 mL) of copper(II) acetate monohydrate (0.20 g, 1 mmol). The resulting green coloured solution was stirred for 8 h at room temperature. The product was precipitated as the perchlorate salt by adding stoichiometric equivalent of NaClO₄ (0.12 g, 1 mmol) in water (3 mL). The bright

green product, [Cu(dppt)₂(H₂O)₂](ClO₄)₂, was collected by suction filtration, washed with cold water and ether and then air-dried. Yield: 76%. Selected IR peaks (v, cm⁻¹): 3447 b (ν_{O-H}), 1500 m, 1527 s and 1600 w $(\nu_{C=N})$ and $(\nu_{N=N})$, 1103 and 1064 (ν_{ClO4}) . Anal. Calcd for C₄₀H₃₂N₈O₁₀Cl₂Cu: C, 52.27; H, 3.51; N, 12.19 %. Found: C, 52.32; H, 3.49; N, 12.24 %. $\Lambda_{\rm M}$ (DMF): 165 Ω^{-1} cm² mol⁻¹. μ_{eff} (27 °C): 1.78 μ_{B} . Electronic spectrum in DMF [$\lambda_{max}/nm~(\epsilon_{max}/dm^3~mol^{-1}~cm^{-1})$]: 278 (8240), 322 (4885), 494 (35) 688 (30). Electronic spectrum in 2% DMF/5 mM Tris-HCl/50 mM NaCl buffer solution [$\lambda_{max}/nm~(\epsilon_{max}/dm^3~mol^{-1}~cm^{-1})$]: 265 (8350), 292 (4900), 482(45), 676 (40). Room temperature polycrystalline EPR spectrum: g_{iso} = 2.061. EPR spectrum in DMF solution at 77 K: g_{\parallel} = 2.292, $g_{\perp} = 2.060$, $A_{||} = 165 \times 10^{-4} \text{ cm}^{-1}$, $g_{||}/A_{||} =$ 139 cm, G = 4.9. Redox behaviour: $E_{1/2} = 0.243 \text{ V}$ (CV) and 0.242 V (DPV), $\Delta E_p = 81 \text{ mV}$, $i_{pa}/i_{pc} = 1.1$, D $= 6.2 \times 10^6 \,\mathrm{cm}^2 \mathrm{s}^{-1}$.

The blocks of bright green single crystals of $[Cu(dppt)_2 (H_2O)_2](ClO_4)_2$ (1) separated upon cooling a solution of 1 in MeOH:MeCN:Et₂O at 5 °C for seven days. The latter were found suitable for X-ray studies.

2.3. X-ray crystallography

A bright green needle-like single crystal of the complex $[Cu(dppt)_2(H_2O)_2](ClO_4)_2$ 1 with dimensions 0.35 × $0.30 \times 0.30 \text{ mm}^3$ was selected under the polarizing microscope and then mounted on glass fiber. The crystal data collections were performed on a Bruker AXS-KAPPA APEX II diffractometer equipped with a CCD area detector utilizing Mo- K_{α} radiation (λ = 0.71073 Å) at 273 K. Data were collected and reduced by SMART and SAINT softwares in the Bruker packages [15]. The structure was solved by direct methods and subsequently refined by full-matrix least squares calculations with the SHELXL-2018/3 software package [16]. All non-hydrogen atoms were refined anisotropically while hydrogen atoms were placed in geometrically idealized positions and constrained to ride on their parent atoms. Also, hydrogens on water oxygen which is connected to Cu are located. The disorder in perchlorate anion is fixed and the ratio of occupancies of disordered moieties is found to be 53:47. The graphics interface package used was PLATON, and the figures were generated using the ORTEP 3.07 generation package [17]. Crystallographic data for the structural analysis of [Cu(dppt), (H₂O)₂](ClO₄)₂ (1) have been deposited with Cambridge Crystallographic Data Center, CCDC No. 1994856. Copies of this information may be obtained free of charge from http://www.ccdc.ac.uk /const/retrieving.html or from the CCDC, 12 Union Road, Cambridge, CB2 1EZ, UK (email: deposit@ccdc.cam.ac.uk).

2.4. Spectroscopic and electrochemical experiments of DNA interactions

The spectroscopic and electrochemical experiments of DNA interactions were carried out by employing the procedure reported by us previously [14].

2.5. Cell viability assays

The in vitro cytotoxicities of test complex 1 (HeLa, 0.1-100 μ M; NIH 3T3, 1-500 μ M), free dppt ligand, Cu(OAc)₂·H₂O against HeLa and NIH 3T3 cell lines were assayed by 3-(4,5-dimethylthiazol-2-yl)-2,5-diphenyltetrazolium bromide (MTT) assay. The inhibitory effect of them on both cancer and normal cells were evaluated by means of their IC₅₀ values (concentration of compound required to inhibit 50% of cell proliferation). Cisplatin was chosen as a positive control.

2.6. Anticancer drug mechanistic studies 2.6.1. Cell cycle

The HeLa cells were seeded in 6 well plates with highglucose DMEM media after the period of the time cells attained the growth and the cells were treated with 1 in its IC₅₀ concentration in the medium for 48 h. After 48 h of incubation, cells were trypsinized and resuspended with complete media. Cells were collected and centrifuged at 1000 rpm for 5 min. Then cell pellet was washed with PBS (Phosphate Buffer Saline) twice and subsequently fixed with 1 ml of 70% of ice cold ethanol overnight at 4°C. Following the ice cold ethanol, the cell pellet were washed twice with cold PBS and added 10 μl of RNase A at 10 g/ml concentration, which was then incubated for 30 min and washed with PBS at the end. Cells were then incubated in 1 ml of PBS with 50 μl of propidium iodide (1 mg/ml stock) for 30 min in darkness. Then cells were analysed to check the cell cycle phase using FACSverse flow cytometer (Becton-Dickinson).

2.6.2. ROS generation

The HeLa cells were seeded in 6 well plates with high glucose DMEM media for the treatment until cell confluency after the cell growth treated with 1 in 3 h, 2 h and 1 h time interval. After the treatment, cells were trypsinized and 10 μ M 2',7'-dichlorodihy drofluorescein diacetate (DCHF-DA, Sigma-Aldrich) dye was added to the pellet. This was kept in incubation under darkness for 10 min. The cells were then analyzed to determine ROS level using FACSverse flow cytometer (Becton-Dickinson).

2.6.3. Apoptosis

The HeLa cells were treated with 1 in high-glucose DMEM media for 48 h. After treatment, the cells were trypsinized, resuspended in PBS, washed twice and centrifuged to remove PBS. The cells were suspended in 100 μl of binding buffer containing 5 μl of Annexin V and propidium iodide (PI) and incubated for 15 mins under darkness. Stained cells were diluted using 450 μl of binding buffer. The cells were analyzed by using FACSverse flow cytometer (Becton-Dickinson) and the data were analyzed by FACSverse software.

2.6.4. DAPI staining

Cell nuclear morphology was evaluated by fluorescence microscopy following DAPI (4',6-diamidino-2-phenylindole) staining. The HeLa cells were treated with 1 for 48 h. The cells were washed with PBS (pH 7.4), fixed with ice cold paraformaldehyde and then cells were then washed with PBS followed by DAPI was added and incubated for 15 min at 37 °C wrapped in aluminium foil. The cells were then washed with PBS and examined under Zeiss Axio Observer fluorescence microscope.

3. RESULTS AND DISCUSSION

3.1. Synthesis and characterization of 1

The bright green complex, [Cu(dppt),(H₂O),](ClO₄), (1) was prepared in good yield (76%) and purity by the reaction of an aqueous solution of Cu(OAc)2·H2O, ethanolic solution of 5,6-diphenyl-3-(2-pyridyl)-1,2,4triazine (dppt) and NaClO₄ in a stoichiometric ratio (1:2:1) at room temperature. The selected frequencies observed in the IR spectra of 1, the broad band appeared at 3447 cm⁻¹ represents the existence of H₂O [18]. The stretching vibrations of the C=N and N=N groups appear at considerable lower values with respect to the $\nu_{\text{\tiny C=N}}$ and $\nu_{\text{\tiny N=N}}$ of the free dppt ligand supporting the coordination of the pyridyl and triazine nitrogen donors to copper(II) ion [19]. It displays two well split bands at 1103 and 1064 cm⁻¹ due to perchlorate anion. Such splitting normally arises due to coordination of or hydrogen bonding [20] of ClO₄; however, none of these is present in the crystal structure. Elemental analysis of 1 was entirely consistent with its determined composition by X-ray crystallography. This is substantiated by conductivity measurements in DMF solution, which is expected for a 1:2 electrolyte in solution.

In DMF solution, 1 exhibits only one broad band (λ_{max}), 688 nm) with very low extinction coefficient (ε_{max} , 30 dm³ mol⁻¹ cm⁻¹) value in the visible region, typical of ligand field (LF) absorption for Cu(II) located in a tetragonal field. The powder EPR spectrum at 298 K of 1 is isotropic while frozen DMF solution shows axial spectral features, typical of mononuclear Cu(II) species $(g_{||}>g_{\perp}>2.0; G=(g_{||}-2)/(g_{\perp}-2)=4.9)$ suggesting the presence of $d_{x^2-\gamma^2}$ ground state in copper(II) located in square-based geometries [21]. The observed g_{11} (2.292) and A_{11} (165×10⁻⁴ cm⁻¹) values are consistent with the presence of a square based CuN₄ coordination plane with strong axial interaction by two oxygen atoms. The $g_{\parallel}/A_{\parallel}$ quotient (139 cm) is suggestive [22] of negligible distortion from the CuN₄ coordination plane. The electrochemical behaviour of 1 in DMF (TBAP as supporting electrolyte) shows a quasi-reversible redox couple, $E_{1/2}$ at 0.243 V versus SCE. The peak potentials separation, ΔE_p is 81 mV, the ratio of cathodic to anodic peak current (i_{pa}/i_{pc}) is close to unity and the reduction process is diffusion controlled. The weak σ bonding caused by the highly electron-withdrawing phenyl groups as well as strong π back bonding [23] involving the phenyl and pyridine rings, rather than the bulkiness of the ligand molecule, is responsible for the positive $E_{1/2}$ value.

In the complex (1), the copper atom is coordinated to two 3-(2-pyridyl)-5,6-diphenyl-1,2,4-triazine (dppt) in *trans* configuration via triazine nitrogen (N_{tz}) and pyridine nitrogen (N_{py}) and two water molecules. The crystallographic data (Table 1) and selected bond lengths and angles (Table 2) are provided.

The two Cu-N_{py} (2.046(2) Å) and Cu-N_{tz} (2.030(2) Å) bond distances are not appreciably different indicating that the donor strength of two nitrogens are equal while the two oxygen atoms of water molecules occupy axial position at longer distances (2.425(3) Å), as a consequence of the Jahn-Teller effect. However, the structure of 1 (Fig. 1) at 273 K is almost the same as that already determined by Palaniandavar et al. [24] at 296 K and Takagi et al. [25] at 200 K and is hence a confirmation of the identity of 1.

Table 1: Selected crystal data and structure refinement parameters for 1

$C_{40}H_{32}N_8Cl_2O_{10}Cu$
919.17
273(2)
0.71073
Monoclinic
C2/c
12.1016(8)
11.3529(8)
29.8689(18)
90
92.782(4)
90
4098.8(5)
4
1.490
0.732
1884
$0.35 \times 0.30 \times 0.30$
2.461-28.159
21988
4940
3665
0.0324
1.081
0.0529
0.1414
0.0965/0.1567

3.2. Spectroscopic and voltammetric studies on DNA interaction

The absorption spectra of 1 in the absence and presence of DNA at different concentrations (R = [DNA]/ [complex] = 1-25) in 2% DMF/5 mM Tris-HCl/50 mM NaCl buffer (pH = 7.1) were recorded (Fig. 2) at 291 nm (π - π * transition). With an increase in concentration of CT DNA, the hypochromism of 61.0% and red-shift of 3 nm for 1 were observed indicating the partial intercalative interaction. The extent of binding was calculated [26] and the intrinsic equilibrium DNA binding constant, K_b has been estimated to be $2.565\pm0.001\times10^5$ M⁻¹, which suggests the enhanced DNA binding propensity of 1 possibly due to the involvement of partial intercalative interaction of the planar 5,6-diphenyltriazine moiety of coordinated dppt into the DNA base pairs leading to high hypochromism. In addition, there is no change in absorption spectral band of dppt upon increasing the CT DNA

concentration indicates that there is no interaction between dppt and the base pairs of DNA.

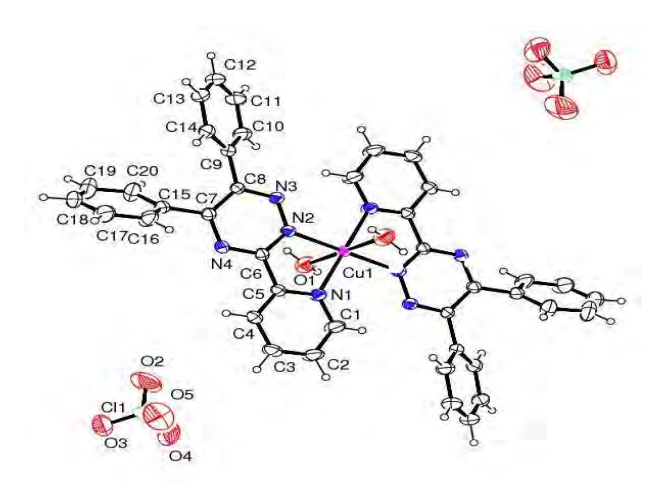


Fig. 1: An ORTEP drawing of $[Cu(dppt)_2(H_2O)_2]$ $(ClO_4)_2$ (1) showing 30% probability thermal ellipsoids with atom labeling scheme

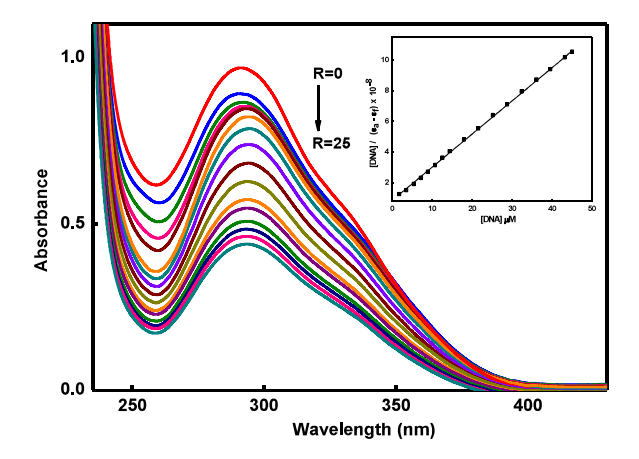


Fig. 2: Absorption spectra of 1 (concentration, 25×10^{-6} M) in 2% DMF/5mM Tris- HCl/50 mM NaCl buffer at pH 7.1 in the absence (R = 0) and presence (R = 25) of increasing amounts of CT DNA. Inset: Plot of [DNA] vs [DNA]/(ε_a - ε_f) at R = 25 of 1.

The intrinsic fluorescence intensity of DNA and that of EthBr are low, while the fluorescence intensity of EthBr will be enhanced on addition of DNA due to its intercalation into the DNA. In our experiment, the fluorescence intensities of EthBr-DNA system show a decreasing trend with increasing concentration of 1 (Fig. 3), indicating that some EthBr molecules are

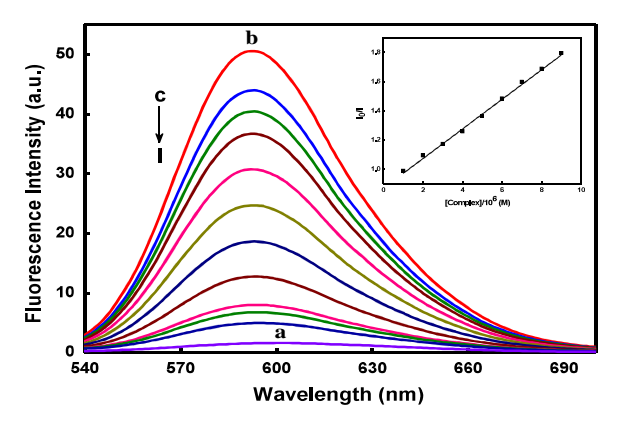
released from EthBr-DNA after an exchange with 1 which results in the fluorescence quenching of EthBr. This may be due to that 1 displaces the EthBr from its DNA-binding sites in the competitive manner. The plot (Fig. 3, inset) illustrates that the quenching of EthBr bound to DNA are in good agreement with the linear

Stern-Volmer equation [27]. The K_{SV} value (1.60 × 10⁵ M^{-1}) of 1 indicates the quenching efficiency and especially significant degree of binding to DNA. The binding strength of 1 (only those samples caused a 50% decrease of fluorescence intensity) with DNA was estimated as apparent binding constant (K_{app}) [28].

Table 2: Selected bond lengths (Å) and bond angles (°) for 1

N(2)-Cu(1)	2.030(2)	N(2)-Cu(1)#1	2.030(2)
N(1)-Cu(1)	2.046(2)	N(1)-Cu(1)#1	2.046(2)
O(1)-Cu(1)	2.425(3)	O(1)-Cu(1)#1	2.425(3)
N(2)-Cu(1)-N(2)#1	180.0 (9)	N(2)-Cu(1)-N(1)#1	100.14(9)
N(2)#1-Cu(1)-N(1)#1	79.86(9)	N(2)- $Cu(1)$ - $N(1)$	79.86(9)
N(2)#1-Cu(1)-N(1)	100.14(9)	N(1)#1-Cu(1)-N(1)	180.0 (9)
N(2)-Cu(1)-O(1)#1	90.39(10)	N(2)#1-Cu(1)-O(1)#1	89.61(10)
N(1)#1-Cu(1)-O(1)#1	88.83(11)	N(1)-Cu(1)-O(1)#1	91.17(11)
N(2)-Cu(1)-O(1)	89.61(10)	N(2)#1-Cu(1)-O(1)	90.40(10)
N(1)#1-Cu(1)-O(1)	91.17(11)	N(1)-Cu(1)-O(1)	88.83(11)
O(1)#1-Cu(1)-O(1)	180.0 (9)		

Symmetry transformations used to generate equivalent atoms: #1 - x + 1/2, -y + 1/2, -z + 1



Inset: Plot of [complex $\times 10^{-6}$] vs I_0/I of 1.

Fig. 3: Fluorescence quenching curves of ethidium bromide bound to DNA in 2% DMF/5mM Tris-HCl/50 mM NaCl buffer at pH 7.1: (a) EthBr (1.25 μ M); (b) EthBr + DNA (125 μ M); (c-m) EthBr + DNA + 1 (0-9 μ M).

The K_{app} value $(2.82 \times 10^5~M^{-1})$ supports a strong interaction of 1 with CT DNA and the mode of binding through partial intercalation [29]. The results are consistent with those obtained from electronic absorption titration studies. The cathodic (0.032~V) and anodic peak potential (0.132~V) values observed from the cyclic voltammetric (CV) responses for 1 in 2% DMF-5 mM Tris-HCl-50 mM NaCl buffer (pH = 7.1), which correspond to Cu^{II}/Cu^{I} redox couple [30]. Upon

addition of DNA, both the cathodic and anodic current decreases drastically (Fig. 4), this is expected of strong binding of the complex with DNA [31] via partial intercalation. The formal potentials of $\text{Cu}^{\text{II}}/\text{Cu}^{\text{I}}$ couple (obtained from differential pulse voltammetry (DPV) s tudies) in the E^0_f (0.116 V) and E^0_b (0.032 V) forms shift negatively (-84 mV) after reacting with DNA. The ratio of equilibrium binding constants, K_+/K_{2+} , is calculated to be 0.04, which suggests that the B form of DNA tends to stabilize Cu(II) over Cu(I) state.

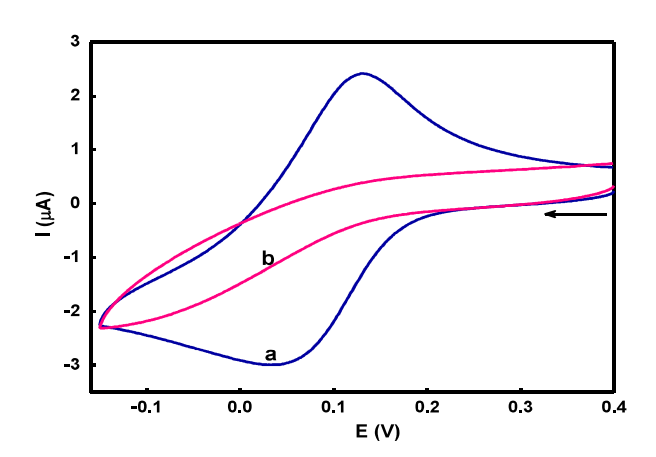


Fig. 4: Cyclic voltammograms of 1 (0.5 mM) in the absence (a) and presence (b) of CT DNA (R = 5) at 25.0 ± 0.2 °C at 50 mV s⁻¹ scan rate in 2% DMF/5mM Tris-HCl/50 mM NaCl buffer at pH 7.1.

3.3. In vitro cytotoxic activity

HeLa cells were treated with increasing concentrations (0.1 to 100 μ M) of 1 for 48 h inhibited the growth of HeLa cells in a dose-dependent manner (IC₅₀, 3.73 \pm 0.57 μ M) (Fig. 5).

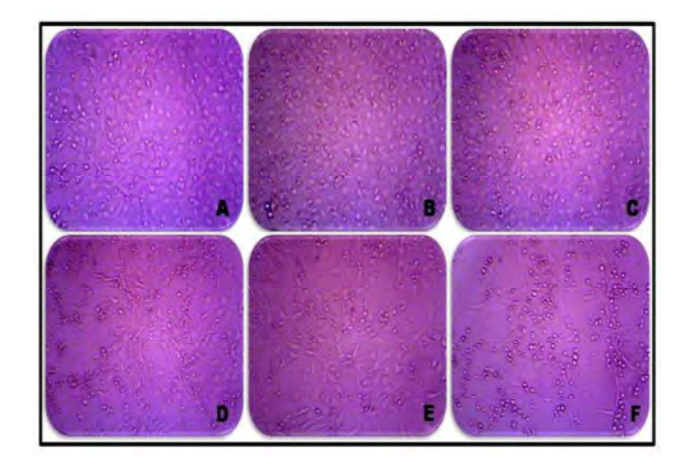


Fig. 5: Photomicrograph of human cervical carcinoma cells (HeLa) after 48 h exposure with 1 (A, control; B, 0.1 μ M; C, 1 μ M; D, 10 μ M; E, 50 μ M; F, 100 μ M).

From the IC $_{50}$ of 1, we can find that it is found to be highly active against the selected cancer cells [32] and 4.5 times better than cisplatin (IC $_{50}$, 16.4 μ M). In comparison, free dppt ligand (IC $_{50}$, 112.48 μ M) and

 $\text{Cu}(\text{OAc})_2 \cdot \text{H}_2\text{O}$ (IC $_{50}$, 705.67 μM) showed no significant growth inhibition activities, which indicated that the chelation of dppt with copper ion was essential for anticancer activities of the copper(II) complex. In addition, the results indicated that the IC $_{50}$ value of 1 against NIH 3T3 mouse embryonic fibroblasts (normal cells) is found to be above 500 μM , which confirmed that 1 is very specific on cancer cells. Finally, the cytotoxic behaviour of 1 is consistent with its ability to bind with DNA.

3.4. Anticancer drug mechanism

The profiles of propidium iodide stained HeLa cells treated with IC₅₀ concentration of 1 for 48 h were analyzed by FACS [33]. As shown in Fig. 6, in the control, the percentage in the cell at G1 phase is 61.94% and the remarkable increase of 17.2% was found. The increase in G1 phase was accompanied by the corresponding reduction in G0, S and G2/M phases. The data mean that 1 induces cell cycle arrest at G1 phase in HeLa cells. The cells treated with 1 and DCFDA for 1 h show significant shift of the histogram towards the right, indicating an increase in the intensity of emission resulting from the generation of DCF from DCFDA [34]. As shown in Fig. 7, in the control, the DCF fluorescence intensity is 100% while the intensity of DCF fluorescence increases to 128% when HeLa cells were incubated with 1.

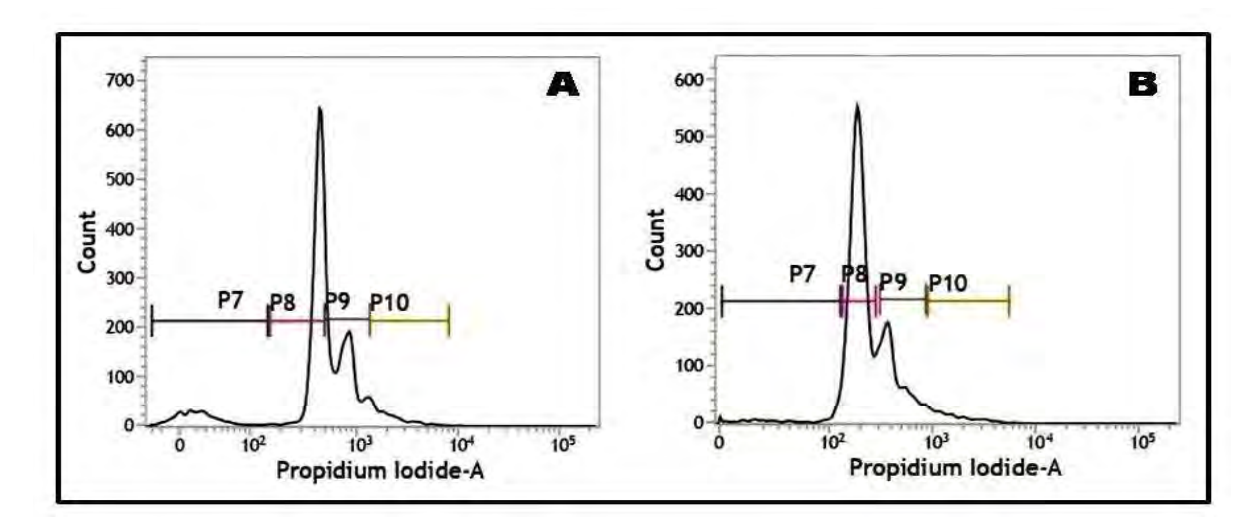


Fig. 6: Flow cytometric analysis showing the G1 phase cell cycle arrest by 1 in HeLa cells (P7, P8, P9 and P10 correspond to G0, G1, S and G2/M phases respectively). A, HeLa cells alone; B, HeLa cells treated with 1.

Greater shift implies higher fluorescence intensity resulting from higher amount of DCF formation and thus greater ROS generation, which is consistent with the apoptotic effect (cf. below) of 1. Moreover, the ROS levels induced by 1 show a time-dependent manner, decreasing the fluorescence intensity for 2 h (119%) and 3 h (116%). The result demonstrates the generation of ROS and this reactive species possibly causing cell apoptosis. We then carried out apoptosis assay to further evaluate the possible mechanism of cell death induced by 1 [35]. In the control cells, the percentage of living, early apoptotic, late apoptotic and necrosis cells were 99.9, 0.0, 0.1 and 0.0%, respectively (Fig. 8).

However, 1 treated HeLa cells displayed a remarkable

average of 56.08% of early apoptotic cells and 18.33% of late apoptotic cells. The increased expression of Annexin V positive cells undoubtedly demonstrated the cells were in apoptosis stage and is consistent with its *in vitro* cell cytotoxicity. Interestingly, there is no sign of cell death via necrotic pathway. To understand the nuclear morphology and the nature of cell death mechanism, we have carried out DAPI (4',6-diamidino-2-phenylindole) staining with 1 (Fig. 9).

The control HeLa cells exhibited evenly stained nucleus with round and intact contours whereas the treated cells showed characteristic fragmentation of the nucleus or condensed nuclei which is supportive of the cell toxicity induced by 1 due to apoptotic mode of cell death.

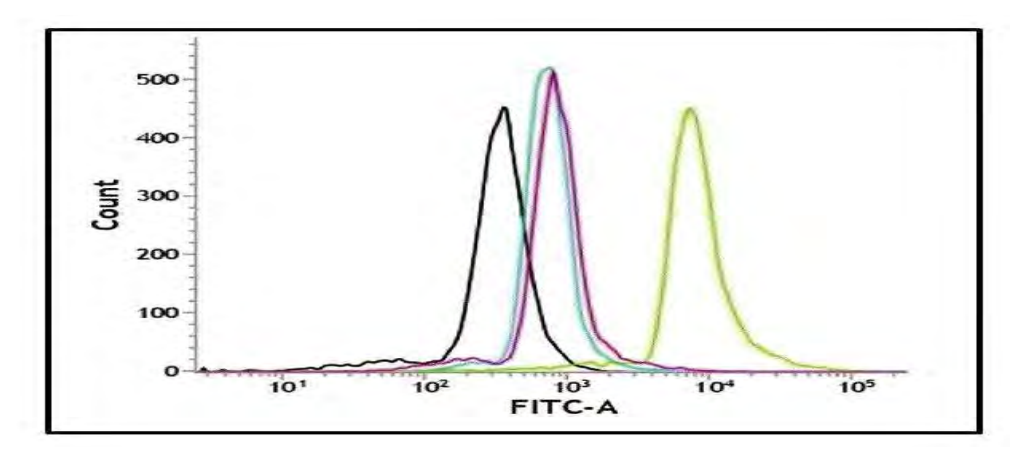


Fig. 7: DCFDA assay in HeLa cells for generation of ROS using the 1 in a time-dependent manner (control, black; 1 h, blue; 2 h, red; 3 h, green).

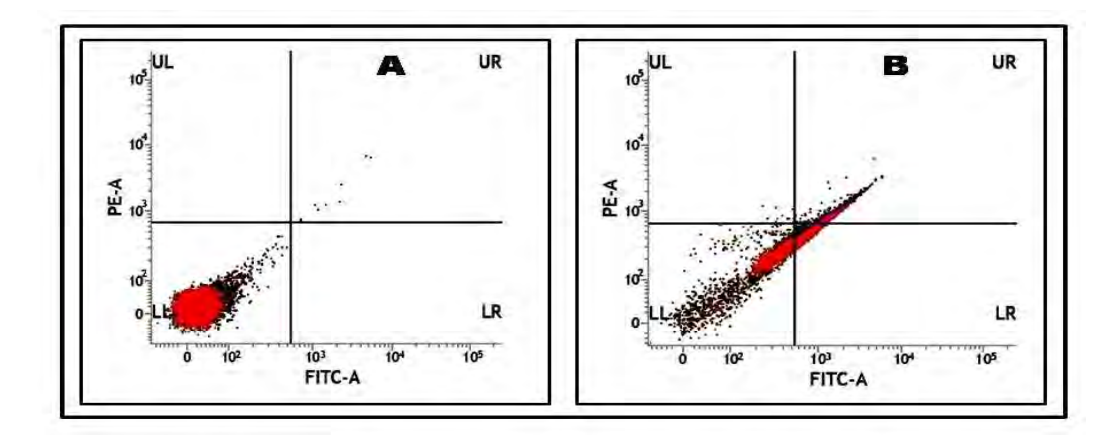


Fig. 8: Cellular apoptosis induced by 1 as determined from the annexin V-FITC/PI staining assay of the HeLa cells with four distinct phenotypes: viable cells (lower left quadrant, LL); cells at an early stage of apoptosis (lower right quadrant, LR); cells at a late stage of apoptosis (upper right quadrant, UR); and necrosis (upper left quadrant, UL). A, HeLa cells alone; B, HeLa cells treated with 1; red dots, gated cells; black dots, ungated cells.

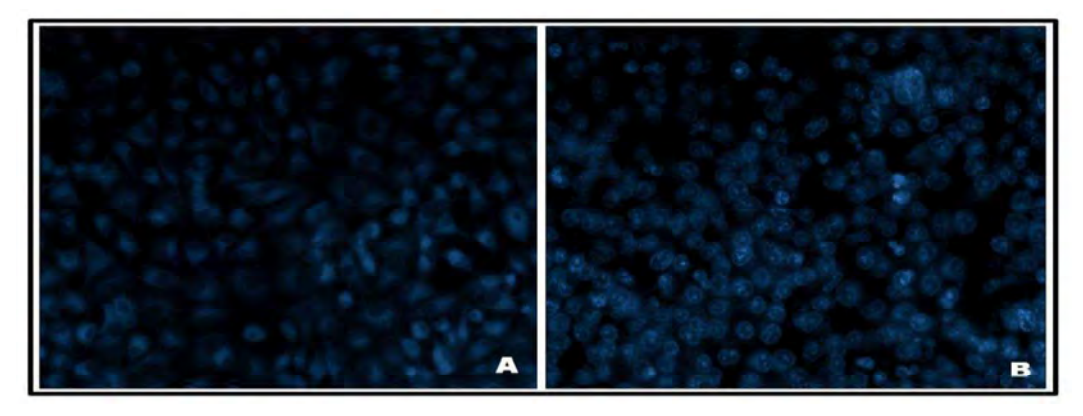


Fig. 9: HeLa cells stained with DAPI (A, HeLa cells alone; B, HeLa cells treated with 1) and visualized under a fluorescence microscope.

4. CONCLUSION

The copper(II) complex, [Cu(dppt)₂(H₂O)₂](ClO₄)₂, has been synthesized and characterized. The complex binds to CT DNA through partial intercalative mode. It exhibits highly active inhibitory effect, which was higher than cisplatin and selective to cancer cells while non-toxic to healthy cells. The biological evaluation provides evidence that it blocked cell cycle at G1 phase and induced apoptosis alone along with the generation of ROS. The present lead complex is a novel therapeutic agent for the treatment of cervical cancer as well as encourages further exploration of non-platinum anticancer agents. It targets the mitochondria of cancer cells and induces apoptosis by a mechanism involving the formation of ROS.

5. ACKNOWLEDGEMENTS

We are grateful to the DST-FIST programme of the National College (Autonomous), Tiruchirappalli. Thanks are due to STIC, Cochin University of Science and Technology for X-ray crystal structure data. We thank SAIF, Indian Institute of Technology Madras for structure solution and refinement (Dr. P. K. Sudhadevi) and for recording EPR spectra.

6. REFERENCES

- 1. Ndagi U, Mhlongo N, Soliman ME. *Drug Des Dev Ther*, 2017; 11:599-616.
- 2. Frezza M, Hindo S, Chen D, Davenport A, Schmitt S, Tomco D, Dou QP. *Curr Pharm Des*, 2010; **16**:1813-1825.
- 3. Marzano C, Trevisan A, Giovagnini L, Fregonal D. *Toxicol In Vitro*, 2002; **16**:413-419.
- 4. Orvig C, Abrams MJ. Chem Rev, 1996; **99**:2201-2204.

- 5. Yaman M, Kaya G, Yekeler H. World J Gastro-enterol 2007; **13**:612-618.
- Thompson KH, Orvig C. Science 2003; 300:936-939.
- 7. Samuni A, Chevion M, Czapski G. *J Biol Chem*, 1981; **256**:12632-12635.
- 8. Wijker CA, Lafleur MV. Mut Res, 1999; 429:27-35.
- 9. Linder MC. Mut Res, 2001; 475:141-152.
- 10. Deegan C, Coyle B, McCann M, Devereux M, Egan DA. Chem-Biol Interact, 2006; **164**:115-125.
- 11. Knox JJ, Hotte SJ, Kollmannsberger C, Winquist E, Fisher B, Eisenhauer EA. *Invest New Drugs*, 2007; **25**:471-477.
- 12. Yuan J, Lovejoy DB, Richardson DR. *Blood*, 2004; **104**:1450-1458.
- 13. Barnham KJ, Masters CL, Bush AI. *Nat Rev Drug Discov*, 2004; **3**:205-214.
- 14. Sangeetha S, Murali M. Int J Biol Macromol, 2018; **107**:2501-2511.
- 15. Bruker AXS. Inc SMART (Version 5.060) and SAINT (Version 6.02), Madison, Wisconsin: USA; 1996.
- 16. Sheldrick GM. Acta Cryst, 2015; C17:3-8.
- 17. Farrugia LJ. J Appl Cryst., 2012; 45:849-854.
- Nakamoto K. Infrared and Raman spectra of inorganic and coordination compounds. 4th edn. Wiley- Interscience, New York; 1986.
- 19. Bereau V, Marrot J. CR Chim, 2005; 8:1087-1092.
- 20. Rosenthal MR. J Chem Educ, 1973; 50:331-335.
- 21. Moradi-Shoeili Z, Amini Z, Boghaei DM, Notash B. *Polyhedron*, 2013; **53**:76-82.
- 22. Loganathan R, Ramakrishnan S, Suresh E, Riyasdeen A, Akbarsha MA, Palaniandavar M. *Inorg. Chem*, 2012; **51**:5512-5532.

- 23. Lever ABP. Inorganic Electronic Spectroscopy. Elsevier: Amsterdam; 1984.
- 24. Uma R, Palaniandavar M, Butcher RJ. J Chem Soc Dalton Trans, 1996; 2061-2066.
- 25. Yamada A, Mabe T, Yamane R, Noda K, Wasada Y, Inamo M, et al. Dalton Trans, 2015; 44:13979-13990.
- 26. Wolfe A, Shimer Jr. GH, Meehan T. *Biochemistry*, 1987; **26**:6392-6396.
- 27. Lakowicz JR, Webber G. *Biochemistry*, 1973; 12:4161-4170.
- 28. Lee M, Rhodes AL, Wyatt MD, Forrow S, Hartley JA. *Biochemistry*, 1993; **32**:4237-4245.
- 29. Kahrovic E, Zahirovic A, Turkusic E. *J Chem Chem Eng*, 2014; **8**:335-343.

- 30. Monica B, Marisa BF, Franco B, Giorgio P, Silvana P, Pieralberto T. *Inorg Chem*, 2003; 42:2049-2055.
- 31. Bard AJ, Faulkner LR. Electrochemical Methods: Fundamentals and Applications. Wiley: New York; 1980.
- 32. Tarafder MTH, Kasbollah A, Crouse KA, Ali AM, Yamin BM, Fun HK. *Polyhedron*, 2001; **20**:2363-2370.
- 33. Crowley LC, Marfell BJ, Scott AP, Waterhouse NJ. *Cold Spring Harb Protoc*, 2016; 11:953-956.
- 34. Takanashi T, Ogura Y, Taguchi H, Hashizoe M, Honda Y. *Investig Ophthalmol Vis Sci*, 1997; **38**:2721-2728.
- 35. Bhattacharjee RN, Park KS, Kumagai Y, Okada K, Yamamoto M, Uematsu S, et al. *J Biol Chem*, 2006; **281**:36897-36904.